EDITORIAL BOARD

Jiri Cizek (Waterloo, Canada)
David P. Craig (Canberra, Australia)
Raymond Daudel (Paris, France)
Ernst R. Davidson (Bloomington, Indiana)
Inga Fischer-Hjalmars (Stockholm, Sweden)
George G. Hall (Nottingham, England)
Jan Linderberg (Aarhus, Denmark)
Frederick A. Matsen (Austin, Texas)
Roy McWeeny (Pisa, Italy)
William H. Miller (Berkeley, California)
Keiji Morokuma (Okazaki, Japan)
Joseph Paldus (Waterloo, Canada)
Ruben Pauncz (Haifa, Israel)
Siegrid Peyerimhoff (Bonn, Germany)
John A. Pople (Pittsburgh, Pennsylvania)
Alberte Pullman (Paris, France)
Pekka Pyykkö (Helsinki, Finland)
Leo Radom (Canberra, Australia)
Klaus Ruedenberg (Ames, Iowa)
Henry F. Schaefer III (Athens, Georgia)
Isaiah Shavitt (Columbus, Ohio)
Per Siegbahn (Stockholm, Sweden)
Au-Chin Tang (Kirin, Changchun, China)
Rudolf Zahradnik (Prague, Czech Republic)

ADVISORY EDITORIAL BOARD

David M. Bishop (Ottawa, Canada)
Giuseppe del Re (Naples, Italy)
Fritz Grein (Fredericton, Canada)
Mu Shik Jhon (Seoul, Korea)
Mel Levy (New Orleans, Louisiana)
Jens Oddershede (Odense, Denmark)
Mark Ratner (Evanston, Illinois)
Dennis R. Salahub (Montreal, Canada)
Harel Weinstein (New York, New York)
Robert E. Wyatt (Austin, Texas)
Tokio Yamabe (Kyoto, Japan)

ADVANCES IN
QUANTUM CHEMISTRY

QUANTUM SYSTEMS IN CHEMISTRY AND PHYSICS, PART II

EDITOR-IN-CHIEF

PER-OLOV LÖWDIN

PROFESSOR EMERITUS

DEPARTMENT OF QUANTUM CHEMISTRY AND QUANTUM THEORY PROJECT
UPPSALA UNIVERSITY
UPPSALA, SWEDEN

QUANTUM THEORY PROJECT
UNIVERSITY OF FLORIDA
GAINESVILLE, FLORIDA

EDITORS

JOHN R. SABIN
MICHAEL C. ZERNER
QUANTUM THEORY PROJECT
UNIVERSITY OF FLORIDA
GAINESVILLE, FLORIDA

ERKKI BRÄNDAS
DEPARTMENT OF QUANTUM CHEMISTRY
UPPSALA UNIVERSITY
UPPSALA, SWEDEN

GUEST EDITORS

S. WILSON
RUTHERFORD APPLETON
LABORATORY
CHILTON, OXFORDSHIRE
UNITED KINGDOM

J. MARUANI
LABORATOIRE DE CHIMIE
PHYSIQUE
CNRS AND UPMC
PARIS, FRANCE

Y. G. SMEYERS
INSTITUTO DE ESTRUCTURA DE
LA MATERIA, CSIC
MADRID, SPAIN

P. J. GROUT
PHYSICAL AND THEORETICAL CHEMISTRY
LABORATORY
UNIVERSITY OF OXFORD
OXFORD, UNITED KINGDOM

R. McWEENY
DIPARTIMENTO DI CHIMICA E CHIMICA
INDUSTRIALE
UNIVERSITA DI PISA
PISA, ITALY

VOLUME 32

ACADEMIC PRESS

San Diego London Boston New York Sydney Tokyo Toronto

This book is printed on acid-free paper. ♾

Copyright © 1999 by ACADEMIC PRESS

All Rights Reserved.
No part of this publication may be reproduced or transmitted in any form or by any means, electronic or mechanical, including photocopy, recording, or any information storage and retrieval system, without permission in writing from the Publisher.
The appearance of the code at the bottom of the first page of a chapter in this book indicates the Publisher's consent that copies of the chapter may be made for personal or internal use of specific clients. This consent is given on the condition, however, that the copier pay the stated per copy fee through the Copyright Clearance Center, Inc. (222 Rosewood Drive, Danvers, Massachusetts 01923), for copying beyond that permitted by Sections 107 or 108 of the U.S. Copyright Law. This consent does not extend to other kinds of copying, such as copying for general distribution, for advertising or promotional purposes, for creating new collective works, or for resale. Copy fees for pre-1999 chapters are as shown on the title pages. If no fee code appears on the title page, the copy fee is the same as for current chapters.
0065-3276/99 $30.00

Academic Press
a division of Harcourt Brace & Company
525 B Street, Suite 1900, San Diego, California 92101-4495, USA
http://www.apnet.com

Academic Press
24-28 Oval Road, London NW1 7DX, UK
http://www.hbuk.co.uk/ap/

International Standard Book Number: 0-12-034833-0

PRINTED IN THE UNITED STATES OF AMERICA
98 99 00 01 02 03 MM 9 8 7 6 5 4 3 2 1

Contributors Volume 32

Numbers in parentheses indicate the pages on which the authors' contributions begin.

C. Amovilli (227), Dipartimento di Chimica e Chimica Industriale, Università di Pisa, 56100 Pisa, Italy

V. Barone (227), Dipartimento di Chimica e Chimica Industriale, Università di Pisa, 56100 Pisa, Italy

M. Bylicki (207), Instytut Fizyki, Uniwersytet Mikolaja Kopernicka, 87-100 Torun, Poland

R. Cammi (227), Dipartimento di Chimica e Chimica Industriale, Università di Pisa, 56100 Pisa, Italy

E. Cancès (227), Dipartimento di Chimica e Chimica Industriale, Università di Pisa, 56100 Pisa, Italy

D. L. Cooper (51), Department of Chemistry, University of Liverpool, Liverpool L69 7ZD, United Kingdom

M. Cossi (227), Dipartimento di Chimica e Chimica Industriale, Università di Pisa, 56100 Pisa, Italy

G. Day (93), Physical and Theoretical Chemistry Laboratory, University of Oxford, Oxford OX1 3QZ, United Kingdom

G. H. F. Diercksen (181), Max Planck Institut für Astrophysik, D-85740 Garching bei München, Germany

A. Famulari (263), Dipartimento di Chimica Fisica ed Elettrochimica, Università di Milano, 20133 Milan, Italy

J. Gerratt (51), School of Chemistry, University of Bristol, Cantocks Close, Bristol BS8 1TS, United Kingdom

E. Gianinetti (263), Dipartimento di Chimica Fisica ed Elettrochimica, Università di Milano, 20133 Milan, Italy

I. P. Grant (1), Mathematical Institute, University of Oxford, Oxford OX1 3LB, United Kingdom

P. J. Grout (93,285), Physical and Theoretical Chemistry Laboratory, University of Oxford, Oxford OX1 3QZ, United Kingdom

M. Hoffmann (109), Department of Chemistry, A. Mickiewicz University, 60-780 Poznan, Poland

A. Kalemos (69), Department of Chemistry, Laboratory of Physical Chemistry, National and Kapodistrian University of Athens, 157 10 Zografou, Athens, Greece

J. Karwowski (181), Instytut Fizyki, Uniwersytet Mikolaja Kopernicka, 87-100 Torun, Poland

G. J. A. Keith (285), Physical and Theoretical Chemistry Laboratory, University of Oxford, Oxford OX1 3QZ, United Kingdom

C. Lavín (181), Departamento de Química Física, Facultad de Ciencias, 47005 Valladolid, Spain

J. Linderberg (315), Department of Chemistry, Aarhus University, DK-8000 Aarhus C, Denmark

A. Maquet (197), Laboratoire de Chimie Physique-Matière et Rayonnement, Université Pierre et Marie Curie, 75231 Paris Cedex 05, France

I. Martin (181), Departamento de Química Física, Facultad de Ciencias, 47005 Valladolid, Spain

A. Mavridis (69), Department of Chemistry, Laboratory of Physical Chemistry, National and Kapodistrian University of Athens, 157 10 Zografou, Athens, Greece

B. Mennucci (227), Dipartimento di Chimica e Chimica Industriale, Università di Pisa, 56100 Pisa, Italy

Y. Pérez-Delgado (181), Departamento de Química Física, Facultad de Ciencias, 47005 Valladolid, Spain

C. Petrongolo (127), Dipartimento di Chimica, Università di Siena, I-53100 Siena, Italy

C. S. Pomelli (227), Dipartimento di Chimica e Chimica Industriale, Università di Pisa, 56100 Pisa, Italy

H. M. Quiney (1), Clarendon Laboratory, Department of Physics, University of Oxford, Oxford OX1 3PU, United Kingdom

M. Raimondi (263), Dipartimento di Chimica Fisica ed Elettrochimica, Università di Milano, 20133 Milan, Italy

J. Rychlewski (109), Department of Chemistry, A. Mickiewicz University, 60-780 Poznan, Poland

M. L. Senent (145), Instituto de Estructura de la Materia, CSIC, E-28006 Madrid, Spain

M. Sironi (263), Dipartimento di Chimica Fisica ed Elettrochimica, Università di Milano, 20133 Milan, Italy

H. Skaane (1), Mathematical Institute, University of Oxford, Oxford OX1 3LB, United Kingdom

Y. G. Smeyers (145), Instituto de Estructura de la Materia, CSIC, E-28006 Madrid, Spain

R. Specchio (263), Dipartimento di Chimica Fisica ed Elettrochimica, Università di Milano, 20133 Milan, Italy

A. Szarecka (93,109), Department of Chemistry, A. Mickiewicz University, 60-780 Poznan, Poland

R. Taïeb (197), Laboratoire de Chimie Physique-Matière et Rayonnement, Université Pierre et Marie Curie, 75231 Paris Cedex 05, France

T. Thorsteinsson (51), Department of Chemistry, Chemistry Laboratory IV, Copenhagen University, DK-2100 Copenhagen, Denmark

J. Tomasi (227), Dipartimento di Chimica e Chimica Industriale, Università di Pisa, 56100 Pisa, Italy

I. Vandoni (263), Dipartimento di Chimica Fisica ed Elettrochimica, Università di Milano, 20133 Milan, Italy

V. Véniard (197), Laboratoire de Chimie Physique-Matière et Rayonnement, Université Pierre et Marie Curie, 75231 Paris Cedex 05, France

M. Villa (145), Departamento de Químia, UAM, Iztapalapa, CP 09340 Mexico, D.F., Mexico

S. Wilson (93,285), Rutherford Appleton Laboratory, Chilton, Oxfordshire OX11 0QX, United Kingdom

R. G. Woolley (167), Department of Chemistry and Physics, Nottingham Trent University, Nottingham NG11 8NS, United Kingdom

Preface

The description of quantum systems is fundamental to an understanding of many problems in chemistry and physics. It is a vibrant field of research in which the countries of Europe have an established tradition of excellence. This volume records a representative selection of the papers delivered at the Second European Workshop on Quantum Systems in Chemistry and Physics. The Workshop was held at Jesus College, Oxford, April 6–9, 1997. The meeting was sponsored by the European Union, as a part of the COST chemistry initiative for stimulating cooperation in science and technology within the states of the European Union and those of Central and Eastern Europe. Workshop participants came from Bulgaria, Denmark, England, Finland, France, Greece, Hungary, Israel, Italy, Mexico, Norway, Poland, Slovakia, Spain, Wales, and the United States.

Like the first Workshop, which was held in San Miniato, near Pisa, Italy, a year earlier, the purpose of the Workshop recorded here was to bring together chemists and physicists with a common interest—the quantum mechanical many-body problem—and to encourage collaboration and exchange of ideas in the fundamentals by promoting innovative theory and conceptual development rather than improvements in computational techniques and routine applications.

The Workshop was opened with a personal view of the status of the quantum mechanical description of systems in chemistry and physics by a leading British authority. Professor Brian T. Sutcliffe, of the University of York, gave a stimulating and often provocative lecture in which he highlighted the formidable problems which stand in the way of further progress in many of the areas addressed during the Workshop. Not all agreed with Sutcliffe's perspective. Indeed, he succeeded in provoking some lively debate. In the article reproduced here, "No alteration has been made from that which was said at the time," since "it seemed honest, if unflattering, to leave things as they were." I am deeply grateful to Professor Sutcliffe for sharing his perspective on the field.

The Workshop was organized into eight sessions, each addressing a different aspect of the quantum mechanical many-body problem. Together with a poster session, the sessions were arranged as follows:

Density matrices and density functionals *(Chair: R. Pauncz)*
Electron correlation effects—Many-body methods and configuration interaction *(Chairs: U. Kaldor and I. P. Grant)*
Relativistic formulations *(Chair: B. T. Sutcliffe)*

Valence theory: Chemical bonds and bond breaking *(Chair: I. G. Kaplan)*
Nuclear motion, vibronic effects, and flexible molecules *(Chair: J. Maruani)*
Response theory—Properties and spectra: Atoms and molecules in strong electric and magnetic fields *(Chair: J. Gerratt)*
Condensed matter: Crystals and clusters, surfaces and interfaces *(Chair: Y. G. Smeyers)*
Reactive collisions and chemical reactions *(Chair: R. G. Woolley)*

A total of 37 lectures were scheduled over a 2½ day period. I express my gratitude to all of the speakers and the participants. They made the Workshop the stimulating and enjoyable experience that it was!

It is a pleasure to thank the members of the scientific organizing committee, Roy McWeeny (Pisa), Jean Maruani (Paris), and Yves G. Smeyers (Madrid), for their enthusiastic support and valuable advice throughout. I am especially grateful to Peter J. Grout (Oxford) for his help with the local organization of the Workshop.

Jesus College was founded in 1571 and is the only Oxford College to date from the Elizabethan period. Indeed, Queen Elizabeth I, who has the title of Foundress, granted timber for the College Buildings. The College provided a splendid venue for the Workshop at the heart of England's oldest University. It is a pleasure to thank the officers and staff of Jesus College, whose tireless attention to detail ensured the comfort of participants throughout the Workshop.

All contributions to this volume were refereed. I am most grateful to Erkki Brändas (Uppsala University) for organizing and executing the refereeing process with impressive proficiency.

Finally, the generous financial support of the European Union COST office is acknowledged. I particularly acknowledge the help with various "administrative details" given by Dr. S. Bénéfice of the COST office in Brussels.

S. WILSON
CHAIR, SCIENTIFIC
ORGANIZING COMMITTEE

Workshop Participants

J. Avery, Department of Chemistry, University of Copenhagen, DK-2100 Copenhagen, Denmark

P. Badger, Department of Chemistry, University of Sheffield, Sheffield, United Kingdom

M. Bylicki, Instytut Fizyki, Uniwersytet Mikolaja Kopernicka, 87-100 Torun, Poland

H. Chojnacki, Institute of Physical and Theoretical Chemistry, I-30, 50-370 Wroclaw, Poland

D. L. Cooper, Department of Chemistry, University of Liverpool, Liverpool L69 7ZD, United Kingdom

G. Day, Physical and Theoretical Chemistry Laboratory, University of Oxford, Oxford OX1 3QZ, United Kingdom

Ya. I. Delchev, Institute of Nuclear Research and Nuclear Energy, Bulgarian Academy of Sciences, 1784 Sofia, Bulgaria

J. Gerratt, School of Chemistry, University of Bristol, Cantocks Close, Bristol BS8 1TS, United Kingdom

E. Gianinetti, Dipartimento di Chimica Fisica ed Elettrochimica, Università di Milano, 20133 Milan, Italy

F. Gianturco, Department of Chemistry, The University of Rome, Città Universitaria, 00185 Rome, Italy

I. P. Grant, Mathematical Institute, University of Oxford, Oxford OX1 3LB, United Kingdom

P. J. Grout, Physical and Theoretical Chemistry Laboratory, University of Oxford, Oxford OX1 3QZ, United Kingdom

I. Hubač, Department of Chemical Physics, Faculty of Mathematics and Physics, Comenius University, 842 15 Bratislava, Slovakia

U. Kaldor, School of Chemistry, Tel Aviv University, 69978 Tel Aviv, Israel

I. G. Kaplan, Instituto de Física, Universidad Nacional Autónoma de México, 01000 México, D.F., Mexico

J. Karwowski, Instytut Fizyki, Uniwersytet Mikolaja Kopernicka, 87-100 Torun, Poland

G. J. A. Keith, Physical and Theoretical Chemistry Laboratory, University of Oxford, Oxford OX1 3QZ, United Kingdom

A. Khoudir, Laboratoire de Chimie Physique, Université Pierre et Marie Curie, 75231 Paris Cedex 05, France

S. Kirkpekar, Department of Chemistry, Odense University, DK-5230 Odense M, Denmark

C. Kozmutza, Department of Theoretical Physics, Institute of Physics, Technical University of Budapest, Budapest, Hungary

J. Linderberg, Department of Chemistry, Aarhus University, DK-8000 Aarhus C, Denmark

N. O. J. Malcolm, Department of Chemistry, University of Manchester, Manchester M20 9PL, United Kingdom

A. Maquet, Laboratoire de Chimie Physique-Matière et Rayonnement, Université Pierre et Marie Curie, 75231 Paris Cedex 05, France

I. Martin, Departamento de Química Física, Facultad de Ciencias, 47005 Valladolid, Spain

J. Maruani, Laboratoire de Chimie Physique, Université Pierre et Marie Curie, 75231 Paris Cedex 05, France

A. Mavridis, Department of Chemistry, Laboratory of Physical Chemistry, National and Kapodistrian University of Athens, 157 10 Zografou, Athens, Greece

R. McWeeny, Dipartimento di Chimica e Chimica Industriale, Università di Pisa, 56100 Pisa, Italy

A. K. Mohanty, IBM Corporation, Poughkeepsie, New York

T. van Mourik, Environmental Molecular Sciences Laboratory, Pacific Northwest Laboratory, Richland, Washington 99352

C. A. Nicolaides, Physics Department, National Technical University, Athens, Greece

J. M. Oliva, School of Chemistry, University of Bristol, Cantocks Close, Bristol BS8 1TS, United Kingdom

A. Papakondylis, Department of Chemistry, Laboratory of Physical Chemistry, National and Kapodistrian University of Athens, 157 10 Zografou, Athens, Greece

D. Parry, Department of Chemistry, University of Wales, Swansea, Singleton Park, Swansea SA2 8PP, United Kingdom

R. Pauncz, Department of Chemistry, Technion-Israel Institute of Technology, 32000 Haifa, Israel

C. Petrongolo, Dipartimento di Chimica, Università di Siena, I-53100 Siena, Italy

H. M. Quiney, Clarendon Laboratory, Department of Physics, University of Oxford, Oxford OX1 3PU, United Kingdom

M. Raimondi, Dipartimento di Chimica Fisica ed Elettrochimica, Università di Milano, 20133 Milan, Italy

T. T. Rantala, Department of Physical Sciences, University of Oulu, FIN-90571 Oulu, Finland

S. Rettrup, Department of Chemistry, Chemistry Laboratory IV, Copenhagen University, DK-2100 Copenhagen, Denmark

I. Roeggen, Institute of Mathematical and Physical Sciences, University of Tromsø, N-9037 Tromsø, Norway

J. Rothman, Department of Chemistry, Columbia University, New York City, New York 10027

J. Rychlewski, Department of Chemistry, A. Mickiewicz University, 60-780 Poznan, Poland

S. P. A. Sauer, Department of Chemistry, Odense University, DK-5230 Odense M, Denmark

L. Schulz, Institute of Physical and Theoretical Chemistry, 50-370 Wroclaw, Poland

H. Skaane, Mathematical Institute, University of Oxford, Oxford OX1 3LB, United Kingdom

Y. G. Smeyers, Instituto de Estructura de la Materia, CSIC, E-28006 Madrid, Spain

B. T. Sutcliffe, Department of Chemistry, University of York, Heslington, York YO1 5DD, United Kingdom

A. Szarecka, Department of Chemistry, A. Mickiewicz University, 60-780 Poznan, Poland

J. Tomasi, Dipartimento di Chimica e Chimica Industriale, Università di Pisa, 56100 Pisa, Italy

C. Valdemoro, Instituto de Matemáticas y Física Fundamental, Conséjo Superior de Investigacious Científicas, 28006 Madrid, Spain

I. Vandoni, Dipartimento di Chimica Fisica ed Elettrochimica, Università di Milano, 20133 Milan, Italy

S. Wilson, Rutherford Appleton Laboratory, Chilton, Oxfordshire OX11 0QX, United Kingdom

R. G. Woolley, Department of Chemistry and Physics, Nottingham Trent University, Nottingham NG11 8NS, United Kingdom

Ab initio relativistic quantum chemistry: four-components good, two-components bad!*

H. M. Quiney
Department of Physics, University of Oxford,
Oxford OX1 3PU, UNITED KINGDOM,

H. Skaane and I. P. Grant
Mathematical Institute, University of Oxford, 24-29 St Giles',
Oxford OX1 3LB, UNITED KINGDOM

Abstract

In view of the debate which resulted from the introductory lecture at this meeting, this article has been submitted to address the issues raised concerning the validity and implementation of relativistic theories of many-electron systems. We present the formulation and construction of BERTHA, our relativistic molecular structure program, and illustrate features of relativistic electronic structure theory with examples. These include magnetic and hyperfine interactions in small molecules, the use of spinor basis functions which include a dependence on a magnetic field strength, NMR shielding constants, *P*-odd interactions in chiral molecules, and computational details of a relativistic *ab initio* treatment of germanocene.

---

*With apologies to George Orwell [1]

ADVANCES IN QUANTUM CHEMISTRY, VOLUME 32
Copyright ©1999 by Academic Press. All rights of reproduction in any form reserved.
0065-3276/99 $30.00

Contents

1 Introduction
2 Dirac equation
3 Variation theory
  3.1 Non-relativistic quantum mechanics
  3.2 Relativistic quantum mechanics
  3.3 Example; hydrogenic ground-state energies
4 Relativistic many-electron theory
  4.1 Electron-electron interaction
  4.2 Bethe-Salpeter equation
  4.3 Continuum dissolution
  4.4 General formulation of the N-electron problem
  4.5 Dirac-Hartree-Fock equations
5 Implementation
  5.1 Relativistic corrections to non-relativistic quantum chemistry
  5.2 Relativistic many-body perturbation theory
  5.3 Virtual electron-positron pairs
  5.4 Matrix elements of charge and current operators
6 Applications
  6.1 Zeeman effect
  6.2 NMR shielding tensors in small molecules
  6.3 Parity violation in chiral molecules
  6.4 Strategy for DHF calculations in large molecules: germanocene
7 Conclusion
8 Acknowledgements
References

1 Introduction

Brian Sutcliffe's introductory lecture at this meeting [2] succeeded admirably in its designed purpose of provoking debate about the aims and shortcomings of quantum chemistry. Given that these comments were made by a co-author of one of the most influential texts on this subject [3], any "hopes and fears" he might have deserve to be taken very seriously. But as practitioners of relativistic quantum mechanics, we were surprised by his criticisms, repeated *verbatim* in this volume, and by the highly selective nature of the material used to support his assertions. For these reasons, we have chosen to depart from our presentation at the meeting in order to present a view of relativistic quantum chemistry which, we hope, will restore balance to the discussion.

The most serious reservation expressed about relativistic formulations of quantum chemistry in [2] is "to know to what question they are supposed to be the answer, in the circumstances in which we find ourselves". This article is intended to demonstrate that one may formulate a valid theory of quantum chemistry without invoking the Schrödinger equation, and that the conventional quantum chemistry that we would find in, say, [3, 4] may be obtained as a limiting case of our formulation. We prefer to keep the relativistic structure of the Dirac theory intact at all times, which means that our formulation does not contain "relativistic corrections". This is quite deliberate, and a feature which we will turn into a computational advantage.

Judging by the contributions to this meeting, the opinions expressed in the introductory lecture to it, or the articles published in any issue of, say, *Journal of Chemical Physics*, the aims and purpose of the whole of quantum chemistry appear to us to be as difficult to define clearly as it is to answer the challenge directed at the comparatively small community performing relativistic calculations. If we recall Coulson's assessment of the Conference on Molecular Quantum Mechanics [5], held at the University of Colorado in 1960, which was dedicated almost wholly to what he perceived to be the nature of quantum chemistry and to what sort of question it is equipped to answer, factional divisions of this type have long been with us. He even went so far as to formalise the divisions, defining Group I quantum chemists, who are driven by electronic computation, and Group II quantum chemists, whose interests are firmly rooted in experimental interpretation, with the minimum of elaborate numerical labour. What, then, *are* the circumstances in which we find ourselves? Happily, Coulson's prediction that there would be a parting of the ways has never been fulfilled, and both Group I and Group II chemists were in evidence at our meeting in Oxford almost forty years later, though he could hardly have anticipated the technical advances that have made the work of Group I quantum chemists viable. It would appear that relativistic formulations are viewed by some card-carrying members of both Groups I and II as a peripheral and utterly unimportant area of quantum chemistry, an opinion which we practitioners can only hope to change by reasoned argument and by example. We have always worked under the assumption that an interdisciplinary approach rooted in chemistry, physics, mathematics and computation cannot fail to yield results of lasting value. This diversity in the constitution of quantum chemistry suggests an analogy with *Animal Farm*, and the various beasts who, at first, put aside their differences and worked together with the common philosophy "all animals are equal" [1]. We subscribe to the view that "all quantum chemists are equal", irrespective of their departmental allegiances, and belong to this long and diverse tradition of quantum chemistry despite our current professional affiliations as mathematical physicists. It is also the clear lesson of [1] that we *must* resist any attempt to qualify this dictum with the rider "...but some quantum chemists are more equal than others". Perhaps our work may not be immediately appealing to some quantum chemists, and a superficial survey may not reveal the extent of its relevence and uselfulness. We invite readers to appreciate it as a gourmet meal, however, rather than regarding it as a "complete dog's breakfast" [2]. As we shall see later, a fully relativistic treatment affords a fresh insight into quantum chemistry. To quote Feynman [6], "there is a pleasure in recognising old things from a new point of view", and such a fresh perspective is almost reason enough to pursue an unconventional line of approach. We shall see also, perhaps surprising some readers, that the relativistic calculation of molecular properties is, in some senses, much simpler than the non-relativistic formulation, and that familiar results arise in unexpected ways. Even in the absence of a fully satisfactory solution of the many-body problem, and fixing our attention to models in which the nuclei are clamped, we are able to extract physical information from our calculations, and to interpret this information in terms of the charge and current densities which constitute the system. Apart from overcoming the formidable challenges posed by high performance scientific computing, this physical information is all we need from a calculation. This is the raw material which all of us must seek in order to provide answers to the challenges posed by quantum chemistry, and the only matter with which we are concerned in this article.

This contribution begins with a brief review of the Dirac equation, and the role of variation theory in non-relativistic and relativistic quantum chemistry. Special features of the relativistic N-body problem are discussed in the context of a general second-quantized formalism. We outline the Dirac-Hartree-Fock theory, which Bertha Swirles first introduced in 1935 [7]. Methods for including "relativistic effects" by perturbative methods are surveyed, and the surprising role of the negative-energy states in relativistic many-body theory is revealed. We present computational algorithms for implementing the *ab initio* relativistic theory emphasising, in particular, how we may include spin-dependent interactions between four-spinor states. In order to illustrate the use of the theory, we discuss calculations of NMR shielding constants, and parity-violating matrix interactions in chiral molecules. Some of the design features of our program, which we have named BERTHA, to acknowledge the prescient contribution made by Bertha Swirles [1], are presented, together with the numerical algorithms on which it is based. We conclude with the heretical suggestion that four-component methods have wider applicability than has been suggested previously.

2 Dirac equation

The manifestly covariant form of the Dirac equation [8] is

$$[\gamma_\mu(p^\mu + eA^\mu) - mc]\Psi(x) = 0 \tag{1}$$

where the space-time four-vector, x, is written

$$\begin{aligned} x &= (x^0, x^1, x^2, x^3) && (2)\\ &= (ct, \boldsymbol{r}). && (3) \end{aligned}$$

The four-momentum is defined by $p_\mu = i\partial/\partial x^\mu$, and A^μ is the classical four-potential, where

$$A^\mu = (\phi(\boldsymbol{r})/c, \boldsymbol{A}(\boldsymbol{r})). \tag{4}$$

The scalar potential is $\phi(\boldsymbol{r})$, and $\boldsymbol{A}(\boldsymbol{r})$ is the vector potential of the external electromagnetic field. The 4 × 4 matrices, γ_μ, satisfy the anticommutation relations

$$\{\gamma_\mu, \gamma_\nu\} = 2g_{\mu\nu} \tag{5}$$

where $g_{\mu\nu}$ is the Minkowski space metric, whose non-zero elements are $g_{00} = 1$ and $g_{11} = g_{22} = g_{33} = -1$. Repeated indices imply summation in the inner product $a_\mu b^\mu$.

Premultiplying by $c\gamma^0$, the Dirac equation is obtained in the non-relativistic variables $(\boldsymbol{x}, t)$,

$$\left\{ i\frac{\partial}{\partial t} + e\phi(\boldsymbol{r}) - c\boldsymbol{\alpha}\cdot(\boldsymbol{p} + e\boldsymbol{A}(\boldsymbol{r})) - \beta mc^2 \right\} \Psi(x) = 0 \tag{6}$$

---

[1] This article is respectfully dedicated to Bertha Swirles, now Lady Jeffreys, who has given her blessing to the use of the name BERTHA.

The 4×4 matrices $\boldsymbol{\alpha}$ and β are given by

$$\boldsymbol{\alpha}_q = \begin{bmatrix} 0 & \boldsymbol{\sigma}_q \\ \boldsymbol{\sigma}_q & 0 \end{bmatrix}, \qquad \beta = \begin{bmatrix} \boldsymbol{I} & 0 \\ 0 & -\boldsymbol{I} \end{bmatrix} \tag{7}$$

where $q = \{x, y, z\}$, $\boldsymbol{\sigma}_q$ are the Pauli spin matrices, $\beta = \gamma^0$, and $\boldsymbol{I}$ is the 2×2 unit matrix.

If we assume that the external electromagnetic field consists only of a time-independent scalar potential, $V(\boldsymbol{r}) = -e\phi(\boldsymbol{r})$, the solutions are of the form

$$\Psi_k(x) = \psi_k(\boldsymbol{r}) e^{-iE_k t} \tag{8}$$

where $\psi_k(\boldsymbol{r})$ is a four-component function of position satisfying the spatial eigenvalue equation

$$\left\{ c\boldsymbol{\alpha} \cdot \boldsymbol{p} + \beta mc^2 + V(\boldsymbol{r}) \right\} \psi_k(\boldsymbol{r}) = E_k \ \psi_k(\boldsymbol{r}) \tag{9}$$

with eigenvalue, E_k. The solution of equations of this type forms the computational basis of the relativistic electronic structure theory of atoms and molecules.

The solutions are classified as being of 'positive-energy' type for $E_k > 0$, and 'negative-energy' type for $E_k < 0$. For attractive potentials, $V(\boldsymbol{r}) < 0$, of the type which most commonly occur in electronic structure theory, the positive-energy solutions are further classified as square-integrable bound states if $-mc^2 < E_k < mc^2$. All other solutions belong to a continuum of states representing scattering in the external field. In the case where there is no external field, the spectrum consists only of positive- and negative-energy continua.

Although this presentation of the Dirac equation is quite conventional, there is one rather important sleight of hand which has occurred in this section which touches on an important point of principle. We assume throughout this article that we are solving an electronic structure problem to which the nuclei contribute a classical time-independent external potential. So our formulation immediately introduces the Born-Oppenheimer approximation, involving the separation into electronic and nuclear coordinates. To do otherwise in non-relativistic theory is a fiendishly difficult problem [9]: to our knowledge there have been only a very few attempts to construct a relativistic theory on this basis, none but the crudest of which appear to offer much hope of a practical implementation. In order to treat nuclear motion strictly on the same footing as electronic motion in relativistic theory, one must face new possibilities. For example, the nuclei may be bosons, which are described by the Klein-Gordon equation, and the nuclei have an internal structure, each with a characteristic distribution of particles and currents. There are many more possible levels of sophistication in the models which we use to describe the system than are available in a non-relativistic treatment. One can no longer simply emulate the non-relativistic treatment utilizing the Schrödinger equation with spin couplings characteristic of the particles; the formidable problem of interacting field equations is involved. So, the reader should regard our presentation with whatever apprehension, or lack of apprehension, he or she usually feels for the Born-Oppenheimer approximation.

3 Variation theory

In order to understand some of misgivings expressed in [2], and what has led Sutcliffe to express them, it is necessary to review the status of the variation principle in relativistic and non-relativistic quantum theory.

3.1 Non-relativistic quantum mechanics

McWeeny's extensive revision of *Methods of molecular quantum mechanics* [4] sets out the commonly-accepted ground-rules of computational quantum chemistry: in Chapter 2, we learn of the Undheim-Hylleraas-Macdonald theorem, and the variation theorem. In practical applications, these theorems are implemented as numerical algorithms, in which one introduces a trial function depending on a set of variational parameters, constructs the Rayleigh quotient, and finds the stationary point of the Rayleigh quotient with respect to the variational parameters. There may be many stationary points, including local maxima and minima, but the "best" solution is obtained when one obtains the global minimum of the Rayleigh quotient with respect to the variable parameters. Any approximate trial function yields an electronic energy which is an upper bound to an exact eigenvalue of the Schrödinger equation, the identity of the eigenvalue being determined by the Undheim-Hylleraas-Macdonald separation theorem.

3.2 Relativistic quantum mechanics

In the one-electron theory of Dirac, one finds that the eigenvalue spectrum consists of two parts. The *positive-energy spectrum* comprises states corresponding to those found in non-relativistic theory, but with energies shifted by mc^2 a.u., corresponding to the rest-mass energy. The energies of these states contain small contributions that are sometimes attributed to mass-velocity effects and spin-orbit coupling in treatments based on perturbations to the non-relativistic Schrödinger operator. The solutions themselves are four-component spinors, instead of two-component spin-orbitals. The second branch of the eigenvalue spectrum consists of states with energies less than $-mc^2$ a.u., and in a second-quantized theory they can be interpreted as states of positrons. The existence of these solutions is a consequence of the relativistic energy-momentum relation, $E^2 = c^2p^2 + m^2c^4$, and rather than being thought of as a shortcoming of the theory, this feature should instead be acknowledged as the explanation for the well-established existence of anti-particles. One may not, therefore, expect basis set expansions of the one-electron Dirac operator to conform strictly to the Undheim-Hylleraas-Macdonald theorem; it is easy to find numerical examples which do not. Similarly, we should not expect approximate trial functions to provide strict upper bounds to bound-state eigenvalues.

However, there is a *stationary* variation principle of precisely the type employed in the quantum chemical linear variation method. In the derivation of the Roothaan equations based on finite basis set expansions of Schrödinger wavefunctions, one insists only that the Rayleigh quotient be *stationary* with respect to the variational parameters, and then *assumes* that the variational principle guarantees an absolute minimum. In the corresponding linear equations based on the Dirac equation, the stationary condition is imposed, but no further assumption is made about the nature of the stationary point.

Any valid formulation of relativistic electronic structure theory must exhibit a clear separation between the elements of the positive- and negative-energy parts of the one-electron spectrum, which, for practical purposes, imposes a strict variational lower bound of $-mc^2$ a.u. on all acceptable approximations of positive-energy solutions for monotonically attractive external field potentials. The kinetic balance prescription for the basis function elements of the four-spinors is now a well-established method for generating basis sets which approach completeness in well-defined limits, and which preserve unambiguously the identity of positive- and negative-energy spinors [10, 11]. Stanton and Havriliak [10] estimate that finite-dimensional approximations to Dirac spinors may fail to satisfy the upper-bounding principle of non-relativistic variation theory at the level $O[(Z\alpha)^4]$, where Z is the nuclear charge and α is the fine-structure constant. In the limit of a complete basis set, however, such matrix representations converge to the exact Dirac spectrum for a given system, though the convergence need not satisfy the Undheim-Hylleraas-Macdonald theorem. In practice, we actually observe *quasi*-variational behaviour if kinetically balanced basis sets are used, because the parts of the four-component spinors which become Pauli two-spinors in the non-relativistic limit $c \rightarrow \infty$

dominate the total electronic energy of bound-state systems. For atomic point nuclear models, we have also utilized basis sets of L-spinors and S-spinors [11, 12, 13], which are generated by a generalization of the kinetic balance prescription. Satisfactory methods exist for solving the one-electron Dirac equation using finite basis sets which exhibit all of the important features found in non-relativistic quantum chemistry. The only thing which must be sacrificed are the *strict* upper-bounds to bound-state eigenvalues. This never poses a problem in practice, since the variational behaviour is dominated by the non-relativistic contributions to the total energy. As an example, the naive use of the variation principle as a non-linear energy minimization procedure succeeds in generating single-particle functions with no hint of trouble, and is now a standard method for obtaining Gaussian basis set parameters for relativistic molecular structure calculations [14].

3.3 Example: hydrogenic ground state energies

The variational treatment of the ground states of point-nuclear hydrogenic ions using a minimal Slater basis set is familiar to every student of quantum chemistry. If we work with the radially reduced Schrödinger equation, the trial function, ψ_T has the form

$$\psi_T = N r \exp\left(-\lambda r\right)$$

where λ is a real, positive parameter, and N is a normalization constant. We construct the Rayleigh quotient, R, according to

$$\begin{aligned} R &= \frac{\langle \psi_T | h | \psi_T \rangle}{\langle \psi_T | \psi_T \rangle} \\ &= \frac{1}{2}\lambda^2 - Z\lambda \end{aligned}$$

for nuclear charge, Z. We impose the variational condition

$$\frac{\partial R}{\partial \lambda} = 0$$

to find that $\lambda = Z$, and the ground state energy, E is given, in a.u., by

$$E = -\frac{Z^2}{2}. \tag{10}$$

We now consider the corresponding variational treatment of the Dirac equation. The radially reduced equation for the the ground state is [11]

$$\begin{bmatrix} c^2 - \frac{Z}{r} & \left(-\frac{d}{dr} - \frac{1}{r}\right) \\ \left(\frac{d}{dr} - \frac{1}{r}\right) & -c^2 - \frac{Z}{r} \end{bmatrix} \begin{bmatrix} P(r) \\ Q(r) \end{bmatrix} = \varepsilon \begin{bmatrix} P(r) \\ Q(r) \end{bmatrix}$$

where $P(r)$ and $Q(r)$ are the radial parts of two-component functions, which by tradition are labelled the large- and small-components, respectively. In order to satisfy the boundary conditions for acceptable bound-state solutions at $r = 0$ and for $r \to \infty$, the radial trial function must be chosen to be

$$\psi_T = \begin{bmatrix} c^L N r^\gamma \exp(-\lambda r) \\ c^S N r^\gamma \exp(-\lambda r) \end{bmatrix}$$

where $\gamma = \sqrt{1 - (Z/c)^2}$, and c^L and c^S are linear expansion coefficients that fix the ratio of the radial amplitudes $P(r)$ and $Q(r)$. We first solve the secular equation in this basis

$$\begin{vmatrix} \left(c^2 - \varepsilon - \frac{Z\lambda}{\gamma}\right) & -\frac{c\lambda}{\gamma} \\ -\frac{c\lambda}{\gamma} & \left(-c^2 - \varepsilon - \frac{Z\lambda}{\gamma}\right) \end{vmatrix} = 0$$

to find that

$$\varepsilon = -\frac{Z\lambda}{\gamma} \pm \frac{c}{\gamma}\sqrt{c^2 - Z^2 + \lambda^2}$$

The variational condition $(\partial\varepsilon/\partial\lambda) = 0$ is satisfied only for the positive sign of the square root, yielding the optimal value $\lambda = Z$, and the positive-energy bound-state energy

$$E_0 = \gamma c^2, \tag{11}$$

while the ratio between the coefficients c^L and c^S is given by

$$\begin{aligned} \frac{c^S}{c^L} &= \frac{(\gamma - 1)c^2}{cZ} \\ &\simeq -\frac{Z}{2c}, \end{aligned}$$

which illustrates the origin of the component labels *large* and *small*, if we remember that $c \simeq 137$ in atomic units. Of course, Eqs (10) and (11) are the exact $1s_{1/2}$ energies, respectively, of the point-nuclear Schrödinger and Dirac equations. No stationary value is obtained for the negative-energy solution, because no negative-energy bound-states exist for monotonely attractive potentials. At first glance, this seems to be a completely different result than we obtained from non-relativistic theory in Eq. (10). However, if we make use of the fact that $Z/c < 1$ and expand γ we find that

$$E_0 = c^2 - \frac{Z^2}{2} - \frac{Z^4}{8c^2} - \frac{Z^6}{16c^4} - \cdots$$

revealing that E_0 contains the electron rest-mass energy as the first term, the non-relativistic result as the term independent of c, and a series of "relativistic corrections" in which Z/c is the expansion parameter. It is significant that in neither the relativistic nor non-relativistic examples have we needed to assume that this energy is a *minimum* with respect to variation in the parameters. In fact, for the example based on the Dirac equation it is not: if we were to vary the exponential parameters for $P(r)$ and $Q(r)$ independently, we would find that this stationary point represents a minimum with respect to variations in $P(r)$, and a maximum with respect to $Q(r)$. This is the min-max principle described by Talman [18]. It is satisfied precisely for the exact solutions of the point-nuclear single-particle Dirac equation, but there is no reason to believe that it is an appropriate principle with which to determine the wavefunction of a many-electron system. As we shall see in the next section, relativistic many-electron theory is derived from quantum electrodynamics [11, 15, 16, 17], which is based on single-particle states and fundamental interactions. Many-electron relativistic wavefunctions are not solutions of an unquantized wave-equation; this is doubtless one of the features that causes such unease amongst quantum chemists. We are aware of no argument which confirms that a general two-electron bound-state wavefunction obtained by the min-max principle has the same physical content as one derived from quantum electrodynamics. Since quantum electrodynamics is the most precisely established of all physical theories, we advocate an adherence to its tenets which is as strict as practical considerations allow.

4 Relativistic many-electron theory

Relativistic treatments of N-electron systems usually start from the so-called *Dirac-Coulomb hamiltonian*, H_{DC}, where

$$H_{DC} = \sum_i h_D(\boldsymbol{r}_i) + \sum_{i>j} \frac{1}{r_{ij}}$$

where $r_{ij} = |\boldsymbol{r}_i - \boldsymbol{r}_j|$, and $h_D(\boldsymbol{r}_i)$ is a single-particle Dirac operator for electron i. This is the physical *ansatz* introduced by Bertha Swirles [7], when she formulated the theory of the relativistic self-consistent field.

A number of objections have been raised regarding the use of operators of this type. In the end, we shall return to H_{DC} and see that it represents a valid starting point for a relativistic theory of atomic and molecular electronic structure, provided that it is interpreted correctly. Before we do so, however, we shall indicate the main areas of concern, and explain why no problem of principle exists.

4.1 Electron-electron interaction

The most obvious objection to the Dirac-Coulomb operator is that the instantaneous Coulomb interaction, $1/r_{ij}$, is manifestly not Lorentz invariant. It is, however, the leading term of the covariant interaction

$$v^T_{ij,\alpha\gamma} = \frac{1}{r_{ij}} - \left(\frac{\boldsymbol{\alpha}_i \cdot \boldsymbol{\alpha}_j}{r_{ij}} \exp\left(i\omega_{\alpha\gamma} r_{ij}\right) + \left(\boldsymbol{\alpha}_i \cdot \boldsymbol{\nabla}_{r_{ij}}\right) \left(\boldsymbol{\alpha}_j \cdot \boldsymbol{\nabla}_{r_{ij}}\right) \frac{\exp\left(i\omega_{\alpha\gamma} r_{ij}\right) - 1}{\omega^2_{\alpha\gamma} r_{ij}} \right),$$

which may be derived from QED by assuming the Coulomb gauge condition, $\boldsymbol{\nabla} \cdot \boldsymbol{A} = 0$, and assuming the electrons are in Dirac stationary states in some effective static potential [19, 11, 17]. This effective configuration-space interaction is derived by further assuming that two one-electron Dirac currents interact by exchanging a single virtual photon of frequency $\omega_{\alpha\gamma}$. These assumptions allow us to perform the time-like integrations in the Feynman diagram involving the exchange of one virtual photon from which this interaction is derived, resulting in the appearance of the single-particle energy difference parameter, $\omega_{\alpha\gamma} = (\varepsilon_\gamma - \varepsilon_\alpha)/c$. The interaction is symmetrized for the interaction of two electrons, yielding

$$v^T_{ij} = \frac{1}{2}\left(v^T_{ij,\alpha\gamma} + v^T_{ij,\beta\delta}\right)$$

In the limit $\omega \to 0$, $v^T_{ij} \to g_{ij} + b_{ij}$, where $g_{ij} = 1/r_{ij}$, and b_{ij} is the low-energy form of the Breit interaction

$$b_{ij} = -\frac{1}{2r_{ij}} \left((\boldsymbol{\alpha}_i \cdot \boldsymbol{\alpha}_j) + \frac{(\boldsymbol{\alpha}_i \cdot \boldsymbol{r}_{ij})(\boldsymbol{\alpha}_j \cdot \boldsymbol{r}_{ij})}{r^2_{ij}} \right)$$

The Breit interaction may be regarded as the $O(\alpha^2)$ correction to the Coulomb interaction, and the covariant form v^T_{ij} represents the complete interaction between two independent electrons due to the exchange of a single transverse photon. In practice, we find that the Breit interaction suffices to describe effects attributed to "spin-spin" and "spin-other-orbit" interactions in atomic and molecular structure calculations. There exists, however, no problem of principle involving the interaction between two electrons.

To summarize this section, the Dirac equation for an electron moving in a time-independent external field, such as a nuclear Coulomb field or a molecular mean-field, is a Lorentz-invariant description of the relativistic kinematics of a single electron. The interaction v_{ij}^T provides a covariant description of the interaction between two such electrons propagating in this external field, and may be represented by the sum of the Coulomb and Breit interactions, correct to $O(\alpha^2)$, provided that the limit $\omega \to 0$ is justified. This low-energy approximation is acceptable for interactions between electrons occupying positive-energy states. If we wish to consider the interactions between positive- and negative-energy electrons, we must include the energy dependences in the interaction. The often-quoted *caveat* regarding the use of the Breit operator for any purpose other than first-order perturbation theory applies only to interactions involving virtual electron-positron pair production, as a careful reading of [20] will confirm. We may use it with complete safety to define mean-field potentials by iteration, because these involve only electron densities of positive-energy bound-states.

The complete theory of quantum electrodynamics introduces additional terms which cannot be expressed simply in terms of v_{ij}^T. These quantities are identified as electrodynamic contributions to the mass of a particle, and corrections to the charge of a particle which cause short-range modifications of Coulomb's law. These cause a discrepancy between the predictions of the Dirac electron theory and experiment, which in one-electron systems is called the Lamb shift. In §5.3 we demonstrate how these effects are incorporated in our formulation.

4.2 Bethe-Salpeter equation

The spectre of the Bethe-Salpeter equation was raised in the discussion at this meeting, in the context of what a covariant relativistic many-electron theory should look like. In §42γ of [20], however, Bethe and Salpeter note that if we restrict ourselves to equal time interactions, such as the Coulomb and low-frequency Breit interactions, the Bethe-Salpeter equation reduces to the Dirac-Coulomb-Breit equation for two electrons. They describe the "radical" difference between the Bethe-Salpeter and Dirac-Coulomb-Breit operators as the use of individual time coordinates for each electron in the former, and equal-time coordinates in the latter. As we have already remarked, this deficiency in the Dirac-Coulomb-Breit operator is remedied if we replace $g_{ij} + b_{ij}$ by v_{ij}^T, because the individual time coordinates embodied in the derivation of v_{ij}^T are the reason that the energy differences $\omega_{\alpha\gamma}$ and $\omega_{\beta\delta}$ appear in v_{ij}^T, after integrating over the *relative* time coordinate $t_i - t_j$. Whilst the Bethe-Salpeter equation has been used to construct covariant bound-state solutions for two-fermion problems, such as the hydrogen atom and positronium, it is formidably difficult to solve and introduces no physics other than that which is embodied in perturbative approaches to quantum electrodynamics. There appear to be no advantages in trying to generalize it to many-fermion problems, and no prospect of finding solutions to it for more general problems involving electron-nuclear interactions.

4.3 Continuum dissolution

The practical question remains: how can we find bound-state solutions of equations based on the Dirac-Coulomb-Breit operator? The naive approach to the solution of a He-like problem would be to assume that the two-electron wavefunction, Ψ, can be written as a complete-set expansion of the form

$$\Psi(x_1, x_2) = \sum_{\mu\nu} c_{\mu\nu} \left(\psi_\mu(x_1)\psi_\nu(x_2) - \psi_\mu(x_2)\psi_\nu(x_1)\right)$$

in which $c_{\mu\nu}$ are the expansion coefficients of antisymmetrized products of one-electron four-spinors, labelled μ and ν. We may define our one-electron basis by solving the Dirac equation for a time-independent potential, so that $x_i = (t_i, \boldsymbol{r}_i)$, consistent with the derivation of v_{ij}^T. The two-electron spinor, Ψ, is a sixteen-component object, written as a sum of sixteen-component antisymmetric two-electron configuration state functions.

The problem with this approach is that the complete set of one-electron basis functions contains both positive- and negative-energy states. The ground-state energy of this He-like system is degenerate with an infinite number of configurations in which one electron occupies a positive-energy state, and the other a negative-energy state. In the course of time, a two-electron atom prepared in a bound state should dissolve into the positive- and negative-energy continua once any form of electron-electron interaction is allowed to act. This is the so-called "continuum dissolution" process described by Sucher [21], which was first discussed in the context of covariant treatments of two-electron systems by Brown and Ravenhall [22].

Their solution was to surround the operator $g_{ij} + b_{ij}$ by projection operators which restrict the expansion of Ψ to include only configurations involving *positive energy* spinors. These projection operators, L_{ij}^{++} have the form

$$L_{ij}^{++} = L_i^+ L_j^+$$

where

$$L_i^+ = \sum_n^+ \psi_n^\dagger(x_i)\psi_n(x_i).$$

If one constructs the projection operators from the same independent particle basis as is used in the expansion of Ψ, then the effect is simply to limit the expansion of Ψ to include only two-electron configurations involving positive energy spinors. Defining $b_\mu^\dagger$ to be a creation operator for the single-particle positive-energy state, ψ_μ, the equation

$$H_{DC}\Psi = E\Psi$$

is equivalent to a set of Fock-space equations which do not couple the positive- and negative-energy sectors of Hilbert space if

$$\Psi(x_1, x_2) = \frac{1}{\sqrt{2}} \sum_{\mu\nu}^{++} \left\{ b_\mu^\dagger(x_1) b_\nu^\dagger(x_2) - b_\mu^\dagger(x_2) b_\nu^\dagger(x_1) \right\} |0\rangle$$

where $|0\rangle$ is the vacuum state consisting of no electrons, positrons. There is no "continuum dissolution", and all valid processes involving the production of virtual electron positron pairs may be treated perturbatively. In relativistic quantum chemistry, such processes are not likely to be of much structural importance, but we can calculate them if we wish, using relativistic many-body perturbation theory. The apparent exclusion of the negative-energy states does not mean we do not know how to deal with them, but rather an indication that we know that it is permissible to ignore them in order to formulate a zero-order model potential. In the next section, we present a complete formulation of the relativistic many-electron problem for a fixed configuration of nuclei, based on our earlier work [11, 23, 17].

4.4 General formulation of the N-electron problem

For a time-independent scalar potential, the electron-positron field operator, $\Psi(x)$, is expanded in a complete basis of four-component solutions of the time-dependent Dirac equation [19],

$$\Psi(x) = \sum_{E_m>0} b_m \psi_m^+(x) + \sum_{E_n<0} d_n^\dagger \psi_n^-(x), \tag{12}$$

where b_m and $d_n^\dagger$ are, respectively, annihilation and creation operators for the positive-energy state $\psi_m^+(x)$ and the negative-energy state $\psi_n^-(x)$. These functions are of the form of Eq (8), and have spatial parts which are solutions of the Dirac equation defined by Eq. (9).

In the absence of interparticle interactions, the total energy is given by [11]

$$H_0 = \sum_{E_m>0} N_m^+ E_m - \sum_{E_n<0} N_n^- E_n \qquad (13)$$

where $N_m^+ = b_m^\dagger b_m$ is the number of particles with energy E_m, and $N_n^- = d_n d_n^\dagger$ is the number of anti-particles, which we may interpret as holes in the negative-energy continuum whose energy is E_n. The infinite energy of the filled negative-energy continuum is eliminated on the grounds that it is not observable.

The operator corresponding to the net charge of the system, Q, is

$$Q = -e\left\{\sum_{E_m>0} N_m^+ - \sum_{E_m<0} N_n^-\right\} + Q_{vac} \qquad (14)$$

comprising the sum of the electron and positron charges, and the polarization charge, Q_{vac}, induced in the vacuum charge distribution by the external scalar field. Since Q is conserved in electromagnetic interactions, real or virtual electrons and positrons are always created and annihilated in pairs.

Normal ordering of the operators is introduced so that annihilation operators are placed to the right of creation operators allowing all anti-commutators to vanish in the process. A normally-ordered product of operators is denoted, for example, by $: b_p^\dagger b_q^\dagger :$, where the normal ordering is indicated by colons. The normal ordering ensures that $Q = 0$ for the *free* vacuum, and that the particle vacuum has zero energy.

For simplicity, we restrict our attention to spherically-symmetric atomic potentials, which may be defined by a single radial coordinate, r; the introduction of molecular electrostatic potentials introduces notational complexity, but no new problems of principle. Retaining only contributions from positive-energy states, the total energy operator of an N-electron system, H, is given by $H = H_0 + H_1$, where

$$\begin{aligned} H_0 &= \overset{+}{\sum} N_p^+ E_p && (15) \\ H_1 &= \overset{+}{\sum} : b_p^\dagger b_q^\dagger b_s b_r : \langle pq|v_{12}|rs\rangle + \overset{+}{\sum} : b_p^\dagger b_q : \langle p| - V(r) - Z(r)/r|q\rangle && (16) \end{aligned}$$

Classification	Energy	Labels
Core	$E \leq F$	$a, b, c, \cdots$
Virtual	$E > F$	$r, s, t, \cdots$
General	any E	$i, j, k, \cdots$

Table 1: Labelling scheme for single particle states.

where $V(r)$ is a mean-field counter-term, $Z(r)$ may be used to represent the effects of finite nuclear charge distributions, and

$$\langle ij|v_{12}|kl\rangle = \int\int \psi_i^\dagger(\mathbf{r}_1)\psi_j^\dagger(\mathbf{r}_2)v_{12}\psi_k(\mathbf{r}_1)\psi_l(\mathbf{r}_2)\ d\mathbf{r}_1 d\mathbf{r}_2.$$

Summation over the single-particle states is restricted to positive energy contributions, which has become known as the 'no virtual pair' approximation. In practice, the interaction v_{12} may be the complete energy-dependent, covariant interaction, v_{12}^T, the Coulomb interaction, g_{12}, or the transverse-gauge Breit operator, $g_{12} + b_{12}$.

Particle-labels are introduced which define the energy ordering of single-particle states with respect to the Fermi level, F (Table 1). A new normal ordering is introduced such that a creation operator $b_i^\dagger$ appears at the right of an operator product if $i = \{a, b, c, \cdots\}$, which is sufficient to specify the occupancy of the reference space of occupied spinors. This space includes the entire negative-energy spectrum, but in Dirac hole theory the energy of the negative energy 'sea' is eliminated, on the grounds that it is unobservable. If we wish to investigate effects which involve negative-energy states, we must first excite an electron into a virtual orbital, generating an electron-positron pair. The prescriptions for treating such processes are well-known, but we shall treat the negative energy sea as chemically inert, and will consider the subset of interactions which involve only positive-energy spinors. This is the *no virtual pair* approximation, which, in familiar chemical terms, is analogous to the "frozen core" approximation; it is particularly effective in this context of molecular structure, because the apparent core-valence excitation energy is at least of order mc^2 a.u.

Defining the energy of the core, E_{core}, and the one-body potential, W, by

$$E_{core} = \sum_a E_a \tag{17}$$

$$\langle i|W|j\rangle = \sum_a \left[\langle ia|v_{12}|ja\rangle - \langle ai|v_{12}|ja\rangle\right] - \langle i|V|j\rangle \tag{18}$$

the second-quantized operator defining the interactions between positive-energy states with the specified partition of particle and hole labels is comprised of

$$\begin{aligned}
H_0 &= E_{core} + \sum : b_i^\dagger b_i : E_i && (19)\\
H_1^0 &= \sum_a \langle a| - V(r)|a\rangle + \frac{1}{2}\sum_{ab}\left[\langle ab|v_{12}|ab\rangle - \langle ba|v_{12}|ab\rangle\right] \\
&= \langle a|W|a\rangle && (20)\\
H_1^1 &= \sum_{ij} : b_i^\dagger b_j : \langle i|W|j\rangle && (21)\\
H_1^2 &= \frac{1}{2}\sum_{ijkl} : b_i^\dagger b_j^\dagger b_l b_k : \langle ij|v_{12}|kl\rangle. && (22)
\end{aligned}$$

The choice $W = 0$ defines the Dirac-Hartree-Fock self-consistent field potential, causing the one-body operators H_1^0 and H_1^1 to vanish. The operator H_1^2 remains, entering the theory as many-body corrections to the Dirac-Hartree-Fock single-particle eigenvalues. In this formulation, the Dirac-Hartree-Fock procedure is identical to its non-relativistic Hartree-Fock analogue, differing only in the replacement of Schrödinger two component spin-orbitals with the four-component positive energy spinors of the Dirac theory, and in the introduction, if desired, of a relativistic correction to the low-energy form of the electron-electron interaction. We initially restrict the sum over core labels to include only positive-energy spinors, consistent with the 'no-virtual pair' approximation. Additional terms which include negative-energy labels correspond to excitations out of the negative-energy sea, and may be thought of as giving rise to an effective vacuum polarization potential. Some of the terms which include the effects of virtual electron-positron pairs are discussed in §5.3.

4.5 Dirac-Hartree-Fock equations

According to our formulation of relativistic electronic structure theory within quantum electrodynamics, we construct an antisymmetric N-electron wavefunction, Ψ, by operating on the electron vacuum, $|0\rangle$, such that

$$\Psi = \frac{1}{\sqrt{N!}}\sum_P (-1)^p \hat{P}\left\{b_1^\dagger b_2^\dagger \cdots b_N^\dagger\right\}|0\rangle.$$

where P is the permutation label, $\hat{P}$ represents the permutation operator which acts on the electron labels, and p is the parity of the permutation.

For molecules, the single-particle Dirac operator for electron a constructed from the sum of the scalar potentials, $V_n(\mathbf{r}_a)$, due to each the N_{nuc} nuclei in the system, is denoted by $\hat{h}_D(\mathbf{r}_a)$, and defined by

$$\hat{h}_D(\mathbf{r}_a) = c\boldsymbol{\alpha} \cdot \mathbf{p}_a + \beta_a mc^2 + \sum_{n=1}^{N_{nuc}} V_n(\mathbf{r}_a), \tag{23}$$

A general matrix element of the electron-repulsion operator, g_{12}, is

$$(ij|g_{12}|kl) = \int\int \psi_i^\dagger(\mathbf{r}_1)\psi_j(\mathbf{r}_1)\frac{1}{|\mathbf{r}_1 - \mathbf{r}_2|}\psi_k^\dagger(\mathbf{r}_2)\psi_l(\mathbf{r}_2)\, d\mathbf{r}_1 d\mathbf{r}_2,$$

where $\psi_i^\dagger(\mathbf{r})$ is the Hermitian transpose of the four spinor, $\psi_i(\mathbf{r})$. These single-particle functions are represented as multi-centre expansions of the form

$$\begin{aligned}\psi_k(\mathbf{r}) &= \begin{bmatrix} \psi_k^L(\mathbf{r}) \\ \psi_k^S(\mathbf{r}) \end{bmatrix} \\ &= \begin{bmatrix} \sum_{\mu=1}^{N} c_{\mu k}^L M[L, \mu, \mathbf{r}] \\ \sum_{\mu=1}^{N} c_{\mu k}^S M[S, \mu, \mathbf{r}] \end{bmatrix}\end{aligned} \tag{24}$$

By convention, the two-spinor functions, $\psi_k^L(\mathbf{r})$ and $\psi_k^S(\mathbf{r})$ are called, respectively, the "large components" and "small components" of $\psi_k(\mathbf{r})$. The quantities $c_{\mu k}^T$ are the expansion coefficients of two-component basis functions, $M[T, \mu, \mathbf{r}]$, corresponding to the component labels $T = L$ and $T = S$.

In BERTHA, we employ a G-spinor expansion in Eq. (24), in which the two-component basis functions are defined by

$$M[L, \mu, \mathbf{r}_{A_\mu}] = \frac{1}{r_{A_\mu}} f_\mu^L(r_{A_\mu})\chi_{\kappa_\mu, m_\mu}(\theta_{A_\mu}, \varphi_{A_\mu}) \tag{25}$$

$$M[S, \mu, \mathbf{r}_{A_\mu}] = \frac{i}{r_{A_\mu}} f_\mu^S(r_{A_\mu})\chi_{-\kappa_\mu, m_\mu}(\theta_{A_\mu}, \varphi_{A_\mu}). \tag{26}$$

The radial basis functions are defined by

$$f_\mu^L(r_{A_\mu}) = N_\mu^L {r_{A_\mu}}^{l_\mu + 1} \exp\left(-\lambda_\mu r_{A_\mu}^2\right), \tag{27}$$

and the restricted kinetically matched small component is

$$f_\mu^S(r_{A_\mu}) = N_\mu^S[(\kappa_\mu + l_\mu + 1) - 2\lambda_\mu r_{A_\mu}^2]{r_{A_\mu}}^{l_\mu} \exp\left(-\lambda_\mu r_{A_\mu}^2\right). \tag{28}$$

where $l_\mu = j_\mu - a_\mu/2$, and $\kappa_\mu = -a_\mu(2j_\mu + 1)/2$. The two-component spin-angular functions are defined in [11]. This basis is referred to as a *restricted*, kinetically balanced basis, because the elements of the large- and small-component basis sets are generated by the one-to-one mapping

$$M[S, \mu, \mathbf{r}_{A_\mu}] \propto (\boldsymbol{\sigma} \cdot \boldsymbol{p})M[L, \mu, \mathbf{r}_{A_\mu}]$$

The expectation value of H_0 and H_1 (Eqs (15) and (16)) with respect to the orbital-based trial function Ψ leads, in the closed-shell case, to the energy functional

$$E = \sum_a (a|\hat{h}_D|a) + \frac{1}{2}\sum_a \sum_b [(aa|\hat{g}|bb) - (ab|\hat{g}|ba)]$$

which is the total electronic energy of an antisymmetrized system comprised of N "core" electrons created out of the electron vacuum. This is *precisely* the energy functional derived by Swirles [7], based on a sensible physical interpretation of the so-called Dirac-Coulomb operator

$$\hat{H}_{DC} = \sum_a \hat{h}_D(\mathbf{r}_a) + \sum_{a>b} \frac{1}{|\mathbf{r}_a - \mathbf{r}_b|}$$

and a trial N-electron wavefunction constructed from a Slater-determinant of occupied, *positive-energy* single-particle four-spinors. This physical *ansatz*, in which the non-relativistic Schrödinger operators of Hartree-Fock theory are replaced by one-electron Dirac operators in Dirac-Hartree-Fock theory, may be justified rigorously within quantum electrodynamics provided that we implement the labelling scheme summarized in Table 1, and enforce normal ordering on our second-quantized operators.

5 Implementation

In the previous sections, we have discussed the variational properties of matrix representations of the one-electron Dirac operator and the interaction between two-electrons occupying single particle configuration states, and derived a general, relativistic N-electron theory which does not suffer from continuum dissolution. For all practical purposes, this theory is identical to second-quantized non-relativistic formulations of many-body theory or configuration interaction, except that the one-electron basis of spin-orbitals is replaced by a one-electron basis of positive-energy four-spinors, and the single-particle Schrödinger equation is replaced by the single-particle Dirac equation. The validity of this theory as a legitimate approximation within quantum electrodynamics is now so well-established that it is surprising that any doubt still remains, particularly if it is remembered that the familiar Bethe-Goldstone second-quantized formulation of many-body perturbation theory [24] is derived from relativistic quantum field theory. In fact, it is nothing other than a configuration-space implementation of the Furry bound-state interaction picture of QED [19].

At the no-virtual-pair level of approximation, there is no numerical evidence that divergences in this theory occur "even when four-component spinors are used", as is suggested in [2]. It is certainly true that the use of the Breit interaction degrades the convergence of the partial wave expansion of the electron-electron interaction, but in an approach based on expansions in single-particle spinors this is hardly of any consequence because the Breit interaction always yields small corrections, compared with those arising because of the instantaneous Coulomb interaction. Beyond the no-virtual-pair approximation, divergences do occur in the evaluation of the Lamb shift, but techniques for handling these are very well-understood. In §5.3 we outline a mass renormalization scheme which we have developed that yields answers in precise agreement with covariant renormalization theory, but which eliminates all divergences without the parametric modification of the electromagnetic interaction. One is on very shaky ground bringing the theory of quantum electrodynamics into question, since it is the most precisely established of all physical theories, and its validity is established using techniques very similar to those described in this article. If one makes the claim which appears to be made in [2], that one cannot construct a valid many-body bound state wavefunction from QED perturbation theory, then one must present something stronger than a vague rumour to back it up; the consequences of such an assertion to high precision studies of quantum electrodynamics and electroweak theory are *very* serious [25]. In §5.2, we discuss a few examples of high-precision calculations of few-electron systems which refute the claim.

5.1 Relativistic corrections to non-relativistic quantum chemistry

One seemingly sensible approach to the relativistic electronic structure theory is to employ perturbation theory. This has the apparent advantage of representing supposedly small relativistic effects as corrections to a familiar non-relativistic problem. In Appendix 4 of *Methods of molecular quantum mechanics*, we find the terms which arise in the reduction of the Dirac-Coulomb-Breit operator to Breit-Pauli form by use of the Foldy-Wouthuysen transformation, broken into electronic, nuclear, and electron-nuclear effects. From a purely aesthetic point of view, this approach immediately looks rather unattractive because of the proliferation of terms at the first order of perturbation theory. To make matters worse, many of the terms listed are singular, and it is presumably the variational divergences introduced by these operators which are referred to in [2]. Worse still, higher-order terms in the Foldy-Wouthuysen transformation used in this way yield a mathematically invalid expansion.

Kutzelnigg [26, 27] has developed a *direct* perturbation theory based on a change in the metric of the four-component spinor space in which some classes of regular relativistic corrections to the non-relativistic limit are obtained to all orders in α and $Z\alpha$. In much the same spirit, Dyall [28] has succeeded in achieving an exact separation of the spin-dependent and spin-independent terms in the Dirac-Coulomb-Breit hamiltonian, except that there is no elimination of the small component. In Dyall's approach, the spin-free equation may be solved as two coupled two-component equations, the solutions of which may be used as a basis for including spin-orbit coupling either perturbatively or variationally.

The reduction of the relativistic many-electron hamiltonian by expansion in powers of the external field is the second-order Douglas-Kroll transformation [29], and has been used with success by Hess and co-workers [30]. The operators which result from this transformation are non-singular, but the integrals over the resulting operators are complicated and have to be approximated, even for finite basis set expansions. The reduction of the Dirac-Coulomb-Breit equation to two-component form using direct perturbation theory has been described by Kutzelnigg and coworkers [26, 27, 31], Rutkowski [32], and van Lenthe *et al.* [33].

Given that the theory from which these perturbative approaches are derived all start with the Dirac-Coulomb-Breit hamiltonian, it is worth pausing to ask if they have any advantage compared a direct assault on the problem. As Kutzelnigg demonstrates, relating components by the kinetic balance prescription eliminates divergences in the perturbative expansion, but one does not then obtain a strict upper bound on the eigenvalues. A strict upper bound on the energy may be obtained if terms proportional to $\ln r$ are introduced into the basis, but convergent behaviour is obtained only if both second-order two-spinor approximations are regularized. The problems related to the perturbative expansion of the wavefunctions in the presence of strong external fields are not ameliorated by the use of a finite nucleus instead of a point nuclear model. Moreover, one may calculate the relativistic correction to explicitly correlated wavefunctions only in first order of perturbation theory because of the presence of a singularity. Ottschofski and Kutzelnigg [31] claim that this is a "virulent" singularity which is "concealed but not absent" in calculations of the type that we describe in §5.2, though no published evidence is offered to support the assertion. The problem is that the mathematical validity of the methods of expansion used in these approaches has not been established, and the dodges devised to hide this unpalatable fact merely succeed in complicating the issue.

Apart from a reduction in the number of basis functions required to generate the wavefunction, the use of an operator partitioned by order of perturbation theory has the clear advantage that one may apply the variation principle to an explicitly correlated trial function without having to worry about the consequences of continuum dissolution. The disadvantage of that approach is that even at the Dirac-Coulomb level of approximation, one must evaluate matrix elements of operators which are more complicated than g_{ij}. Nevertheless, Cencek and Kutzelnigg [27] have calculated accurate energy eigenvalues for He, H_2^+, and H_2 values which are correct to $O(Z\alpha)^2$.

5.2 Relativistic many-body perturbation theory

The alternative approach, which we have adopted, utilizes is a direct expansion of the many-electron state function in a single-particle basis of four-component Dirac spinors. One solves matrix Dirac-Hartree-Fock equations in a G-spinor basis to self-consistency. This defines a finite set of second-quantization operators, a time-independent potential, and a model space consisting of occupied *positive-energy* spinors. Many-body corrections to the mean-field potential, the molecular energies, and the state vector are incorporated by perturbation theory. If one restricts attention to the positive-energy spinors and to the no-virtual-pair approximation, no divergences are encountered, and at the Dirac-Coulomb-Breit level of approximation, all electron-electron interaction integrals which are encountered can be calculated using standard techniques borrowed from non-relativistic quantum chemistry. We have devised computational algorithms to evaluate these integrals in a kinetically balanced G-spinor basis using methods based on the McMurchie-Davidson algorithm [34], and have been able to reduce the amount of computational work involved in performing these calculations by treating the two-spinor basis functions as the primary computational entities.

It proves to be a straightforward matter to implement conventional integral screening and convergence acceleration algorithms, and a generalization of the $O(N)$ multipole expansion method for small component interactions which greatly reduces the computational workload. Spinor matrix elements are constructed by successive contractions of the spinor amplitudes on the two-spinor basis, and used to evaluate many-body corrections by a sum-over-spinors extension of conventional many-body theory. Like the relativistic self-consistent field procedure, this many-body method has been implemented using a direct approach, in which integrals are evaluated in batches as they are required, and then discarded. Our recent calculations of electronic parameters which violate parity- and time-reversal symmetry in the molecule YbF $^2\Sigma$, and which are the subject of current experimental interest [35], will appear elsewhere [36].

The type of "concealed" singularity described by Ottschofski and Kutzelnigg [31] must be *very* well-concealed indeed, because it has never made its presence felt in the type of QED-based many-body theory that we describe, even in high-precision relativistic coupled-cluster calculations of the helium-like ground-state energy, which is a formally exact representation of a two-electron system within the no-virtual pair approximation. In the calculations of Plante *el al.* [37], for example, all-order calculations of all helium-like ions with nuclear charges in the range $1 \leq Z \leq 100$ have been performed without difficulty. There is no suggestion that the partial-wave contributions to the correlation energy do not form a convergent series, or that the iterative coupled cluster procedure is divergent. We have already performed relativistic many-body calculations for atoms using finite basis sets, including the Breit interaction in the definition of the self-consistent field potential [38]. There have been subsequent developments along these lines, including the coupled-cluster calculations described by Kaldor at this meeting, and the recent many-body molecular calculations of Visscher *et al.* [39].

Once one has solved the technical problem of evaluating integrals over G-spinors, the operation of our program follows closely that of most non-relativistic quantum chemical codes. Spin symmetry is replaced in our approach by the time-reversal symmetry which is the basis of Kramers' theorem [40]. Point group theory conforms, therefore to the theory of double-groups, and we have already made a preliminary study of this, based on the computational implementation of Meyer *et al.* [41], which conforms to the spinor conventions which we have adopted. All of the technical features specific to the use of relativistic spinor functions is absorbed into the definition of intermediate quantities involved in the McMurchie-Davidson algorithm [34]. A careful definition of these quantities allows us to write down compact expressions for all quantities of interest which are the precise analogues of the non-relativistic formulae presented by Saunders [42] and Helgaker and Taylor [43]. Details of our computational algorithms will appear elsewhere [44].

5.3 Virtual electron-positron pairs

Cautious readers may feel uneasy about the apparently surreptitious disappearance of the negative-energy states from this theory. The anti-commutation relations between the creation and annihilation operators of electrons and positrons are sufficient to derive how the the negative-energy states enter in electron correlation problems. Labzowsky [15] and Sapirstein [16] have derived the second-order energy correction to bound-state energy levels, E_2, from QED perturbation theory, bringing into play the creation and annihilation operators for positrons in Eq. (12). In the notation of Table 1, the result is

$$E_2 = \frac{1}{4}\sum_{ab}\left\{\sum_{rs}^{++}\frac{\langle ab||rs\rangle\langle rs||ab\rangle}{\varepsilon_a+\varepsilon_b-\varepsilon_r-\varepsilon_s} - \sum_{cd}^{--}\frac{\langle ab||cd\rangle\langle cd||ab\rangle}{\varepsilon_a+\varepsilon_b-\varepsilon_c-\varepsilon_d}\right\}$$

where $\langle ab||rs\rangle = \langle ab|v_{12}|rs\rangle - \langle ab|v_{12}|sr\rangle$. The first term is simply the usual second-order correlation energy correction, while the second term corresponds to a correlation correction to the pair $\{a, b\}$ due to virtual excitations out of the negative-energy 'sea'. Calculations of this term which use $v_{12} = 1/r_{12}$ [23] reveal that it is a correction of $O[(Z\alpha)^4]$, and that it is readily calculated using finite basis set methods. We may not use b_{12} to calculate the second term, because the assumption of small single-particle energy differences inherent in the Breit operator is violated. For this, we must use v_{12}^T, as discussed by Bethe and Salpeter [20].

The lowest-order radiative correction gives rise to the Lamb shift, in which the negative-energy states play a crucial role. This consists of two energy correction terms. The first is the vacuum polarization, E_P, which for electron a has the form

$$E_P = \frac{1}{2}\sum_i \mp\langle ai|g_{12}|ai\rangle$$

where the upper sign is taken for positive-energy ψ_i, and the lower for negative-energy ψ_i. This is just a classical electrostatic interaction in which the bound-state density interacts with an effective potential V_P, given by

$$V_P(x) = \frac{1}{2}\sum_i \mp \int \frac{\psi_i^\dagger(y)\psi_i(y)}{|x-y|}d^3y,$$

corresponding to the potential induced in the vacuum by the external electrostatic field. This potential was first derived by Uehling [45], and is readily calculated using standard numerical methods.

The second energy correction, known as the electron self-energy, corresponds to the self-interaction of an electron with the electromagnetic field. Here we encounter the first true divergence, which is removed by renormalization of the free-electron mass. The renormalized electron self energy for electron a, E_S, is

$$\begin{aligned} E_S \;=\; & \frac{\alpha}{\pi}mc^2\int_0^\infty dk \sum_i \frac{\langle ai|v_{12}^F|ia\rangle}{\varepsilon_i-\varepsilon_a\pm ck} \\ & -\frac{\alpha}{\pi}mc^2\int_0^\infty dk \sum_{p_1p_2p_3}\frac{\langle a|p_1\rangle\langle p_1p_2|v_{12}^F|p_2p_3\rangle\langle p_3|a\rangle}{\varepsilon_{p_2}^0-\varepsilon_{p_3}^0\pm ck}\end{aligned}$$

in which p_1, p_2 and p_3 are labels for the free-particle states whose energies are given by $E_i^2 = c^2p_i^2 + m^2c^4$. The first term represents the interaction of the bound state with the electromagnetic field, in which external-field states are the intermediate states, and the second term represents the electrodynamic mass of of the free-electron wavepacket ψ_a. For convenience, we use the Feynman gauge representation of the electron-electron interaction

$$v_{12}^F(k) = (1 - \boldsymbol{\alpha}_1 \cdot \boldsymbol{\alpha}_2)\frac{\sin kr_{12}}{r_{12}}$$

We have shown [46] that if a multipole expansion of the interaction v_{12}^F is adopted and the mass renormalization procedure carried out at the partial wave level, a convergent representation is obtained for E_S which is in precise agreement with the parametric methods which were introduced by Feynman [47] and implemented in the numerical calculations of Mohr [48]. For both the self energy and vacuum polarization, the positive- and negative-energy states are equally important in the calculation of the physical effect, with respect to both the numerical value of the energy shift and the finiteness of the theory.

Sceptical readers may suspect that the negative-energy states play an important role only in the calculation of small QED corrections, and that they are, therefore, of no consequence to quantum chemistry. In fact, we show in §6.2 that they play an important part in the calculation of magnetic interactions, and their existence may be turned to a computational and theoretical advantage.

5.4 Matrix elements of charge and current operators

The success and applicability of the approach presented in this article depends on whether it can be implemented in practical algorithms. In order to facilitate the evaluation of integrals involving single-particle charge and current spinor densities, we introduce a tensor-valued generalization of the McMurchie-Davidson algorithm [34]. The relativistic one-electron charge-current density may be reduced in a G-spinor basis to elements of the form

$$M^\dagger[T,\mu,\boldsymbol{r}]\sigma_q M[T',\nu,\boldsymbol{r}] = \sum_{\alpha\beta\gamma} E_q[T,\mu;T',\nu;\alpha,\beta,\gamma]H[\lambda_{\mu\nu},\boldsymbol{P}_{\mu\nu};\alpha,\beta,\gamma] \quad (29)$$

where we define σ_0 to be the 2×2 identity matrix, $T' = T$ if $q = 0$, $T' = \bar{T}$ if $q = \{x, y, z\}$, and $\bar{T} \neq T$. The quantities labelled $E_q[T,\mu;T',\nu;\alpha,\beta,\gamma]$ are expansion coefficients of the Hermite Gaussian-type functions (HGTF) defined by

$$H[\lambda_{\mu\nu}, \boldsymbol{P}_{\mu\nu}; \alpha, \beta, \gamma] = \left(\frac{\partial}{\partial P_{\mu\nu,x}}\right)^{\alpha} \left(\frac{\partial}{\partial P_{\mu\nu,y}}\right)^{\beta} \left(\frac{\partial}{\partial P_{\mu\nu,z}}\right)^{\gamma} \exp\left(-\lambda_{\mu\nu} r^2_{P_{\mu\nu}}\right)$$

where $\lambda_{\mu\nu} = \lambda_\mu + \lambda_\nu$ and $\boldsymbol{P}_{\mu\nu} = (\lambda_\mu \boldsymbol{P}_\mu + \lambda_\nu \boldsymbol{P}_\nu)/\lambda_{\mu\nu}$, and $\boldsymbol{r}_{P_{\mu\nu}} = \boldsymbol{r} - \boldsymbol{P}_{\mu\nu}$.

We evaluate the E_q-coefficients in our computer program, BERTHA, by performing a Cartesian tensor contraction on the components of a *general* 2×2 hermitian tensor operator using the scalar quantities defined by Eq. (54) of [42], which allows us to evaluate all tensor components using a single computer code. Consequently, one may also transform between Cartesian and spherical tensor formulations, simply by modifying the entries in the set of 2×2 hermitian matrices which are used to construct the E_q-coefficients, and redefining the tensor indices and the summation convention. The transformation of the scalar quantities into the tensor basis involves a negligible fraction of the total processor time in any practical application of our formulation.

The definition of the E_q-coefficients greatly simplifies the evaluation of the one- and two-electron matrix elements of H_{DCB} and H_I in the two-spinor basis, $M[T, \mu; \boldsymbol{r}]$. It is convenient to define

$$\begin{aligned} N^{TT'}_{\mu\nu} &= N^T_\mu N^{T'}_\nu \\ K_{\mu\nu} &= \exp\left(-\frac{\lambda_\mu \lambda_\nu}{\lambda_{\mu\nu}} (\boldsymbol{P}_\mu - \boldsymbol{P}_\nu)^2\right) \end{aligned}$$

$$[p, \boldsymbol{P}; \alpha, \beta, \gamma | q, \boldsymbol{Q}; \alpha', \beta', \gamma'] = \iint H(p, \mathbf{r}_{P,1}; \tau, \mu, \nu) \frac{1}{r_{12}} H(q, \mathbf{r}_{Q,2}; \tau', \mu', \nu') d^3 r_1 d^3 r_2$$

Using the definitions of the E_q-coefficients in Eq. (29), and methods described in [42, 43] to evaluate spatial integrals over a HGTF basis, we may derive the following results which prove useful in our formulation of relativistic molecular quantum electrodynamics.

Charge-current operator

The spinor product $\psi_k^\dagger \psi_k$ represents the charge density associated with the four-spinor ψ_k, while $c\psi_k^\dagger \alpha_q \psi_k$ represents the q-component of the current. The matrix elements of these operators may be reduced to elementary G-spinor integrals of the form

$$\begin{aligned}(\mu;T|\sigma_q|\nu;T') &= \int M^\dagger[T,\mu,\mathbf{r}]\sigma_q M[T',\nu,\mathbf{r}]d\mathbf{r} \\ &= N^{TT'}_{\mu\nu}K_{\mu\nu}\left(\frac{\pi}{\lambda_{\mu\nu}}\right)^{3/2} E_q[\mu,T;\nu,T';0,0,0]\end{aligned}$$

Moment integrals

The generalized spin-dependent moment integrals occur in the evaluation of matrix elements of H_I, and are defined by

$$\begin{aligned}(\mu,T|\sigma_q x_C|\nu,T') &= \int M^\dagger[T,\mu,\boldsymbol{r}]\sigma_q x_C M[T',\nu,\boldsymbol{r}]d^3r \\ &= N^{TT'}_{\mu\nu}K_{\mu\nu}\left(\frac{\pi}{\lambda_{\mu\nu}}\right)^{3/2} (E_q[\mu,T;\nu,T';1,0,0] \\ &\quad +PC_x E_q[\mu,T;\nu,T';0,0,0])\end{aligned}$$

where $\boldsymbol{r}_C = \boldsymbol{r} - \boldsymbol{P}_C$, and x_C, y_C, and z_C are the components of $\boldsymbol{r}_C$. Expressions for the integrals over $\sigma_q y_C$ and $\sigma_q z_C$ are obtained by permuting indices. Scalar matrix elements of the position operator involve the $q = 0$ component. In the relativistic theory of nuclear magnetic resonance chemical shifts, we also require matrix elements of the tensor operator $\boldsymbol{\alpha} \times \boldsymbol{r}$, which are obtained using the Cartesian tensor summation

$$\begin{aligned}&\langle\psi_m|\boldsymbol{\alpha}\times\boldsymbol{r}_C|\psi_n\rangle = \\ &\qquad \hat{\boldsymbol{e}}_p\epsilon^{pqq'}\sum_{\mu,\nu}\left\{c^{*L}_{\mu m}c^{S}_{\nu n}(\mu,L|\sigma_q r_{q'_C}|\nu,S) - c^{*S}_{\mu m}c^{L}_{\nu n}(\mu,S|\sigma_q r_{q'_C}|\nu,L)\right\}\end{aligned} \tag{30}$$

where $\epsilon^{pqq'}$ is the antisymmetric tensor and $\hat{\boldsymbol{e}}_p$ is a unit vector in the direction $p = \{x,y,z\}$. Higher-order generalized moments are obtained using Eq. (42) of [42].

Coulomb operator

Electron repulsion integrals may be evaluated by a straightforward generalization of the McMurchie-Davidson algorithm [34], using the definition of the two-spinor charge operator. The Coulomb interaction involves only the E_q-coefficients for $q = 0$, and results in G-spinor integrals of the form

$$\begin{aligned}&(\mu,T;\nu,\bar{T}|g_{12}|\sigma,T';\tau,\bar{T}') = \\ &\qquad \iint M^\dagger[T,\mu,\mathbf{r}_1]M[\bar{T},\nu,\mathbf{r}_1]g_{12}M^\dagger[T',\sigma,\mathbf{r}_2]M[\bar{T}',\tau,\mathbf{r}_2]d\mathbf{r}_2 d\mathbf{r}_2 \\ &= K_{\mu\nu}K_{\sigma\tau}\sum_{\alpha\beta\gamma}\sum_{\alpha'\beta'\gamma'} E_0[\mu,T;\nu,\bar{T};\alpha,\beta,\gamma] \\ &\qquad \times E_0[\sigma,T';\tau,\bar{T}';\alpha',\beta',\gamma'][\lambda_{\mu\nu},\boldsymbol{P}_{\mu\nu};\alpha,\beta,\gamma|\lambda_{\sigma\tau},\boldsymbol{P}_{\sigma\tau};\alpha',\beta',\gamma']\end{aligned}$$

Breit operator

It is here that the simplifications made possible by defining the E_q-coefficients is most apparent, since integrals over b_{12} may be be obtained by a simple extension of the McMurchie-Davidson algorithm for electron repulsion integrals. This approach conveys the advantages of simplicity, generality and efficiency when compared with those which exist in the literature [49, 50].

$$\begin{aligned}
&(\mu, T; \nu, \bar{T}|b_{12}|\sigma, T'; \tau, \bar{T}') = \\
&\qquad \iint M^{\dagger}[T, \mu, \mathbf{r}_1] M[\bar{T}, \nu, \mathbf{r}_1] b_{12} M^{\dagger}[T', \sigma, \mathbf{r}_2] M[\bar{T}', \tau, \mathbf{r}_2] d\mathbf{r}_2 d\mathbf{r}_2 \\
&= \quad -\frac{1}{2} K_{\mu\nu} K_{\sigma\tau} \sum_{q} \sum_{\alpha\beta\gamma} \sum_{\alpha'\beta'\gamma'} E_q[\mu, T; \nu, \bar{T}; \alpha, \beta, \gamma] \\
&\qquad \Big\{ E_q[\sigma, T'; \tau, \bar{T}'; \alpha', \beta', \gamma'][\lambda_{\mu\nu}, \boldsymbol{P}_{\mu\nu}; \alpha, \beta, \gamma | \lambda_{\sigma\tau}, \boldsymbol{P}_{\sigma\tau}; \alpha', \beta', \gamma'] \\
&\qquad + \sum_{q'} E_{q'}[\sigma, T'; \tau, \bar{T}'; \alpha', \beta', \gamma'][\lambda_{\mu\nu}, \boldsymbol{P}_{\mu\nu}; \alpha, \beta, \gamma | B^{qq'} | \lambda_{\sigma\tau}, \boldsymbol{P}_{\sigma\tau}; \alpha', \beta', \gamma'] \Big\}
\end{aligned}$$

where

$$\begin{aligned}
&[p, \boldsymbol{P}; \alpha, \beta, \gamma | B^{xy} | q, \boldsymbol{Q}; \alpha', \beta', \gamma'] = \\
&\quad (-1)^{\alpha'+\beta'+\gamma'+1} \left\{ \left(\frac{p+q}{2pq} \right) [p, \boldsymbol{P}; \alpha+\alpha'+1, \beta+\beta'+1, \gamma+\gamma' | q, \boldsymbol{Q}; 0, 0, 0] \right. \\
&\quad + PQ_y [p, \boldsymbol{P}; \alpha+\alpha'+1, \beta+\beta', \gamma+\gamma' | q, \boldsymbol{Q}; 0, 0, 0] \\
&\quad \left. + \, (\beta+\beta')[p, \boldsymbol{P}; \alpha+\alpha'+1, \beta+\beta'-1, \gamma+\gamma' | q, \boldsymbol{Q}; 0, 0, 0] \right\}
\end{aligned}$$

$$\begin{aligned}
&[p, \boldsymbol{P}; \alpha, \beta, \gamma | B^{xx} | q, \boldsymbol{Q}; \alpha', \beta', \gamma'] = \\
&\quad (-1)^{\alpha'+\beta'+\gamma'+1} \left\{ \left(\frac{p+q}{2pq} \right) [p, \boldsymbol{P}; \alpha+\alpha'+2, \beta+\beta', \gamma+\gamma' | q, \boldsymbol{Q}; 0, 0, 0] \right. \\
&\quad + PQ_x [p, \boldsymbol{P}; \alpha+\alpha'+1, \beta+\beta', \gamma+\gamma' | q, \boldsymbol{Q}; 0, 0, 0] \\
&\quad \left. + \, (\alpha+\alpha')[p, \boldsymbol{P}; \alpha+\alpha', \beta+\beta', \gamma+\gamma' | q, \boldsymbol{Q}; 0, 0, 0] \right\}
\end{aligned}$$

The complete set of tensor components $B^{qq'}$ is obtained by permuting the Cartesian indices. The integrals $[p, \boldsymbol{P}; \alpha, \beta, \gamma | q, \boldsymbol{Q}; 0, 0, 0]$ may be calculated efficiently using algorithms described in [42, 43].

6 Applications

We now abandon conventional quantum chemical wisdom, and embrace the relativistic theory of electromagetic interactions wholeheartedly. In a single-particle theory, the interaction between an electron and a vector potential, $\boldsymbol{A}(\boldsymbol{r})$, is included in the Dirac hamiltonian by modifying the canonical momentum, so that

$$\left\{c\boldsymbol{\alpha}\cdot(\boldsymbol{p}+e\boldsymbol{A}(\boldsymbol{r}))+\beta mc^2+V(\boldsymbol{r})\right\}\psi_k(\boldsymbol{r})=E_k\ \psi_k(\boldsymbol{r}) \tag{31}$$

subject to appropriate boundary conditions. This is the relativistically invariant separation of the interaction of the four-potential, A_μ, into its scalar part, $A_0 = V(\boldsymbol{r})/c$, and its vector potential part, $\boldsymbol{A}(\boldsymbol{r})$. We may separate the Dirac operator into the scalar part defined by Eq (9), and an interaction hamiltonian, H_I, of the form

$$H_I = c\boldsymbol{\alpha}\cdot\boldsymbol{A}(\boldsymbol{r}) \tag{32}$$

It is immediately apparent that the linearity of the Dirac equation with respect to $\boldsymbol{p}$ imparts a linearity of H_I with respect to $\boldsymbol{A}(\boldsymbol{r})$. To quantum chemists this result may seem perplexing. The minimal coupling substitution $\boldsymbol{p}\to\boldsymbol{p}+e\boldsymbol{A}(\boldsymbol{r})$ is common to both the relativistic theory and the more familiar non-relativistic theory. Consequently, the gauge transformation of potentials and amplitudes according to

$$\begin{aligned}\boldsymbol{A}(\boldsymbol{r}) &\to \boldsymbol{A}(\boldsymbol{r})+\nabla f(\boldsymbol{r})\\ \psi(\boldsymbol{r}) &\to \exp(-if(\boldsymbol{r}))\psi(\boldsymbol{r})\end{aligned}$$

for an arbitrary function $f(\boldsymbol{r})$, preserves the fields and leaves all interactions invariant, provided that the original assumption that $V(\boldsymbol{r})$ is independent of time continues to be satisfied. The non-relativistic theory contains a term proportional to A^2, whose validity is well-established but which is not, apparently, a part of the relativistic theory. We shall see in §6.2 that such terms occur in second-order of relativistic many-body perturbation theory, and that they arise because of interactions involving the negative-energy states.

6.1 Zeeman effect

In order to demonstrate how the E_q-coefficients are used, we consider the simple example of interaction of a relativistic one-electron atom with an external magnetic field, $\boldsymbol{B}$. For a weak external field, the first-order interaction energy, E_Z, of an electron in the one-electron state ψ_0 with the magnetic field is given by

$$E_Z = \left\langle \psi_0 | \frac{c}{2} \boldsymbol{\alpha} \cdot (\boldsymbol{B} \times \boldsymbol{r}) | \psi_0 \right\rangle \tag{33}$$

which is the relativistic expression for the anomalous Zeeman shift in the energy of the state ψ_0. While this expression is linear in $\boldsymbol{B}$, it bears only a superficial resemblance to the non-relativistic result, E_Z^{nr}, which is

$$E_Z^{nr} = \left\langle \psi_0^{nr} | -\frac{1}{2} \boldsymbol{B} \cdot (\boldsymbol{L} + 2\boldsymbol{S}) | \psi_0^{nr} \right\rangle$$

in which ψ_0^{nr} is a Breit-Pauli two-spinor. If we make the naive substitutions $c\boldsymbol{\alpha} \to \boldsymbol{v}$, $\boldsymbol{p} = m\boldsymbol{v}$, and $\boldsymbol{l} = \boldsymbol{r} \times \boldsymbol{p}$ in Eq (33), we obtain the spin-independent effective operator $-\frac{1}{2}\boldsymbol{B} \cdot \boldsymbol{L}$. We shall now see that the correct spin-coupling is automatically taken care of by using Dirac four-spinors.

A computational expression for E_Z may be obtained by a simple modification of Eq (30), yielding

$$\begin{aligned}
&\left\langle \psi_0 | \frac{c}{2} \boldsymbol{\alpha} \cdot (\boldsymbol{B} \times \boldsymbol{r}) | \psi_0 \right\rangle \\
&\quad = \left\langle \psi_0 | -\frac{c}{2} \boldsymbol{B} \cdot (\boldsymbol{\alpha} \times \boldsymbol{r}) | \psi_0 \right\rangle \\
&\quad = \langle \psi_0 | -\boldsymbol{B} \cdot \boldsymbol{m} \; | \psi_0 \rangle \\
&\quad = \frac{c}{2} B_p \epsilon^{pqq'} \sum_{\mu,\nu} \left\{ c_{\mu 0}^{*L} c_{\nu 0}^{S} (\mu, L | \sigma_q r_{q'_C} | \nu, S) - c_{\mu 0}^{*S} c_{\nu 0}^{L} (\mu, S | \sigma_q r_{q'_C} | \nu, L) \right\} \qquad (34)
\end{aligned}$$

where $\boldsymbol{m}$ is the effective magnetic moment operator. The tensor sum over p in Eq (34) reduces to a single term in the case of a homogeneous field in which $\boldsymbol{B} = B_z \hat{\boldsymbol{k}}$.

In Table 2 we present the expectation values of the operator $\mu_z = \frac{c}{2}(\boldsymbol{\alpha} \times \boldsymbol{r})_z$, which determines the interaction strength of a state ψ_0 with a homogeneous magnetic field of magnitude B_z. Here, each one-electron four-spinor, ψ_0, is determined for the Dirac-Hartree-Fock ground-state of the neon atom using BERTHA.

The relativistically corrected anomalous Zeeman effect for one-electron atoms has been presented by Bethe and Salpeter [20], and is given by

$$\begin{aligned}
m_z &= \left| \left\langle \psi_0 | \frac{c}{2} (\boldsymbol{\alpha} \times \boldsymbol{r})_z | \psi_0 \right\rangle \right| \\
&= \frac{j + 1/2}{\ell + 1/2} \left[1 - \frac{2\kappa}{\kappa - 1/2} \int_0^\infty Q^2(r) dr \right] \qquad (35) \\
&= g_{j\ell} - \Delta_{j\kappa}
\end{aligned}$$

Table 2: Calculations of $m_z = |\langle c(\boldsymbol{\alpha} \times \boldsymbol{r})_z/2\rangle|$ for H-like neon, using Eq. (34) and four-spinors generated by BERTHA, are compared with the analytic values of $g_{j\ell}$, $\Delta_{j\kappa}$ and m_z obtained from Eq. (35)

$n\ell_j$	$g_{j\ell}$	$\Delta_{j\kappa}$	m_z (Eq. (34))	m_z (Eq. (35))
$1s_{1/2}$	2.000000000	3.55468(-3)	1.996445300	1.996445319
$2s_{1/2}$	2.000000000	8.88899(-4)	1.999111009	1.999111010
$2p_{1/2}$	0.666666667	8.88895(-4)	0.665777668	0.665777772
$2p_{3/2}$	1.333333333	7.10250(-4)	1.332623083	1.332623083

The first term is the non-relativistic result derived from Breit-Pauli theory, and is the Landé g-factor, $g_{j\ell}$, while the second is the first-order relativistic correction, $\Delta_{j\kappa}$, which is proportional to the small-component electron density. We compare, in Table 2, the values which we have calculated directly from Eq. (34) with those derived from Eq. (35). The excellent agreement between these results gives us confidence in our finite basis set representations of Dirac spinors, in the interaction hamiltonian formalism, and in the formulation of the E_q-coefficients in Eq. (29).

6.2 NMR shielding tensors in small molecules

In order to demonstrate how a term proportional to A^2 arises in the relativistic theory, and to demonstrate how simple the relativistic theory really is, we will consider a textbook example: the nuclear magnetic shielding tensor. In this case, we have

$$H_I = c\boldsymbol{\alpha}\cdot\left\{\frac{1}{2}\boldsymbol{B} \times \boldsymbol{r} + \frac{1}{c^2}\frac{\boldsymbol{\mu} \times \boldsymbol{r}_n}{r_n^3}\right\} \tag{36}$$

where the first term corresponds to the interaction with the external magnetic field, and the second is the nuclear hyperfine interaction with a nuclear magnetic moment, $\boldsymbol{\mu}$. Since the components of $\boldsymbol{\alpha}$ are constant 4×4 matrix operators we may permute cyclically the operators containing $\boldsymbol{\alpha}$ to obtain the equivalent interaction operator

$$H_I = -\frac{c}{2}\boldsymbol{B} \cdot (\boldsymbol{\alpha} \times \boldsymbol{r}) - \frac{1}{c}\frac{\boldsymbol{\mu}\cdot(\boldsymbol{\alpha} \times \boldsymbol{r}_n)}{r_n^3} \tag{37}$$

The calculation of the first-order effects are straightforward. The matrix element

$$\left\langle \psi_0 \middle| -\frac{c}{2}\boldsymbol{B}\cdot(\boldsymbol{\alpha}\times\boldsymbol{r}) \middle| \psi_0 \right\rangle$$

is the first-order Zeeman shift in the four-component single-particle state, ψ_0, which we have already studied. The first-order nuclear hyperfine interaction energy of that state is

$$\left\langle \psi_0 \middle| -\frac{1}{c}\frac{\boldsymbol{\mu}\cdot(\boldsymbol{\alpha}\times\boldsymbol{r}_n)}{r_n^3} \middle| \psi_0 \right\rangle$$

where $\boldsymbol{r}_n = \boldsymbol{r} - \boldsymbol{R}_N$, and $\boldsymbol{R}_N$ is the position of the nucleus in whose hyperfine interaction we are interested.

The second-order effects comprise three contributions. The second-order Zeeman and hyperfine interactions involve obvious extensions of second-order Rayleigh-Schrödinger perturbation theory using the appropriate operators. If we introduce an arbitrary gauge origin $\boldsymbol{R}_G$, and the variable $\boldsymbol{r}_G = \boldsymbol{r} - \boldsymbol{R}_G$, the second-order term involving both Zeeman and hyperfine operators is

$$\begin{aligned} E_2 &= \sum_{qq'} B_q\mu_{q'} \sum_{ak} \left\{ \frac{\langle\psi_a|(\boldsymbol{\alpha}\times\boldsymbol{r}_G)_q|\psi_k\rangle\langle\psi_k|(\boldsymbol{\alpha}\times\boldsymbol{r}_n/r_n^3)_{q'}|\psi_a\rangle}{E_a - E_k} \right. \\ &\quad \left. + \frac{\langle\psi_a|(\boldsymbol{\alpha}\times\boldsymbol{r}_n/r_n^3)_q|\psi_k\rangle\langle\psi_k|(\boldsymbol{\alpha}\times\boldsymbol{r}_G)_{q'}|\psi_a\rangle}{E_a - E_k} \right\} \\ &= \sum_{qq'} B_q\mu_{q'}\sigma^2_{qq'} \end{aligned} \tag{38}$$

where the sums over q and q' include the Cartesian components $\{x, y, z\}$, the quantity $\sigma_{qq'}$ is known as the shielding tensor, and the sum over k includes the *complete* set of states, *including those of negative energy*, but excluding the occupied positive-energy states. We expect that if we restrict the sum over k to include only unoccupied positive-energy states, we should obtain the paramagnetic shielding tensor components, with small relativistic corrections, because the non-relativistic paramagnetic shielding tensors may be deduced from Eq. (38) by the substitution $c\boldsymbol{\alpha} \rightarrow \boldsymbol{v}$. If we now consider the sum over the negative-energy states, each operator factor of $\boldsymbol{\alpha}$ increases the magnitude of the matrix element in which it appears by a factor c if ψ_k is a negative-energy state, because the relative magnitudes of the large and small components are reversed. The energy denominator is now of order $2mc^2$, and consequently the sum over the negative energy states appears on an equal footing, and with approximately equal weight, in the evaluation of E_2. This term corresponds to the diamagnetic shielding of non-relativistic theory, but is readily incorporated in our scheme simply by summing over all states, without prejudice.

Approximate forms of this theory, in which the negative-energy contributions are estimated using closure relations, have already been given by Pyykkö [51] and Pyper [52]. One may readily construct a relativistic theory for all of the electric and magnetic properties described in, for example, McWeeny [4], by extending this linear interaction hamiltonian formalism. Here, we shall repeat earlier non-relativistic calculations of the NMR shielding constants in small molecules, in order to demonstrate how this familiar quantity is obtained using Dirac four-spinors.

There is a cancellation of contributions from the paramagnetic and diamagnetic terms in the non-relativistic theory, and the individual contributions depend on the gauge origin which is chosen for the external magnetic field [53]. If complete sets are chosen to calculate Eq. (38) however, the complete shielding tensor is gauge independent. Of course, we never actually have a complete basis set, and gauge dependencies from this basis set truncation can be reduced by the use of gauge-dependent spinor basis functions of the form

$$\exp\left(-\frac{i}{2}\boldsymbol{B}\cdot(\boldsymbol{R}_{GP_\mu}\times\boldsymbol{r})\right)M[T,\mu,\boldsymbol{r}] \tag{39}$$

where $\boldsymbol{R}_{GP_\mu} = \boldsymbol{R}_G - \boldsymbol{R}_{P_\mu}$, and $T = L$ or $T = S$, which eliminates all reference to the gauge origin in one-electron matrix elements. For consistency with our usual nomenclature, we shall call the basis functions defined by Eq. (39) B-spinors, which are intended as a two-component generalization of so-called London orbitals [53]. In order to make a direct comparison with non-relativistic methods, we select the simplest realistic model, in which the intermediate states $\{\psi_k\}$ are generated in a DHF potential using a large basis set. The components of the shielding tensor can be defined by

$$\sigma_{qq'} = \left.\frac{\partial^2 E(\boldsymbol{B},\boldsymbol{\mu})}{\partial B_q \partial \mu_{q'}}\right|_{\boldsymbol{B}=0,\boldsymbol{\mu}=0}$$

where $E(\boldsymbol{B},\boldsymbol{\mu})$ is the total energy of the system including the effect of the external magnetic field and the nuclear hyperfine interaction. In a B-spinor basis, the complete calculation of the shielding tensors involves calculating the first- and second-order terms

$$\sigma_{qq'} = \sigma^1_{qq'} + \sigma^2_{qq'} \tag{40}$$

where

$$
\begin{aligned}
\sigma^{1}_{qq'} &= \sum_{a}\sum_{\mu\nu}\left\{c^{L*}_{\mu a}c^{S}_{\nu a}\left\langle L,\mu\left|\frac{i}{2}\left(\boldsymbol{P}_{\mu\nu}\times\boldsymbol{r}\right)_{q}\left(\frac{\boldsymbol{\sigma}\times\boldsymbol{r}_{n}}{r_{n}^{3}}\right)_{q'}\right|S,\nu\right\rangle\right. \\
&\quad \left. +c^{S*}_{\mu a}c^{L}_{\nu a}\left\langle S,\mu\left|\frac{i}{2}\left(\boldsymbol{P}_{\mu\nu}\times\boldsymbol{r}\right)_{q}\left(\frac{\boldsymbol{\sigma}\times\boldsymbol{r}_{n}}{r_{n}^{3}}\right)_{q'}\right|L,\nu\right\rangle\right\}, \\
\sigma^{2}_{qq'} &= \sum_{ak}\left\{\frac{\langle\psi_a|(\boldsymbol{\alpha}\times\boldsymbol{r}_G)_q|\psi_k\rangle\langle\psi_k|(\boldsymbol{\alpha}\times\boldsymbol{r}_n/r_n^3)_{q'}|\psi_a\rangle}{E_a-E_k}\right. \\
&\quad \left. +\frac{\langle\psi_a|(\boldsymbol{\alpha}\times\boldsymbol{r}_n/r_n^3)_q|\psi_k\rangle\langle\psi_k|(\boldsymbol{\alpha}\times\boldsymbol{r}_G)_{q'}|\psi_a\rangle}{E_a-E_k}\right\},
\end{aligned}
$$

in which $\boldsymbol{P}_{\mu\nu} = \boldsymbol{P}_{\mu} - \boldsymbol{P}_{\nu}$, and $\boldsymbol{r}_n = \boldsymbol{r} - \boldsymbol{R}_N$. The terms which constitute $\sigma^1_{qq'}$ involve atomic integrals in which the effective operator depends on the separation of the origins of the coordinate systems in which the basis sets are defined. The first-order term is obtained simply by differentiating the first-order nuclear hyperfine energy with respect to B_q and $\mu_{q'}$ in a field-dependent basis set.

In Table 3 we present a Dirac-Hartree-Fock calculation of the first- and second-order contributions to $\sigma_{qq'}$ for the ground state of the water and ammonia molecules, using a double zeta quality two-spinor basis augmented by polarization functions on all centres. We have checked that the spherically-averaged results are independent of the orientation of the molecule, and that they are, to a very good approximation, independent of the gauge origin. For water, we obtain the spherically averaged value 330.96 ppm, which is in excellent agreement with the corresponding non-relativistic value of 330.74 obtained by Gauss [54], and in good agreement with the experimental value of 344 ppm. Similarly, the spherically averaged value for ammonia is 268.9 ppm, in excellent agreement with the non-relativistic value of 265.2 ppm, and the experimental value of 264.5 ppm [54]. Unsurprisingly, in a system in which no relativistic effects are expected, none are found. It is gratifying that the agreement between the approaches is as precise as it is, and is convincing evidence that we have formulated our relativistic theory correctly. It is also worth emphasising that *almost all of our result comes from the sum over negative-energy states*: these states evidently can play an important chemical role in an *ab initio* relativistic theory, though one must look to magnetic properties to discern their influence. The contribution from the first-order gauge correction is, on the other hand very small, particularly if we compare it with the non-relativistic value obtained using London orbitals. Nevertheless, we must include the gauge correction in order to obtain good agreement between the relativistic and non-relativistic

Table 3: Components of the first- and second-order shielding tensor defined by Eq. (40) for H_2O and NH_3 (in ppm). The spherical average, σ_{av} is defined by $\sigma_{av} = (\sigma_{xx} + \sigma_{yy} + \sigma_{zz})/3$. The water molecule is aligned in the xz-plane with the oxygen nucleus located at the origin of coordinates. The ammonia molecule has its nitrogen nucleus located at the origin, and two of its hydrogen nuclei lying in the xy-plane. The second-order contribution, σ^2, is divided into the contribution from positive-energy intermediate states, σ^2_+ and from negative-energy intermediate states, σ^2_-.

H_2O	σ_{xx}	σ_{yy}	σ_{zz}	σ_{av}
σ^1	3.54	11.73	8.52	7.93
σ^2_+	-12.11	-48.01	-35.60	-31.91
σ^2_-	355.94	354.70	354.18	354.94
σ	347.37	318.41	327.10	330.96

NH_3	σ_{xx}	σ_{yy}	σ_{zz}	σ_{av}
σ^1	-1.90	-1.90	-1.88	-1.89
σ^2_+	-34.08	-34.08	-61.44	-43.20
σ^2_-	313.66	313.66	314.65	313.99
σ	277.68	277.68	251.33	268.90

treatments at the same formal level of approximation. We are currently performing calculations of shielding constants in organometallic compounds, in which the relativistic effects are much larger.

6.3 Parity violation in chiral molecules

The standard model of the electroweak interaction introduces an effective interaction between nucleons and electrons which violates parity-reversal symmetry. This P-odd interaction, H_P, is given by

$$H_P = \frac{G_F}{2\sqrt{2}} \sum_{i,n} Q_{W,n} \gamma_i^5 \varrho(\boldsymbol{r}_i)$$

where the sum over i includes occupied positive-energy spinors, the sum over n includes all nuclei, and $\varrho(\boldsymbol{r}_i)$ is the normalized nucleon density at $\boldsymbol{r}_i$. The interaction is parametrized by the Fermi interaction constant, G_F which has the value $G_F = 10^{-14}$a.u. Each nucleus is associated with a weak charge, $Q_{W,n}$, which is given by

$$Q_{W,n} = -N + Z(1 - 4\sin^2\theta_W)$$

where N is the number of neutrons in the nucleus, Z is both the number of protons and the nuclear charge, and θ_W is the Weinberg angle, which measures the relative strength of the neutral and charged current parts of the P-odd interaction. The electronic 4 × 4 matrix operator, γ^5, has the explicit representation

$$\gamma^5 = \begin{bmatrix} 0 & 0 & 1 & 0 \\ 0 & 0 & 0 & 1 \\ 1 & 0 & 0 & 0 \\ 0 & 1 & 0 & 0 \end{bmatrix}$$

and is sometimes called the *chirality* operator. The validity of H_P has now been established by numerous experiments, the most recent and precise of which may be found in [25]. These are matched by high-precision atomic many-body calculations [55] which differ from the ones described in this article mainly by exploiting separability into radial and angular contributions, and the numerical methods used to solve the resulting radial equations. In atomic vapour experiments, the P-odd interaction mixes atomic states of opposite parity, and makes possible dipole transitions which would otherwise be forbidden on symmetry grounds. The most recently-reported experiment [25] detects P-odd effects by studying nuclear hyperfine structure in the forbidden $6s$-$7s$ transition in atomic caesium. The impressive agreement between the value of θ_W deduced from the combination of atomic theory and experiment with the fundamental predictions of electroweak theories is rather strong evidence that the relativistic many-body divergences hinted at by Kutzelnigg [31] arise only in connection with the manipulative procedures of the Foldy-Wouthuysen transformation.

In the context of relativistic molecular electronic structure calculations, we may define the chemical concept of chirality by the requirement that a chiral molecule has a non-vanishing electronic expectation value of γ^5. This is consistent with the prescription of Barron [56], who notes that the hallmark of a truly chiral system is that it can support time-even pseudoscalar observables. We require, therefore, enantiomeric states which are related by parity inversion, but not by time reversal combined with any proper rotation. In a relativistic description, γ^5 is a pseudoscalar interaction, and if ψ^+ and ψ^- represent the state vectors of two enantiomers related by parity inversion, we have

$$\langle\psi^+|\sum_i \gamma_i^5|\psi^+\rangle = -\langle\psi^-|\sum_i \gamma_i^5|\psi^-\rangle$$

Since the expectation value of the molecular chirality operator is different for two enantiomeric states of a molecule, the first-order energy shift due to H_P is also different. If the electroweak interaction is included in the molecular hamiltonian, two molecular enantiomers differ in energy by an amount, ΔE, where

$$\Delta E = 2\left|\langle\psi^{\pm}|H_P|\psi^{\pm}\rangle\right|$$

where the superscript ± indicates that we may evaluate the expectation value in either enantiomer. In a non-relativistic approximation, it is necessary to invoke a magnetic perturbation, such as spin-orbit coupling, to obtain a non-vanishing energy difference between enantiomers. In our case, we need evaluate only a simple one-electron matrix element in the bound-state wavefunction.

Based on scaling arguments, Hegstrom *et al.* [57] showed that the magnitude of this parity-violating energy satisfies the scaling law

$$\Delta E \simeq G_F Z^5 \alpha^3 \eta$$

where α is the fine-structure constant, and η is a structural parameter, which depends on the molecule: typically, $\eta \simeq 10^{-3}$. In all cases which have been treated using non-relativistic methods, the *L*-amino acids and *D*-sugars, which are the ones found in living organisms, are the enantiomers which are stabilized by H_P [56]. However, one must remember that these energy differences are of the order of 10^{-20} a.u. in organic molecules, and that any link between the predominance of one enatiomer over another in Nature is unlikely to have evolved solely due to this tiny thermodynamic factor. Some of the speculations about the link between the handedness of biological molecules and the electroweak interaction are discussed, and largely discounted, by Khriplovich [58].

Clearly there is a strong enhancement of the *P*-odd interaction if the molecule contains a heavy element, and a suitable candidate for experimental study is the chiral system CHBrClF. The rovibrational spectrum and synthesis of this molecule is surveyed in [59], and it has been discussed in the context of PNC by Khriplovich [58]. In Table 3, we present a analysis of the chiral energy difference in CHBrClF calculated using BERTHA. For each centre, the orbital contributions cancel strongly, particularly in the core region. The reason for this is that core orbitals are weakly perturbed atomic spinors, and the formation of a molecular bond has the effect of adding admixtures of spinors which are close in energy, in proportions which preserve their orthogonality. Most of the total effect comes from Br-centred valence electron contributions.

From these calculations we deduce an energy difference of 0.15 MHz between the ground state energies of the enantiomers of CHBrClF. Since this is only 0.015% of the $2s$-$2p$ Lamb shift in atomic hydrogen, it is amazing that energy differences of this magnitude may nowadays be measured routinely. Non-linear laser spectroscopy experiments have already been performed on *D*- and

L-camphor [60] which provide a direct probe of energy differences due to the electroweak interaction, since parity-conserving contributions to the energy are equal in the two enantiomeric forms. Alternatively, one could detect a difference between enantiomeric forms of a molecule by measuring the fluctations in optical activity which could arise, under suitable circumstances, due to the tunnelling between its the left- and right-handed forms. We are not in possession of all the experimental details, but understand that an *indirect* measurement of the P-odd effect on vibrational energy level differences has been proposed. This experimental situation has been anticipated and discussed in general terms by Khriplovich [58], from whose analysis we derive an estimate of around 1-10 Hz for the vibrational energy splittings caused by the weak interaction. In our formulation, we would have to take the vibrational average of a perturbing P-odd interaction hypersurface in the adiabatic vibrational wavefunctions (obtained, perhaps, using conventional quantum chemistry), which raises some rather delicate questions about the validity, or otherwise, of the Born-Oppenheimer separation at the 1 Hz level of accuracy. There may well be an experimentally observable vibrational frequency shift, and we emphasise that none of these *theoretical* concerns undermines the experimental viability of studying the P-odd interaction in CHBrClF, which, if successful, would be the first observation of parity violation in molecules. Some very formidable theoretical analysis remains to be done, however, if we are to calculate the magnitude of the effect from first principles to an accuracy which is sufficient to verify the validity of H_P for molecular systems. The difficulty of averaging such a small effect in wavefunctions derived from the Born-Oppenheimer separation touches on another of the "hopes and fears" expressed in [2, 9]; we are simply unable to offer further insight on this aspect of the problem at present.

6.4 Strategy for DHF calculations of large molecules: germanocene

We were asked by several participants at the meeting whether it would ever be possible to use BERTHA to calculate the electronic structures of large molecules, particularly organo-metallic species. Of course, one must learn to walk before one runs, and BERTHA is currently restricted to a DHF treatment of electronic structure. One can still learn a great deal from such studies, and they are a necessary precursor to treatments which include many-body effects, either from first principles using many-body theory, or in a more approximate way, using density functional theory. We believe that BERTHA, and the programs like it which are under development, have much to offer to the study of organo-metallic compounds. It now appears quite possible that one could

Table 4: Orbital eigenvalues (in a.u.) and orbital contributions to ΔE (in Hz) for the chiral molecule CHBrClF reduced to an atom-centred expansion. Contributions from the hydrogen nucleus are negligible and have been omitted.

i	ε_i	^{12}C	^{35}Cl	^{19}F	$^{80}\mathrm{Br}$
1	-498.50250	0.0	0.0	0.0	287.3
2	-105.26765	0.0	-94.5	0.0	0.0
3	-67.11230	0.0	0.0	0.0	3754.0
4	-60.17953	0.0	0.0	0.0	-3215.4
5	-58.42375	0.0	0.0	0.0	-4974.7
6	-58.42251	0.0	0.0	0.0	5162.8
7	-26.37118	0.0	0.0	29.5	0.0
8	-11.46854	2.0	0.0	0.0	0.0
9	-10.66042	0.0	-916.6	0.0	0.0
10	-10.18792	0.0	0.0	0.0	4209.4
11	-8.08927	0.0	915.2	0.0	0.6
12	-8.02763	0.0	-285.0	0.0	-0.2
13	-8.02581	0.0	-136.0	0.0	-0.1
14	-7.71700	0.0	0.0	0.0	-1126.6
15	-7.45504	0.0	0.0	0.0	-45998.7
16	-7.44914	0.0	0.0	0.0	51757.6
17	-3.16908	-0.3	0.5	0.0	-15607.6
18	-3.15913	0.0	-0.2	0.0	19270.9
19	-3.12751	0.3	0.2	0.0	193.3
20	-3.12241	0.0	-0.5	0.0	-6176.8
21	-3.11420	0.0	0.0	0.0	1482.0
22	-1.67621	-0.2	-10.4	269.0	-84.0
23	-1.19488	5.6	-717.3	-9.9	2920.0
24	-1.08264	-18.5	11.7	-14.3	-2857.9
25	-0.90724	91.4	-3927.9	162.5	66642.0
26	-0.77270	-126.9	103178.7	-372.1	-1590058.7
27	-0.73704	-319.2	-274286.4	-148.5	3817709.1
28	-0.71463	276.0	174776.4	-212.4	-2197809.1
29	-0.59236	67.6	-69889.9	-410.5	401760.8
30	-0.55040	441.6	185303.3	812.0	-1559326.0
31	-0.49215	720.6	-109932.5	-4901.2	1273043.1
32	-0.46788	-2196.5	35343.9	1433.6	-932496.3
33	-0.44177	-179.3	-276810.2	18994.6	3247597.9
34	-0.42698	1280.3	231660.2	-14758.6	-2453232.3
TOTAL		44.5	-5817.5	873.6	82826.3

study fragments of molecules which are of biochemical interest, and it is partially for this reason that we have begun implement a relativistic treatment of NMR interactions, and optical properties such as circular dichroism.

In order to be able to do anything at all, we require a wavefunction, constructed in a basis set of sufficient quality to describe the phenomena of interest. On the face of it, the task of constructing such a many-electron DHF wavefunction would appear hopeless: it is scarcely a trivial undertaking in *ab initio* non-relativistic quantum chemistry. There are, roughly speaking, four times as many basis functions in a relativistic calculation as there would be in a non-relativistic study, because of the presence of the four-spinor structure. We recover one degree of freedom by exploiting time reversal symmetry, but the factor of two remaining in the basis set dimension is deceptive. The allowed combinations of components in the two-electron integral generation stages of the calculation are blocked by the spinor structure, and there are only three distinct combinations at the DHF level of approximation. If kinetically balanced basis sets are employed of the type defined by Eq. (25), however, the effective angular quantum number in the small component basis function is always one unit larger that the large component function which it is constructed to match. Consequently, multi-centre integrals involving small-component functions are intrinsically more expensive to calculate than those involving large-component basis functions. Since the chemistry is dominated by large-component densities, the DHF approach doesn't look too practical at first sight.

In practice, we must use direct methods for large systems, in which two-electron integral batches are recalculated as they are required at each iteration. The amount of external storage required for a large system is prohibitive using non-relativistic programs, and the situation is worse for relativistic calculations. One need not, of course, calculate all integrals at every iteration, but neither may one neglect integrals simply because of their magnitude. The important consideration is whether an integral contributes significantly to a *change* in the Fock matrix, based on some crude estimate of the value of the integral and the change in the density matrix which multiplies the direct and exchange contributions. These constructions are summarized by the definitions

$$\mathbf{F}^{n+1} = \mathbf{F}^{n} + \mathbf{I}\,\Delta\mathbf{D}^{n} \tag{41}$$

where

$$\Delta\mathbf{D}^{n} = \mathbf{D}^{n} - \mathbf{D}^{n-1}. \tag{42}$$

where $\mathbf{F}^n$ is the Fock matrix at iteration n, $\mathbf{D}^n$ is the corresponding density matrix, and I is the matrix containing the antisymmetrized list of two-electron integrals. Since our scheme is based on Eq. (29), it is easy to show that Schwartz' inequality

$$0 \leq (\mu, \nu; T|\sigma, \tau; T') \leq \sqrt{|(\mu, \nu; T|\mu, \nu; T)||(\sigma, \tau; T'|\sigma, \tau; T')|} \qquad (43)$$

is satisfied by G-spinor integrals, and that Eq. (43) may be used to provide strict upper bounds on the magnitude of any two-electron two-spinor integral. We have implemented such a scheme in order to reduce the amount of computational labour expended in calculating two-electron integrals. A similar integral screening scheme has been reported by Saue [61], and applied to four-component calculations using a basis set of scalar Gaussian functions. We note in passing the very recent article by Schwegler *et al.* [62], in which it is demonstrated that a development of the general approach described here, in which non-local exchange contributions receive more careful treatment, is able to construct non-relativistic Fock matrices, in favorable circumstances, using an algorithm which scales linearly with the number of particles in the system.

Here we follow the classic work of Almlöf *et al.* [63] on direct self-consistent field calculations, and apply our scheme to a calculation of germanocene, Ge(cp)$_2$, an organo-metallic sandwich compound, using a double zeta quality basis set. This system contains 21 nuclei, and has been performed *without* exploiting point-group symmetry: each nuclear centre has been regarded as independent, so that we could test the effectiveness of the screening algorithm, and so that we could compare with non-relativistic results.

The efficiency of the relativistic screening algorithm is very high, and the results which are summarized in Table 4 are surprising, and reflect a characteristic feature of DHF wavefunctions. After the first couple of iterations, the change in the density matrix due to the overlap of small-component functions is negligibly small, and such change is concentrated in the one-centre contributions. After about ten iterations, even this variation in the density matrix vanishes, and the computational labour is comparable to a non-relativistic calculation.

One might be tempted to think that this rapid convergence of the small-component contributions is due to the size of the amplitudes, compared with the dominant large-component density. In fact, the reason for this extraordinary behaviour is that small component functions are highly localized to the nuclear sites. For a heavy element, the small-component amplitude may be very large near the nucleus; it can quite easily be comparable with some large-component amplitudes. The crucial difference is that the small component amplitude decays very rapidly away from the nucleus, while the large component functions are extended structures that determine the chemical bonding of the system. Two-centre small-component overlap densities are negligibly

Table 5: Snapshot of the percentage of integrals calculated in a Dirac-Hartree-Fock calculation of Ge(cp)$_2$. The labels LL, LS and SS refer to the blocks of the Fock matrix which receive contributions from the specified classes of integral.

	LL	LS	SS
One-centre integrals	51.3	27.5	2.5
Two-centre integrals	40.0	25.1	0.6
Multi-centre integrals	11.8	6.3	0.006

small, and one-centre small component overlap densities converge very rapidly, because their behaviour is dominated by the nuclear Coulomb potential. Even for germanium, which has a nuclear charge of only $Z = 32$, this effect is sufficient to suppress participation of small component basis functions in the self-consistent field procedure. Visscher [64] was the first to note that this localization of small component density could be turned to a computational advantage, and has devised a scheme which models this density as a point charge. Recently, we have adapted this idea to calculate the moments of the multipole field generated by the small component charge density [44], using extensions of the methods described by White and Head-Gordon [65]. The result is that DHF calculations of extended molecules are quite straightforward, if challenging, and follow non-relativistic lines. Of course, they are still more expensive than their non-relativistic counterparts, but the difference is less than one would think was decent, given the much higher level of theory involved in the relativistic treatment. One could not describe the calculations as "cheap and cheerful" [2], but they are certainly encouraging. Close to convergence, after about fifteen iterations without convergence acceleration techniques, there is very little to choose between a HF and DHF iterative scheme: only the large component amplitudes continue to change sufficiently to contribute significant changes to the Fock matrix.

7 Conclusion

We believe that these results will speak for themselves. Relativistic electronic structure calculations based on the Dirac equation are now not only possible, but they have many advantages over the standard non-relativistic formulation, particularly in the calculation of electric and magnetic properties. We are evidently not alone in this belief: relativistic electronic structure programs are under development in Oslo [66], Groningen [67] NASA (Ames) [68] and IBM (Poughkeepsie) [69]. The program, BERTHA, has been constructed from scratch entirely within our group at the cost of about three or four man-years of effort, a rapid development made possible by our experience in atomic physics and modern techniques of program development, including the use of symbolic manipulation to simplify algebraic problems. It is now possible to carry out calculations for small molecules using BERTHA using a standard personal computer running under the Linux operating system; for larger problems we use high-performance workstations. Clearly, more time must be invested before we will have a satisfactory treatment of many-body effects, but we may borrow much of this technology directly from existing programs, now that we have the core relativistic modules in place. From our point of view, the purpose of such a program is to extract the maximum amount of physical information from what we have at each stage of development, rather than to see the development as an end in itself, with an uncertain physical application. Our accumulated experience in relativistic electronic structure theory spans over fifty years, and we have drawn heavily on this in the design of BERTHA. We have deliberately chosen to regard the spinors as the natural computational objects to form the basis of relativistic electron structure calculations, largely because of this experience. Not all members of the relativistic community agree with this strategy, as the extensive bibliography by Pyykkö [70] will attest, but this diversity of opinion merely adds to the growing vitality of the subject.

Relativistic many-body calculations are more expensive than their non-relativistic counterparts, both because of the presence of the small component, but also because more functions are needed to represent the core orbitals if properties involving the electron density near heavy nuclei are required. But the calculation of many body corrections, as Sutcliffe has observed sagely [2], is always with us irrespective of the operator we choose for our zero-order approximation; the relativistic many-body problem is just slightly more onerous than its non-relativistic analogue. We have no comfort to offer regarding the Born-Oppenheimer separation, and it is certainly true that in this regard a relativistic formulation is even more formidable than its already complicated non-relativistic counterpart. Although one must dedicate more resources to an *ab initio* relativistic quantum chemical calculation, more information inevitably comes out as a result, and very often the relativistic four-component structure and division into charge-current contributions clarifies the physics of the system. Such a judgement is certainly a matter of taste, but after many years experience, we have developed quite a taste for the Dirac equation, and regard it as providing the natural language in which to discuss electronic properties. So we finish as we began, with the revolutionary suggestion, borrowed from *Animal Farm* [1], that the time has now come to stand up and proclaim: "*four-components good, two-components bad!*". At the risk of being trampled underfoot in the counter-revolution, we hope that this will at least kindle as lively a debate as did Sutcliffe's introductory lecture!

8 Acknowledgements

EPSRC are thanked for the award of an Advanced Fellowship to HMQ, and for the generous provision of computing resources to HMQ and IPG for this research. HS is supported by a scholarship from the Norwegian Research Council, and receives computing resources from the Norwegian Programme for Supercomputing. We thank Brian Sutcliffe for his courtesy in forwarding the text of his introductory lecture, which allowed us to structure our contribution to meet his criticisms.

References

[1] G. Orwell, *Animal Farm; a fairy story*, Secker and Warburg, (1945).

[2] B. T. Sutcliffe, *Adv. Quantum. Chem.*, this volume.

[3] R. McWeeny and B. T. Sutcliffe, *Methods of molecular quan tum mechanics*, Academic Press, (1969).

[4] R. McWeeny, *Methods of molecular quantum mechanics* (second edition), Academic Press, (1989).

[5] C. A. Coulson, *Rev. Mod. Phys.*, **32** 171 (1960).

[6] R. P. Feynman, *Rev. Mod. Phys.*, **20** 367 (1948)

[7] B. Swirles, *Proc. R. Soc. (London) A*, **A152**, 625-649 (1935).

[8] P. A. M. Dirac, *Proc. R. Soc. (London)*, **A117**, 610-624 (1928).

[9] B. T. Sutcliffe, *Theoretical models of chemical bonding. Part I: atomic hypothesis and the concept of molecular structure*, ed. Z. B. Macsič, p1, Springer-Verlag (1990).

[10] R. Stanton and S. Havriliak, *J. Chem. Phys.*, **81** 1910 (1984).

[11] I. P. Grant and H. M. Quiney, *Adv. At. Mol. Phys.*, **23**, 37-86 (1988).

[12] H. M. Quiney, *The effects of relativity in atoms, molecules and the solid state*, (eds. S. Wilson, I. P. Grant and B. L. Gyorffy), pp 83-123, Plenum Press, New York (1991)

[13] I. P. Grant, *Relativistic, quantum electrodynamic and weak interaction effects in atoms*, (eds. W. R. Johnson, P. J. Mohr and J. Sucher), pp 235-253, AIP Conference Proceedings 189 (1989).

[14] K. G. Dyall and K. Fægri jr., *Theoret. Chim. Acta.*, **94**, 39 (1996)

[15] L. N. Labzowsky, *Sov. Phys. JETP*, **32** 94 (1971).

[16] J. Sapirstein, *Physica Scripta*, **36** 801 (1987).

[17] I. P. Grant, *Atomic, molecular & optical physics handbook*, ed. G. W. F. Drake, Chapt. 22, p287, AIP Press, Woodbury, New York (1996).

[18] J. D. Talman, *Phys. Rev. Lett.*, **57**, 1091 (1986).

[19] W. H. Furry, *Phys. Rev.*, **81** 115 (1951).

[20] H. A. Bethe and E. E. Salpeter, *Quantum mechanics of one- and two-electron systems*, (Vol. *XXXV* of *Handbuch der Physik*, Springer-Verlag, Berlin, Göttingen, Heidelberg (1957).

[21] J. Sucher, *Relativistic, quantum electrodynamic and weak interaction effects in atoms*, (eds. W. R. Johnson, P. J. Mohr and J. Sucher), pp 28-46, AIP Conference Proceedings 189 (1989).

[22] G. E. Brown and D. G. Ravenhall, *Proc. R. Soc. (London) A*, **208**, 552-559 (1951).

[23] H. M. Quiney, I. P. Grant and S. Wilson, Lecture notes in chemistry, **52**, ed. U. Kaldor, p307 Springer-Verlag (1989).

[24] I. Lindgren and J. Morrison, *Atomic many-body theory*, Springer-Verlag, Berlin (1982).

[25] C. S. Wood, S. C. Bennett, D. Cho, B. P. Masterson, J. L. Roberts, C. E. Tanner, C. E. Wieman, *Science*, **275**, 1759 (1997).

[26] W. Kutzelnigg, *Z. Phys. D.*, **11**, 15 (1989); *Z. Phys. D.*, **15**, 27 (1990).

[27] W. Cencek and W. Kutzelnigg, *J. Chem. Phys.*, **105** 5878 (1996).

[28] K. G. Dyall, *J. Chem. Phys.*, **100**, 2118 (1994).

[29] B. A. Hess, *Phys. Rev. A*, **32** , 756 (1986).

[30] V. Kellö, A. J. Sadlej, and B. A. Hess, *J. Chem. Phys.*, **105**, 1995 (1996).

[31] E. Ottschofski and W. Kutzelnigg, *J. Chem. Phys.*, **106** 6634 (1997).

[32] A. Rutkowski, *J. Phys. B: At. Mol. Phys.*, **19**, 149 (1986); *J. Phys. B: At. Mol. Phys.*, **19**, 3431 (1986); *J. Phys. B: At. Mol. Phys.*, **19**, 3443 (1986).

[33] E. van Lenthe, E. J. Baerends, and J. G. Snijders, *J. Chem. Phys.*, **99** 4597 (1993).

[34] L. E. McMurchie and E. R. Davidson, *J. Comp. Phys.*, **26**, 218 - 231 (1978).

[35] E. A. Hinds and B. E. Sauer, *Physics World*, **10**, 37 (1997).

[36] H. M. Quiney, H. Skaane, and I. P. Grant, *J. Phys. B: At. Mol. Opt. Phys.*, (submitted, 1997)

[37] D. R. Plante, W. R. Johnson and J. Sapirstein, *Phys. Rev. A*, **49** 3519 (1994).

[38] H. M. Quiney, I. P. Grant, and S. Wilson, *J. Phys. B: At. Mol. Opt. Phys.*, **23** L271 (1990).

[39] L. Visscher, T. J. Lee, and K. G. Dyall, *J. Chem. Phys.*, **105**, 6769 (1996).

[40] H. A. Kramers, *Proc. Acad. Amsterdam*, **33**, 959 (1930).

[41] J. Meyer, W. D. Sepp, B. Fricke and A. Rosén, *Comput. Phys. Commun.*, **96**, 263 (1996)

[42] V. R. Saunders, *Methods of Computational Molecular Physics*, (eds. G. H. F.Diercksen & S. Wilson), pp. 1-36 Reidel, Dordrecht (1983).

[43] T. U. Helgaker and P. R. Taylor, *Modern electronic structure theory, Part II*, ed. D. R. Yarkony, p. 725, World Scientific, Singapore (1995).

[44] H. M. Quiney, H. Skaane, and I. P. Grant, to be submitted (1997).

[45] E. A. Uehling, *Phys. Rev.*, **48**, 55 (1935).

[46] H. M. Quiney and I. P. Grant, *J. Phys. B: At. Mol. Opt. Phys.* **27**, L299 (1994).

[47] R. P. Feynman, *Phys. Rev.*, **74**, 1430 (1948).

[48] P. J. Mohr, *Phys. Rev. A*, **26**, 2388 (1982).

[49] F. Rosicky, *Chem. Phys. Lett.*, **85** 195 (1982).

[50] A. K. Mohanty, *Int. J. Quant. Chem.* **42** 627 (1992).

[51] P. Pyykkö, *Chem. Phys.*, **74**, 1 (1983).

[52] N. C. Pyper, *Chem. Phys. Lett.*, **96**, 204 (1983).

[53] K. Ruud, Masters thesis, University of Oslo, (unpublished) (1993).

[54] J. Gauss, *Chem. Phys. Lett.*, **191**, 614 (1992).

[55] W. R. Johnson, J. Sapirstein and S. A. Blundell, *Physica Scripta*, **T46**, 184-192 (1993).

[56] L. D. Barron, *Theoretical models of chemical bonding. Part I: atomic hypothesis and the concept of molecular structure*, ed. Z. B. Macsič, p115, Springer-Verlag (1990).

[57] R. A. Hegstrom, D. A. Rein and P. G. H. Sandars, *J. Chem. Phys.*, **73**, 2329 (1980).

[58] I. B. Khriplovich, *Parity nonconservation in atomic phenomena*, Gordon and Breach (1991).

[59] A. Beil, D. Luckhaus, and M. Quack, *Ber. Bunsenges. Phys. Chem.*, **100**, 1853 (1996).

[60] E. Arimondo, P. Glorinex, and T. Oka, *Opt. Commun.*, **23**, 369 (1977).

[61] T. Saue, *Principles and applications of relativistic molecular calculations*, PhD thesis (unpublished), University of Oslo (1995).

[62] E. Schwegler, M. Challacombe, and M. Head-Gordon, J. Chem. Phys., **106**, 9708 (1997).

[63] J. Almlöf, K. Fægri jr, and K. Korsell, *J. Comput. Chem.*, **3**, 385 (1982).

[64] L. Visscher, *Theor. Chim. Acta*, (accepted for publication, 1997).

[65] C.A.White and M. Head-Gordon, *J. Chem. Phys.*, **105** (1996).

[66] T. Saue, K. Fægri jr, T. Helgaker and O. Gropen, *Mol. Phys.*, **91**, 937 (1997).

[67] L. Visscher, O. Visser, P. J. C. Aerts, H. Merenga, and W. C. Nieuwpoort, *Comp. Phys. Commun.*, **81**, 120 (1994)

[68] K. G. Dyall, K. Fægri jr., and P. R. Taylor, *The effects of relativity in atoms, molecules and the solid state*, (eds. S. Wilson, I. P. Grant and B. L. Gyorffy), pp 167-184, Plenum Press, New York (1991)

[69] F. A. Parpia, A. K. Mohanty, *Phys. Rev.*, **52**, 962 (1995).

[70] P. Pyykkö, *Relativistic theory of atoms and molecules*, vol I (1986), vol II (1993), *Lecture Notes in Chemistry*, Springer-Verlag, Berlin; the database *RTAM Version 3.0: Relativistic theory of atoms and molecules* may be accessed at *http://www.csc.fi/lul/rtam.*

Modern VB representations of CASSCF wave functions and the fully-variational optimization of modern VB wave functions using the CASVB strategy

DAVID L. COOPER
Department of Chemistry, University of Liverpool, P.O. Box 147, Liverpool L69 7ZD, United Kingdom

THORSTEIN THORSTEINSSON
Chemistry Laboratory IV, Copenhagen University, Universitetsparken 5, DK-2100 Copenhagen Ø, Denmark.

JOSEPH GERRATT
School of Chemistry, University of Bristol, Cantocks Close, Bristol BS8 1TS, United Kingdom

Abstract

We outline the CASVB strategy, which may be used either to generate very compact modern valence bond representations of CASSCF wave functions or to optimize general types of modern VB wave function. Various aspects of the methodology are illustrated by means of applications to the ground state of benzene, to the $X^4\Delta$ and $a^6\Delta$ state of FeH, and to the two lowest ^1A_g states of various model polyene systems.

1 Introduction
2 The CASVB strategy
3 Results
  3.1 Benzene
  3.2 FeH
  3.3 Model polyene systems
4 Conclusions
References

Key words: CASVB — modern VB — CASSCF — benzene — FeH — polyenes

ADVANCES IN QUANTUM CHEMISTRY, VOLUME 32
Copyright © 1999 by Academic Press. All rights of reproduction in any form reserved.
0065-3276/99 $30.00

1 Introduction

We use the label 'modern valence bond' to signify one or more spatial configurations constructed from completely general, nonorthogonal orbitals, and combined with all allowed ways of coupling together the electron spins so as to obtain the required resultant. The CASVB strategy [1–7] exploits the invariance of CASSCF wave functions to arbitrary nonsingular linear transformations of the active orbitals: the basic idea is to carry out a (typically) nonunitary orbital transformation so that the total CASSCF wave function becomes dominated by a compact, easy-to-interpret component of modern VB form. In order to be able to realize this goal, we require efficient procedures for carrying out exactly the transformation of the structure space induced by a given general orbital transformation, as well as schemes for determining orbital transformations that lead to 'useful' representations of the CASSCF wave function. These key features are incorporated in the CASVB procedures already distributed as part of the MOLPRO package [8], in which they are interfaced to a very efficient CASSCF program [9], and we intend to incorporate them into many other packages in due course. Inexpensive and generally available procedures could lead to CASVB becoming a standard tool for analyzing CASSCF wave functions, bridging the traditional MO/VB divide. Furthermore, CASVB algorithms may be adapted so as to enable fully-variational optimization of fairly general types modern VB wave functions, so that the CASVB strategy also represents a significant advance in the development of VB methodology.

2 The CASVB strategy

All of the key features of the CASVB algorithms have been described in detail elsewhere [1–7], and so we present here a brief overview. We write a normalized CASSCF wave function in the form

$$\Psi_{\mathrm{CAS}} = \sum_{I}^{N_{\mathrm{CI}}} c_I \Phi_I \tag{1}$$

in which the N_{CI} structures Φ_I correspond to all distributions of the N active electrons in m active orbitals that are consistent with the overall symmetry. The CASSCF wave function typically also incorporates an (optimized) inactive component that is common to all the structures. We are concerned here with nonunitary $m \times m$ linear transformations of the orthogonal active orbitals ϕ_μ that result in sets of nonorthogonal orbitals ϕ'_μ. An $m \times m$ orbital transformation $\mathbf{O}$ induces an $N_{\mathrm{CI}} \times N_{\mathrm{CI}}$ transformation $\mathbf{T}(\mathbf{O})$ of the structure space, so that:

$$\begin{aligned} \mathbf{H}' &= \mathbf{T}^{\dagger}(\mathbf{O})\,\mathbf{H}\,\mathbf{T}(\mathbf{O}) \\ \mathbf{S}' &= \mathbf{T}^{\dagger}(\mathbf{O})\,\mathbf{S}\,\mathbf{T}(\mathbf{O}) \\ \mathbf{c}' &= \mathbf{T}^{-1}(\mathbf{O})\,\mathbf{c} = \mathbf{T}(\mathbf{O}^{-1})\,\mathbf{c} \end{aligned} \tag{2}$$

in which **H** and **S** are hamiltonian and overlap matrices, and **c** is a CI vector. Consequently, we may circumvent the usual problems implicit in evaluating matrix elements between structures constructed from nonorthogonal orbitals.

The basic property

$$\mathbf{T}(\mathbf{O}_1\mathbf{O}_2) = \mathbf{T}(\mathbf{O}_1)\mathbf{T}(\mathbf{O}_2) \tag{3}$$

allows us to decompose the full orbital transformation **O** into a sequence of m^2 simple updates of the type $\phi_\nu \rightarrow \phi_\nu + \lambda\phi_\mu$, for which the corresponding structure transformations take a particularly simple form [1,2,10]. In this way, we may realize exactly the effects of the structure transformation **T(O)** without explicit construction. All of the required algorithms are described in detail in Refs. [3,5], together with procedures for evaluating the first and second derivatives of **T(O)** with respect to the orbital parameters, as is required for efficient optimization schemes.

This still leaves completely open the question of how to choose the orbital transformation **O**. Perhaps the most obvious approach is to partition the total CASSCF wave function according to

$$\Psi_{\mathrm{CAS}} = S_{\mathrm{VB}}\Psi_{\mathrm{VB}} + (1-S_{\mathrm{VB}}^2)^{1/2}\Psi_{\mathrm{VB}}^{\perp}\,, \tag{4}$$

in which

$$S_{\mathrm{VB}} = \frac{\langle\Psi_{\mathrm{CAS}}|\Psi_{\mathrm{VB}}\rangle}{\langle\Psi_{\mathrm{VB}}|\Psi_{\mathrm{VB}}\rangle^{1/2}} \tag{5}$$

and $\langle\Psi_{\mathrm{VB}}|\Psi_{\mathrm{VB}}^{\perp}\rangle=0$. We refer to maximization of S_{VB} as the overlap-based criterion.

An attractive alternative is to minimize the energy expectation value

$$E_{\mathrm{VB}} = \frac{\langle\Psi_{\mathrm{VB}}|\hat{\mathrm{H}}|\Psi_{\mathrm{VB}}\rangle}{\langle\Psi_{\mathrm{VB}}|\Psi_{\mathrm{VB}}\rangle}\,, \tag{6}$$

but it is our experience that analogous overlap- and energy-optimized wave functions are always in very good qualitative agreement. Minimization of E_{VB} is necessarily computationally more expensive than is maximization of S_{VB}, because of the requirement to determine the effect of applying hamiltonian matrices to CI vectors. Nonetheless, it has proved possible to develop highly efficient strategies [1–7]. Maximization of S_{VB} or minimization of E_{VB} is achieved using modified Newton-Raphson second-order procedures that allow for the elimination of redundant parameters [7] that arise from e.g. orbital normalization and from any constraints that may have been applied to the form of Ψ_{VB}.

When interpreting 'N in N' CASSCF wave functions, our usual choice of Ψ_{VB} is motivated by the well-documented success of the spin-coupled approach, as exemplified by the various applications reviewed in Refs. [11,12]. Such a wave function takes the form

$$\Psi_{\mathrm{VB}} = \mathcal{A}(\varphi_1^2\varphi_2^2\ldots\varphi_n^2\,\Theta_{\mathrm{pp}}^{2n}\,\phi_1\phi_2\ldots\phi_N\,\Theta_{SM}^{N}) \tag{7}$$

in which the singly occupied nonorthogonal orbitals ϕ_μ accommodate the N active electrons, and the doubly occupied orthogonal orbitals φ_i accommodate the $2n$ inactive ones. The normalized N-electron spin eigenfunction of $\hat{S}^2$ and $\hat{S}_z$, Θ^N_{SM}, is expanded in the full space of f^N_S linearly-independent spin functions [13], and Θ^{2n}_{pp} corresponds to perfect pairing of the spins of the inactive electrons. Especially when the numbers of active electrons and active orbitals are different, it can prove more appropriate to choose instead a Ψ_{VB} of multiconfiguration form [7].

Combining the CASVB procedures with CASSCF codes makes possible the fully-variational optimization of modern VB wave functions using 'standard' packages. The basic idea is to alternate optimization of the active parameter set (via minimization of E_{VB}) and of the external parameter set (using CASSCF procedures) in an iterative two-step procedure. The MOLPRO package [8] already features fully-variational optimization of quite general types of modern VB wave function, including multiconfiguration spin-coupled wave functions. We have presented practical approaches [5] for the proper utilization of molecular point group symmetry in modern VB approaches that involve the optimization of nonorthogonal orbitals. Furthermore, given that the final variational wave function is essentially a constrained form of CASSCF function, much of the impressive technology of CASSCF procedures immediately becomes available to variational calculations of modern VB wave functions. Of immediate significance is the efficient evaluation of energy gradients, as required, for example, to carry out geometry optimization. Further examples include on-the-fly evaluation of integrals over basis functions and perturbative methods for the incorporation of dynamical correlation.

3 Results

We concentrate here on the type of information made available by the use of the overlap criterion to generate very compact modern VB representations of ground and excited state CASSCF wave functions. Applications of the CASVB codes are presented for the ground state of benzene, the $X^4\Delta$ and $a^6\Delta$ state of FeH, and the two lowest ^1A_g states in various model polyene systems.

3.1 Benzene

The ground state of the benzene molecule, treated as a π-electron system, is by now a rather familiar example for the spin-coupled approach, with a description based on six singly-occupied deformed $C(2p_\pi)$ functions, as shown in Figure 1, and symmetric coupling of the electron spins around the ring. The relatively small amounts of delocalization onto neighbouring carbon atoms, not present in the classical VB covalent description, play a crucial role in reducing the contribution from 'ionic' structures, with double occupancy of one or more orbitals. We have recently analyzed the corresponding '6 in 6' CASSCF wave function using the overlap criterion (Eq. (5)) and a Ψ_{VB} of spin-coupled form, with the active orbitals constrained to transform into one another under successive $\hat{C}_6$ rotations [6]. The resulting description is very similar indeed to the fully-variational spin-coupled result. We examined the relative importance of the different modes of spin-coupling in Ψ_{VB} and analyzed the orthogonal complement, $\Psi_{VB}^{\perp}$, in terms of weights calculated using the conventional Chirgwin-Coulson definition [13]. As is well known, such weights must add to 100%, but individual weights need not lie in the range [0,100]%. It has been suggested to us that it could be informative to repeat these analyses with alternative definitions for the weights.

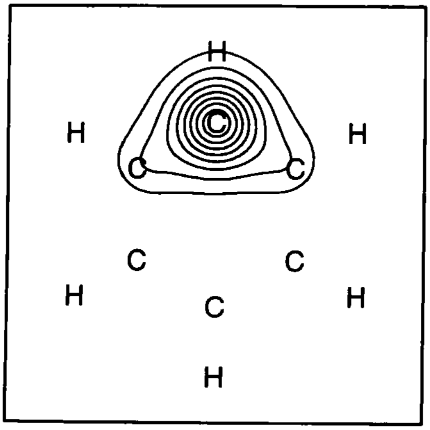

Figure 1. Symmetry-unique modern VB π orbital for the ground state of benzene. Contours are shown in the horizontal plane 1 bohr above the molecular plane, with projected positions of the nuclei denoted by their chemical symbols.

All of the details of the basis set, geometry and CASVB calculations are given in Ref. [6]. The overlap-optimized Ψ_{VB} of spin-coupled form (cf. Eq. 7) gives an impressive S_{VB}=0.99546 and the corresponding value of E_{VB}, without further optimization, incorporates 89.14% of the (nondynamical) electron correlation recovered by the '6 in 6' CASSCF wave function. It is convenient to expand Θ_{SM}^{N} (Eq. 7) in the Rumer basis, so that modes 1,4 correspond to Kekulé-like structures and modes 2,3,5 correspond to *para*-bonded structures [12]. We report in Table I the weights of these f_S^N=5 different modes in Ψ_{VB}, augmenting our earlier Chirgwin-Coulson weights with values obtained using Löwdin's scheme for symmetric orthogonalization [15] and the inverse-overlap definition promoted by Gallup and Norbeck [16,17]. The inverse-overlap weights, unlike those from the more traditional Chirgwin-Coulson definition, must lie in the range [0,100]% but, at least in the case of benzene, we find that these two schemes show much the same pattern, with very much larger contributions from the Kekulé-like modes than from the *para*-bonded structures. The symmetric orthogonalization scheme leads to functions which deviate as little as possible (in a root mean square sense) from the original set, but, at least in the case of benzene, it appears that the corresponding weights (in the range [0,100]%) do not accord with the values obtained from alternative procedures.

TABLE I. Weights of the f_S^N=5 different VB structures in Ψ_{VB}, with the spin function expressed in the Rumer basis.

Structure	Chirgwin-Coulson	'Löwdin'	inverse-overlap
1	36.44%	22.01%	42.71%
2	9.04%	18.66%	4.86%
3	9.04%	18.66%	4.86%
4	36.44%	22.01%	42.71%
5	9.04%	18.66%	4.86%

TABLE II. Weights of different classes of modern VB structures in the total CASSCF wave function for benzene. Weights of ionic structures are based on analysis of $\Psi_{\mathrm{VB}}^{\perp}$.

Class	Chirgwin-Coulson	'Löwdin'
Covalent	99.0942%	99.0993%
Singly-ionic	0.3424%	0.1615%
Doubly-ionic	0.5537%	0.5985%
Triply-ionic	0.0097%	0.1408%

Although S_{VB} exceeds 0.995 and the weight of Ψ_{VB} in Ψ_{CAS} exceeds 99%, the orthogonal complement is far from unimportant: it accounts for slightly more than 10% of the electron correlation recovered by the CASSCF wave function. As such, it seems worthwhile to include in our analysis the various contributions to $\Psi_{\mathrm{VB}}^{\perp}$, and so we report in Table II the weights of the different classes of modern VB structures in the total CASSCF wave function. The two definitions we examined do differ in the relative importance attached to singly-ionic and triply-ionic structures, but both of them indicate that the largest component of $\Psi_{VB}^{\perp}$ is the set of doubly-ionic structures (ca. 0.6% of the total wave function). As might be expected from the importance in the total wave function of Kekulé-like structures based on functions which deform towards neighbouring positions in the ring, singly-ionic structures with charges in adjacent positions possess particularly small weights; in either mode of analysis, the most important of the singly-ionic structures are those with charges in *meta* positions.

3.2 FeH

Low-lying states of FeH have been studied both experimentally and theoretically by many groups, and it is now well established that the ground state is a quartet ($X^4\Delta$), lying 0.24 eV below the lowest sextet state ($a^6\Delta$). An extensive theoretical study of the plethora of low-lying states of various symmetries has been presented by Langhoff and Bauschlicher [18].

For the purposes of the present account, we constructed full-valence CASSCF wave functions for the $X^4\Delta$ and $a^6\Delta$ states. In $C_{\infty v}$ symmetry, the valence orbitals comprise four σ orbitals, the two components of a π orbital, and the two components of a δ orbital. Calculations were actually carried out in C_{2v} symmetry, so that the full-valence active space is based on all distributions of the 9 valence electrons in 8 orbitals: five a_1, one b_1, one b_2 and one a_2. For each state, we carried out a state-averaged calculation using both Δ components (degenerate A_1 and A_2 roots), adopting bond lengths of 3.015 bohr and 3.193 bohr, respectively, for the $X^4\Delta$ and $a^6\Delta$ states [18]. Basis sets for Fe [19] and H [20], consisting of (14s9p5d/4s1p) cartesian GTOs contracted to [8s5p3d/2s1p], were taken directly from the MOLPRO library by means of keywords W140905 and VDZ [8].

Each '9 in 8' CASSCF wave function was transformed into modern VB form by maximizing the overlap with the configuration:

$$\Psi_{VB}=\mathcal{A}(\Psi_{CORE}\,\sigma_1\,\sigma_2\,\sigma_3\,\sigma_4\,\pi^2(^3\Sigma^-)\,\delta^3(^2\Delta)\,\Theta_{SM}^N)\ . \tag{8}$$

with Θ_{SM}^N expanded in the full allowed spin space. The resulting values of S_{VB} (see Table III) exceed 0.9995 and the corresponding values of E_{VB} are very close to the CASSCF energies. The further energy lowerings that can be achieved by minimizing E_{VB} are insignificant, especially for the $a^6\Delta$ state.

The symmetry restrictions on the coupling of the π orbitals and of the δ orbitals ensure that the wave functions possess the correct overall symmetry (Δ). Of course, the size of the full-valence CASSCF active space is then such that each component of the spin-coupled π and δ orbitals is expanded in just one CASSCF natural orbital. As a consequence, the π and δ orbitals in Ψ_{VB} must match exactly the corresponding CASSCF natural orbitals, which take the form of fairly unremarkable d functions centred on the Fe atom. As such, the impressive values of S_{VB} and E_{VB} reflect the fact that the free parameters in each Ψ_{VB} are essentially those of a '4 in 4' system. The four nonorthogonal σ orbitals for each state are depicted in Figure 2, with the corresponding overlap integrals in Table IV. The description of the bonding that emerges from maximizing S_{VB} is analogous to that we have observed previously in fully-variational calculations on a wide range of diatomic transition metal hydrides and their ions [21–23].

TABLE III. Full-valence CASSCF and CASVB results for FeH.

Calculation	Quantity	$X^4\Delta$	$a^6\Delta$
CASSCF	E_{CAS}/hartree	−1262.883015	−1262.881429
Maximize S_{VB}	S_{VB}	0.999517	0.999996
	E_{VB}/hartree	−1262.882518	−1262.881419
Minimize E_{VB}	E_{VB}/hartree	−1262.882542	−1262.881419

TABLE IV. Overlap integrals between (normalized) modern VB σ orbitals for FeH. Values in the lower triangle relate to the $X^4\Delta$ state and those in the upper triangle to the $a^6\Delta$ state.

	σ_1	σ_2	σ_3	σ_4
σ_1		0.81	0.59	0.16
σ_2	0.78		0.25	0.13
σ_3	0.64	0.26		−0.00
σ_4	0.13	0.05	−0.30	

The bonding in these states of FeH arises from the overlap of a characteristic 'bonding hybrid' on the metal (σ_1) with a slightly deformed H(1s) function (σ_2). The remaining σ orbitals take the characteristic forms of 'nonbonding hybrids' on the metal (σ_3) and functions that resembles 'd_{z^2}' on iron (σ_4). The strength of the σ bond is linked to the high overlap of σ_1 and σ_2 (see Table IV), and the predominance of singlet coupling of the associated electron spins. The most significant difference between these two states arises from the different mode of coupling of the spins associated with the electrons accommodated in orbitals σ_3 and σ_4: 74% singlet for $X^4\Delta$ but overwhelmingly triplet for $a^6\Delta$. At this level of theory, the difference in energy between the two states is indeed rather small. We find that expanding the active space to include also a second π orbital (i.e. another b_1 and b_2 pair) does lead to a slightly larger energy difference, but ultimately it

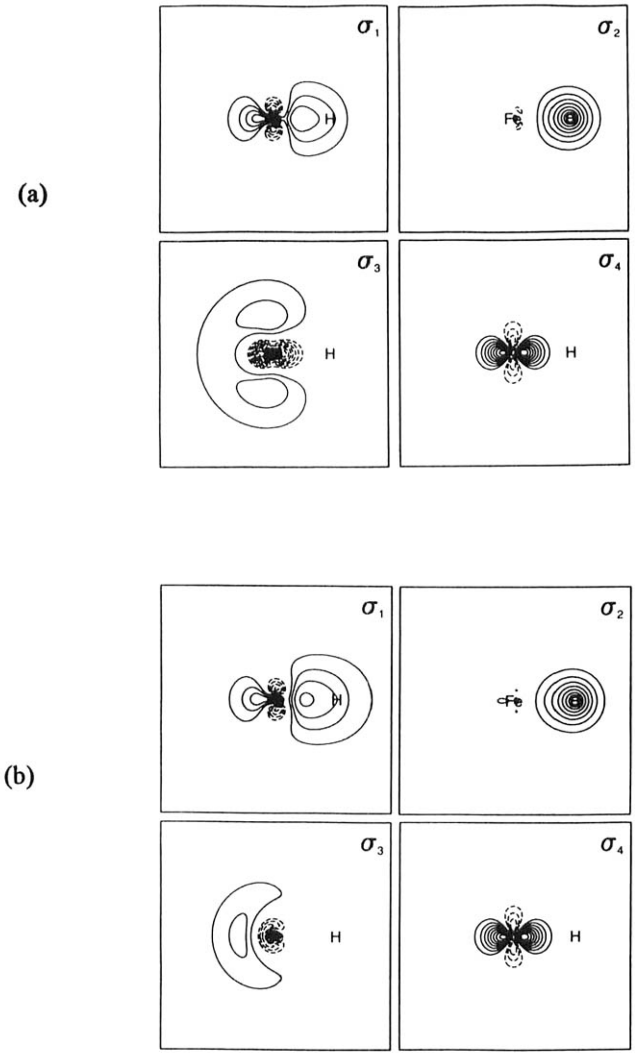
(a)
σ1
H
σ2
Fe
σ3
H
σ4
H
(b)
σ1
H
σ2
Fe
σ3
H
σ4
H

Figure 2. Modern VB σ orbitals for FeH: (a) $X^4\Delta$ state; (b) $a^6\Delta$ state. Contours are shown in a plane containing both nuclei. The nuclear positions are marked by their chemical symbols.

proves necessary to take proper account of dynamical electron correlation effects [18] if we are to match the experimental value of T_e.

3.3 Model polyene systems

Exploratory calculations on *trans*-regular model polyene chains were carried out in C_{2h} symmetry using bond lengths r_{CC}=139 pm, r_{CH}=109 pm and angles of 120° [24], using a minimal STO-3G basis set. For systems with n_C carbon atoms (n_C=4,8,6,10) we carried out CASSCF calculations for the two lowest roots of ^1A_g symmetry using an active space consisting of n_C 'π' electrons and n_C π orbitals, with all of the 'σ' electrons accommodated in an optimized core. Total CASSCF energies (E_{CAS}) are recorded in Table V. Of course, further studies of these states will need to use more realistic basis sets and may need to take account of dynamical electron correlation effects to place correctly the $(2)^1A_g$ state relative to other excited states. Nonetheless, we do expect to obtain a faithful description of the key features of the bonding.

TABLE V. CASSCF and CASVB results for ^1A_g roots of the model polyene system with n_C=10.

n_C	root	E_{CAS} (hartree)	S_{VB}	E_{VB} (hartree)
4	1	−153.091025	0.9999158	−153.090807
	2	−152.857556	0.9999665	−152.857488
6	1	−229.071285	0.9994594	−229.070170
	2	−228.894391	0.9989062	−228.892301
8	1	−305.052294	0.9987436	−305.049874
	2	−304.911100	0.9969754	−304.905616
10	1	−381.033618	0.9978681	−381.029661
	2	−380.916468	0.9951752	−380.908184

For the purposes of interpretation, we transformed each set of CASSCF orbitals so as to maximize the overlap (S_{VB}) with a spin-coupled-like modern VB configuration based on n_C active orbitals of π symmetry and an inactive σ core (cf. Eq. (7)). The resulting values of S_{VB} are listed in Table V, together with the expectation value of the energy (E_{VB}) for the dominant modern VB component of each CASSCF wave function. Although the value of S_{VB} decreases with increasing n_C, it still exceeds 0.995 even in the worst case. Especially for the smaller values of n_C, E_{VB} lies within very few millihartrees of E_{CAS}; these differences could of course be reduced, even with a single spatial configuration, by choosing the transformation of the CASSCF orbitals so as to minimize E_{VB}, but our experience for numerous systems suggests that the corresponding modern VB wave functions would be little different from those described here. We return to this point later.

For each case, we find a modern VB description based on C(2p$_\pi$) functions associated with particular atoms in the chain, but deformed towards neighbouring atoms. It is convenient to label the orbitals π_i according to the carbon atoms with which they are associated. As is to be expected, the 'boundary' effects on the total wave function become less significant as n_C increases, and so we concentrate here on the description afforded by the calculations for the largest system. The overlaps between normalized modern VB orbitals for $n_C=10$ are shown in the lower (upper) triangles of Table VI for the first (second) roots of ^1A_g symmetry, and contours of the symmetry-unique orbitals are depicted in Figures 3 and 4. The most immediate observation is that the orbitals for these two roots are rather similar, but that those for the second root are more uniform along the chain. This can be seen particularly clearly from the nearest-neighbour overlaps, which exhibit much less alternation for the higher root than for the ground state.

TABLE VI. Overlap integrals between (normalized) modern VB π orbitals for the model polyene system with $n_C=10$. Values in the lower triangle relate to the $(1)^1A_g$ root and those in the upper triangle to the $(2)^1A_g$ root.

	π_1	π_2	π_3	π_4	π_5	π_6	π_7	π_8	π_9	π_{10}
π_1		0.54	0.14	−0.03	−0.07	−0.11	−0.01	0.00	0.01	0.01
π_2	0.58		0.55	0.13	−0.08	−0.05	0.04	0.00	0.01	0.01
π_3	0.13	0.40		0.55	0.11	−0.01	−0.04	−0.07	0.00	0.00
π_4	0.05	0.10	0.58		0.52	0.11	−0.11	−0.04	0.04	−0.01
π_5	−0.02	−0.10	0.10	0.42		0.56	0.11	−0.01	−0.05	−0.11
π_6	0.00	−0.02	0.01	0.10	0.58		0.52	0.11	−0.08	−0.07
π_7	0.01	0.03	−0.02	−0.10	0.10	0.42		0.55	0.13	−0.03
π_8	0.00	0.01	0.00	−0.02	0.01	0.10	0.58		0.55	0.14
π_9	0.00	−0.01	0.01	0.03	−0.02	−0.10	0.10	0.40		0.54
π_{10}	0.00	0.00	0.00	0.01	0.00	−0.02	0.05	0.13	0.58	

We find much larger differences between the total spin functions for these two roots. For a system with $N=10$ and $S=0$, such a spin function consists of a linear combination of $f_S^N=42$ modes of spin coupling. Rather than quote weights of particular modes, it proves particularly convenient for systems such as these to examine instead matrix elements $\langle \hat{s}_i.\hat{s}_j \rangle$ [25,26], in which the i,j subscripts correspond directly to those on the orbitals. Spin correlation matrices, evaluated over the total spin function [27], are reported in the lower (upper) triangles of

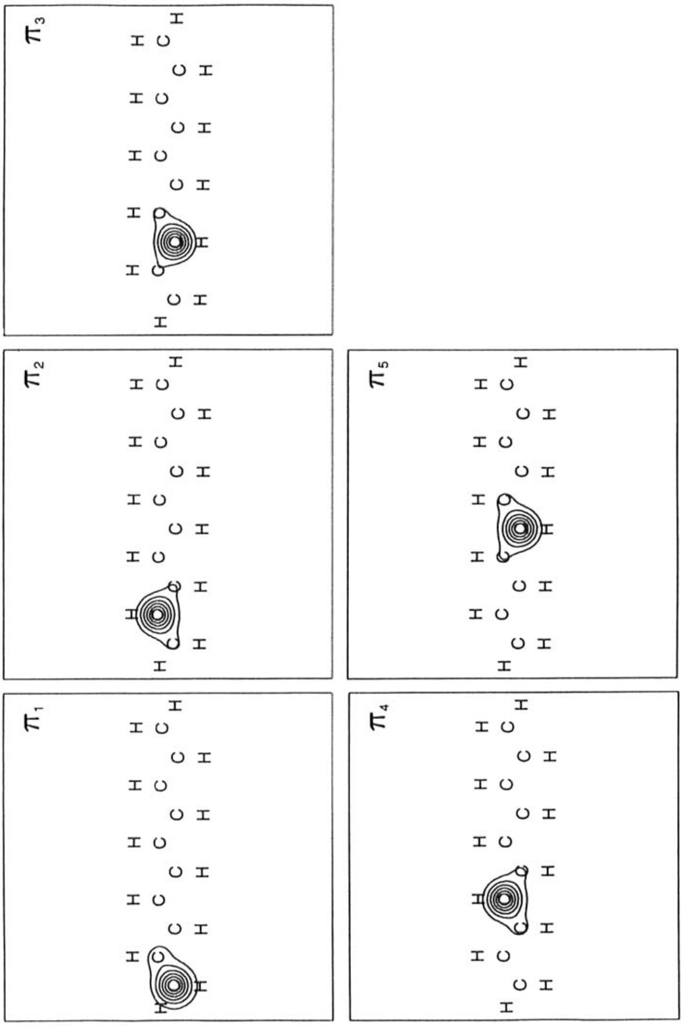

Figure 3 Symmetry-unique modern VB π orbitals for the $(1)^1A_g$ root of the model polyene system with n_C=10. The representation is analogous to that in Figure 1.

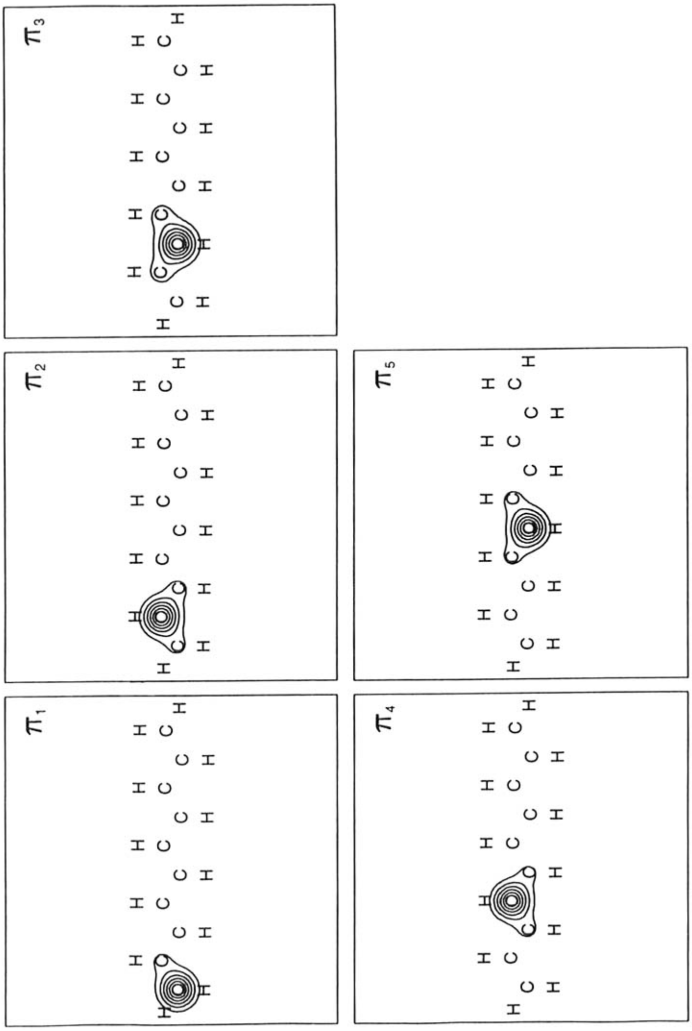

Figure 4 Symmetry-unique modern VB π orbitals for the $(2)^1A_g$ root of the model polyene system with n_C=10. The representation is analogous to that in Figure 1.

Table VII for the first (second) roots of ^1A_g symmetry. The value $\langle \hat{s}_i.\hat{s}_j \rangle = -\frac{3}{4}$ indicates that the spins of electrons i and j are strictly singlet coupled, whereas $\langle \hat{s}_i.\hat{s}_j \rangle = +\frac{1}{4}$ indicates that they are strictly triplet coupled. The corresponding matrix element in the case of no coupling between the two spins is zero.

The spin correlation matrix for the ground state indicates a clear alternation in nearest-neighbour values, with values approaching $-\frac{3}{4}$ for sites $(2i+1,2i)$ associated with larger orbital overlaps, as in the conventional Kekulé-like structure for a *trans*-alternating polyene. The corresponding nearest-neighbour values for the second root also show a clear alternation, but with the most negative values ($\approx -\frac{1}{2}$) associated instead with sites $(2i,2i+1)$, as in the alternative Kekulé-like structure for a *trans*-alternating polyene. It is noticeable, in this context, that $\langle \hat{s}_1.\hat{s}_2 \rangle$ and $\langle \hat{s}_1.\hat{s}_{10} \rangle$ adopt almost the same value. The ground state shows a very simple propagation of spin-spin correlation along the chain, with alternating positive and negative values which decrease in magnitude with increasing distances between the sites. This does not appear to be true in the CASVB wave function for the second root, for which the corresponding pattern is very much more complicated.

TABLE VII. Spin correlation matrices $\langle \hat{s}_i.\hat{s}_j \rangle$ evaluated over the total spin function for the model polyene system with $n_C=10$. Values in the lower triangle relate to the $(1)^1A_g$ root and those in the upper triangle to the $(2)^1A_g$ root.

	1	2	3	4	5	6	7	8	9	10
1		–0.37	0.16	0.07	–0.15	0.12	–0.17	–0.13	0.07	–0.36
2	–0.70		–0.53	0.06	0.00	–0.09	0.10	–0.04	0.02	0.07
3	0.16	–0.20		–0.18	–0.02	0.12	–0.17	0.05	–0.04	–0.13
4	–0.16	0.14	–0.65		–0.50	0.01	0.02	–0.19	0.11	–0.17
5	0.10	–0.08	0.18	–0.30		–0.25	0.03	0.10	–0.08	0.11
6	–0.12	0.08	–0.19	0.17	–0.64		–0.51	0.00	–0.02	–0.14
7	0.05	–0.04	0.09	–0.09	0.16	–0.24		–0.18	0.06	0.07
8	–0.07	0.05	–0.12	0.09	–0.17	0.16	–0.60		–0.53	0.16
9	0.03	–0.02	0.06	–0.05	0.07	–0.07	0.14	–0.20		–0.35
10	–0.04	0.03	–0.09	0.06	–0.10	0.08	–0.16	0.16	–0.70	

The CASVB representations of the CASSCF wave functions for these model *trans*-regular polyenes indicate that excitation from the ^1A_g ground state to the second root of the same symmetry is mainly a matter of spin recoupling, with somewhat less significant changes to the orbitals.

As we have indicated, the CASVB procedures may also be used for the fully-variational optimization of modern VB wave functions. This allows us to investigate for the ground states of these model polyene systems the extent to which the modern VB representations obtained from the CASSCF wave functions by means of the overlap criterion resemble the corresponding fully-variational spin-coupled results. The energies from such fully-variational calculations, which include full optimization of the core orbitals, are labelled 'SC' in Table VIII. All of the CASVB wave functions were found to be symmetry pure, without the need to impose any symmetry relationships amongst the orbitals.

TABLE VIII. CASVB and CASSCF energies (in hartree) for $(1)^1A_g$ roots of the model polyene systems.

	n_C=4	n_C=6	n_C=8	n_C=10
`max`(S_{VB})	−153.0908073	−229.0701699	−305.0498741	−381.0296606
`min`(E_{VB})	−153.0908098	−229.0702304	−305.0500691	−381.0300478
SC	−153.0908098	−229.0702305	−305.0500693	−381.0300484
CASSCF	−153.0910254	−229.0712853	−305.0522941	−381.0336176

As anticipated earlier, in our discussion of the results obtained by maximizing S_{VB}, we find that the wave functions are little changed if we choose instead to minimize E_{VB} (see Table VIII). In addition, we find for these systems that the further changes associated with fully-variational optimization of the modern VB wave functions are even smaller. Thus, the representations obtained simply by maximizing S_{VB} are very similar indeed to the best one may achieve with fully-variational optimization of wave functions of this type. The differences in energy between the full CASSCF wave functions and the dominant modern VB components obtained by means of the overlap criterion, arise mostly from ionic structures rather than from changes to the orbital spaces. Even in the largest system, with n_c=10, the total weight of all the ionic structures is only 0.43%, but this translates into an energy contribution of nearly 4 millihartree.

4 Conclusions

The CASVB strategy provides a very practical means for transforming the total CASSCF wave function into representations in which a very compact and easy-to-interpret modern VB component is dominant. Much the same technology can be, and has been, used to generate fully-variational single and multiconfigurational modern VB wave functions [7], but this is not an aspect that we have pursued in much detail in the present account.

Examples of some of the types of information that may be obtained from such modern VB wave functions have been illustrated here by means of applications to the ground state of benzene, to the $X^4\Delta$ and $a^6\Delta$ state of FeH, and to the two lowest ^1A_g states of various model polyene systems. It has to be hoped that widespread use of the CASVB procedures via packages such as MOLPRO [8] could diminish the traditional barriers between molecular orbital and valence bond theory.

References

1 T. Thorsteinsson, D.L. Cooper, J. Gerratt, P.B. Karadakov, and M. Raimondi, *Theor. Chim. Acta* **93**, 343 (1996).

2 T. Thorsteinsson, Ph.D. thesis (University of Liverpool, UK, 1995).

3 T. Thorsteinsson and D.L. Cooper, *Theor. Chim. Acta* **94**, 233 (1996).

4 T. Thorsteinsson, D.L. Cooper, J. Gerratt, and M. Raimondi, Molec. Eng. (in press).

5 T. Thorsteinsson, D.L. Cooper, J. Gerratt, and M. Raimondi, Theor. Chim. Acta **95**, 131 (1997).

6 T. Thorsteinsson and D.L. Cooper, J. Math. Chem. (in press).

7 D.L. Cooper, T. Thorsteinsson and J. Gerratt, Int. J. Quant. Chem. (in press).

8 MOLPRO is a package of *ab initio* programs written by H.-J. Werner and P.J. Knowles, with contributions from J. Almlöf, R.D. Amos, A. Berning, M.J.O. Deegan, F. Eckert, S.T. Elbert, C. Hampel, R. Lindh, W. Meyer, A. Nicklaß, K. Peterson, R. Pitzer, A.J. Stone, P.R. Taylor, M.E. Mura, P. Pulay, M. Schütz, H. Stoll, T. Thorsteinsson and D.L. Cooper.

9 H.-J. Werner and P.J. Knowles, J. Chem. Phys. **82**, 5053 (1985); P.J. Knowles and H.-J. Werner, Chem. Phys. Lett. **115**, 259 (1985).

10 P.Å. Malmqvist, Int. J. Quant. Chem. **30**, 479 (1986) .

11 D.L. Cooper, J. Gerratt and M. Raimondi, Chem. Rev. **91**, 929 (1991).

12 J. Gerratt, D.L. Cooper, P.B. Karadakov and M. Raimondi, Chem. Soc. Rev. **26**, 87 (1997).

13 R. Pauncz, Spin Eigenfunctions (Plenum Press, New York, 1979)

14 B.H. Chirgwin and C.A. Coulson, Proc. Roy. Soc. Lond. A **201**, 196 (1950).

15 P.-O. Löwdin, Arkiv. Mat. Astr. Fysik. **35A**, 9 (1947).

16 G.A. Gallup and J.M. Norbeck, Chem. Phys. Lett. **21**, 495 (1973).

17 G.A. Gallup, R.L. Vance, J.R. Collins, and J.M. Norbeck, Adv. Quant. Chem. **16**, 229 (1982).

18 S.R. Langhoff and C.W. Bauschlicher, J. Mol. Spec. **141**, 243 (1990).

19 A.J.H. Wachters, J. Chem. Phys. **52**, 1033 (1970).

20 T.H. Dunning, J. Chem. Phys. **90**, 1007 (1989).

21 S.D. Loades, D.L. Cooper, J. Gerratt and M. Raimondi, J. Chem. Soc. Chem. Comm., 1604 (1989).

22 D.L. Cooper, S.D. Loades and N.L. Allan, J. Mol. Struct. (THEOCHEM) **229**, 189 (1991).

23 S.D. Loades, Ph.D. thesis (University of Liverpool, UK, 1992).

24 D.L. Cooper, N.L. Allan and P.J. Grout, J. Chem. Soc. Faraday Trans. 2 **85**, 1519 (1989).

25 G. Raos, J. Gerratt, D.L. Cooper and M. Raimondi, Chem. Phys. **186**, 233 (1994); *ibid* **186**, 251 (1994).

26 G. Raos, S.J. McNicholas, J. Gerratt, D.L. Cooper, and P.B. Karadakov, J. Phys. Chem. A (in press).

27 D.L. Cooper, R. Ponec, T. Thorsteinsson, and G. Raos, Int. J. Quant. Chem. **57**, 501 (1996).

On the Electronic Structure of ScB^+ : Ground and Low-Lying Excited States

APOSTOLOS KALEMOS and ARISTIDES MAVRIDIS

National and Kapodistrian University of Athens, Department of Chemistry, Laboratory of Physical Chemistry, P.O. Box 64004, 157 10 Zografou, Athens-Greece.

Abstract

The electronic structure of the ScB^+ cation has been studied using MRCI (CASSCF + single + double replacements) techniques and large basis sets, (21s16p9d6f/10s5p2d1f) generalized contracted to [7s6p4d3f/4s3p2d1f]. From the manifold of molecular states emanating from the ^3D_g, ^1D_g, ^3F_g atomic states of Sc^+ and the ground ^2P_u state of the B atom, we have analyzed a series of eight low-lying excited states of symmetries $^4\Sigma^-$, $^2\Sigma^+(2)$, $^2\Sigma^-$, $^2\Pi(2)$, and $^2\Delta(2)$, spanning an energy range of about 1 eV. For all states full potential energy curves have been constructed and spectroscopic constants have been extracted via a standard Dunham analysis. The ground $X^4\Sigma^-$ state of ScB^+ traces its ancestry to the $Sc^+(^3D_g;M=+1)+B(^2P_u;M=-1)$ atomic fragments, with a binding energy of 44.9 kcal/mol at R_e=2.160 Å. The binding mode of the $X^4\Sigma^-$ state can be considered as the result of three half bonds, a σ and two π bonds.

List of contents

1. Introduction
2. Some technical details
3. Atomic States
4. Results and Discussion
5. Synopsis and final remarks
References

ADVANCES IN QUANTUM CHEMISTRY, VOLUME 32
Copyright ©1999 by Academic Press. All rights of reproduction in any form reserved.
0065-3276/99 $30.00

1. Introduction

Compounds containing transition metal atoms are of considerable interest due to their catalytic and other important material properties [1]. The multifaceted and intricate chemistry of the transition metal elements and their cations derives mainly from the many low-lying atomic states [2], which in turn are due to the similarity of nd, (n+1)s, and (n+1)p orbitals both in spatial extension and energy [3]. The high density of states is, of course, responsible for creating unusual binding modes in such systems, imposing at the same time stringent computational conditions if one wishes to examine their properties by ab-initio methods. Therefore, the quantitative examination of molecules containing transition metal atoms forces us to investigate rather simple systems with the purpose of gleaning some insight in their behaviour, particularly their binding mechanisms and dissociation energies.

We have performed ab initio calculations on the diatomic molecule scandium boride cation, ScB^+, determining the electronic structure both of its ground state and of a series of low-lying excited states.

In the last fifteen years, concerning the first and second row elements of the periodic table, the following diatomic molecules containing the Sc atom have been examined by ab initio post–HF methods : ScH [4], ScH^+ [5], $ScHe^+$ [6], ScLi [7], $ScLi^+$ [8], ScN [9], ScN^+ [10], ScN^{2+} [11], ScO [12], ScO^+ [13], ScF [14], and $ScNe^+$ [6]. We see that the ScB^+ (and the ScB) is in obvious omission and the present work intends to fill this gap, while work is in progress on the TiB^+, VB^+ and CrB^+ systems. As far as we know, no experimental data are available on ScB^+.

2. Some technical details

With the purpose of obtaining accurate dissociation energies (D_e) and binding mechanisms for all nine states considered, a method is required that will ensure a balanced description for all states involved, at all nuclear geometries, from equilibrium to dissociation limits. In the present case with five valence (active) electrons, the CASSCF+1+2 (Complete Active Space SCF + single + double replacements = MRCI) method seems to be the most suitable, being at the same time computationally tractable. Although the MRCI method is not size-extensive [15, 16], due to the relative small number of active electrons, the effect on our results is for all practical purposes negligible.

The (reference) CAS space selected is comprised of ten orbital functions, six of which correspond to the valence space of the Sc^+(4s, 3d), and the rest to the valence space of the B atom (2s, 2p). The number of configuration functions (CFs) resulting from distributing five electrons among ten orbitals, ranges from 500 to 800 CFs depending on the symmetry. Although our calculations were performed under C_{2v} symmetry, all CASSCF wave functions display pure (axial) angular momentum symmetry, i.e., Λ=0, 1 or 2, Σ, Π, and Δ respectively.

Dynamical correlation was extracted mainly by single and double excitations out of the reference CAS-space. To keep the calculations manageable the approach of "internally contracted" CISD was employed (icMRCI) [17]. Thus our largest CI-expansion reached the number of approximately half a million CFs. Despite the fact that on the CI calculations no $C_{\infty v}$ restrictions were imposed, no serious symmetry breaking problems were detected.

The basis set expansion of the metal is the ANO set of Bauschlicher [18] but with the functions of g-symmetry removed : (21s16p9d6f) contracted to [7s6p4d3f]. For the B atom the correlation consistent basis set of Dunning [19], cc-pVTZ, (10s5p2d1f) contracted to[4s3p2d1f], was employed.

Due to the nature of our PECs (*vide infra*) we were forced to use the state-average (SA) technique [20, 21]. Numerical experiments for some of the states performed with-and-without the SA-method around equilibrium geometries, showed that losses in total energies due to the SA approach were less than 1 mh.

All calculations were done with the MOLPRO suite of codes [22] ; around equilibrium geometries and for certain states, our results were also checked by the COLUMBUS [23] code.

3. Atomic States

The Hartree-Fock energies of the Sc and Sc^+ in their ground states are -759.735546 and -759.538831 h, the former being 0.34 mh higher than the numerical HF value [24] ; corresponding valence-CISD (4s3d) energies are -759.777570 and -759.545129 h. The SCF, CISD and valence full-CI energies of the ground ^2P state of the B atom are -24.528098, -24.596634, and -24.598722 h respectively. While our atomic HF calculations display full rotational symmetry, correlated calculations were done under C_{2v} symmetry conditions. Because the excited states of the Sc^+ atom, ^1D_g and ^3F_g, and the first excited ^4P_g state of the B atom are involved in the molecular states studied, the accurate calculation of the corresponding atomic energy separations is obviously of interest.

Table I contrasts relative energies of the relevant atomic states with corresponding experimental values [2]. Notice the good agreement between the calculated and experimental $^4P_g \leftarrow {}^2P_u$ energy splitting of the B atom. On the contrary, the calculated separations $^1D_g \leftarrow {}^3D_g$ and $^3F_g \leftarrow {}^1D_g$ of the Sc^+ atom are not in satisfactory agreement with the experimental results, the largest discrepancy being 0.137 eV ($^3F_g \leftarrow {}^1D_g$), due to differential correlation effects [25].

Table I. Theoretical vs Experimental Atomic Energy Separations, ΔE(eV) of Sc^+ and B atoms.

	Sc^+			B
Method/ΔE	$^1D_g \leftarrow {}^3D_g$	$^3F_g \leftarrow {}^1D_g$	$^3F_g \leftarrow {}^3D_g$	$^4P_g \leftarrow {}^2P_u$
SCF	0.470	0.323	0.793	2.091
CISD	0.272	0.431	0.703	3.521
Exp[a]	0.302	0.294	0.596	3.571

[a] Ref. 2, average over M_J values.

4. Results and Discussion

Table II presents total energies, bond lengths and dissociation energies for nine states of Σ, Π and Δ symmetry at CASSCF, icMRCI and icMRCI+Q (icMRCI + Davidson correction) level of theory. Depending on the morphology of the PECs, harmonic frequencies (ω_e) are also given for some of the states. An overall picture of the computed PECs at the icMRCI level is given in Figure 1 ; notice that the energy range in which all nine states are embedded is about 1 eV. In what follows, and for reasons of clarity, we examine each state separately ordering the states according to their symmetry.

Ground, X $^4\Sigma^-$ (1 $^4\Sigma^-$) state. At infinity the wave function is represented by the combination, $\left|X\,^4\Sigma^-\right\rangle \propto \left|4s3d_{xz}2p_y\right\rangle + \left|4s2p_x3d_{yz}\right\rangle$ or in terms of the $Sc^+(^3D_g)$ and $B(^2P_u)$ atomic states,

$$\left|X\,^4\Sigma^-\right\rangle \propto \left|^3D_g;M=+1\right\rangle \otimes \left|^2P_u;M=-1\right\rangle - \left|^3D_g;M=-1\right\rangle \otimes \left|^2P_u;M=+1\right\rangle$$

A schematic representation of the binding mechanism is given by the valence-bond-Lewis diagram

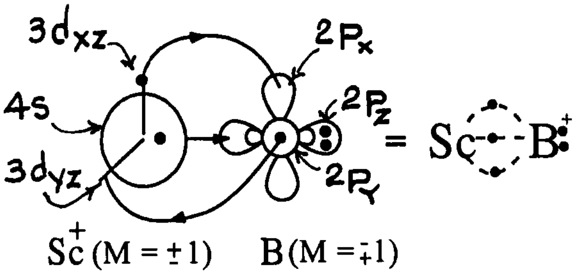

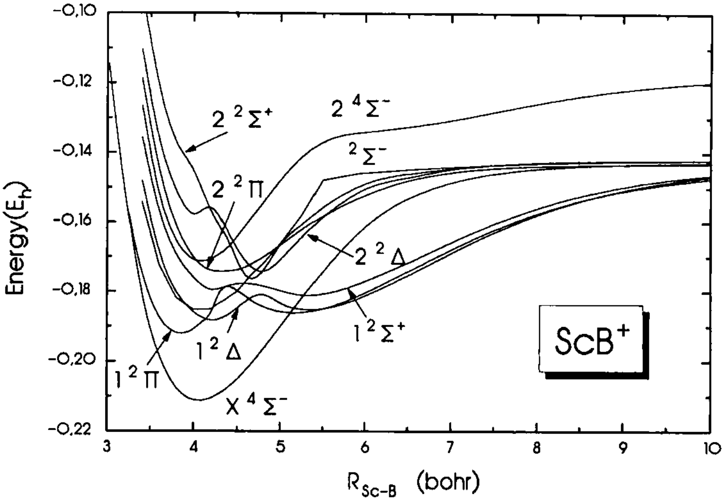

Figure 1. Potential energy curves of ScB^+ at the icMRCI level of theory.

Table II. Energies E(hartree), Bond Distances R_e(Å), Dissociation Energies D_e(kcal/mol), and Harmonic Frequencies ω_e(cm^{-1}) of the $X\ ^4\Sigma^-$, $1\ ^2\Pi$, $1\ ^2\Delta$, $1\ ^2\Sigma^-$, $1\ ^2\Sigma^+$, $2\ ^2\Sigma^+$, $2\ ^2\Pi$, $2\ ^2\Delta$ and $2\ ^4\Sigma^-$ States of ScB^+ in Ascending Energy Order.

State[a]	Method[b,c]	-E	R_e	D_e[d]	ω_e
$X\ ^4\Sigma^-$	CASSCF	784.15011	2.181	38.4	452
	icMRCI	784.21000	2.160	44.9	513
	icMRCI+Q	784.213	2.16	45	500
$1\ ^2\Pi_{(g)}$	CASSCF	784.14775	2.016	21.6	
	icMRCI	784.19190	2.064	31.5	
	icMRCI+Q	784.194	2.05	32	
$1\ ^2\Pi_{(l)}$	CASSCF	784.14307	2.904		
	icMRCI	784.18647	2.737		

(Table II continues)

$1\,^2\Delta_{(g)}$	CASSCF	784.12667	2.211	17.4	
	icMRCI	784.18826	2.233	29.1	
	icMRCI+Q	784.192	2.24	31	
$1\,^2\Delta_{(l)}$	CASSCF	784.13229	2.930		
	icMRCI	784.18528	2.835		
	icMRCI+Q	784.188	2.83		
$1\,^2\Sigma^-$	CASSCF	784.12392	2.109	16.3	
	icMRCI	784.18563	2.167	27.4	
	icMRCI+Q	784.188	2.12	27.6	
$1\,^2\Sigma^+_{(g)}$	CASSCF	784.12697	2.953	17.6	
	icMRCI	784.18118	2.816	24.6	
	icMRCI+Q	784.184	2.80	26	
$1\,^2\Sigma^+_{(l)}$	CASSCF	784.11542	2.206		
	icMRCI	784.17962	2.251		
	icMRCI+Q	784.184	2.26		
$2\,^2\Sigma^+$	CASSCF	784.10716	2.453	5.8	
	icMRCI	784.17682	2.490	21.9	
$2\,^2\Pi$	CASSCF	784.11859	2.280	3.0	
	icMRCI	784.17466	2.293	20.0	438
	icMRCI+Q	784.181	2.28	23	
$2\,^2\Delta$	CASSCF	784.11145	2.483	8.4	
	icMRCI	784.17431	2.532	20.3	
	icMRCI+Q	784.178	2.54	22	
$2\,^4\Sigma^-$	CASSCF	784.11905	2.173	18.9	
	icMRCI	784.17144	2.168	18.1	
	icMRCI+Q	784.174	2.17		

---

[a] “*g*” and “*l*” refers to “global” and “local” minimum respectively, see text.

[b] With the exception of the 1 $^2\Pi$ state the CASSCF results have been obtained by the state-average method.

[c] +Q refers to Davidson correction for quadruples.

[d] With respect to the ground state products.

which suggests that the two atoms are held together by three-half bonds, one half-σ and two half-π bonds. The CASSCF atomic populations at the equilibrium separation

$$\mathrm{Sc} : 4s^{0.28}\ 4p_z^{\ 0.10}\ 3d_\sigma^{\ 0.42}\ 3d_{xz}^{\ 0.56}\ 3d_{yz}^{\ 0.56}$$

$$\mathrm{B} \ :\ 2s^{1.52}\ 2p_z^{\ 0.63}\ 2p_x^{\ 0.40}\ 2p_y^{\ 0.40}\ ,$$

clearly corroborate the above picture. The electronic traffic along the reaction coordinate is shown in the evolution population diagram of Figure 2. We observe how the 4s e$^-$ on Sc$^+$ plummets from 1 e$^-$ at infinity to ~ 0.3 e$^-$ around R_e, the gradual increase of the 2p$_z$ e$^-$ on B to ~ 0.6 e-, and the almost symmetric increase and decrease in electron counts of the d$_\pi$(Sc$^+$) and p$_\pi$(B) respectively. Figure 3 shows the X $^4\Sigma^-$ PEC at the CASSCF and icMRCI level of theory. The former captures the chemistry of the system fairly well as is also obvious from the corresponding D_e and R_e values, Table II : At the icMRCI level the D_e increases by less than 7 kcal/mol, with a decrease in bond length by 0.02 Å as compared to the CASSCF values.

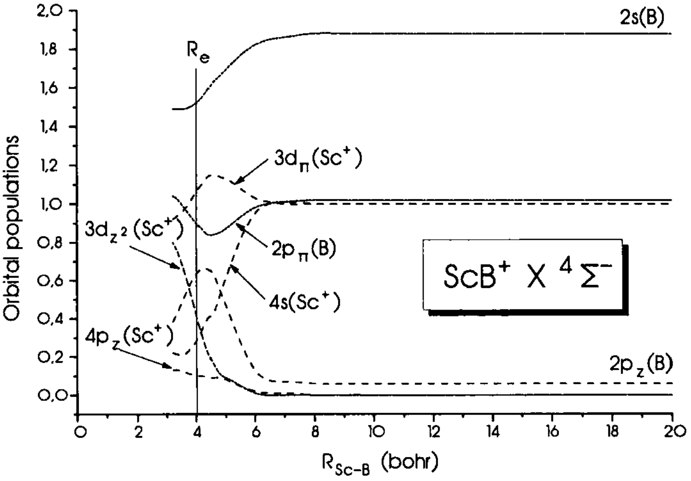

Figure 2. CAS-population evolution diagram of the X $^4\Sigma^-$ state. The perpendicular line R_e refers to equilibrium separation.

2 $^4\Sigma^-$ state. The binding mode in this state is similar to that of the X $^4\Sigma^-$ state, i.e., three-half bonds, one half-σ and two-half π bonds, but the details are entirely different. At infinity the wave function is written as

$$|2\,^4\Sigma^-\rangle \propto \sqrt{4/5}\,|2p_z 3d_{xz} 3d_{yz}\rangle - \sqrt{1/5}\,|2p_z 3d_{x^2-y^2} 3d_{xy}\rangle \;,$$

or in terms of the Sc$^+$ and B atomic states

$$|2\,^4\Sigma^-\rangle \propto |\,^3F_g;M=0\rangle \otimes |\,^2P_u;M=0\rangle \;.$$

At equilibrium the *in situ* Sc$^+$ cation finds itself in the excited ~ ^{3}F state tracing its ancestry there as the PEC shows, Figure 4. A pictorial representation of the wave function at equilibrium, depicting the $\sqrt{4/5}$ component of the function only, is

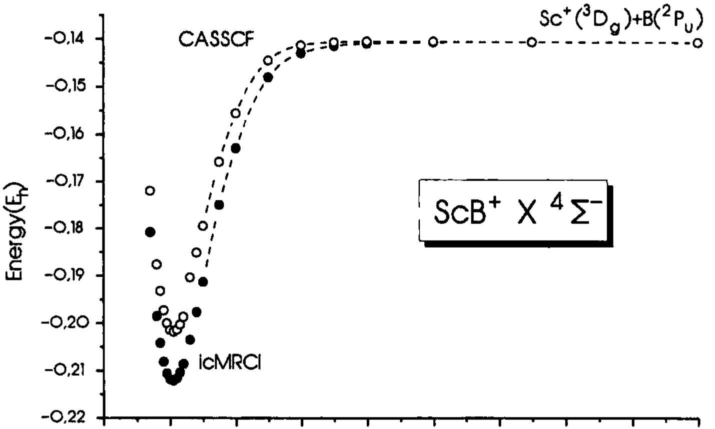

Figure 3. Potential energy curves of the ground $^4\Sigma^-$ state at the CASSCF and icMRCI level of theory.

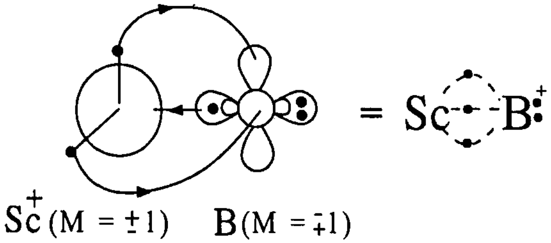

The CAS atomic populations at R_e are

$$\mathrm{Sc} : 4s^{0.67}\, 4p_z^{0.10}\, 3d_\sigma^{0.57}\, 3d_{xz}^{0.38}\, 3d_{yz}^{0.38}$$

$$\mathrm{B} : 2s^{1.57}\, 2p_z^{0.08}\, 2p_x^{0.58}\, 2p_y^{0.58}\ ,$$

in agreement with the above icon. Notice the clear formation of the two half-π bonds, the complete transfer of the $2p_z$-boron electron to the metal with the synchronous formation on the latter of a ~ $4s3d_\sigma$ hybrid. Overall we observe a transfer of 1.35 e^- from the B to the Sc^+ atom via the σ-frame with a concomitant "back donation" of 1.16 e^- via the π-frame from the Sc^+ to the B atom. All of these changes along the reaction path are succinctly shown in the evolution population diagram, Figure 5. The bond lengths of the X $^4\Sigma^-$ and 2 $^4\Sigma^-$ states differ by less than 0.01 Å (Table II) which also reflects the bonding similarity between these two states. Now from ~ 5 to 9 bohr the 2 $^4\Sigma^-$ PEC shows a depression, Figure 4, which is probably due to an avoided crossing between the 2 $^4\Sigma^-$ and 3 $^4\Sigma^-$ states. The latter, shown also in Figure 4, has been calculated at the CASSCF level only due to technical difficulties. At the CASSCF level the 3 $^4\Sigma^-$ state is slightly bound; assuming that the binding energy would increase at a higher level of calculation, the 2 $^4\Sigma^-$ – 3 $^4\Sigma^-$ PECs would interact, creating the aforementioned depression in the 2 $^4\Sigma^-$ state.

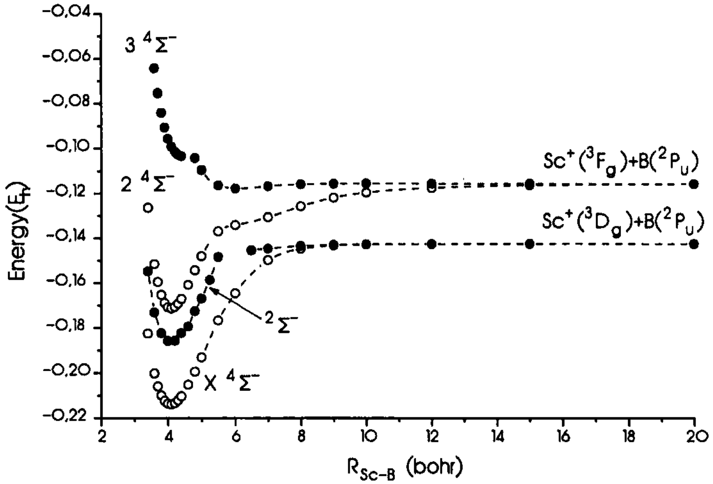

Figure 4. Potential energy curves of Σ^- symmetry states ; the 3 $^4\Sigma^-$ state is at the CASSCF level while the rests at the icMRCI level of theory.

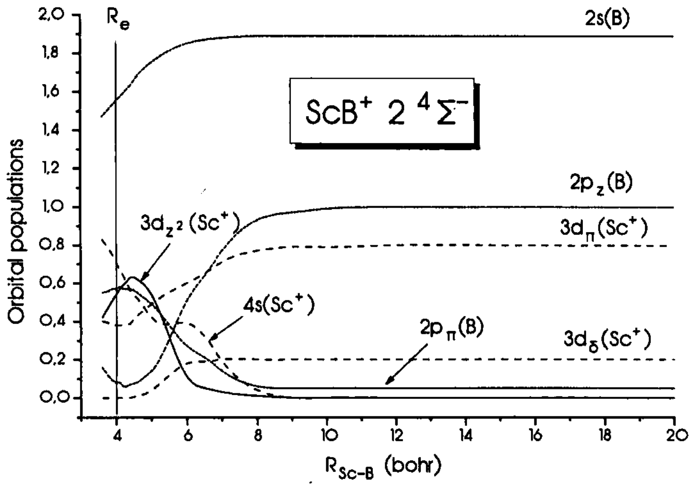

Figure 5. CAS-population evolution diagram of the 2 $^4\Sigma^-$ state.

1 $^2\Pi$ state. As Figure 1 (also see Table II) shows this is the first excited state of the ScB^+ system, being 11.4 kcal/mol above the X $^4\Sigma^-$ state at the icMRCI level of theory. The 1 $^2\Pi$ PEC shown in Figure 6 presents two distinct minima, one "global" (*g*) at 3.90 bohr (Table II) and one "local" (*l*) at 5.18 bohr and higher in energy from the first one by ~ 5.5 mh.

Asymptotically we start with $Sc^+(^3D_g$; M=±1) + $B(^2P_u$; M=0). As the two atoms approach each other a pure σ-bond is formed by coupling into a singlet the 4s e^- on Sc^+ and the $2p_z$ e^- on the B atom : $|^2\Pi\rangle \propto |(4s3d_\pi)_T 2p_z\rangle$, where the subscript T means "coupled into a triplet". The $3d_{xz}(\pi)$ electron remains strictly localized on the metal, while ~ 0.2 e^- are transferred from B to Sc^+ via the σ-frame. As we move in, passing the *l*-minimum at 5.18 bohr, the *g*-minimum is formed at 3.90 bohr while the bond character changes drastically. The overall reaction, from infinity to *l* to *g* can be represented with the following valence-bond-Lewis pictures

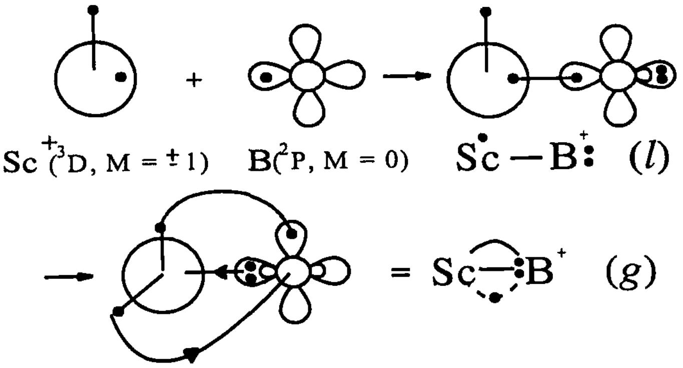

At the *g*-minimum the *in-situ* metal finds itself in the ~ ^3F excited state with M=0, while the B atom has to change its M value to ±1. That is, between the *l*-*g* minima a switching of the M-values occur between the Sc^+ and B atoms. At equilibrium the CASSCF atomic populations of the two minima are as follows

(*l*) $Sc : 4s^{1.08}\, 4p_z^{0.05}\, 3d_\sigma^{0.04}\, 3d_{xz}^{1.0}$

$B : 2s^{1.84}\, 2p_z^{0.84}\, 2p_x^{0.06}\, 2p_y^{0.06}$

(*g*) $Sc : 4s^{0.16}\, 4p_z^{0.10}\, 3d_\sigma^{0.16}\, 3d_{xz}^{0.49}\, 3d_{yz}^{1.05}$

$B : 2s^{1.50}\, 2p_z^{0.06}\, 2p_x^{0.49}\, 2p_y^{0.87}$

As the populations show at the *g*-minimum we have a π-bond, a σ-bond, and a half π-bond from the Sc^+ to the B atom. Also this state has the shortest bond length of all states studied here and the largest intrinsic bond strength, ~ 48 kcal/mol with respect to $Sc^+(^3F_g) + B(^2P_u)$; 0.44 e^- are transferred from B to Sc^+ and ~ 0.5 e^- from Sc^+ to B via the π-frame. It is of interest to mention at this point that we were unable to calculate correctly this 1 $^2\Pi$ state using the COLUMBUS code. As a matter of fact, despite of all our efforts, we obtained two crossing curves of $^2\Pi$ symmetry (Figure 7). The lowest in energy presents a minimum at R_e=3.88 bohr with an energy E=-784.19078 h and correlating to $Sc^+(^3F_g) + B(^2P_u)$, obviously corresponding to the *g* part of the 1 $^2\Pi$ state (Figure 6), while the other one presents its minimum at R_e=5.22 bohr, E=-784.18507 h dissociating to $Sc^+(^3D_g)+B(^2P_u)$ corresponding to the (*l*) part of the 1 $^2\Pi$ state. Somehow, and inadvertently, we have constructed the two "diabatic" PECs that give rise to the morphology of the adiabatic 1 $^2\Pi$ curve (Figure 6).

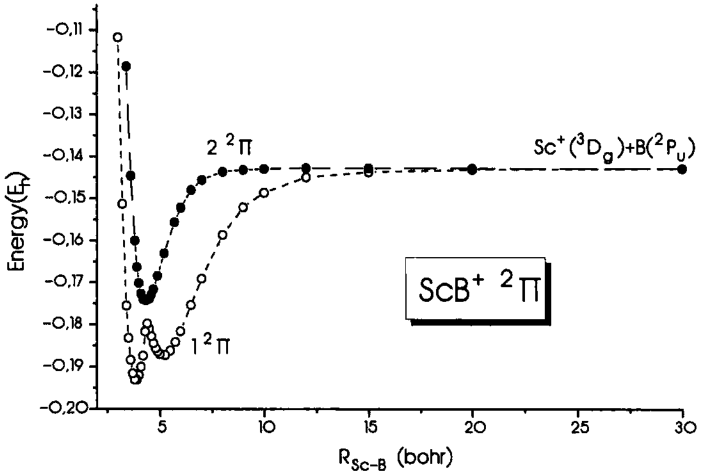

Figure 6. Potential energy curves of the 1 $^2\Pi$ and 2 $^2\Pi$ states at the icMRCI level of theory ; the double well of the 1 $^2\Pi$ is due to an avoided crossing.

The population evolution diagram of the 1 $^2\Pi$ PEC shown in Figure 8 summarizes essentially our conclusions for this state. For instatnce, the 4s orbital on Sc^+ maintains up to 5 bohr, where the *l*-minimum occurs, a constant population of

~ 1 e^-, but around 4 bohr plummets to ~ 0.15 e^- where the *g*-minmum occurs. This situation is similar but more pronounced with the $2p_z$ function on B : it starts asymptotically with 1 e^- and almost retains its population up to the first min, ~ 5 bohr. Passing the 5 bohr point it plummets and its population practically vanishes. The $3d_{xz}$ and $3d_{yz}$ on the metal follow an opposite route, i.e., the former starts from 1 e^- at infinity and ends up at ~ 0.5 e^- around the equilibrium while the latter at infinity is empty, aquiring ~ 1 e^- around the equilibrium.

2 $^2\Pi$ state. The PEC of the 2 $^2\Pi$ state is shown in Figure 6 along with the 1 $^2\Pi$ PEC for reasons of comparison. Notice that both these states correlate to the same asymptotic products, $Sc^+(^3D_g)$ + $B(^2P_u)$. Numerical equilibrium results are presented in Table II. Here, the molecule is created via a half π-bond as the result of electron transfer from B to Sc^+, and a σ-bond as the result of electron transfer along the molecular axis from Sc^+ to B.

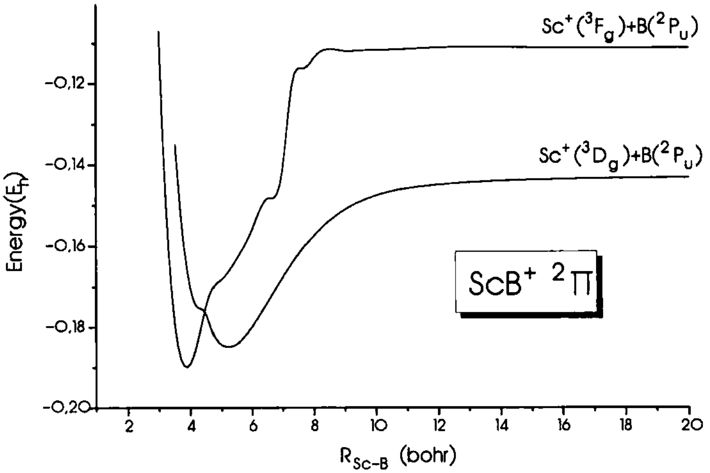

Figure 7. Potential energy curves of $^2\Pi$ symmetry with erroneous crossing. Calculated by the COLUMBUS code at the MRCI level.

We have the following valence-bond-Lewis cartoon

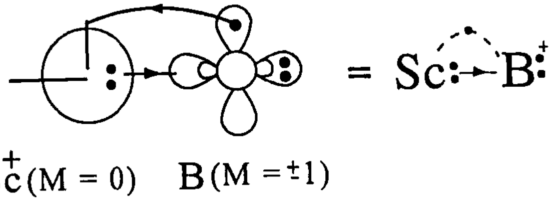

with the CASSCF equilibrium populations

$$\mathrm{Sc} : 4s^{0.75}\, 4p_z^{0.08}\, 3d_\sigma^{0.77}\, 3d_{xz}^{0.37}$$

$$\mathrm{B} : 2s^{1.56}\, 2p_z^{0.67}\, 2p_x^{0.60}\, 2p_y^{0.09}$$

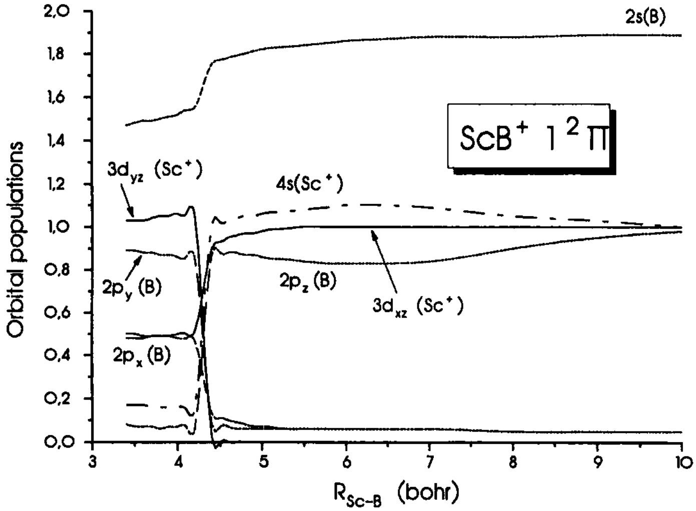

Figure 8. CAS-population evolution diagram of the 1 $^2\Pi$ state.

Approximately 0.8 e$^-$ are "circling" around, ~ 0.4 e$^-$ from the $2p_x$ of B are trasferred to the $3d_{xz}$ of Sc$^+$, and ~ 0.4 e$^-$ from the hybrid ~ $4s3d_\sigma$ to the $2p_z$ of B.

1 $^2\Delta$ and 2 $^2\Delta$ states. Figure 9 displays the icMRCI PECs of these two states and Table II the equilibrium numerical results. Asymptotically we start with the metal in its $\left|{}^3D_g;M=\pm2\right\rangle$ state and with the B atom in the $\left|{}^2P_u;M=0\right\rangle$ state, i.e., $\left|{}^3D_g;M=\pm2\right\rangle\otimes\left|{}^2P_u;M=0\right\rangle$, or in terms of the atomic orbitals, $\sim\left|(4s3d_\Delta)_T 2p_z\right\rangle$. As the B moiety moves in with the p_z e^- along the internuclear axis a σ-bond is formed around 5.37 bohr (*l*-minimum) with a d_Δ electron strictly localized, playing no essential rôle in the bonding, but simply carrying the symmetry of the state. Forcing the B atom closer a global (*g*) minimum is formed, with synchronous change in the M values of both atoms, $Sc^+(M=\pm1)$ and $B(M=\pm1)$ to satisfy the Δ symmetry. Now the two atoms are held together by a π-bond and a half σ-bond. The valence-bond-Lewis icons and the corresponding atomic populations are as follows

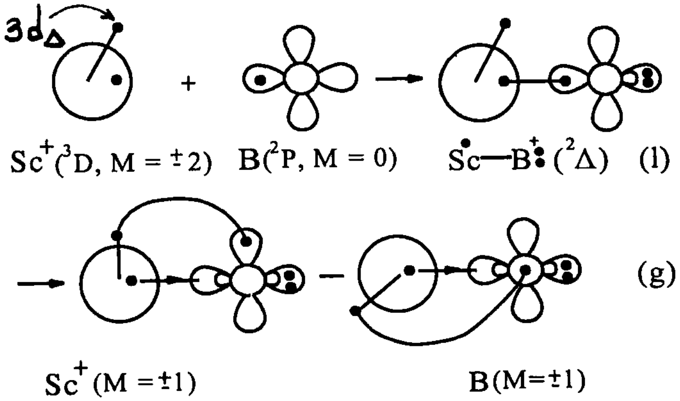

(*l*) $Sc: 4s^{1.06}\,4p_z^{0.06}\,3d_\sigma^{0.05}\,3d_\Delta^{1.00}$

$B: 2s^{1.84}\,2p_z^{0.86}\,2p_x^{0.06}\,2p_y^{0.06}$

(*g*) $Sc: 4s^{0.37}\,4p_z^{0.08}\,3d_\sigma^{0.30}\,3d_{xz}^{0.58}\,3d_{yz}^{0.58}$

$B: 2s^{1.53}\,2p_z^{0.67}\,2p_x^{0.40}\,2p_y^{0.40}$.

From the "*l*" to the "*g*" minimum, notice the dramatic bond shortening (by ~ 0.6 Å), while the total energy drops by 3 mh (Table II). At this point an observation is pertinent : The $^2\Delta$ has two components, $^2A_1$ and $^2A_2$ under C_{2v} symmetry. At the *g*-minimum the $^2A_1$ component can be written as $\sim (|\sigma\pi_x^2\rangle - |\sigma\pi_y^2\rangle)(\alpha\beta - \beta\alpha)\alpha$ and this is shown pictorially in the previous icon. However, the $^2A_2$ component, of course degenerate with the $^2A_1$, can be written as

$$\sim |\sigma\pi_x\pi_y\rangle[0.77(2\alpha\alpha\beta - \alpha\beta\alpha - \beta\alpha\alpha) - 0.45(\alpha\beta - \beta\alpha)\alpha] \;,$$

This last wave function can be represented pictorially by

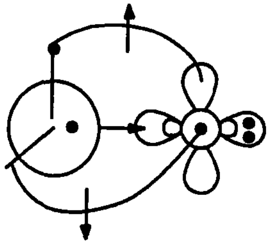

This last picture suggests that we have three half bonds, two π half bonds, from Sc^+ to B and from B to Sc^+ and one σ half bond from Sc^+ to B. The above discussion shows that in molecules of this type an "objective" interpretation of the binding mode is not always plaussible.

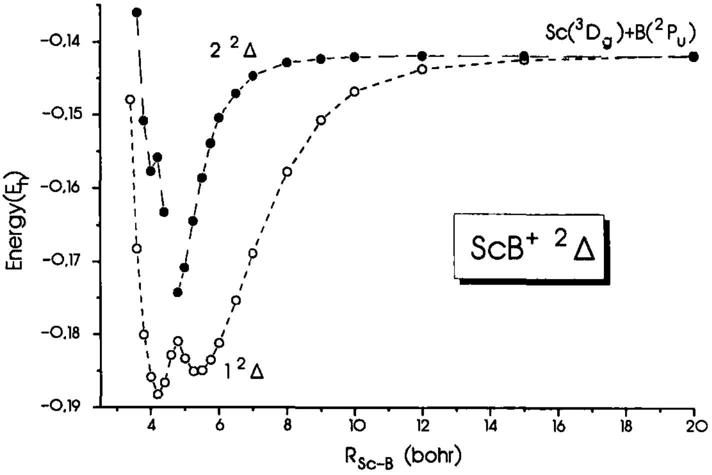

Figure 9. Potential energy curves of $1\,^2\Delta$ and $2\,^2\Delta$ states at the icMRCI level presenting avoided crossing.

The asymptote of the 2 $^2\Delta$ state ($^2A_1$ component) can be written, $|2\,^2\Delta\rangle \propto |4s(2p_x3d_{xz})_S\rangle - |4s(2p_y3d_{yz})_S\rangle$ or in terms of the atomic functions $|2\,^2\Delta\rangle \propto |^3D_g;M=\pm1\rangle \otimes |^2P_u;M=\pm1\rangle$, with its PEC shown in Figure 9. Observe a second avoided crossing around the distance of 4 bohr which originates from the ^1D_g state of the Sc^+ atom. At equilibrium this 2 $^2\Delta$ state can be represented by the wave function $|2\,^2\Delta\rangle \propto 0.7|(\sigma^2)\sigma^2\delta^1\rangle + 0.4(|\sigma^1\pi_x^2\rangle - |\sigma^1\pi_y^2\rangle)$ with CASSCF populations

$$\begin{aligned} Sc &: 4s^{0.78}\,4p_z^{0.07}\,3d_\sigma^{0.13}\,3d_{xz}^{0.25}\,3d_{yz}^{0.25}\,3d_\Delta^{0.60} \\ B &: 2s^{1.70}\,2p_z^{0.78}\,2p_x^{0.21}\,2p_y^{0.21}\;. \end{aligned}$$

The equilibrium bond length, 2.532 Å (Table II) occurs approximately at the average of the *l* and *g* minima of the 1 $^2\Delta$ state. Overall ~ 0.1 e^- are transferred from B to Sc^+.

1 $^2\Sigma^+$ and 2 $^2\Sigma^+$ states. As Figure 10 shows the 1 $^2\Sigma^+$ PEC presents two minima as the result of an avoided crossing between the two $^2\Sigma^+$ states, but the first minimum, i.e., the one that appears at longer distance, 5.33 bohr (Table II) is lower in energy by 1.5 mh from the second which occurs at 4.25 bohr. As a matter of fact and within the accuracy of the present methodology these two minima are degenerate. However as before the bonding mechanism from the one to the other is totally different. Observe the schematic valence-bond-Lewis icons.

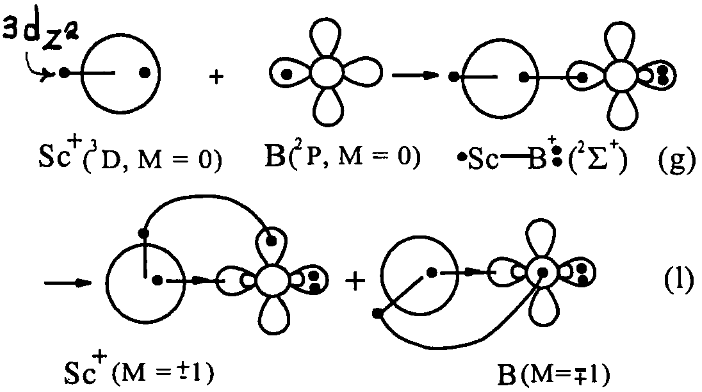

The equilibrium CASSCF populations are

(*l*) $\mathrm{Sc} : 4s^{1.09}\,4p_z^{0.05}\,3d_\sigma^{1.01}$

$\mathrm{B} \;:\; 2s^{1.85}\,2p_z^{0.85}\,2p_x^{0.06}\,2p_y^{0.06}$

(*g*) $\mathrm{Sc} : 4s^{0.38}\,4p_z^{0.08}\,3d_\sigma^{0.30}\,3d_{xz}^{0.57}\,3d_{yz}^{0.57}$

$\mathrm{B} \;:\; 2s^{1.52}\,2p_z^{0.66}\,2p_x^{0.41}\,2p_y^{0.41}$.

At the first minimum, the "*g*", both atoms are in their M=0 state ; we have a pure σ-bond, a transfer of ~ 0.2 e^- from B to Sc^+ and a very large bond length. At the "*l*" minimum, and at a much shorter distance (2.251 Å), both atoms aquire an M=±1 value. The result is a pure π-bond and a half σ-bond from Sc^+ to B. No total charge transfer is observed. This 1 $^2\Sigma^+$ state is $^2A_1$ under C_{2v} symmetry and at equilibrium can be written as $\sim \left(\left|\sigma\pi_x^2\right\rangle + \left|\sigma\pi_y^2\right\rangle\right)(\alpha\beta - \beta\alpha)\alpha$, similar to the 1 $^2\Delta$ ($^2A_1$) but with "+" instead of a "–" sign (*vide supra*).

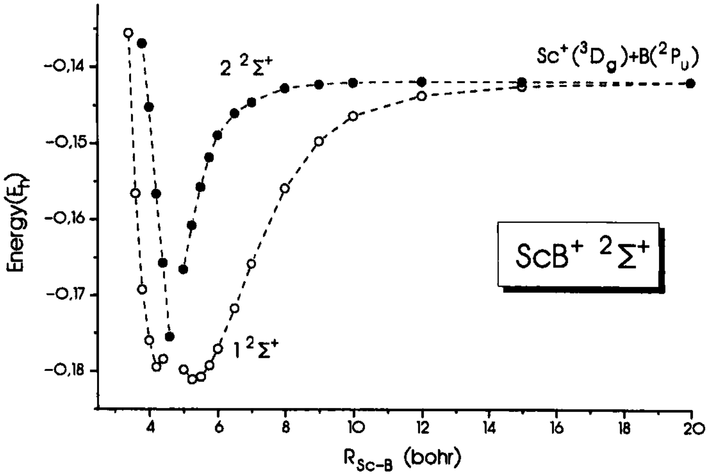

Figure 10. Potential energy curves of 1 $^2\Sigma^+$ and 2 $^2\Sigma^+$ states at the icMRCI level presenting avoided crossing.

The 2 ${}^2\Sigma^+$ state correlating to the $Sc^+({}^3D_g) + B({}^2P_u)$ as the 1 ${}^2\Sigma^+$ (Figure 10), has an asymptotic wave function $|{}^2\Sigma^+\rangle \propto |4s(2p_x 3d_{xz})_S\rangle + |4s(2p_y 3d_{yz})_S\rangle$ or in terms of the atomic states

$$|{}^2\Sigma^+\rangle \propto |{}^3D_g;M=1\rangle \otimes |{}^2P_u;M=-1\rangle + |{}^3D_g;M=-1\rangle \otimes |{}^2P_u;M=1\rangle.$$

The molecule is formed through a π-bond and a half σ-bond as the following icon indicates and the equilibrium CASSCF populations corroborate.

$$\begin{aligned} &Sc: 4s^{0.62}\, 4p_z^{0.06}\, 3d_\sigma^{0.17}\, 3d_{xz}^{0.56}\, 3d_{yz}^{0.56} \\ &B\ :\ 2s^{1.62}\, 2p_z^{0.53}\, 2p_x^{0.41}\, 2p_y^{0.41}\ . \end{aligned}$$

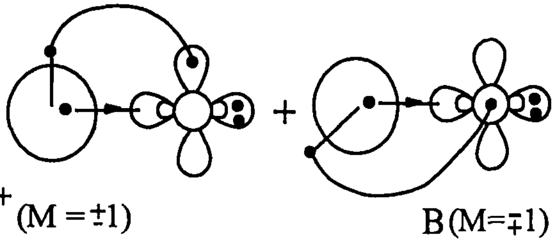

No net charge transfer is observed.

1 ${}^2\Sigma^-$ state. This is exactly similar to the X ${}^4\Sigma^-$ state but with one spin flip to form the doublet. The asymptotic wave function and the valence-bond-Lewis icon are identical with that of the X ${}^4\Sigma^-$ state. The binding mechanism is also similar with that of the X ${}^4\Sigma^-$ state, i.e., it comprises of two half π-bonds and a half σ-bond. This is clear from the equilibrium CASSCF atomic populations

$$\begin{aligned} &Sc: 4s^{0.20}\, 4p_z^{0.12}\, 3d_\sigma^{0.52}\, 3d_{xz}^{0.55}\, 3d_{yz}^{0.55} \\ &B\ :\ 2s^{1.55}\, 2p_z^{0.56}\, 2p_x^{0.41}\, 2p_y^{0.41}\ , \end{aligned}$$

which are practically the same with the populations of the X ${}^4\Sigma^-$ state. Figure 4 shows the 1 ${}^2\Sigma^-$ PEC, as well as the X ${}^4\Sigma^-$ PEC for reasons of comparison ; at the icMRCI level the bond distance (Table II) between the two states differ by

0.015 Å, again indicating the similarity of the states. At equilibrium the wave function of the $1^2\Sigma^-$ ($^2A_2$) state can be written as

$$\sim\left|\sigma\pi_x\pi_y\right\rangle[0.77\,(2\alpha\alpha\beta-\alpha\beta\alpha-\beta\alpha\alpha)+0.45(\alpha\beta-\beta\alpha)\alpha]$$

which differs from the $^2A_2$ component of the $^2\Delta$ state in the sign of the spin function, "+" here, "–" in the $^2\Delta$ state (*vide supra*). Notice finally the kink in the $1\ ^2\Sigma^-$ PEC around 5 bohr, Figure 4 ; the cause of this is shown in Figure 11. This last figure presents the $1\ ^2\Sigma^-$ and $2\ ^2\Sigma^-$ PECs at the CASSCF level of theory only. It is obvious that the kink of the $1\ ^2\Sigma^-$ PEC is due to an avoided crossing between a repulsive $^2\Sigma^-$ state correlating to $Sc^+(^3D_g)$ + $B(^2P_u)$ and the $2\ ^2\Sigma^-$ which traces its ancestry to $Sc^+(^1D_g)$ + $B(^2P_u)$. We have another avoided crossing between the repulsive $2\ ^2\Sigma^-$ PEC and the $3\ ^2\Sigma^-$ PEC which correlates to $Sc^+(^3F_g)$ + $B(^2P_u)$. As previously mentioned we were unable to calculate the $2\ ^2\Sigma^-$ PEC at the icMRCI level because of technical reasons.

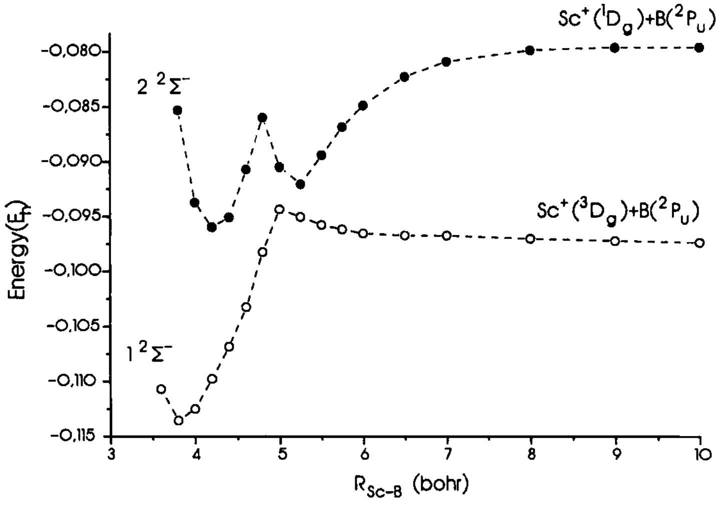

Figure 11. Potential energy curves of $1\ ^2\Sigma^-$ and $2\ ^2\Sigma^-$ states at the CASSCF level.

5. Synopsis and final remarks

At the icMRCI level of theory we have calculated full PECs for nine states of the scandium boride cation, ScB$^+$. The symmetry of the ground state is $^4\Sigma^-$ with a bond distance of 2.160 Å and a binding energy of 44.9 kcal/mol. We believe that the first excited state is of $^2\Pi$ symmetry, ~ 11.5 kcal/mol above the X $^4\Sigma^-$ state. Table III presents a summary of D$_e$'s, R$_e$'s of all states, as well as, their binding mechanism in a schematic way by employing simple Lewis-like pictures. It is worth emphasizing the following points

1. A very large number of bound states is packed in a short, ~ 1 eV, energy range. Some of the states are essentially degenerate within the accuracy of our calculations ; for instance the 2 $^2\Pi$ and 2 $^2\Delta$ states differ by ~ 0.5 mh, Tables II and III.

2. We have a variety of binding schemes (codified in Table III) ranging from three half-bonds to simple σ-bonds.

3. In the states 1 $^2\Sigma^+_g$, 1 $^2\Delta_l$ and $^2\Pi_l$, where the molecule is held together by a pure σ-bond, the binding energy is practically the same for all three states, ranging from 25 to 28 kcal/mol.

4. Bond lengths vary significantly from state-to-state, the shorter and larger bond distances being 2.064 (1 $^2\Pi_g$) and 2.835 (1 $^2\Delta_l$) Å.

5. During bond formation and for the states 2 $^4\Sigma^-$, 2 $^2\Delta$, 1 $^2\Sigma^+$ about 0.2 e$^-$ are transferred from B to Sc$^+$, for the rest of the states no significant charge movement occurs.

6. Due to avoided crossings the PECs of the states 1 $^2\Pi$, 1 $^2\Delta$ and 1 $^2\Sigma^+$ present double minima characterized formally as "*g*" and "*l*", global and local respectively. Due to very small energy barriers between the *g* and *l* minima bond distances for these states are not well defined. This is particularly obvious in the state 1 $^2\Sigma^+$, Figure 10, where the energy barrier between the two minima is ~ 1 mh.

7. All our MRCI calculations are size extensive within 0.5 mh.

Table III. Summary of "Schematic" Binding Modes, Bond Distances R_e(Å), and Dissociation Energies D_e(kcal/mol), of the Ground (X $^4\Sigma^-$) and Eight Low-Lying States in Ascending Energy Order of ScB^+, and at the icMRCI level of theory.

State[a]	Binding Mode[b]	R_e	D_e[c]
X $^4\Sigma^-$	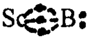	2.160	44.9
1 $^2\Pi_{(g)}$	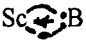	2.064	31.5
1 $^2\Pi_{(l)}$	Sċ—B:	2.737	
1 $^2\Delta_{(g)}$	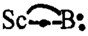	2.233	29.1
1 $^2\Delta_{(l)}$	Sċ—B:	2.835	
$^2\Sigma^-$	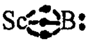	2.167	27.4
1 $^2\Sigma^+_{(g)}$	•Sc—B:	2.816	24.6
1 $^2\Sigma^+_{(l)}$	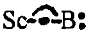	2.251	
2 $^2\Sigma^+$	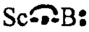	2.490	21.9
2 $^2\Pi$	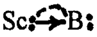	2.293	20.0
2 $^2\Delta$		2.532	20.3
2 $^4\Sigma^-$	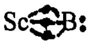	2.168	18.1

[a] *g* and *l* refer to "global" and "local" min, see text.

[b] Bend lines represent π-bonds, straight lines represent σ-bonds, while dashed lines with a dot represent half bonds.

[c] All D_e's are with respect to the ground state products.

References

[1] N. N. Greenwood and A. Earnshaw, *Chemistry of the Elements*, Pergamon Press, Oxford (1984)

[2] C. E. Moore, *Atomic Energy Levels*, NSRDS-NBS Cirular No. 35, Washington, D. C. (1971)

[3] S. R. Langhoff and C. W. Bauschlicher, Jr., Ann. Rev. Phys. Chem. **39**, 213 (1988)

[4] C. W. Bauschlicher, Jr., and S. P. Walch, J. Chem. Phys. **76**, 4560 (1982)

[5] A. E. Alvarado-Swaisgood and J. F. Harrison, J. Phys. Chem. **89**, 5198 (1985)

[6] H. Partridge, C. W. Bauschlicher, Jr., and S. R. Langhoff, J. Phys. Chem. **96**, 5350 (1992)

[7] J. F. Harrison, J. Phys. Chem. **87**, 1323 (1983)

[8] D. B. Lawson and J. F. Harrison, J. Phys. Chem. **100**, 6081 (1996)

[9] K. L. Kunze and J. F. Harrison, J. Am. Chem. Soc. **112**, 3812 (1990)

[10] K. L. Kunze and J. F. Harrison, J. Phys. Chem. **93**, 2983 (1989)

[11] K. L. Kunze and J. F. Harrison, J. Phys. Chem. **95**, 6418 (1991)

[12] C. W. Bauschlicher, Jr., and P. Maitre, Theor. Chim. Acta **90**, 189 (1995)

[13] J. L. Tilson and J. F. Harrison, J. Phys. Chem. **95**, 5097 (1991)

[14] J. F. Harrison, J. Phys. Chem. **87**, 1312 (1983)

[15] R. J. Bartlett, Annu. Rev. Phys. Cnem. **32**, 359 (1981)

[16] W. Duch and G. H. F. Diercksen, J. Chem. Phys. **101**, 3018 (1994)

[17] H.-J. Werner and P. J. Knowles, J. Chem. Phys. **89**, 5803 (1988) ; P. J. Knowles and H.-J. Werner, Chem. Phys. Lett. **145**, 514 (1988) ; H.-J. Werner and E. A. Reinsch, J. Chem. Phys. **76**, 3144 (1982) ; H.-J. Werner, Adv. Chem. Phys. **LXIX**, 1 (1987)

[18] C. W. Bauschlicher, Jr., Theor. Chim. Acta **92**, 183 (1995)

[19] T. H. Dunning, Jr., J. Chem. Phys. **90**, 1007 (1989)

[20] K. Docken and J. Hinze, J. Chem. Phys. **57**, 4928 (1972)

[21] H.-J. Werner and W. Meyer, J. Chem. Phys. **74**, 5794 (1981)

[22] MOLPRO is a package of *ab initio* programs written by H.-J. Werner and P. J. Knowles, with contributions from J. Almlof, R. D. Amos, A. Berning, M. J. O. Deegan, F. Eckert, S. T. Elbert, C. Hambel, R. Lindh, W. Meyer, A. Nicklass, K. Peterson, R. Pitzer, A.J. Stone, P. R. Taylor, M. E. Mura, P. Pulay, M. Schuetz, H. Stoll, T. Thorsteinsson, and D. L. Cooper.

[23] R. Shepard, I. Shavitt, R. M. Pitzer, D. C. Comeau, M. Pepper, H. Lischka, P. G. Szalay, R. Ahlrichs, F. B. Brown and J.-G. Zhao, Intern. J. Quantum Chem. **S22**, 149 (1988)

[24] P. J. Hay, J. Chem. Phys. **66**, 4377 (1977)

[25] B. H. Botch, T. H. Dunning, Jr., and J. F. Harrison, J. Chem. Phys. **75**, 3466 (1981)

On the effects of basis set truncation and electron correlation in conformers of 2-hydroxy-acetamide

A. Szarecka[†], G. Day[†], P. J. Grout[†] and S. Wilson[‡]
[†] *Physical and Theoretical Chemistry Laboratory,*
University of Oxford, South Parks Road,
Oxford, OX1 3QZ
and
[‡] *Rutherford Appleton Laboratory,*
Chilton, Oxfordshire, OX11 0QX

Abstract

Ab initio quantum chemical calculations have been used to study the differences in energy between two gas phase conformers of the 2-hydroxy-acetamide molecule that possess intramolecular hydrogen bonding. In particular, rotation around the central C-C bond has been considered as a factor determining the structure of the hydrogen bond and stabilization of the conformer. Energy calculations include full geometry optimization using both the restricted matrix Hartree-Fock model and second-order many-body perturbation theory with a number of commonly used basis sets. The basis sets employed ranged from the minimal STO-$3G$ set to 'split-valence' sets up to 6-31G. The effects of polarization functions were also studied. The results display a strong basis set dependence.

Contents

1. Introduction
2. Methods
3. Results
4. Discussion
5. Conclusions
Acknowledgements
References

ADVANCES IN QUANTUM CHEMISTRY, VOLUME 32
Copyright ©1999 by Academic Press. All rights of reproduction in any form reserved.
0065-3276/99 $30.00

1 Introduction

The conformational analysis of the 2-hydroxy-acetamide molecule, a fragment of a tartaric acid monoamide derivative, is viewed as a prototype for the study of amide derivatives of tartaric acid. 2-hydroxy-acetamide, $CH_2(OH)CONH_2$, can adopt one of two intramolecular hydrogen-bonding conformers. These conformers, designated *syn*- and *anti*-, are shown in Figures 1 and 2, respectively. The relative stability of these two conformers is, in part, dictated by the stabilization resulting from the hydrogen-bond formed. The two conformers are distinguished by the mutual arrangement of the hydroxyl and amide functional groups, and, therefore, rotation about the central *C-C* bond. The hydrogen-bond in the *syn*-conformer is formed between the proton-donating hydroxyl group and the proton-accepting carbonyl oxygen, while, in the *anti*-conformer, the amide group and the hydroxyl oxygen act as proton donator and acceptor, respectively.

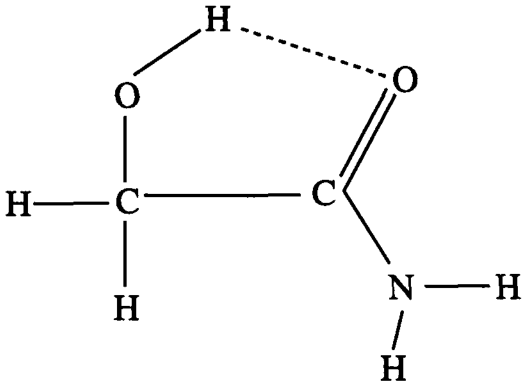

Figure 1: The *syn*-conformer of 2-hydroxy-acetamide.

Interest in the structure of the hydrogen-bond in tartaric acid and its derivatives stems from their increasingly important roles as chiral auxiliaries in asymmetric synthesis [1] [2] [3], which is important in organic and, particularly, pharmaceutical chemistry, as well as their use as racemate resolving agents in chromatography [4] [5]. It is the hydrogen-bonding in tartaric acid and its derivatives which is believed to be central to their resolving and chiral-specific catalytic activity[4]. For these reasons, a study of the hydrogen-bonding in a simple model molecule can be seen to be important.

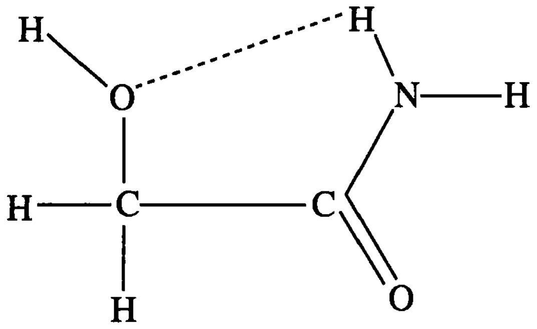

Figure 2: The *anti*-conformer of 2-hydroxy-acetamide.

The purpose of the present study is to determine the conformational preference of 2-hydroxy-acetamide using *ab initio* quantum chemical methods. Intramolecular hydrogen-bonding is believed to have a strong influence on the relative stability of the conformers. The study of intramolecular hydrogen-bonding by *ab initio* quantum chemical calculations is made difficult by the approximation techniques which are necessary for a theoretical description of a system such as this. The small energy differences calculated by *ab initio* quantum mechanical techniques are very sensitive to the choice of basis set used to parametrize the orbitals and to the calculation of electron correlation effects.

In the present study, the difference between the energies of the two conformers are determined for restricted Hartree-Fock calculations using nine commonly used basis sets. Calculations are made using unaugmented basis sets ranging from the minimal $STO\text{-}3G$ to split-valence $6\text{-}31G$ basis sets and the effects of supplementary polarization functions is also investigated. The same basis sets are used in calculations including second-order electron correlation energy corrections and the basis set dependence of the correlation energies is also studied.

It should be emphasized that the computational characteristics of the methods and basis sets used in this study are such that applications to larger systems, and, in particular, tartaric acid and its derivatives, would be feasible with moderate computer resources. More sophisticated correlation treatments, for example, higher order perturbation theory or cluster expansions[6] [7], and basis sets capable of supporting a higher accuracy, for example, the universal basis sets[8] [9] or the correlation consistent basis sets developed by Dunning and his coworkers[10]-[15], could be used for the 2-

hydroxy-acetamide molecule but, at present, could not be applied so readily to larger systems, such as the amide derivatives of tartaric acid.

It is well known that for intermolecular hydrogen-bonded systems[16] *"the weakness of the bond causes problems in that the basis set superposition error can be a sizeable percentage of the interaction energy"* and this *"produces a distortion in the optimal geometry"*. For intermolecular hydrogen bonded systems the so-called counterpoise corrections[17]-[25] widely used in studies of van der Waals interactions can be employed[8] [26] . Such corrections are not applicable to intramolecular interactions. For basis sets which are sufficiently large and flexible the basis set superposition error is small. Indeed, when systematic sequence of even-tempered basis sets are employed in studies of van der Waals interactions the basis set can be extended until the superpositions error (as measured by the counterpoise correction) is negligible [25] [27]. However, except for small systems, this approach remains computationally intractable at present. In the present work, attention has been focussed on a range of standard basis sets of a size that would facilitate applications to larger systems and, in particular, the amide derivatives of tartaric acid.

Electron correlation effects are known to be important in systems with weak interactions. Studies of van der Waals interactions have established the importance of using methods which scale linearly with the number of electrons[28] [29]. Of these methods, low-order many-body perturbation theory, in particular, second order theory, offers computational tractability combined with the ability to recover a significant fraction of the electron correlation energy. In the present work, second order many-body perturbation theory is used to account for correlation effects. Low order many-body perturbation theory has been used in accurate studies of intermolecular hydrogen bonding (see, for example, the work of Xantheas and Dunning[30]).

There have been previous studies of intramolecular hydrogen bonding using *ab initio* quantum chemical methods which take account of electron correction effects [31]-[34]. Teppen *et al*[32] investigated both the basis set dependence and the effects of electron correlation in the conformational analysis of 1,2-ethanediol and 1,2,3-propanetriol. They reported calculations at the "HF/4-21G", "HF/6-311G**" and "MP2/6-311G**" levels of theory. They found that electron correlation has a significant effect on the internal coordinates and the depths of the associated energy minima. Teppen *et al* found that the inclusion of electron correlation effects in an *ab initio* calculation selectively stabilizes those conformers with more intramolecular hydrogen bonds.

2 Methods

Finite basis set (matrix) restricted Hartree-Fock calculations were performed and then used as a reference for the many-body perturbation theory expansion for electron correlation effects[35]-[36], which, in this work, is truncated at second order in the energy.

Four standard basis sets introduced by Pople and his co-workers[38]-[47] were used for geometry optimizations and energy calculations, while calculations are also presented with *d*-type polarization functions added to first row and heavier atoms only (designated by a *, *e.g.* $6\text{-}21G^*$) and with *p*-type polarization functions added to hydrogens as well as the *d*-type functions added to heavier atoms (designated by a **, *e.g.* $6\text{-}21G^{**}$). This gives a sequence of nine basis sets used to study the relative energies of the two conformers of 2-hydroxy-acetamide; $STO\text{-}3G$, $3\text{-}21G$, $3\text{-}21G^{**}$, $6\text{-}21G$, $6\text{-}21G^*$, $6\text{-}21G^{**}$, $6\text{-}31G$, $6\text{-}31G^*$, and $6\text{-}31G^{**}$.

The algorithm[1] using internal coordinates due to Schlegel[48]-[50] was employed, at both the restricted Hartree-Fock and correlated level of theory, to fully optimize the geometries of both conformers, for each basis set. The energies were determined for the calculated stationary geometries. The choice of initial geometry used to start calculations has a very small effect on the stationary geometry and, therefore, energy found. An initial guess for the geometry of the molecule was taken from average bond lengths (*e.g.* 1.54Å for $C\text{-}C$ and 1.21Å for $C{=}O$) and standard angles (*e.g.* 109.5° around a tetrahedral carbon atom and 120° around a trigonal planar nitrogen atom). This guess for the geometry was used to start a restricted Hartree-Fock $STO\text{-}3G$ geometry optimization. The resulting geometry was then used as an initial geometry for all other restricted Hartree-Fock calculations. The initial geometries used for calculations which took account of correlation effects were the optimized geometries from the matrix Hartree-Fock calculations on the same conformer using the same basis set.

The calculations reported in the present paper have been carried out using the *GAUSSIAN94* programs of Frisch *et al*[37] using various computers in the Physical and Theoretical Chemistry Laboratory, University of Oxford, at the Rutherford Appleton Laboratory and at the Poznań Supercomputing and Networking Center.

---

[1] designated the 'Berny' algorithm in the GAUSSIAN94 program[37]

3 Results

3.1 Restricted matrix Hartree-Fock energies

The restricted Hartree-Fock energies, in Hartree, calculated from the optimized structures of both conformers (*syn-* and *anti-*) of 2-hydroxy-acetamide are given in Table 1 for all nine basis sets used in this study. The difference between the calculated energies of the *syn-* and *anti-* conformers is also given in milliHartree. A negative energy difference shows a more stable *syn-*conformer and a positive energy difference showing that the *anti*-conformer is calculated to be energetically preferred for a given choice of basis set at the restricted Hartree-Fock level of theory.

Table 1

Calculated restricted Hartree-Fock energies and energy differences between the *syn-* and *anti-* conformers. Energies are given in Hartree (H); energy differences in milliHartree (mH)

Basis Set	E_{syn}/H	E_{anti}/H	$\Delta E_{syn-anti}/\text{mH}$
$STO\text{-}3G$	-279.109335	-279.108041	-1.294
3-21G	-281.248683	-281.249306	+0.623
3-21G^{**}	-281.294484	-281.294886	+0.402
6-21G	-282.427302	-282.428056	+0.754
6-21G^{*}	-282.568932	-282.567674	-1.258
6-21G^{**}	-282.592485	-282.591039	-1.446
6-31G	-282.701907	-282.704948	+3.041
6-31G^{*}	-282.824705	-282.824595	-0.110
6-31G^{**}	-282.842712	-282.842497	-0.215

3.2 Total Energies Through Second-Order

The total energies calculated through second-order in the many-body perturbation expansion with respect to a Møller-Plesset reference hamiltonian for the optimized structures of both the *syn-* and *anti-* conformers of 2-hydroxy-acetamide are given in Table 2 for all nine basis sets considered in this study. The difference between these calculated total energies of the *syn-* and *anti-*conformers is also given in milliHartree. Again, a negative energy difference

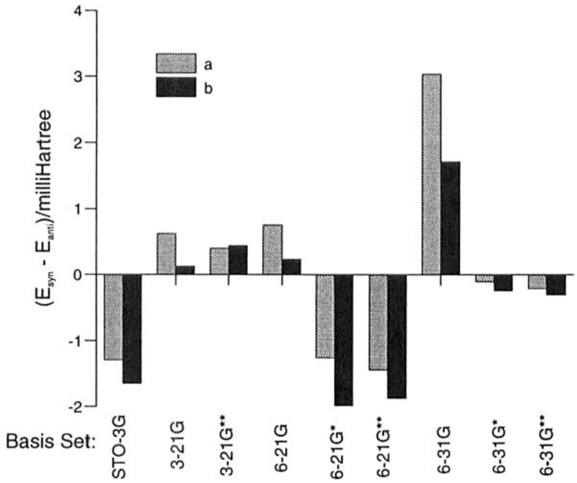

Figure 3: Energy difference between the *syn*- and *anti*-conformer for a) restricted matrix Hartree-Fock energies b) total energies through second-order.

shows a more stable *syn*-conformer and a positive energy difference showing that the *anti*-conformer is calculated to be more stable.

A histogram showing the calculated total energy differences between the *syn*- and *anti*- conformers at both the restricted Hartree-Fock and correlated levels of theory for all nine basis sets used is given in Figure 3. In this Figure, the 'lightly' shaded bars are the energy differences resulting from the restricted matrix Hartree-Fock calculations whilst the 'heavily' shaded bars refer to the difference between the total energies through second-order.

Table 2

Calculated total energies including second order correlation effects.
Energies are given in Hartree (H); energy differences
are given in milliHartree (mH).

Basis Set	E_{syn}/H	E_{anti}/H	$\Delta E_{syn-anti}$/mH
STO-$3G$	-279.366160	-279.364508	-1.652
3-21G	-281.772370	-281.772498	+0.128
3-21G^{**}	-281.857426	-281.857863	+0.437
6-21G	-282.951454	-282.951690	+0.236
6-21G^{*}	-283.328247	-283.326263	-1.984
6-21G^{**}	-283.380550	-283.378680	-1.870
6-31G	-283.233720	-283.235434	+1.714
6-31G^{*}	-283.593947	-283.593700	-0.247
6-31G^{**}	-283.640210	-283.639903	-0.307

Table 3

Calculated second order correlation energies.
Energies and energy differences are given in milliHartree (mH).

Basis Set	$E_{corr,syn}$/mH	$E_{corr,anti}$/mH	ΔE_{corr}/mH
STO-$3G$	-256.825	-256.468	-0.357
3-21G	-523.687	-523.192	-0.495
3-21G^{**}	-562.942	-562.977	+0.035
6-21G	-524.152	-523.634	-0.518
6-21G^{*}	-759.315	-758.589	-0.726
6-21G^{**}	-788.065	-787.641	-0.424
6-31G	-531.812	-530.486	-1.326
6-31G^{*}	-769.242	-769.105	-0.137
6-31G^{**}	-797.498	-797.407	-0.091

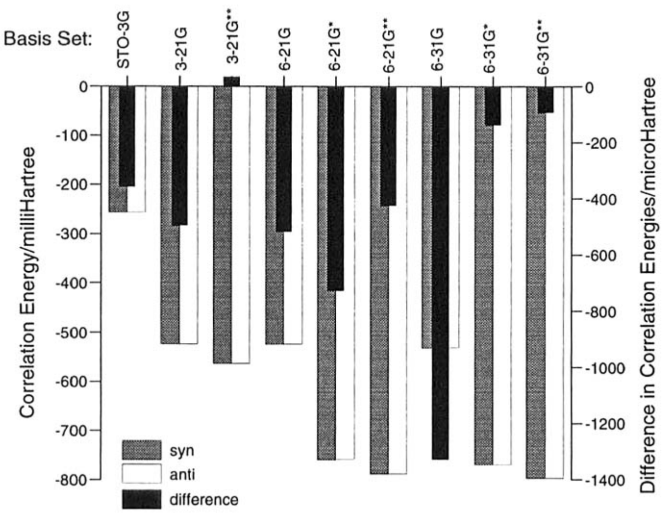

Figure 4: Calculated second-order correlation energies (left-hand axis) and the difference between the calculated correlation energies for the *syn-* and *anti-* conformers (right-hand axis).

3.3 Correlation Energies

The second-order correlation energies calculated with all nine basis sets used in this study are given in Table 3 for both the *syn-* and *anti-*conformers. The difference in the second-order correlation energies between the *syn-* and *anti-*conformers is also given for each basis set used. These results are also displayed graphically in Figure 4 where the 'lightly' shaded bars designate the second-order correlation energy component for the *syn-*conformer, the 'white' bars show it for the *anti-*conformer, and the 'heavily' shaded bars are the differences between the correlation energy components for the two conformers. Note that the correlation energy components should be read from the left-hand axis, which is calibrated in milliHartree, whilst the correlation energy difference refers to the right-hand axis, which is calibrated in μHartree.

4 Discussion

4.1 Matrix restricted Hartree-Fock Energies

Among the nine "standard" basis sets used in this study of the two conformers of 2-hydroxy-acetamide, there is no consistent energetic preference for either the *syn-* or *anti-* conformer at the restricted matrix Hartree-Fock level of theory. While the 3-21G, 3-21G^{**}, 6-21G , and 6-31G basis set calculations indicate that the *anti*-conformer is energetically favoured, the other five basis sets used in this study (STO-3G, 6-21G^{*}, 6-21G^{**}, 6-31G^{*}, 6-31G^{**}) indicate that the *syn*-conformer has a lower energy. Increasing the size of the basis set used in the restricted Hartree-Fock calculations does not increase or decrease the magnitude of the energy difference between the *syn-* and *anti*-conformers nor do larger basis sets consistently lead to a conformational preference.

Basis sets augmented by polarization functions in the restricted Hartree-Fock calculations favour the *syn-* conformer more than the corresponding basis set without the polarization functions. Although the calculations using the 3-21G^{**} basis set indicates that the *anti-* is more stable than the *syn*-conformer, the *anti*-conformer is less favoured in these calculations than the calculations with the corresponding basis set without polarization functions, *i.e.* 3-21G. Furthermore, comparison between the energies calculated with the 6-21G^{*} and 6-21G^{**} basis sets and between the calculations using the 6-31G^{*} and 6-31G^{**} basis sets shows that augmenting the hydrogen atoms as well as the heavier atoms with polarization functions results in an additional stabilization of the *syn*-conformer with respect to the *anti*-conformer.

4.2 Total Energies Through Second-Order

As with the restricted matrix Hartree-Fock results, the total energies through second-order show no consistent energetic preference for either the *anti-* or *syn*-conformer. Also, there is no trend in the magnitude or sign of the energy difference as the basis set is increased in size. Inspection of Figure 3 shows that the total energies through second-order display the same conformational preferences as the corresponding calculations at the restricted matrix Hartree-Fock level of theory.

The augmentation of the basis sets with polarization functions has the same effect in the correlated calculations as they do in the restricted matrix Hartree-Fock calculations, *i.e.* basis sets with d-polarization functions added to the heavy atoms show a greater energetic stabilization for the *syn*-conformer and further augmentation with p-polarization functions added to the hydrogens stabilizes the *syn* -conformer even further. The only exception to this trend in calculations with any of the basis sets used in this study is that the correlated calculations using the 3-21G^{**} basis set favour the *anti* -configuration of the molecule more than the calculations made with the 3-21G basis set.

4.3 Second-Order Correlation Energies

The second-order correlation energies were determined to show whether electron correlation effects might favour one conformation of the 2-hydroxy-acetamide molecule over the other. The effects of the basis set on the calculated correlation energy is also of interest.

Except for the calculations made using the 3-21G basis set, all correlation energies were larger in magnitude for the *syn* -conformer, *i.e.* the electron correlation energy favours the *syn* -conformer for all basis sets besides 3-21G, where the correlation energy is very small, but favours the *anti*-conformer.

In addition, Figure 4 shows that the magnitude of the correlation energies, for both conformers of the molecule, has a general increasing trend as the basis set is enlarged, is increased by the addition of polarization functions on the heavy atoms and further increased by further polarization functions on the hydrogen atoms.

5 Conclusions

This study has explored the reliability of *ab initio* quantum chemical calculations in predicting the relative stability of the conformers of a system involving intramolecular hydrogen bonding. The 2-hydroxy-acetamide molecule was employed as a model for studies of the amide derivatives of tartaric acid. “Standard” quantum chemical techniques were employed with “standard” molecular basis sets. The techniques and basis sets were chosen so as to render calculations on the tartaric acid derivatives computationally feasible with moderate computational resources. Full geometry optimizations were carried out for the two possible conformers of the 2-hydroxy-acetamide molecule. The results displayed a strong dependence on basis set employed. The choice of basis set is a crucial factor when finding the energetically preferred conformer for a system which has multiple possibilities for intramolecular hydrogen bonding.

In our conformational studies of the 2-hydroxy-acetamide molecule with nine commonly used basis sets using the restricted matrix Hartree-Fock theory and the second-order many-body perturbation theory, there was no universal agreement as to the energetic preference between the conformers. However, both the restricted matrix Hartree-Fock and the second-order perturbation theory correlated calculations there was a consistent trend in that basis sets augmented with polarization functions all predicted a more stable *syn*-conformer than the corresponding calculations using basis sets without the polarization functions. Furthermore, that the second-order many-body perturbation theory correlation energy components displayed a preference for the *syn*-conformer except in the case of the 3-21G^{**} basis set. For the 3-21G^{**} basis set the correlation energy was found to be slightly larger for the *anti*-conformer. The calculations using basis sets augmented with polarization functions resulted in larger correlation energies, but smaller differences between the correlation energies in both conformers.

Acknowledgments
One of the authors (A.S.) is grateful to the Soros Foundation and the British Foreign and Commonwealth Office for a scholarship held at the University of Oxford. G.D. would like to thank the British Council and the Association of Commonwealth Universities for a scholarship also held at the University of Oxford. S.W. acknowledges the support of E.P.S.R.C. under Grant GR/L65567.

References

[1] T. Katsuki and K. B. Sharpless, *J. Am. Chem. Soc.* **103**, 7690 (1981)

[2] P. Pitchen, E. Duñach, M. N. Deshmukh and H.B. Kagan, *J. Am. Chem. Soc.* **106**, 8188 (1984)

[3] M. Hoffmann, A. Szarecka and J. Rychlewski, *Adv. Quantum Chem. (this volume)*

[4] Y. Dobashi and S. J. Hara, *J. Am. Chem. Soc.* **107**, 3406 (1985)

[5] F. Toda and K. J. Tanaka, *J. Org. Chem.* **53**, 3607 (1988)

[6] S. Wilson, *Electron Correlation in Molecules*, Clarendon Press, Oxford (1984)

[7] S. Wilson (editor), *Electron Correlation in Atoms and Molecules*, Methods in Computational Chemistry, vol. 1, Plenum Press, New York (1987)

[8] S. Wilson, *Adv. Chem. Phys.* **67**, 439 (1987)

[9] D. Moncrieff and S. Wilson, *J. Phys. B: At. Mol. Opt. Phys.* **27**, 1 (1994)

[10] T.H. Dunning, Jr., *J. Chem. Phys.* **90**, 1007 (1989)

[11] R.A. Kendall, T.H. Dunning, Jr. and R.J. Harrison, *J. Chem. Phys.* **96**, 6796 (1992)

[12] D.E. Woon and T.H. Dunning, Jr., *J. Chem. Phys.* **98**, 1358 (1993)

[13] D.E. Woon and T.H. Dunning, Jr., *J. Chem. Phys.* **100**, 2975 (1994)

[14] D.E. Woon and T.H. Dunning, Jr., *J. Chem. Phys.* **103**, 4572 (1995)

[15] T. van Mourik, A.K. Wilson, K.A. Peterson, D.E. Woon and T.H. Dunning, Jr., *this volume*

[16] E.R. Davidson and D. Feller, *Chem. Rev.* **86**, 681 (1986)

[17] E. Clementi, *J. Chem. Phys.* **46**, 3851 (1967)

[18] S.F. Boys and F. Bernardi, *Molec. Phys.* **19**, 553 (1970)

[19] A. Johansson, P. Kollman and S. Rothenberg, *Theoret. chim. Acta* **29**, 167 (1973)

[20] B. Lui and A.D. McLean, *J. Chem. Phys.* **59**, 4557 (1973)

[21] M. Urban and P. Hobza, *Theoret. chim. Acta* **29**, 215 (1975)

[22] N.S. Ostlund and D.L. Merrifield, *Chem. Phys. Lett.* **39**, 612 (1976)

[23] P.D. Dacre, *Chem. Phys. Lett.* **50**, 147 (1977)

[24] S.L. Price and A.J.S. Stone, *Chem. Phys. Lett.* **65**, 127 (1979)

[25] B.H. Wells and S. Wilson, *Molec. Phys.* **50**, 1295 (1983)

[26] J.H. van Lenthe, J.G.C.M. van Duijneveldt-van de Tijdt and F.B. van Duijneveldt, Adv. Chem. Phys. **69**, 521 (1987)

[27] B.H. Wells and S. Wilson, *Chem. Phys. Lett.* **101**, 429 (1983)

[28] B.H. Wells and S. Wilson, *Molec. Phys.* **54**, 787 (1985)

[29] B.H. Wells and S. Wilson, *Molec. Phys.* **55**, 199 (1985)

[30] S.S. Xantheas and T.H. Dunning, Jr., *J. Chem. Phys.* **99**, 8774 (1993)

[31] K.B. Borisenko, C.W. Bock and I. Hargittai, *J. Phys. Chem.* **98**, 1442 (1994)

[32] B.J. Teppen, M. Cao, R.F. Frey and C. van Alsenoy, *J. Molec. Struct. (THEOCHEM)* **120** (1994) 169

[33] K.B. Borisenko, K. Zauer and I. Hargittai, *J. Phys. Chem.* **100**, 19303 (1996)

[34] K.B. Borisenko and I. Hargittai, *J. Molec. Struct.* (THEOCHEM) **388**, 107 (1996)

[35] N.H. March, W.H. Young and S. Sampanthar, *The Many-Body Problem in Quantum Mechanics*, Cambridge University Press (1967)

[36] R. McWeeny, *Methods of Molecular Quantum Mechanics*, Academic Press, London (1989)

[37] M.J. Frisch, G.W. Trucks, H.B. Schlegel, P.M.W. Gill, B.G. Johnson, M.A. Robb, J.R. Cheeseman, T.A. Keith, G.A. Petersson, J.A. Montgomery, K. Raghavachari, M.A. Al-Laham, V.G. Zakrzewski, J.V. Ortiz, J.B. Foresman, J. Cioslowski, B.B. Stefanov, A. Nanayakkara, M. Challacombe, C.Y. Peng, P.Y. Ayala, W. Chen, M.W. Wong, J.L. Andres, E.S. Replogle, R. Gomperts, R.L. Martin, D.J. Fox, J.S. Binkley, D.J. Defrees, J. Baker, J.P. Stewart, M. Head-Gordon, C. Gonzalez and J.A. Pople, *GAUSSIAN94* (Revision D.4), Gaussian, Inc., Pittsburgh, PA (1995)

[38] W.J. Hehre, R.F. Stewart and J.A. Pople, *J. Chem. Phys.* **51**, 2657 (1969)

[39] J.B. Collins, P. v. R. Schleyer, J.S. Binkley and J.A. Pople, *J. Chem. Phys.* **64**, 5142 (1976)

[40] J.S. Binkley, J.A. Pople and W.J. Hehre, *J. Amer. Chem. Soc.* **102**, 939 (1980)

[41] M.S. Gordon, J.S. Binkley, J.A. Pople, W.J. Pietro and W.J. Hehre, *J. Amer. Chem. Soc.* **104**, 2797 (1982)

[42] W.J. Pietro, M.M. Francl, W.J. Hehre, D.J. Defrees, J.A. Pople and J.S. Binkley, *J. Amer. Chem. Soc.* **104**, 5039 (1982)

[43] R. Ditchfield, W. Hehre and J.A. Pople, *J. Chem. Phys.* **54**, 724 (1971)

[44] W. Hehre, R. Ditchfield and J.A. Pople, *J. Chem. Phys.* **56**, 2257 (1972)

[45] P.C. Hariharan and J.A. Pople, *Molec. Phys.* **27**, 209 (1974)

[46] M.S. Gordon, *Chem. Phys. Lett.* **76**, 163 (1980)

[47] P.C. Hariharan and J.A. Pople, *Theo. Chim. Acta.* **28**, 213 (1973)

[48] H. B. Schlegel, *J. Comp. Chem.*, **3**, 137 (1984)

[49] H. B. Schlegel, in *New Theoretical Concepts for Understanding Organic Reactions*, Ed. J. Bartran, Kluwer Academic, The Netherlands (1989)

[50] H. B. Schlegel, "Geometry Optimization on Potential Energy Surfaces", in *Modern Electronic Structure Theory*, Ed. D.R. Yarkony, World Scientific Publishing, Singapore (1994)

Gas-phase Conformational Analysis of (R,R)-Tartaric Acid, its Diamide, N,N,N',N' - Tetramethyldiamide and Model Compounds

Marcin HOFFMANN, Agnieszka SZARECKA, Jacek RYCHLEWSKI
Quantum Chemistry Group Department of Chemistry, A. Mickiewicz University,
Grunwaldzka 6 60-780 Poznań, Poland

Abstract: A review over most recent *ab initio* studies carried out at both RHF and MP2 levels on (R,R)-tartaric acid (TA), its diamide (DA), tetramethyldiamide (TMDA) and on three prototypic model systems (each of them constitutes a half of the respective parental molecule), i.e. 2-hydroxyacetic acid (HA), 2-hydroxyacetamide (HD) and 2-hydroxy-N,N-dimethylacetamide (HMD) is presented. (R,R)-tartaric acid and the derivatives have been completely optimized at RHF/6-31G* level and subsequently single-point energies of all conformers have been calculated with the use of second order perturbation theory according to the scheme: MP2/6-31G*//RHF/6-31G*. In the complete optimization of the model molecules at RHF level we have employed relatively large basis sets, augmented with polarisation and diffuse functions, namely 3-21G, 6-31G*, 6-31++G** and 6-311++G**. Electronic correlation has been included with the largest basis set used in this study, i.e. MP2/6-311++G**//RHF/6-311++G** single-point energy calculations have been performed. General conformational preferences of tartaric acid derivatives have been analysed as well as an attempt has been made to define main factors affecting the conformational behaviour of these molecules in the isolated state, in particular, the role and stability of intramolecular hydrogen bonding. In the case of the model compounds, our study principally concerned the conformational preferences and hydrogen bonding structure within the α-hydroxy-X moiety, where X=COOH, $CONH_2$, $CON(CH_3)_2$.

I. Introduction 1
II. Methods 4
III. Results 6
IV. Discussion and Conclusions 12
References 15

I. INTRODUCTION

Optically active derivatives of tartaric acid (2,3-dihydroxy-butanedioic acid) are of steadily increasing importance in numerous fields of organic and pharmaceutical chemistry as chiral auxiliaries (Katsuki and Sharpless, 1980; Finn et al., 1983) or racemate resolving agents. (Toda et al., 1988; Jaques et al., 1981) Currently they are also gaining interest from material science. (Aakeroy et al., 1992,

Copyright © 1999 by Academic Press. All rights of reproduction in any form reserved.
0065-3276/99 $30.00

1993) This is believed to be mainly due to their enormous capability of creating various types of hydrogen bonding.

At present there is a large amount of experimental data available - mostly X-ray diffraction studies, (Stern and Beevers, 1950; Van Bommel, Bijvoet,1958; Tapscott et al., 1969; Rychlewska, 1992; Szczepańska et al., 1994-1995) VCD, (Polvarapu et al, 1985; Su and Keiderling, 1980) ROA, (Barron, 1978; Barron et al., 1992) NMR (Ascenso and Gil, 1980; Hasa, 1980) measurements and dibenzoate exciton chirality analysis (Gawroński et al., 1989) for both ionic and covalent derivatives of (R,R)-tartaric acid (Fig. 1a).

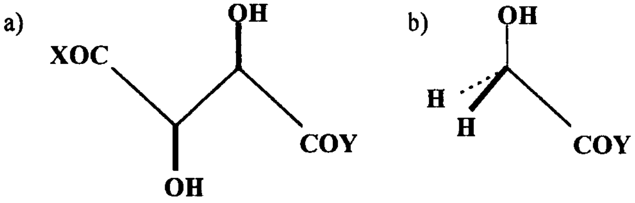

Fig 1. (a) general formula of (R,R)-tartaric acid and its derivatives; (b) general formula of the model compounds.

However, there has not been done much in the field of theoretical conformational analysis of these compounds. Surprisingly this is even the case for the model molecules with the skeleton of hydroxyacetic acid (Fig. 1b). They appear very useful in studying the energetics of certain types of hydrogen bonds occurring in more complex systems such as tartaric acid derivatives and even macromolecules. An investigation of these models is also computationally advantageous since they are significantly smaller and simpler than the parental molecules of the (R,R)-tartaric acid derivatives and therefore we are enabled to employ more accurate methods to examine them with the resources available.

Most recent theoretical studies employed semiempirical methods (Hoffmann et al., 1996; Szarecka et al., 1996) such as based on NDDO formalism: AM1 (Dewar et al., 1985) and PM3 (Stewart, 1989) methods as well as *ab initio* RHF approach (Hehre et al., 1986) to investigate potential energy surfaces of several amide and ester derivatives (Gawroński et al., 1997) of (R,R)-tartaric acid. It has been shown that many local energy minima exist which in some cases differ between one another substantially in both the conformation of the carbon chain and the internal hydrogen bonding structure. However, the energy differences between the conformers obtained from those calculations were often not significantly large. In the gas-phase, the **T** (i.e. trans) conformation (see Fig. 2) of the carbon chain of (R,R)-tartaric acid (R=COOH) and its dimethyldiester (R=$COOCH_3$), with the 5-membered ring type of hydrogen bonds (C=O...HO(α); see Fig. 3) has been found to be of the lowest energy which is in agreement with the solid state, solution and early theoretical (RHF/STO-3G) data (Polvarapu et al., 1985).

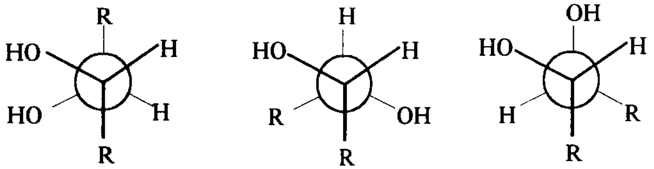

T (trans) G^+ (gauche$^+$) G^- (gauche$^-$)

Fig. 2 Newman projections of 3 staggered conformations of the main carbon chain.

Unlike the acid, its amides that have been so far examined theoretically appear to favour the G+ (i.e. gauche+) conformation of the carbon chain with 6-membered ring type of hydrogen bonding, namely: C=O...HO(β) (cf. Fig. 3). The G+ conformation in the gas phase, on the semiempirical level, has also been found favoured in a non-symmetric derivative: methyl ester of tartaric acid monoamide (In Fig. 1: X=NH_2, Y=OCH_3). This type of conformation has been observed experimentally only in TMDA via NMR in a non-polar solvent. (Gawroński et al., 1997) Solid state data as well as VCD and NMR spectra of the amides in a polar solvent have pointed to the G- (i.e. gauche-) (TMDA: R=$CON(CH_3)_2$) or the T (DA: R=$CONH_2$) conformation (cf. Fig. 2).

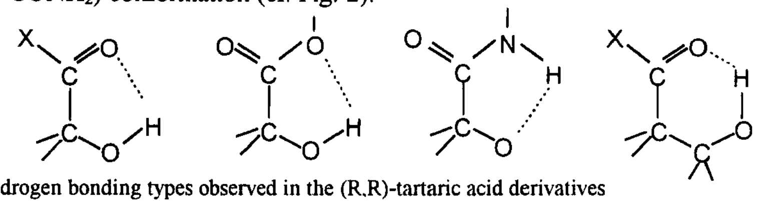

Fig. 3 Hydrogen bonding types observed in the (R,R)-tartaric acid derivatives

In this work we present some further results on TA, TMDA and DA molecules. For the model compounds we have examined their potential energy hipersurfaces and focused on localizing the potential energy minima for all molecules studied.

It is generally accepted that a correct theoretical description of weak interactions, such as hydrogen bonding, depends strongly on the accuracy of method used in calculations and such error sources like neglecting of electronic correlation, finite basis set expansions etc. can strongly affect subtle energy differences between conformers resulting from RHF calculations. (Davidson and Feller, 1986) Therefore we have expected that including electronic correlation via Møller-Plesset second order perturbation theory (Head-Gordon et al., 1988; Pople and Beveridge, 1970) can improve the results considerably.

Experimental studies that have been carried out so far on the model systems were X-ray and neutron diffraction analysis of hydroxyacetic acid (Ellison et al., 1971; Pijper, 1971) and several of its salts, namely rubidium (Golic and Speakman, 1968) and potassium (Mayers et al., 1968) hydrogen bisglycollates as well as lithium glycollate monohydrate.(Colton and Henn, 1965) Glycolic (hydroxyacetic) acid molecule appears nearly planar except for aliphatic and hydroxylic hydrogen atoms. Intermolecular hydrogen bonding networks are observed in all crystal structures. From microwave spectra (Blom and Bauder, 1982) of glycolic acid the O=C-C-OH moiety has also been found planar and internally hydrogen bonded. Theoretical research done on hydroxyacetic acid employed *ab initio* methods (RHF/4-31G - no geometry optimization has been done) (Newton and Jeffreys, 1977), molecular mechanics energy minimisation and molecular dynamics simulations (with the use of GROMOS package). (Stouten et al., 1989) Both quantum-chemical and molecular mechanics methods -in agreement with the experimental data- resulted in the minimum energy conformation being the one with planar O=CC-OH moiety and with the intramolecular hydrogen bonding formed between carbonyl oxygen and α-hydroxyl hydrogen atom. Planar arrangement of the α-hydroxy-carboxylic moiety has also been postulated in Cram (1959) and Cornforth (1959) models of mechanisms of stereospecific additions to carbonyl group.

According to Davidson and Feller (1986): „small split valence (e.g. 3-21G (...)) or split-valence plus polarisation (e.g. 6-31G*) basis sets perform adequately in SCF and correlated geometry optimizations of closed shell organic compounds, but (...) very extended sets with flexible valence spaces and several sets of polarization functions are needed for energy differences accurate to 2-5 kcal mol^{-1} (...)". Therefore in this work we report the RHF results of complete geometry optimisations of three systems containing α-hydroxy - amide/carboxylic moiety at 6-31G*, 6-31++G** and 6-311++G** basis sets (Hehre et al., 1986), where „*" and „+" designates a set of polarisation and diffuse functions respectively. These RHF calculations have been followed by the MP2 correlation energy calculations at the largest basis set used in this study, namely 6-311++G**. We have concentrated on the issue of rotation around C_{sp3}-C_{sp2} which decides about the existence and structure of intramolecular hydrogen bonding. In order to determine the most favoured interactions between these groups, we have considered, and optimised, many structures with different mutual arrangements of α-hydroxyl group and carboxylic/amide group.

II. METHODS

TA, DA, and TMDA

Molecules of (R,R)-tartaric acid (TA), its diamide (DA) and its N,N,N',N'-tetramethyl diamide (TMDA) have been systematically examined using semiempirical AM1 and PM3 methods as described elsewhere. (Hoffmann et al., 1996) It is worth to note, however, that we used a large set of starting structures (270 for each compound), chosen on the basis of all possible combinations of five dihedrals, that we considered conformationally crucial, namely C-C*-C*-C, both H-O-C*-C* and both O=C-C*-O torsion angles. Details of the sequence of computations are shown in Scheme 1.

In the case of the TA and DA molecules all stable conformers obtained from semiempirical methods have been examined at RHF/3-21G level. For TMDA, due to limited computer resources, we have had to limit the number of starting geometries and we have selected several conformers of the lowest energy. (Gawroński et al., 1997) These structures have been examined at 3-21G basis set. After having obtained the results for the TA, DA and TMDA at RHF/3-21G level we have fully reoptimised the geometries with the use of the restricted Hatree-Fock method at another commonly used basis set: 6-31G*. Finally we have performed calculations at MP2/6-31G*//RHF/6-31G* level of theory.

Scheme 1. Computational methods used in examination of the TA, DA and TMDA.

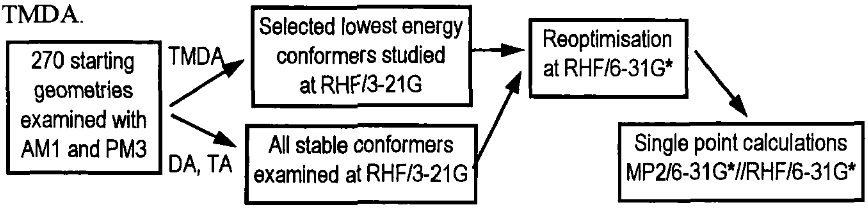
270 starting geometries examined with AM1 and PM3
TMDA
DA, TA
Selected lowest energy conformers studied at RHF/3-21G
All stable conformers examined at RHF/3-21G
Reoptimisation at RHF/6-31G*
Single point calculations MP2/6-31G*//RHF/6-31G*

Scheme 2. Computational methods used in examination of the HA, HD, HDM

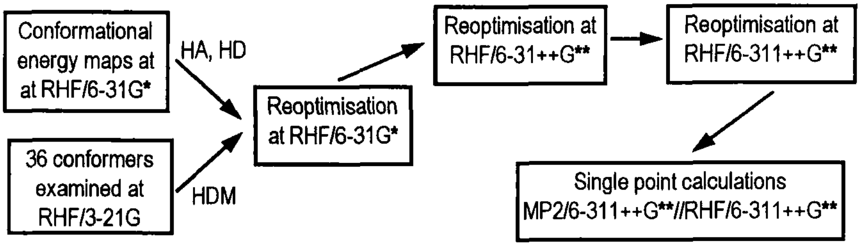
Conformational energy maps at at RHF/6-31G*
HA, HD
36 conformers examined at RHF/3-21G
HDM
Reoptimisation at RHF/6-31G*
Reoptimisation at RHF/6-31++G**
Reoptimisation at RHF/6-311++G**
Single point calculations MP2/6-311++G**//RHF/6-311++G**

HA, HD, HMD

Details of the sequence of computations on the model systems are shown in Scheme 2. For HA and HD we systematically scanned, at 30° grid, the rotation around C_{sp2}-C_{sp3} as well as around C_{sp3}-O(H) bonds at RHF/6-31G*. No optimisation has been done during the scanning. In the case of HMD such a scan at RHF/6-31G* level was not practical therefore we have considered and fully optimised at

RHF/3-21G level 36 starting structures that originated from considering all possible combinations of two torsion angles defining mutual arrangement of α-hydroxyl and carboxylic/amide groups, i.e. O=CC-O and H-OC$_{sp3}$-C$_{sp2}$. We have considered structures with O=CC-O angle varied from 0° to 360° with the step 30° and HOCC equal to 180°, 60° and -60°. Resulting minima have been subsequently reoptimised at 6-31G*, 6-31++G** and 6-311++G** with the starting structure in each calculation being the optimised one from the previous calculation. In the case of HA we additionally examined two conformers with HOC$_{sp2}$-C$_{sp3}$ angle equal 0° and -60° respectively. In MP2 single-point energy calculations we have used the structures optimised at RHF/6-311++G**.

Software

The calculations reported in this work have been carried out using the GAUSSIAN94 (Frisch et al., 1995) and GAMESS (Schmidt et al., 1993) packges implemented on the Silicon Graphics Power Challenge and CRAY J-916 computers at the Poznań Supercomputing and Networking Centre, Poland.

III. RESULTS

In Tables I-III we present RHF and MP2 relative energies as well as selected geometrical parameters of the conformers of (R,R)-tartaric acid diamide (Table I), (R,R)-tartaric acid (Table II), and (R,R)-tartaric acid N,N.N'N'-tetramethyl diamide (Table III). Each of the conformers of these molecules has been designated by a set of 5 characters.

TABLE I

RHF and MP2 study of (R,R)-tartaric acid diamide

conformer	ΔE(RHF) [kcal mol^{-1}]	μ [D]	E_{corr} [hartree]	ΔE(MP2) [kcal mol^{-1}]	CCCC [deg.]	OCCO [deg.]	OCCO [deg.]	HOC*C [deg.]	HOC*C [deg.]
G+aag-g-	0.00	0.83	-1.5362421	0.00	62.6	160.5	160.5	-71.7	-71.7
G+ssg+g+	3.16	0.06	-1.5383617	1.83	51.7	-10.4	-10.5	25.8	25.8
G-aste	3.27	2.68	-1.5371735	2.68	-94.0	172.2	1.3	-146.1	1.9
Taatt	3.64	1.41	-1.5337995	5.17	168.5	154.5	154.5	171.2	171.1
Taag-t	5.79	3.76	-1.5339530	7.23	-175.1	141.6	176.7	-74.8	160.4
Tasg-e	7.21	2.07	-1.5351650	7.89	-160.4	175.9	2.2	-85.0	9.7
G+aag-e+	8.18	1.69	-1.5348881	9.03	53.4	143.4	173.5	-69.4	111.8
Tssg+g+	10.29	2.57	-1.5359710	10.46	161.6	-24.0	-23.9	25.0	24.9
G+aste	11.45	7.19	-1.5359054	11.66	48.3	155.2	-4.1	162.2	-17.1
Tasg+e	10.48	2.95	-1.5338247	12.00	-175.5	166.1	11.0	74.2	-16.6
Taag-g-	11.97	3.78	-1.5344174	13.11	-148.5	161.0	161.0	-50.4	-50.3
G-aag+g+	15.62	3.15	-1.5338857	17.10	-27.0	157.7	-157.7	83.3	83.4

Absolute values (in hartree) of energy (RHF): -564,5148481; (MP2): -566,0510902

TABLE II
RHF and MP2 study of (R,R)-tartaric acid

conformer	ΔE(RHF) [kcal mol^{-1}]	μ [D]	E_{corr} [hartree]	ΔE(MP2) [kcal mol^{-1}]	CCCC [deg.]	OCCO [deg.]	OCCO [deg.]	HOC*C [deg.]	HOC*C [deg.]
Tssee	0.00	2.72	-1.5601811	0.00	174.1	3.5	3.5	-14.0	-14.1
Tsaeg-	1.11	0.78	-1.5599153	1.27	-175.1	-6.0	-171.2	14.4	-56.7
G+aag-g-	1.78	1.64	-1.5604366	1.62	59.8	153.5	153.5	-56.8	-56.8
G+psg-e	3.06	1.12	-1.5611112	2.47	58.4	67.2	-9.2	-60.6	18.1
G+ssg-g-	3.47	1.47	-1.5616626	2.54	47.4	19.0	19.0	-25.8	-25.8
Tsag-g+	2.90	3.23	-1.5596888	3.21	-177.4	8.3	171.8	-34.3	32.8
G+sag-g-	4.55	3.12	-1.5612131	3.90	54.6	-11.6	144.7	-36.8	-58.7
G+speg-	4.82	4.14	-1.5613272	4.10	62.6	-6.6	-116.5	19.0	-62.6
Taag+g-	3.68	3.26	-1.5594885	4.11	-169.2	167.5	-173.7	42.7	-57.5
Taag-g-	4.45	3.05	-1.5598252	4.67	-170.3	-172.6	-172.6	-30.0	-30.0
Tsptg-	5.27	3.33	-1.5610349	4.73	-175.3	7.2	109.5	167.7	-83.4
Taptg-	5.09	1.57	-1.5605840	4.84	-171.7	-172.5	105.9	167.9	-81.2
G-spet	5.30	2.12	-1.5607306	4.96	-66.7	14.0	-124.3	-14.5	-167.6
G+apg+g-	5.84	4.86	-1.5607457	5.48	71.2	166.9	-108.2	45.1	-71.8
G-spet	5.70	2.75	-1.5600771	5.77	-78.9	-14.0	86.8	19.8	-165.6
Tsptg-	7.65	2.39	-1.5616693	6.72	-168.5	7.0	-127.1	173.9	-82.4
G-pptg+	5.65	2.78	-1.5583387	6.81	-69.7	100.8	123.2	-171.9	69.3
Tpptt	5.73	2.24	-1.5583907	6.85	-179.7	123.2	123.2	172.8	172.8
Tpag-t	7.65	3.49	-1.5612468	6.98	-165.5	-126.1	-174.5	-78.5	173.1
G-sag-g-	7.75	3.39	-1.5607865	7.37	-55.8	27.7	-137.3	-30.9	-53.0
G+pag-t	8.08	2.00	-1.5609027	7.63	71.2	-124.2	175.9	-74.8	-178.9
G-apg+t	7.24	5.01	-1.5592147	7.84	-62.4	139.8	-96.8	63.0	-174.5
Taptg+	6.84	2.83	-1.5582676	8.04	-178.5	176.6	132.0	167.0	70.3
G+aag+g+	7.67	0.23	-1.5595607	8.05	45.5	150.1	150.1	39.0	39.0
Tsatg+	7.72	5.23	-1.5592846	8.28	175.8	-3.2	139.2	164.4	61.0
G+sptg-	9.77	2.48	-1.5617987	8.75	62.7	0.9	-128.5	-179.6	-65.0
G-aag-g-	9.09	0.06	-1.5602206	9.06	-56.3	-137.3	-137.3	-56.5	-56.5
G-apg+g-	8.42	2.80	-1.5590272	9.15	-60.2	137.9	68.5	60.9	-55.1
Tpptt	9.71	1.64	-1.5608746	9.28	-161.3	-125.4	-125.4	-160.4	-160.4
G-ppg+g+	8.15	0.09	-1.5579515	9.54	-63.5	108.1	108.1	76.8	76.8
G-apg+g-	10.52	4.79	-1.5599617	10.66	-53.8	151.1	-106.6	54.7	-57.8
G-ppg+g+	10.48	1.63	-1.5592383	11.07	-57.1	-71.2	-71.2	70.6	70.5
G-aatt	11.02	2.35	-1.5591528	11.66	-64.5	-136.0	-136.0	153.4	153.4

Absolute values(in hartree) of energy (RHF): -604,1638845; (MP2): -605,7240656

First character (capital) refers to the conformation of the carbon chain, next two characters describe the mutual arrangement of both COX groups and „their" α-hydroxyl groups; and last two characters describe the positions of hydroxyl hydrogen atoms with respect to the carbon chain. For example, '**T***ssee*' designates the conformer with extended conformation of the carbon chain (CC*C*C is about 180°) and with both COX group in such positions that C=O bonds tend to or nearly eclipse α-C-O bonds (conformation syn; OCC*O about 0°). In this conformation hydroxyl hydrogen atoms are in the *ee* positions, i.e. each OH bond tends to or nearly eclipses C*C bond. Reversely, in the ***a*** conformation C*-O bond is eclipsed by C-X bond of COX group (conformation anti; OCC*O about 180°). Intermediate position of COX group is designated as the ***p*** conformation. Other possible conformations of hydroxyl hydrogen atom are the *g* or the *t* position with respect to the carbon chain. The main carbon chain can in turn be bent to adopt the G+ (CC*C*C is about 60°) or the G- (CC*C*C is about -60°) conformation. Energies are given in atomic units, relative energies (ΔE : the energy differences between each of the conformers and the conformer of the lowest energy) in kcal/mol, torsional angles in degrees.

TABLE III

RHF and MP2 study on N,N,N',N'-tetramethyldiamide

conformer	ΔE(RHF) [kcal mol^{-1}]	μ [D]	E_{corr} [hartree]	ΔE(MP2) [kcal mol^{-1}]	CCCC [deg.]	OCCO [deg.]	OCCO [deg.]	HOC*C [deg.]	HOC*C [deg.]
G+_aag-g-_	0.00	0.17	-2.0673919	0.00	65.1	140.5	140.5	-60.1	-60.0
G+_ssee_	2.72	0.96	-2.0702523	0.92	49.7	25.2	25.2	-16.6	-16.6
♣ **E+_ssee_**	4.95	5.24	-2.0687827	4.07	132.6	15.1	15.1	-15.3	-15.3
T_asg-e_	5.27	3.40	-2.0675284	5.19	-152.7	155.6	8.7	-81.2	-1.5
G-_sag-t_	7.26	4.40	-2.0693140	6.05	-69.6	31.9	-149.3	-24.8	-163.5
[c] **G-_ppg-g-_**	6.91	4.89	-2.0685026	6.21	-58.5	47.8	47.8	-39.3	-39.3
G-_pptt_	8.53	2.18	-2.0639392	10.69	-73.5	108.3	108.3	160.5	160.3
G-_aag+t_	11.14	3.24	-2.0675099	11.07	-38.5	-140.0	-141.5	72.6	-177.9
T_aag+g+_	11.92	4.90	-2.0650373	13.40	-170.6	-159.2	-159.2	73.6	73.6

[c] results of optimisation of crystal structure; ♣ **E+**-eclipsed conformation of the carbon chain
Absolute values (in hartree) of energy (RHF): -720,6107466; (MP2): -722,6781384

Model systems

In Tables IV-VI we present the results of geometry optimizations at RHF level of selected conformers of hydroxyacetic acid, hydroxyacetamide and dimethylhydroxyacetamide respectively. In Tables VII-IX correlation contributions calculated at MP2 level as well as relative energies of the conformers are presented. All conformers of the model compounds are designated in a manner corresponding to the tartaric acid derivatives, i.e. we use the ***s*** and the ***a*** designations for

TABLE IV. Hydroxyacetic acid (HA) - RHF data

	ΔE [kcal mol^{-1}]			O=C-C-O [deg.]			H-O-C-C [deg.]		
	6-31G*	6-31++G**	6-311++G**	6-31G*	6-31++G**	6-311++G**	6-31G*	6-31++G**	6-311++G**
se	0.00	0.00	0.00	0.0	0.1	0.0	-0.1	-0.1	-0.1
ag+	2.11	2.05	2.03	154.7	154.6	154.5	52.7	52.0	52.4
at	5.01	4.75	4.64	172.6	164.7	159.8	178.8	176.0	171.8
st	4.72	4.59	4.33	0.0	0.0	0.0	180.0	180.0	180.0
at*	4.36	3.91	3.79	180.0	180.0	180.0	179.8	179.9	179.9

6-31G*: -302.6569672; 6-31++G**: -302.6846261; 6-311++G**: -302.7594066 (in hartree)

TABLE V. Hydroxyacetamide (HD) - RHF data

	ΔE [kcal mol^{-1}]			O=C-C-O [deg.]			H-O-C-C [deg.]		
	6-31G*	6-31++G**	6-311++G**	6-31G*	6-31++G**	6-311++G**	6-31G*	6-31++G**	6-311++G**
se	0.00	0.09	0.00	0.0	0.0	0.0	0.0	0.0	0.0
ag-	0.07	0.00	0.16	170.9	171.3	171.5	-82.7	-93.5	-93.6

6-31G*: -282.8247052; 6-31++G**: -282.8544491; 6-311++G**: -282.9207174 (in hartree)

TABLE VI. N,N-dimetylo-2-hydroxyacetamide(HMD) - RHF data

	ΔE [kcal mol^{-1}]			O=C-C-O [deg.]			H-O-C-C [deg.]		
	6-31G*	6-31++G**	6-311++G**	6-31G*	6-31++G**	6-311++G**	6-31G*	6-31++G**	6-311++G**
se	0.00	0.00	0.00	0.0	0.0	0.0	0.0	0.0	0.0
ag-	3.79	3.73	3.73	126.1	122.5	123.2	-66.3	-70.7	-68.5
at	5.22	4.92	4.90	-128.2	-127.9	-128.0	166.7	158.7	159.6
st	8.34	8.30	7.85	0.0	-0.2	0.8	179.8	179.7	-179.5

6-31G*: -360.8799373; 6-31++G**: -360.9099125; 6-311++G**: -360.9883944 (in hartree) syn and anti arrangement of COX and α-OH groups and the *e*, *g* and *t* designations for conformations of hydroxyl hydrogen atom. Energies are given in atomic units, relative energies (ΔE: the energy differences between each of the conformers and the conformer of the lowest energy) in kcal mol^{-1}, torsional angles in degrees.

TABLE VII:
Hydroxyacetamide(HD)-MP2 data

Conformer	Correlation energy [hartree]	Relative Energy [kcal mol^{-1}]
se	-0.8594134	0.00
ag-	-0.8593112	0.06

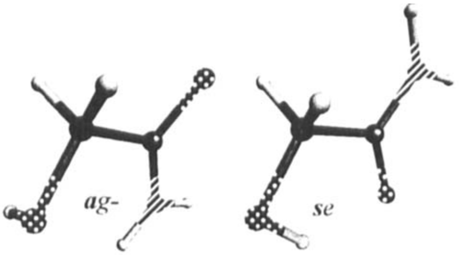

Fig. 4 Stable conformers of hydroxyacetamide (HD)

TABLE VIII
Hydroxyacetic acid (HA) - MP2 data

Conformer	Correlation energy [hartree]	Relative Energy [kcal mol^{-1}]
se	-0.8762181	0.00
ag+	-0.8770513	1.50
at	-0.8767591	4.30
st	-0.8766820	4.04
*at**	-0.8774677	3.01

TABLE IX
N,N-dimetylo-2-hydroxyacetamide(HMD) - MP2 study

Conformer	Correlation energy [hartree]	Relative Energy [kcal mol^{-1}]
se	-1.1642603	0.00
ag-	-1.1652008	3.14
at	-1.1649872	4.44
st	-1.1649124	7.44

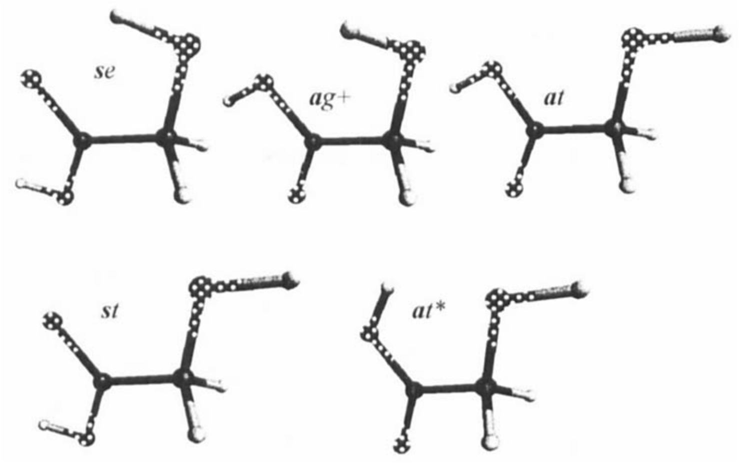
se
ag+
at
st
at*

Fig. 5 Stable conformers of hydroxyacetic acid (HA)

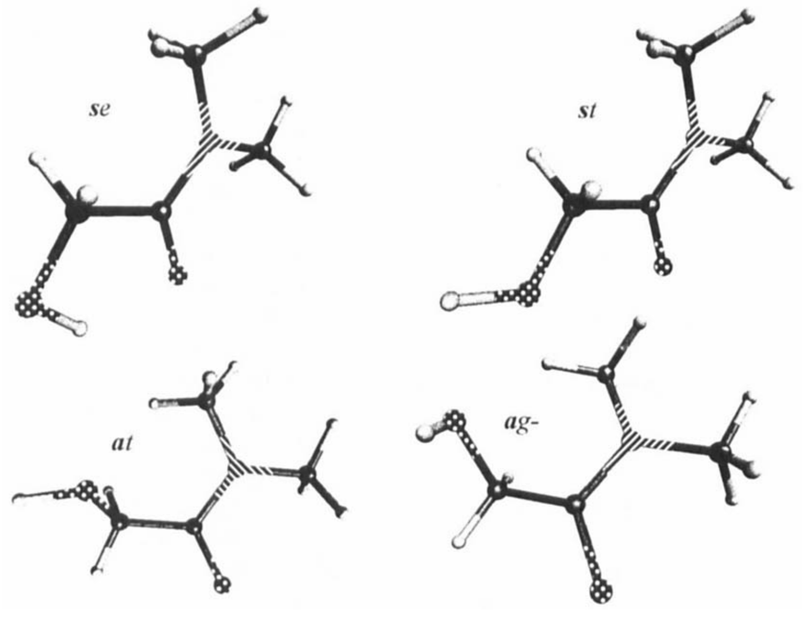

Fig. 6 Stable conformers of N,N-dimetylo-2-hydroxyacetamide(HMD)

IV. DISCUSSION AND CONCLUSIONS

(R,R)-tartaric acid

The minimum energy conformation of (R,R)-tartaric acid is the **T***ssee* that has an extended carbon chain and two hydrogen bonds occurring between carbonyl oxygen atom and the hydroxyl group of the same half of the molecule, i.e. α-hydroxyl group. Both hydrogen bonds close 5-membered rings. This conclusion agrees well with all former findings both experimental and theoretical. It is, however worth to note that we have obtained many various conformers with different conformations of the carbon chain and different hydrogen bonding patterns. Two conformers closest energetically to the favoured **T***ssee* are the **T***saeg-* with OH...OH...O=C hydrogen bonding bonding and the **G+***aag-g-* with two hydrogen bonds joining both halves of the molecules and formed between carbonyl oxygen atoms and β-hydroxyl groups i.e. OH groups from the other half of the molecule. The latter conformer is of energy higher then the **T***ssee* by only 1.78 and 1.62 kcal mol^{-1} at RHF and MP2 level respectively. Conformer possessing the same pattern of hydrogen bonding as the **T***ssee* (5-membered rings) but the carbon chain bent into the **G+** conformation (**G+***ssg-g-*) is of energy higher by 3.47 (RHF) / 2.54 (MP2) kcal mol^{-1}. Trans conformation of the carbon chain going together with 6-membered ring type of hydrogen bonds has the relative energy of 5.73 (RHF) / 6.83 (MP2) kcal mol^{-1}, significantly higher than for example another trans conformer (**T**s*ag-g+*), nonsymmetric, with two hydrogen bond type interactions, namely C=O...HO(α) interaction in one half of the molecule and OH...OH interaction between aliphatic and carboxylic hydroxyl groups from the other half of the molecule. Within the set of the **G-** conformations we have found the **G-***spet* to be of the lowest energy with the following hydrogen bonding pattern : OH(β)...OH(α)...O=C.

(R,R)-tartramide and (R,R)-tertramethyltartramide

Unlike the acid itself whose nonsymmetrical conformations surprisingly appear relatively stable and favoured, amide derivatives markedly prefer symmetric conformations. They both consistently prefer the **G+***aag-g-* conformation and the **G+***ssg+g+* one goes directly thereafter, although in DA the energy difference between them both is slightly bigger. In the **G+***aag-g-* conformation two hydrogen bonds closing 6-membered rings are formed, each involving both halves of the molecule while in the **G+***ssg+g+* one each of the two hydrogen bonds (5-membered ring) is formed within one half of the molecule only. In the case of DA in conformations with anti arrangement of amide group additional hydrogen bonding occurs according to the scheme : NH...OH(α). This type of bonding occurs also in the lowest energy nonsymmetrical conformer of gauche- type, i.e. the **G-***aste*. It has three hydrogen bonds each closing 5-membered ring and one hydrogen bond closing 7-membered ring. The 5-membered rings are formed between: NH...OH(α), OH(α)...OH(β), and OH(β)...O=C, while 7-membered ring is between the distal NH and proximal O=C groups. Trans conformation of DA that possess the same type of hydrogen bonding as the **G+*aag-g-*** is of energy higher by 3.64 (RHF) / 5.17 (MP2) kcal mol^{-1}. In the case of TMDA we have also obtained a conformer with the carbon chain in a nearly **E** (eclipsed) conformation. Both hydrogen bonds formed in this structure are of 5-membered ring type (C=O...OH(α)). Importantly the **G-** conformer, that closely resemble the one observed in the crystal lattice of TMDA was of high relative energy i.e. 8.53 kcal mol^{-1} at RHF/6-31G* and 10,69 kcal mol^{-1} when the electronic correlation was included at MP2 level.

MP2 corrections

Generally, electronic correlation corrected relative energies (ΔE(MP2)) even decreased within the sets of low energy conformers and increased within the rest of high energy structures, except for TMDA molecule in which the MP2 relative energies are smaller than their RHF counterparts even for high energy conformations.

Model molecules

From our result one can notice that all model molecules in the isolated state appear to favour *se* (Fig. 4-6) conformation with planar HOCC(OH)=O moiety and intramolecular hydrogen bonding formed between carbonyl oxygen and hydroxylic hydrogen atoms. This preference is clearly marked for hydroxyacetic acid (Fig. 5), which agrees well with former findings, and also for N,N-dimethyl-hydroxyacetamide (Fig. 6). Only in the case of hydroxyacetamide (Fig. 4) the energy difference between two conformations is very small and, in fact, negligible. Generally we notice quite surprising tendency of the relative energies to decrease with the increase of the basis set size and with inclusion of electronic correlation effects. In hydroxyacetamide we even observe a change in conformational preferences in favour of anti conformer at 6-31++G** basis set.

Hydroxyacetic acid and dimethyl-hydroxy-amide have quite similar sets of conformations corresponding to their local energy minima, i.e. the ***ag***, ***at*** and ***st***. However these types of conformations of hydroxyacetic acid are significantly more planar than their amide counterparts. In the ***ag+*** conformation of HA we observe the hydrogen bond interaction between both hydroxyl groups with the aliphatic hydroxyl being a proton donor. In both the ***st*** and the ***at*** conformations there is no hydrogen bonding and conformers are of very high energy.

In the ***ag-*** conformation of HMD C=O bond eclipses one of the CH bonds - O=CC-O angle is about 120° and the dimethylamine group is in *gauche(-)* position with respect to hydroxyl oxygen. The hydroxyl hydrogen atom is twisted towards carbonyl oxygen into a *gauche(-)* conformation with respect to the carbon chain. In the ***at*** hydrogen is in *trans* arrangement and dimethylamine group in a *gauche(+)* position with respect to the hydroxyl oxygen atom. The ***st*** conformer of the highest energy with planar OCCO group but with hydrogen pointing in the opposite direction with respect to carbonyl possesses no hydrogen bonding.

Hydroxyacetic acid has also additional conformation with hydrogen bonding between the two hydroxylic groups with carboxylic hydroxyl group being a proton donor. This conformation, however, appears significantly less favoured ($\Delta E=4.72$ kcal mol^{-1}) than the structure described above i.e. *ag*+ ($\Delta E=2.11$ kcal mol^{-1}). Generally the energy differences between particular conformers are bigger in HMD than in HA, which is marked especially in the case of the last conformer possessing no hydrogen bonding.

Unlike HMD and HA the hydroxyacetamide molecule (HD) appears to have only two stable conformations. Both of them possess intramolecular hydrogen bonds. In the *se* conformation we observe hydrogen bonding of exactly the same structure as occurring in HA and HMD although its dominance is not as clear as it is in these molecules. In the *ag*- conformer hydrogen bonding is formed between NH_2 and α-OH group according to the scheme: HNH...αO(H). Hydroxyl hydrogen atom is twisted away of N-H bond and its position with respect to the carbon chain, described by the HOCC torsion angle, is from about -83° (6-31G*) to about -93° (6-31++G**, 6-311++G**). As we mentioned earlier the energy differences between these two structures are extremely small and point to a conclusion that both conformations are equally favoured in the gas-phase.

Fortunately, as the geometry of hydroxyacetic acid in the gas-phase has been already determined experimentally (Blom and Bauder, 1982), a direct comparison between experimental data and theoretical predictions on the structure of the molecule in the isolated state could be made in order to evaluate the reliability of the methods used in this work.

TABLE X

Comparison of experimental and theoretical geometries of HA

Parameter	STO-3G	6-31G*	6-31++G**	6-311++G**	MP2/ opt. 6-311++G**	Experiment
C-C [Å]	1.5485	1.5091	1.5085	1.508	1.5124	1.495(6)
C_{sp2}-O [Å]	1,3829	1,3324	1,3211	1,3206	1,3465	1.349(6)
C_{sp2}=O [Å]	1,218	1,1888	1,1902	1,1837	1,2117	1.210(6)
C_{sp3}-O [Å]	1,4323	1,385	1,3854	1,3841	1,4064	1.406(4)
C-H [Å]	1,0969	1,0855	1,0857	1,086	1,0957	1.097(3)
O-H_{carb} [Å]	0,9901	0,9528	0,9487	0,9466	0,9683	0.989(19)
O-H_{hydr} [Å]	0,9925	0,9528	0,9487	0,9466	0,9683	0.956(3)
CC=O [deg]	122,34	123,71	123,79	123,86	123,64	124.2(4)
CCO_{hydr} [deg]	109,93	111,30	111,61	111,81	111,31	111.3(4)
COH_{carb} [deg]	104,95	108,84	109,61	109,44	106,65	105.5(11)
COH_{hydr} [deg]	102,96	108,86	109,86	109,50	106,03	105.2(1)
OCCO [deg]	0,0	0,0	0,1	0,0	0,1	(0.0)

We have performed additional test calculations, namely full geometry optimisations of the *se* conformer of hydroxyacetic acid at RHF/STO-3G and MP2/6-311++G**. Several selected bond lengths, bond angles and torsional angles are collected in Table X according to the method with use of which they have been determined.

As one can conclude from the data gathered in Table X the best agreement between the experimental and theoretical results can be achieved when performing the geometry optimization at MP2 level. This concerns principally bond lengths. 6-31G and 6-311G basis sets, augmented with polarisation/diffuse functions, in general yield correct bond angles and dihedrals but systematic bond length shortening is observed. Should there be needed a higher level of accuracy and agreement with experimental parameters, then complete geometry optimisation with the use of MP2 method would have to be performed rather than only single-point energy calculations.

If the accurate assessment of the relative energies between the conformers is concerned, it has been concluded by Gronert and O'Hair (Gronert and O'Hair, 1995) that the MP2/6-31+G*//RHF/6-31G* level appears to be sufficient for the amino acids studied by them. Those compounds are of comparable size and complexity as the systems considered in this study. It therefore seemed that further increase in the basis set size would put much larger demand on the computer resources without a significant change in the results.

ACKOWLEDGEMENTS

The authors gratefully ackowledge stimulating discussions with Prof. U. Rychlewska and Prof. J. Gawroński. We thank Poznań Supercomputing and Networking Centre for the access to the computer resources there. Finanacial support from KBN (grants: T11F01008p01 and 128/F-336/SPUB/COST/T-9/DZ05/96) is gratefully acknowledged.

REFERENCES

Aakeroy, C.B., Hitchcock, P.B., Seddon, K.R. (1992). *J. Chem. Soc. - Chem. Communications* 553.

Aakeroy, C.B., Hitchcock, P.B. (1993). *J. Materials Chemistry* **3**, 1129.

Ascenso, J., Gil, V.M.S. (1980). *Can. J. Chem.* **58**, 1376.

Blom, C.E., Bauder, A. (1982). *J. Am. Chem. Soc.* **104**, 2993.

Barron, L.D. (1978). *Tetrahedron* **34**, 607.

Barron, L.D., Gargano, A.R., Hecht, L., Polvarapu, P.L., Sugeta, H. (1992). *Spectrochim. Acta* **48A**, 1051.

Colton, R.H., Henn, D.A. (1965). *Acta. Cryst.* **18**, 820.

Cornforth, J.W., Cornforth, R.H., Mathew, K.K. (1959). *J. Chem. Soc.* 112.

Cram, D.J., Kopecky, K.R. (1959). *J. Am.Chem.Soc.* **81**, 2748.

Davidson, E.R., Feller, D. (1986). *Chem. Rev.* **86**, 681.

Dewar, M.J.S., Zoebisch, E.G., Healy, E.F., Stewart, J.J.P. (1985). *J.Am.Chem. Soc.* **107**, 3902.

Ellison, R.D., Johnson, C.K., Levy, H.A. (1971). *Acta Cryst.* **B27**, 333.

Finn, M.G., Sharpless, K.B. (1983). „Asymmetric Synthesis"; vol. 5, chapter 8, Morrison, J.D. (ed), Academic Press: New York.

Gaussian 94, Revision C.3, Frisch, M.A., Trucks, G.W., Schlegel, H.B., Gill, P.M.W., Johnson, B.G., Robb, M.A., Cheeseman, J.R., Keith, T., Petersson, G.A., Montgomery, J.A., Raghavachari, K., Al.-Laham, M.A., Zakrzewski, V.G., Ortiz, J.V., Foresman, J.B., Cioslowski, J., Stefanov, B.B., Nanayakkara, A., Challacombe, M., Peng, C.Y., Ayala, P.Y., Chen, W., Wong, M.W., Andres, J.L., Replogle, E.S., Gomperts, R., Martin, R.L., Fox, D.J., Binkley, J.S., Defrees, D.J., Baker, J., Stewart, J.P., Head-Gordon, M., Gonzalez, C., Pople, J.A., Gaussian Inc., Pittsburgh PA, 1995.

Gawroński, J., Gawrońska, K., Rychlewska, U. (1989). *Tetrahedron Lett.* **30**, 6071.

Gawroński, J., Gawrońska, K., Skowronek, P., Rychlewska, U., Warżajtis, B., Rychlewski, J.,

Gronert, S., O'Hair, R.A.J. (1995). *J. Am.Chem.Soc.* **117**, 2071.

Hoffmann, M., Szarecka, A. (1997). *Tetrahedron* **53**, 6113.

Golic, L., Speakman, J.C. (1968). *J. Chem. Soc.* 2521.

Hasa, M. (1980). *Org. Magn. Res.* **14**, 309.

Head-Gordon, M., Pople, J.A., Frisch, M.J. (1988). *Chem. Phys.Lett.* **153**, 503.

Hehre, W.J., Radom L., Schleyer P.v.R., Pople J.A. (1986) „Ab Initio Molecular Orbital Theory", Wiley, New York.

Hoffmann, M., Rychlewski, J., Rychlewska, U. (1996). *Computational Methods in Science and Technology -Poznań Supercomputing and Networking Center* vol. **2**, 51.

Jacques, J., Collet, A., Wilen, S. H. (1981). „Enantiomers, Racemates and Resolutions", Wiley, New York.

Katsuki, T., Sharpless, K.B. (1980). J. Am. Chem. Soc. **102**, 5974.

Mayers, R.F., Keve, E.T., Skapski, A.C. (1968). *J.Chem. Soc.* (A), 2258.

Newton, M.D., Jeffreys, G.A. (1977). *J. Am. Chem. Soc.* **99**, 2413.

Pijper, W.P. (1971) *Acta Cryst.* **B27**, 344.

Polvarapu, P.L., Ewig, C.S, Chandramouly, T. (1985). *J. Am. Chem. Soc.* **109**, 6213.

Pople, J.A., Beveridge, D.L. (1970). „Approximate Molecular Orbital Theory", McGraw-Hill, New York.

Rychlewska, U. (1992). *Acta Cryst.* **C48**, 965.

Rychlewska, U., Warżajtis, B., Hoffmann, M., Rychlewski, J. (1997). *Molecules* **2**, in press

Schmidt, M.W., Baldridge, K.K., Boatz, J.A., Elbert, S.T., Gordon, M.S., Jensen, J.H., Koseki, S., Matsunaga, N., Nguyen, K.A., Su, S.J., Windus, T.L., Dupois, M., Montgomery, J.A. (1993). *J.Comput. Chem.* **14**, 1347.

Stern, F., Beevers, C.A. (1950). *Acta Cryst.* **3**, 341.

Stewart, J.J.P. (1989). *J.Comput. Chem.* **10**, 209.

Toda, F., Tanaka, K., Nassimbeni, L., Niven, M. (1988). *Chem. Lett.* 1371.

Stouten, P.F.W., Kroon-Batenburg,, L.M.J., Kroon, J. (1989). *J.Mol. Struct. (Theochem)* **200**, 169.

Su, C.N., Keiderling, T.A. (1980). *J. Am. Chem. Soc.* **102**, 511

Szarecka, A., Hoffmann, M., Rychlewski, J., Rychlewska, U. (1996). *J. Mol. Struct.* **374**, 363.

Szczepańska, B., Rychlewska, U. (1994). In „Correlations, Transformations and Interactions in Organic Chemistry" pp. 23-244, Jones, D.W., Katrusiak, A., (ed.), Oxford University Press.

Szczepańska, B., Gdaniec, M., Rychlewska, U. (1995). *J. Incl. Phenom.* **22**, 211.

Tapscott, R.E., Belford, R.L., Paul, I.C. (1969). *Coord. Chem. Rev.* **4**, 323.

Van Bommel, A.J., Bijvoet, J.M. (1958). *Acta Cryst.* **1**,61.

RECENT THEORETICAL DEVELOPMENTS IN CONICAL-INTERSECTION EFFECTS IN TRIATOMIC SPECTRA

Carlo Petrongolo

Dipartimento di Chimica, Universita' di Siena,
Pian dei Mantellini 44, I-53100 Siena, Italy
petro@carlo.icqem.pi.cnr.it

ABSTRACT

The Born-Oppenheimer (BO) approximation breaks down whenever two electronic states are coupled by rovibronic operators. We briefly review the theory of the conical intersections between two adiabatic electronic species and discuss a diabatic representation which strongly reduces the nonadiabatic couplings. We also report some results on the $\tilde{X}^2A_1/\tilde{A}^2B_2$ conical intersection of NO_2 which strongly affects the structure and dynamics of this molecule. The nonadiabatic states have been expanded in the BO vibrational basis of both diabatic electronic species, the energy levels and the cold Franck-Condon absorption intensities have been calculated, several molecular states have been assigned, and the vibrational and vibronic mixings have been discussed by analyzing the expansion coefficients. The theoretical results are in semi-quantitative agreement with and explain some accurate experimental data.

ADVANCES IN QUANTUM CHEMISTRY, VOLUME 32
Copyright ©1999 by Academic Press. All rights of reproduction in any form reserved.
0065-3276/99 $30.00

CONTENTS

1. INTRODUCTION

2. THEORY
    - 2.1. Nonadiabatic formalism
    - 2.2. Conical intersections
    - 2.3. Diabatic electronic representation

3. NO_2 $\tilde{X}\,^2A_1/\tilde{A}\,^2B_2$ NONADIABATIC SPECTRUM
    - 3.1 Method
    - 3.2 Beginning of the nonadiabatic effects
    - 3.3 Development of the nonadiabtic effects

4. CONCLUSIONS

1. INTRODUCTION

The current model of the molecular structure and dynamics relies on the approximate separation of the translational, rotational, vibrational, and electronic motions, and on one-degree-of-freedom and one-particle schemes. Only the translation of an isolated molecule can be exactly separated off, whereas the other motions are separated as far as possible by using body-fixed (BF) reference frames with the origin at the nuclear center of mass, the Eckart conditions, normal coordinates, the Born-Oppenheimer (BO) separation of the nuclear and electronic motions, and the HF one-electron theory. The Eckart conditions and the normal coordinates give the maximum separation of the rotational and vibrational motions; in studying however high-lying energy levels, coupled electronic states, or large amplitude vibrations, other BF axes and vibrational coordinates are more suitable. The BO and HF approximations play a central role in molecular quantum mechanics, even when are nor valid, because they give the canonical reference model for understanding the nuclear and electronic dynamics and are the starting point of more accurate theories.

In order to define the method and the notation of this paper, we shall present in Sec. 2 some theoretical aspects of the rotationless nonadiabatic formalism, of the conical intersections, and of the diabatic representation. The theory is then applied to the $\tilde{X}^2A_1/\tilde{A}^2B_2$ conical intersection of NO_2 in Sec. 3

2. THEORY

2.1. Nonadiabatic formalism

We shall here discuss only the nonadiabatic effects due to the conical intersection between two adiabatic electronic states. By therefore considering only the electronic and vibrational motion, the molecular Schrödinger equation

$$(\hat{H} - E_n)\,|n\rangle = 0\,, \qquad (2.1)$$

is solved by means of the expansion [1]

$$|n> = \Sigma_e \, |e> \, <e|n>_q = \Sigma_e \, |e> \, |n_e> \, , \tag{2.2}$$

where $|e>$ and q are electronic states and coordinates, and $|n_e>$ are generalized Born-Oppenheimer (GBO) vibrational functions. By defining the BO vibrational states and energies by means of

$$(<e|\hat{H}\,|e>_q - E_{fe}) \, |f_e> = 0 \, , \qquad \text{any } e \, , \tag{2.3}$$

the GBO functions are then expanded as

$$|n_e> = \Sigma_f \, |f_e> \, <f_e|n_e> = \Sigma_f \, |f_e> \, <ef_e|n> \, . \tag{2.4}$$

By inserting Eq. (2.2) or (2.4) in (2.1), we obtain the coupled equations

$$(<e|\hat{H}\,|e>_q - E_n\mathbf{1}) \, |n_e> = \mathbf{0} \, , \tag{2.5}$$

or the secular problem

$$(<\mathbf{f_e}|<e|\hat{H}\,|e>_q|\mathbf{f_e}> - E_n \, \mathbf{1}) \, <\mathbf{ef_e}|n> = \mathbf{0} \, , \tag{2.6}$$

respectively.

The off-diagonal operators $<e'|\hat{H}\,|e>_q$, with $e' \neq e$, couple the electronic states and give rise to nonadiabatic effects which can strongly affect the molecular properties. The second-order perturbation theory shows that these couplings can be neglected with respect to the diagonal BO terms of Eqs. (2.3) when

$$|<f'_{e'}|<e'|\hat{H}\,|e>_q|f_e>| << |E_{f'e'} - E_{fe}| \, , \qquad \text{any } e' \neq e \text{ and any } f',f \, . \tag{2.7}$$

These conditions are in general fulfilled for low-lying energy levels and for well separated electronic potential surfaces. In this case, the nonadiabatic species $|n>$ and

E_n of Eq. (2.1) are approximated by the BO ones $|ef_e\rangle$ and E_{fe} of Eqs. (2.3). On the other hand, this formalism breaks down whenever two electronic states $|e\rangle$ or their vibrational BO functions $|f_e\rangle$ are (nearly) degenerate, and we must therefore consider in Eqs. (2.5) and (2.6) all the coupled electronic states.

2.2. Conical intersections

Let us consider for example a triatomic molecule. By using Jacobi coordinates r_1, r_2, and θ, and Legendre basis functions $|l(\theta)\rangle$, the angular-electronic matrix elements of the Hamiltonian are equal to [2]

$$\begin{aligned} \langle l'|\langle e'|\hat{H}\,|e\rangle_q|l\rangle_\theta = {} & \delta_{e'e}\,\delta_{l'l}\,[\,-(1/2\mu_1)\partial^2/\partial r_1{}^2 - (1/2\mu_2)\partial^2/\partial r_2{}^2 + l(l+1)/2\mu_\theta\,] \\ & + \langle l'|\,-\Sigma_Q\,(1/\mu_Q)\,g^Q_{e'e}\,\partial/\partial Q - (1/2\mu_\theta)\,g^\theta_{e'e}\cot\theta \\ & - \Sigma_Q\,(1/2\mu_Q)\,h^Q_{e'e} + V_{e'e}\,|l\rangle_\theta\,. \end{aligned} \tag{2.8}$$

Here μ_Q is the reduced mass corresponding to the nuclear coordinate Q, $g^Q_{e'e}$ and $h^Q_{e'e}$ are the vibronic matrix elements

$$g^Q_{e'e} = \langle e'|\partial/\partial Q|e\rangle_q\,, \quad h^Q_{e'e} = \langle e'|\partial^2/\partial Q^2|e\rangle_q\,, \tag{2.9}$$

and $V_{e'e}$ are the matrix elements of the electronic Hamiltonian $\hat{H}^{el}$ on the basis $|e\rangle$. In a general electronic representation, $g^Q_{e'e}$, $h^Q_{e'e}$, and $V_{e'e}$ are all different from zero, couple the electronic states, and thus give rise to the breakdown of the BO approximation. In the adiabatic representation wich diagonalizes the matrix **V**, the vibronic couplings diverge along the intersection locus of two adiabatic potential surfaces, according to the Hellmann-Feynman theorem

$$g^Q_{e'e} = \langle e'|\partial\hat{H}^{el}/\partial Q|e\rangle_q\,/(V_e - V_{e'})\,. \tag{2.10}$$

Since [3]

$$h^Q_{e'e} = \partial g^Q_{e'e}/\partial Q - \langle \partial e'/\partial Q | \partial e/\partial Q \rangle_q , \tag{2.11}$$

also the second-derivative terms are singular when $V_e = V_{e'}$.

2.3. Diabatic electronic representation

By using suitable Hamiltonians and vibrational basis functions, the singularities of some vibronic couplings in the adiabatic representation can be analytically removed, except those of the diagonal terms h_{ee} which behave as Dirac δ^2 functions near the intersection locus [2]. Nevertheless, the large number of these couplings, the difficulties in calculating them and their matrix elements on the vibrational basis, and their huge values near the intersection locus call for an orthogonal transformation of the adiabatic basis to a diabatic representation. The latter does not diagonalize $\hat{H}^{el}$, but its diagonal vibronic terms should be nearly constant and equal for all the electronic states of interest and its off-diagonal vibronic couplings should be negligible when divided by the reduced masses.

According to different physical and mathematical conditions, we can define different diabatic bases, provided the couplings g^Q and $g^{Q'}$ due to two different vibrations are not both zero [4]. Quasi-diabatic states are very useful in studying structural and dynamical properties due to nonadiabatic effects, and several diabatization techniques have thus been suggested. In previous works [5,6], we have employed the Macias-Riera method [7] which can be easily implemented in large-scale CI electronic computer codes and gives small electronic couplings and negligible vibronic terms. Because the adiabatic states change very quickly near an avoided crossing or a conical intersection, both the vibronic couplings (2.9) and the electronic matrix elements of some operator $\hat{P}$ undergo sharp variations and are strongly peaked near the (quasi-) degeneration locus. Therefore, the adiabatic-to-diabatic transformation matrix must remove the strong peaks of the $P_{e'e}$ matrix elements in the diabatic representation.

The method is very simple in a two-state problem. If |X>, |A> and |1>, |2> are adiabatic and diabatic electronic states, respectively, the transformation is

$$|1\rangle = |X\rangle \cos\tau + |A\rangle \sin\tau ,$$

$$|2\rangle = - |X\rangle \sin\tau + |A\rangle \cos \tau . \tag{2.12}$$

Under the hypotheses that either $|P_{XA}|$ or $|P_{AA} - P_{XX}|$ be peaked near the conical intersection, the angle τ, which gives P_{12} or $(P_{22} - P_{11}) = 0$, is equal to

$$\tau_1 = (1/2) \arctan[2P_{XA}/(P_{AA} - P_{XX})] , \tag{2.13}$$

or to

$$\tau_2 = (1/2) \arctan[(P_{AA} - P_{XX})/2P_{XA}] , \tag{2.14}$$

modulo $\pi/2$, respectively. This method has been succesfully applied to the conical intersections $\tilde{A}^2A_1/\tilde{B}^2B_2$ of NH_2 and $\tilde{X}^2A_1/\tilde{A}^2B_2$ of NO_2, by using a component of the electric quadrupole or dipole moment, respectively [5,6]. In the first case, even large vibronic couplings g_{XA} and huge diagonal terms h_{XX} and h_{AA} become very small in the diabatic representation. In the NO_2 molecule, the transformation also gives nearly constant diabatic electronic dipole moments, which justify the use of the Franck-Condon approximation in the calculation of the absorpion spectrum.

3. NO_2 $\tilde{X}^2A_1/\tilde{A}^2B_2$ NONADIABATIC SPECTRUM

3.1. Method

In 1975, Gillispie *et al.* [8,9] and Smalley *et al.* [10] found that the very complex near-infrared and visible spectrum of NO_2 is due to a conical intersection between the first two electronic states $\tilde{X}^2A_1$ and $\tilde{A}^2B_2$. Later on, the Heidelberg [11], Grenoble [12-16], and Siena [17-19] groups have investigated both theoretically and experimentally this spectrum, by going beyond the BO approximation. Our method has been fully discussed in previous papers, and we shall give here only a brief summary.

By using a bond lengths-bond angle vibronic Hamiltonian, the nonadiabatic states |n> and energies E_n have been calculated by means of the expansions (2.2) and (2.4), where e = 1 or 2 labels the $\tilde{X}^2A_1$ or $\tilde{A}^2B_2$ diabatic electronic state, respectively, and the BO vibrational species $|f_e>$ (2.3) have been obtained in a finite basis representation of primitive and optimized functions.

The Hamiltonain matrix has been diagonalized by means of conventional Householder tridiagonalization, bisection, and inverse iteration techniques [20], by calculating the eigenvalues and the corresponding eigenvectors up to an energy maximum. We have therefore assigned several states |n> and discussed their vibrational and vibronic mixings, by analyzing the expansion coefficients $D_{ef,n} = <ef_e|n>$ and the nodal structure of the BO basis functions $|f_e>$ and of the GBO states $|n_e>$, by calculating the electronic weights

$$w_{en} = \Sigma_f D^2{}_{ef,n} , \tag{3.1}$$

and by fitting the vibrational manifolds with Dunham expansions [17,18]. We have finally calculated the Franck-Condon (FC) nonadiabatic and diabatic intensities I_n and I_{f2}, respectively, for the absorption from the ground vibronic state $\tilde{X}^2A_1(0,0,0)$ and the Fourier transform (FT) of the spectrum [19].

3.2. Beginning of the nonadiabatic effects

The calculated zero point energy (zpe) of NO_2 is at 1896 cm^{-1} and the nonadiabatic interactions due to the $\tilde{X}^2A_1/\tilde{A}^2B_2$ conical intersection are small up to about 9500 cm^{-1}, *i.e.* below the $\tilde{A}^2B_2(0,0,0)$ vibrational origin. The vibronic couplings perturb however some nonadiabatic bands of the ground electronic species well below the $\tilde{A}^2B_2(0,0,0)$ level [17]. Indeed, the states $(v_1,v_2,0)$ and $(v_1-3,v_2+1,2)$ can be vibrationally mixed, giving rise to the resonances which have been observed in

[12] and are described by the GBO states $|n_1>$. Moreover, the nonadiabatic bands due to $\tilde{X}^2A_1$ high-bending overtones are in general shifted to the red of their main vibrational species and have non negligible contributions from other $\tilde{X}^2A_1$ basis functions.

Table 1 reports the levels of B_2 symmetry in the energy range 9400 - 10600 cm^{-1}, and shows that the beginning and the development of the nonadiabatic interactions are gradual and selective in the near-infrared spectrum, where only few nonadiabatic states are strongly mixed between the two electronic species. As it has been predicted [12], the conical intersection first couples highly excited $\tilde{X}^2A_1$ bending states with near $\tilde{A}^2B_2$ partners with $\Delta v_3 = \pm 1$. The first two strongly mixed B_2 bands 68 and 72 at 9534 and 9747 cm^{-1} are both assigned as $\tilde{X}^2A_1(0,11,1) + \tilde{A}^2B_2(0,0,0)$, according to their main vibrational configurations. Other large vibronic mixings occur for the band 81 at 10128 cm^{-1}, of type $\tilde{X}^2A_1(1,10,1) + \tilde{A}^2B_2(0,1,0)$, and for the states 85 and 92 at 10296 and 10523 cm^{-1}, which are mainly due to the interaction $\tilde{X}^2A_1(0,12,1) + \tilde{A}^2B_2(0,1,0)$.

The first strongly mixed A_1 nonadiabatic bands are at higher energies, near the $\tilde{A}^2B_2(0,0,1)$ vibrational level which interacts with the $\tilde{X}^2A_1(0,15,0)$ one, giving two electronically coupled states at 10924 and 11201 cm^{-1} [18]. The number of strongly coupled A_1 nonadiabatic levels is smaller than that of the B_2 ones, owing to the smaller density of the $\tilde{A}^2B_2$ basis functions of B_2 symmetry: 134 A_1 and 238 B_2 nonadiabatic states have $\tilde{A}^2B_2$ weights w_{2n} larger than 15%, out of a total of 797 and 707 up to 18735 cm^{-1}, respectively.

The $\tilde{X}^2A_1$ vibrational levels with 3 or 5 antisymmetric-stretch quanta are in general unmixed in the near-infrared spectrum, but they can also be shifted to the red by the nonadiabatic interactions. On the other hand, some states $|n>$ are equal to linear combinations of many $\tilde{X}^2A_1$ basis functions and of one dominant $\tilde{A}^2B_2$ partner, at most, up to 11900 cm^{-1}. For example, the weight of the main $\tilde{X}^2A_1$ components of the B_2 states 68, 85, and 92 is equal to 25, 32, and 39%, respectively, but the overall contribution of other unassigned $\tilde{X}^2A_1$ basis functions is equal to 22, 29, and 23%, respectively. The conical intersection can therefore mix simultaneously both the vibrational states of the ground electronic species and those of both electronic states;

Table 1. NO_2 B_2 bands between 9400 and 10600 cm^{-1}. Energy in cm^{-1} with respect to the zpe.

Nonadiabatic		$\tilde{X}^2A_1$ main $\vert f_1\rangle$		$\tilde{A}^2B_2$ main $\vert f_2\rangle$		Experiment [12]	
n	E_n	E_{f1}	v_1,v_2,v_3	E_{f2}	v_1,v_2,v_3	E	v_1,v_2,v_3
65	9426	9556	1,9,1			9437	1,9,1
66	9466	9467	4,0,3			9500	1,5,3
67	9504	9541	4,4,1			9518	4,4,1
68	9534	9839	0,11,1	9714	0,0,0	9531	4,0,3
69	9594	9647	1,5,3			9624	1,1,5
70	9650	9660	1,1,5			9654	0,11,1
71	9715	9773	3,6,1			9714	3,6,1
72	9747	9839	0,11,1	9714	0,0,0	9734	**0,0,0**^{a}
73	9751	9756	6,1,1			9736	0,7,3
74	9801	9815	3,2,3			9753	3,2,3
75	9826	9908	0,7,3			9797	6,1,1
76	9893	9948	0,3,5			9836	0,3,5
77	9937	10015	2,8,1			9928	2,8,1
78	9991	10013	5,3,1			9977	2,4,3
79	10025	10027	2,0,5			10007	5,3,1
80	10064	10102	2,4,3			10081	2,0,5
81	10128	10278	1,10,1	10451	0,1,0	10161	1,10,1
82	10159	10161	?			10200	1,6,3
83	10204	10248	?			10214	4,1,3
84	10218	10221	7,0,1			10271	7,0,1
85	10296	10571	0,12,1	10451	0,1,0	10305	1,2,5
86	10317	10373	1,6,3			10363	0,12,1
87	10364	10383	1,2,5				
88	10415	10479	?				
89	10433	10435	5,0,3			10436	0,8,3

Table 1. Continued.

Nonadiabatic		$\tilde{X}^2A_1$ main $\|f_1>$		$\tilde{A}^2B_2$ main $\|f_2>$		Experiment [12]	
n	E_n	E_{f1}	v_1,v_2,v_3	E_{f2}	v_1,v_2,v_3	E	v_1,v_2,v_3
90	10459	10470	?			10479	**0,1,0**[a]
91	10514	10536	?			10488	6,2,1
92	10523	10571	0,12,1	10451	0,1,0	10523	0,4,5
93	10563	10642	0,8,3	10451	0,1,0		

[a] $\tilde{A}^2B_2$ assignment [13].

as the energy increases, these vibrational and vibronic couplings make very difficult, or meaningless, the usual assignment of the vibrational quantum numbers to the states |n>.

We compare in Table 1 our results with the experimental B_2 bands and assignments [12,13], in increasing energy order. Above 10000 cm^{-1}, the errors of the calculated nonadiabatic levels are similar to the root mean square deviation (RMSD) of 17.8 cm^{-1} we have found for the A_1 and B_2 bands up to 10000 cm^{-1} [17]. Nevertheless, only 9 theoretical and experimental assignments are equal, out of a total of 29 bands of this table. This result is probably due to a too large coupling potential V_{12} and to inaccuracies of the diagonal ones, and to the theoretical and experimental difficulties of assigning excited and mixed bands. The recent effective potentials of the $\tilde{X}^2A_1$ state, with RMSD smaller than 3 cm^{-1} [21,22], point out that our potentials must be improved in a future work.

3.3. Development of the nonadiabatic effects

The conical-intersection effects increase with the energy, up to their full development at about 16000 cm^{-1}, where the density of the nonadiabatic levels is about four times larger than that at 10000 cm^{-1} and nearly all of them are vibrationally and/or vibronically mixed. For example, 5 and 64 states |n> are strongly mixed, with

$w_{2n} > 15\%$, in the ranges 10000-11000 cm^{-1} and 16000-17000 cm^{-1}, respectively. Above 11900 cm^{-1}, the coupling does not in general allow the assigning of the main $\tilde{X}^2A_1$ vibrational character of the levels and often involves two or three $\tilde{A}^2B_2$ main configurations with belong to Fermi or to other vibrational resonances [18].

Table 2 compares some strongly mixed theoretical bands [17,18] with equally-assigned experimental ones [12-14] up to 16000 cm^{-1}. Our RMSD of 73 cm^{-1} is satisfactory, by considering the energy range, the level density, and the high-lying levels of this table. The reported $\tilde{X}^2A_1$ and $\tilde{A}^2B_2$ assignments confirm the mixings among high $\tilde{X}^2A_1$ bending overtones and near $\tilde{A}^2B_2$ bending species. The intensity calculations show that the nonadiabatic bands with large $\tilde{A}^2B_2(1,v_2,0)$ character are the strongest ones up to about 15000 cm^{-1}, with a mean energy spacing of 714 cm^{-1} and a 50 fs recurrence of the FT of the spectrum up to 16150 cm^{-1} [19].

Table 3 shows the nonadiabatic levels of B_2 symmetry and their absorption intensities between 16000 and 16300 cm^{-1}. The equilibrium symmetric-stretch and bending coordinates of the electronic species are different by about 6 and 24%, respectively [17], whereas the antisymmetric stretch is equal. Therefore, the conical intersection preferably couples $\tilde{A}^2B_2(v_1,v_2,0)$ combination states with their $\tilde{X}^2A_1$ partners, but this interaction is perturbed by the $\tilde{A}^2B_2$ antisymmetric-stretch species. Above 15000 cm^{-1}, the nonadiabatic intensity distribution is thus modulated by the maxima due to $|n>$ states with large $\tilde{A}^2B_2$ symmetric stretch-bending character, whereas $\tilde{A}^2B_2$ pure overtones are much weaker (*e.g.* bands 409 and 415 of Table 3). As the energy increases, these vibronic interactions give rise to a more and more irregular spectrum.

The B_2 level 407 of Table 3 is the strongest one up to about 17300 cm^{-1} and is a good example of the nonadiabatic effects on the spectrum. It is at 16149 cm^{-1}, has $I_n = 22.82$ μhartree and $w_{2n} = 44\%$, and its main $\tilde{A}^2B_2$ components are (2,5,0) and (1,3,2). At the diabatic level, the first $\tilde{A}^2B_2$ basis function is bright, with $I_{f2} = 69.38$ μhartree, whereas the latter is dark; moreover, the $\tilde{A}^2B_2(2,5,0)$ state contributes also to other 4 nonadiabatic bands of this table, which do not follow a regular progression. Therefore, the conical intersection lowers the $\tilde{A}^2B_2$ vibrational intensities and gives rise to a rather chaotic visible spectrum, by mixing bright and dark basis functions and by spreading the intensities of the strong ones on several nonadiabatic states.

Table 2. Some strongly mixed NO$_2$ bands between 9500 and 16000 cm^{-1}. The theoretical levels are compared with the experimental ones with the same assignment[a]. Energy in cm^{-1} with respect to the zpe.

Theory[b]		Experiment	$\tilde{X}^2A_1$ main $\|f_1>$	$\tilde{A}^2B_2$ main $\|f_2>$
n	E_n	[12-14]	v_1,v_2,v_3	v_1,v_2,v_3
68-	9534	9654	**0,11,1**	0,0,0
72-	9747	9734	0,11,1	**0,0,0**
81-	10128	10161	**1,10,1**	0,1,0
85-	10296	10363	**0,12,1**	0,1,0
92-	10523	10479	0,12,1	**0,1,0**
101-	10848	10864	**1,11,1**	0,2,0
143+	10924	11116	0,15,0	**0,0,1**
112-	11175	11211	0,13,1	**0,2,0**
153+	11201	11071	**0,15,0**	0,0,1
184+	11924	11867		0,1,1
140-	11973	11948-11961	0,14,1	**0,3,0**
162-	12506	12502		0,0,2
216+	12587	12552	0,17,0	**1,0,1**
169-	12640	12658		0,4,0
209-	13436	13396		0,5,0
252-	14141	14129		0,6,0
301-	14885	14835		0,7,0
362-	15650	15554		0,8,0

[a] When two assignments are given, that in boldface type is the same in theory and experiment.

[b] The A_1 or B_2 bands are labelled by + or -, respectivly.

Table 3. NO_2 B_2 bands between 16000 and 16300 cm^{-1} and some B_2 strong bands between 16300 and 18735 cm^{-1}. Energy in cm^{-1} with respect to the zpe and intensity in μhartree.

	Nonadiabatic		Diabatic $\tilde{A}^2B_2$ main $\|f_2>^a$	
n	E_n	I_n	v_1,v_2,v_3	v_1',v_2',v_3'
392	16004	0.01		
393	16109	0.21	2,1,2	
394	16032	2.01		
395	16038	2.93		
396	16055	0.04		
397	16061	0.79		
398	16072	1.10		
399	16074	0.18		
400	16086	3.85	2,5,0	2,1,2
401	16093	0.87		
402	16103	0.33		
403	16109	12.30	2,5,0	1,3,2
404	16112	1.67		
405	16120	4.57		
406	16133	2.32		
407	16149	22.82	2,5,0	1,3,2
408	16159	3.91	5,0,0	2,5,0
409	16173	0.04	5,0,0	
410	16181	2.84		
411	16186	13.45	2,5,0	1,3,2
412	16212	0.61		
413	16232	0.69		
414	16234	4.51	1,3,2	
415	16245	0.16	5,0,0	

Table 3. Continued.

	Nonadiabatic		Diabatic $\tilde{A}^2B_2$ main $\|f_2\rangle$[a]	
n	E_n	I_n	v_1,v_2,v_3	v_1',v_2',v_3'
416	16265	5.43	5,0,0	1,7,0
417	16276	0.58		
418	16286	6.70	0,5,2	1,7,0
419	16291	9.73	1,7,0	0,5,2
420	16299	0.67	0,5,2	
454	16641	15	3,4,0	
480	16878	17	2,6,0	5,1,0
513	17176	15	4,3,0	0,10,0
531	17360	43	3,5,0	3,1,2
543	17452	31	3,5,0	
555	17571	74	2,7,0	5,2,0
594	17866	45	0,11,0	4,4,0
621	18098	113	3,6,0	3,2,2
648	18314	98	2,8,0	7,0,0
650	18328	52	2,8,0	
685	18565	91	4,5,0	
686	18578	97	4,5,0	

[a] When the $\tilde{A}^2B_2$ assignment is not shown, the band is of $\tilde{X}^2A_1$ type.

Table 3 also shows the most important intensity maxima of the nonadiabtic spectrum between 16500 and 18735 cm^{-1}. They are mainly due to a chaotic progression of the symmetric stretch-bending combination states $\tilde{A}^2B_2(v_1,v_2,0)$ within the nonadiabatic species, mixed with and perturbed by high-bending overtones and antisymmetric-stretch basis functions. The strongest band at 18089 cm^{-1} has I_n= 133 μhartree, is due to a fifty/fifty $\tilde{X}^2A_1/\tilde{A}^2B_2$ coupling, and its $\tilde{A}^2B_2$ main components are (3,6,0) and (3,2,2), with weights equal to 40 and 5%, respectively. Above 17500 cm^{-1}, and up to 22000 cm^{-1} at least [19], the spectrum is nearly fully chaotic, except a residual low-resolution intensity modulation which corresponds to few very strong bands, and to a time recurrence in the FT of the spectrum up to 18735 cm^{-1}. For example, the mean energy spacing of the B_2 levels 531, 555, 594, 621, 648, and 686 of Table 3 is equal to 244 cm^{-1} and is reflected by a calculated maximum at 136 fs of the FT of the spectrum [19].

4. CONCLUSIONS

Our method allows a detailed understanding of the conical-intersection effects in the NO_2 spectrum. We have not only calculated the levels and the intensities, but we have also assigned several nonadiabatic states by analyzing their expansion coefficients on the BO basis, and we have discussed the vibrational and vibronic mixings. BO spectra have been also calculated by means of orthogonal Hamiltonians and of Discrete Variable Representation [23], Lanczos [20], and Recursive Residue Generation [24] methods, which are probably less costly than ours, but can hardly give the present amount of information. However, we are now implementing these methods within our nonadiabatic formalism which is also currently extended to the time-dependent dynamics of the wave-packet on the intersecting potential surfaces. This conventional expansion of the wave-packet on the stationary basis $|n>$ will give energy and time results which will be compared both between themselves and with those of the direct solution of the time-dependent Schrödinger equation.

ACKNOWLEDGEMENTS

This work has been made possible by the collaboration with R. Brandi, R.J. Buenker, G. Hirsch, R. Jost, E. Leonardi, and F. Santoro, and by the financial support of the Consiglio Nazionale delle Ricerche and of the Ministero dell'Universita' e della Ricerca Scientifica e Tecnologica.

REFERENCES

[1] M. Born and K. Huang, *Dynamical Theory of Crystal Lattices*, Oxford Academic, Oxford, 1954, p. 406 .

[2] C. Petrongolo, J. Chem. Phys. **89**, 1297 (1988).

[3] D.R. Yarkony, in *Modern Electronic Structure Theory I*, D.R. Yarkony, Ed., World Scientific, Singapore, 1995, p. 642.

[4] C.A. Mead and D.G. Truhlar, J. Chem. Phys. **77**, 6090 (1982).

[5] C. Petrongolo, G. Hirsch, and R.J. Buenker, Mol Phys. **70**, 825 (1990).

[6] G. Hirsch, R.J. Buenker, and C. Petrongolo, Mol Phys. **70**, 835 (1990).

[7] A. Macias and A. Riera, Int. J. Quantum Chem. **17**, 181 (1980).

[8] G.D. Gillispie, A.U. Khan, A.C. Wahl, R.P. Hostny, and M. Krauss, J. Chem. Phys. **63**, 3425 (1975).

[9] G.D. Gillispie and A.U. Khan, J. Chem. Phys. **65**, 1624 (1975).

[10] R.E. Smalley, L. Wharton, and D.H. Levy, J. Chem Phys. **63**, 4977 (1975).

[11] H. Köppel, W. Domcke, and L.S. Cederbaum, Adv. Chem. Phys. **57**, 59 (1984).

[12] A. Delon and R. Jost, J. Chem. Phys. **95**, 5686 (1991).

[13] B. Kirmse, Diplomarbeit, Universität Fridericiana, Karlsruhe, 1994.

[14] R. Georges, These, Universite' J. Fourier, Grenoble, 1994.

[15] R. Georges, A. Delon, F. ylicki, R. Jost, A. Campargue, A. Charvat, M. Chenevier, and F. Stoeckel, Chem Phys. **190**, 207 (1995).

[16] A. Delon, R. Georges, and R. Jost, J. Chem Phys. **103**, 1732 (1995).

[17] E. Leonardi, C. Petrongolo, G. Hirsch, and R.J. Buenker, J. Chem. Phys. **105**, 9051 (1996).

[18] E. Leonardi and C. Petrongolo, J. Chem. Phys. **106**, in press (1997).

[19] R. Brandi, F. Santoro, and C. Petrongolo, Chem. Phys. submitted (1997).

[20] G.H. Golub and C.F. Van Loan, *Matrix Computations*, Noth Oxford Academic, London, 1986.

[21] D. Xie and G. Yan, Mol. Phys. **88**, 1349 (1996).

[22] J.H. Schryber, O.L. Polyansky, P. Jensen, and J. Tennyson, private communication.

[23] M.J. Bramley and T. Carington Jr., J. Chem. Phys. **101**, 8494 (1994).

[24] R.E. Wyatt and C. Iung, in *Dynamics of Molecules and Chemical Reactions*, R.E. Wyatt and J.Z.H. Zhang, Eds., Dekker, New York, 1996, p. 59.

AB INITIO DETERMINATION OF BAND STRUCTURES OF VIBRATIONAL SPECTRA OF NON-RIGID MOLECULES. APPLICATIONS TO METHYLAMINE AND DIMETHYLAMINE.

Y.G. Smeyers, M.L. Senent and M. Villa[1]
Instituto de Estructura de la Materia, C.S.I.C.
calle Serrano, n° 123, E-28006 MADRID

Abstract

The ab initio determination of the band structures of infrared spectra is described giving as examples the methyl torsion and amine wagging in methylamine and the double torsion in dimethylamine. In addition, the influence of the amine hydrogen symmetric bending and the CNC skeleton symmetric bending is considered in methylamine and dimethylamine, respectively. For this purpose, the potential energy sufaces and kinetic parameters are determined at the RHF/MP2 levels with large basis sets. The numerical results are fitted as a function of the vibrational angles to conveniently symmetry adapted functional forms. The Schrödinger equations for the nuclear motions solved by expanding the solutions into products of trigonometric functions. From the energy levels, the vibrational functions and the electric dipole moment variations the bands locations and intensities are determined. The calculated spectra are compared with the available experimental data. In the case of methylamine, the torsional splittings and frequencies are relatively well reproduced, whereas the wagging frequencies appear to be slightly too high. In the case, of dimethylamine, the symmetric and antisymmmetric torsion modes are very well reproduced, whereas the CNC bending frequencies appear also to be too high.

List of Contents

1. Introduction
2. Theory
3. Applications
    3.1. Methyl Torsion and Amine Hydrogen Wagging in Methylamine
    3.2. Amine Hydrogen Wagging and Bending in Methylamine
    3.3. Double Torsion in Dimethylamine
    3.4. Double Torsion + Bending in Dimethylamine
4. Conclusions

---

[1] Permanent Address: Departamento de Química, UAM, Iztapalapa,Av.Purisima y Michoacan, CP 09340, MEXICO D.F.

ADVANCES IN QUANTUM CHEMISTRY, VOLUME 32
Copyright ©1999 by Academic Press. All rights of reproduction in any form reserved.
0065-3276/99 $30.00

1. INTRODUCTION

A non-rigid molecule is defined as a molecular system possessing large amplitude vibrational modes. These large amplitude motions occur when the molecule is flexible and especially when it possesses various isoenergetic conformations separated by relatively low energy barriers. These motions use to be internal rotations or inversions which give rise to large *progressions* in the electronic, far infrared (FIR) and Raman spectra [1-3].

In the following, the calculations of the methylamine and dimethylamine far infrared spectra will be considered. Methylamine will be considered in two different ways: the methyl torsion and the amine hydrogen atom wagging; and the amine hydrogen wagging, and symmetric bending discarding the methyl torsion, in order to study the influence of the bending on the wagging mode. Dimethylamine will be considered also in two different ways: the double methyl rotation, and the double methyl rotation plus the CNC angle symmetric bending.

In this aim, the technique developed for determining the acetone far infrared spectrum [4] is adopted . In this, the potential energy surface on which the nuclei are moving is determined, the nuclear motion Schrödinger equation is solved, and from the energy levels, torsional functions and the dielectric moment variations the FIR spectrum is built up.

2. THEORY

The potential energy surface on which the nuclei are moving is determined assuming the Born-Oppenheimer approximation as well as the separability of the small and large amplitude motions. It is not always easy to distinguish between large and not so large amplitude motions. One criterion can be the energy levels. Usually, motions between isoenergetic conformations as well as vibrational motions affected seriously by the former are considered together.

Under these conditions, the molecule is supposed to be in equilibrium with respect to the small amplitude vibration modes. As a result, the total energy of each conformation of the non-rigid coordinate space is determined by a reliable ab initio procedure with full optimization of the geometry with respect to the other coordinates.

From the optimized geometry the kinetic parameters are deduced, for each conformation, by inversion of the inertial matrix according to the Harthcock and Laane's procedure [5]:

$$\begin{pmatrix} I & X \\ X^t & Y \end{pmatrix} \tag{1}$$

where I is the inertial tensor corresponding to the overall rotation Y is the vibrational submatrix (here diagonal), and X is the interaction matrix between the external and internal motions.

In particular we have:

$$X_{ix} = \sum_a m_a \left(\vec{r}_a \times \frac{\partial \vec{r}_a}{\partial \alpha_i} \right)_x$$

$$Y_{ij} = \sum_a m_a \left(\frac{\partial \vec{r}_a}{\partial \alpha_i} \right) \bullet \left(\frac{\partial \vec{r}_a}{\partial \alpha_j} \right) \tag{2}$$

where m_a is the mass of atom a, and $\vec{r}_a$ its displacement vector.

Finally, the numerical results for the potential and kinetic parameters are adjusted to a symmetry adapted functional form.

In order to solve the Schrödinger equation for the nuclear motions, the vibrational solutions are developed in terms of some basis functions, and the Hamiltonian matrix diagonalized, yielding the energy levels and the wave functions. As basis functions, the symmetry vectors which factorize into boxes the Hamiltonian matrix are conveniently used.

This technique assumes previous knowledge of the symmetry eigenvectors which may be deduced by using Group Theory for Non-Rigid Molecules as well as some information about the necessary basis length [2,3].

In the spectrum calculations the band frequencies and intensities are determined in absolute value without any scale factor. The band frequencies are determined by the difference between the energy levels, of initial and final states. The intensities are determined through the electric dipole moment variation approach [6]:

$$I_{if} = \frac{g}{3BR^2e^2}[\epsilon_i - \epsilon_f][C_i - C_f] < \varphi_i|\vec{\mu}|\varphi_g >^2 \tag{3}$$

where ϵ, C and φ are the energies, populations and vibrational functions of the initial (i) and final (f) states. R and B are the average rotation radii and kinetic parameters, $\vec{\mu}$ is the dipole moment written as a function of the large amplitude coordinates. $\vec{\mu}$ is obtained in the same calculations for the potential. The populations are given by the Boltzmann statistics and the dipole moment components are conveniently shifted along the principal inertial axes of the molecule.

In order to determine the band profiles, the shape of the molecule has to be considered [7]. As is well known, in symmetric prolate or oblate tops, the dipole variation along the main principal axis (A or C) gives rise to **a** or **c** type bands, respectively, with a sharp Q branch. On the contrary, the perpendicular dipole moment variation gives rise to **b-c** or **a-b** type bands with broad PR branches. Generally, only the sharp bands, which can be more easily compared with the experimental data are considered.

Furthermore, we have to remark that Group Theory for Non-Rigid Molecules may be advantageously used to deduce a symmetry adapted analytical form for the potential, as well as the symmetry eigenvectors for simplifying the Hamiltonian matrix solution. In the same way, Group Theory permits to label and classify the energy levels and the vibrational functions. Finally, it may be also used to deduce selection rules for the infrared transitions.

3.APPLICATIONS

3.1. Methyl Torsion and Amine Hydrogen Wagging in Methylamine

Let us consider first the methyl internal rotation and the amine hydrogen wagging in methylamine (Fig. 1), taking as origin for the torsion and wagging angles the molecular plane of methylamine in a planar conformation. The Non-Rigid Group for the methyl torsion and amine hydrogen waging in methyl amine has been derived in [8] into the Longuet-Higgins formalism, and in [9] into the physical operations formalism.

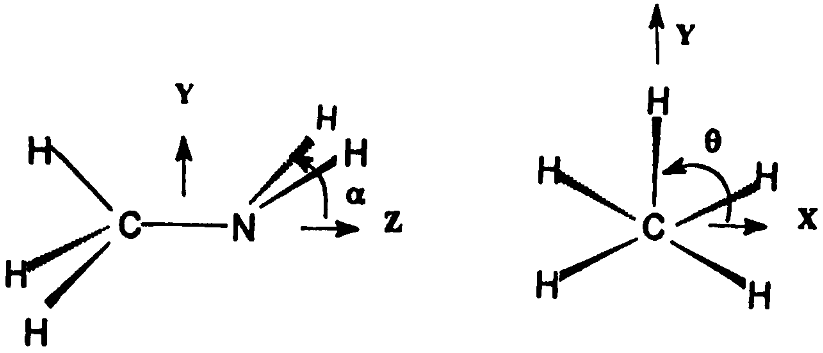

Figure 1. Large amplitude motions in methylamine: torsion (θ) and wagging (α).

The Hamiltonian operator restricted to these two motions takes the form:

$$H(\theta,\alpha) = -\frac{\partial}{\partial\theta}B_\theta(\theta,\alpha)\frac{\partial}{\partial\theta} - \frac{\partial}{\partial\theta}B_{\theta,\alpha}(\theta,\alpha)\frac{\partial}{\partial\alpha} - \frac{\partial}{\partial\alpha}B_{\alpha,\theta}(\theta,\alpha)\frac{\partial}{\partial\theta} - \frac{\partial}{\partial\alpha}B_\alpha(\theta,\alpha)\frac{\partial}{\partial\alpha} + V(\theta,\alpha) \qquad (4)$$

It is easily seen to be invariant under the following operations [9]:

1) A threefold rotation of the methyl group:

$$\hat{C}_3 f(\theta,\alpha) \equiv f(\theta + \frac{2\pi}{3}, \alpha) \qquad (5)$$

2) A twofold rotation of the methyl group followed by a sign change of the rotation:

$$\hat{U} f(\theta,\alpha) \equiv f(\pi - \theta, \alpha) \qquad (6)$$

3) A simultaneous sign change of rotation and wagging angles, (or double switch):

$$\hat{V} f(\theta,\alpha) \equiv f(-\theta, -\alpha) \qquad (7)$$

Notice that the double switch operation exists always when there are symmetry plane in the moving moities and the frame of the molecule [10]. These operations are illustrated in figure 2. With these definitions, the restricted Non-Rigid Group (r-NRG) for the torsion and wagging mode is a group of order twelve, isomorphic to the C_{6v} symmetry point group:

$$C_3^I \wedge [V^I \times U^I] = G_{12} \sim C_{6v} \qquad (8)$$

The subgroups C_3^I, U^I and V^I are defined by the operations (5),(6) and (7), respectively. The character table as well as the symmetry eigenvectors of this group are given in Ref [9].

In particular, we have for the potential energy function, the symmetry adapted analytical form:

$$V(\theta,\alpha) = \sum_{k=even,L} A_{KL}\cos 3K\theta \cos L\alpha + \sum_{k=odd,L} B_{KL}\sin 3K\theta \sin L\alpha \qquad (9)$$

where no cos × sin mixed term appears.

The far infrared spectrum of methylamine has bee studied mainly by Onashi and coworkers [11,12], and Kreglewski et al [13,14].

The potential energy calculations were performed, at the RHF/MP2 level, with the 6-311G++(3fd,3dp) basis set, for 36 selected values of the torsion and wagging angles. In this aim, the GAUSSIAN 92 program package was resorted [15]. The following values were used for the torsion, 0°, 30°, 60° and 90°, and for the wagging, -69.0°, -54.540845°, -38.0°, -19.0°, 0.0°, 19.0°, 38.0°, 54.540845° and 69.0°. The preferred conformations were found at $\theta = 0.0°$ and $\alpha = \pm 54.540845°$ The fit of the relative energy values with respect to the lowest one by a least square method to the equation (9) yields an expression given in Ref.[16].

The B_i kinetic parameters were recalculated for each of the 36 configurations, without the corrections given in Ref. [14,16], and fitted to the same symmetry adapted analytical form (9). The torsion kinetic parameters resemble those of Ref. [16]. In contrast the wagging ones (equilibrium value 26.729 cm^{-1}) differ substantially from those used in [16] (9.602 cm^{-1}), as well as to the approximate experimental value proposed by Onashi et al.[11] (9.19 cm^{-1}).

The torsional-wagging nuclear equation was solved at two levels of approximations: using either the variable kinetic parameters either the equilibrium value. In this aim, 31 × 41 trigonometric functions were used for describing the methyl torsion and the amine hydrogen atom wagging, respectively. The energy levels encountered are given in Table 1, where it is seen that the both approaches yield similar results. The levels are clustered into quartets. In fact it is a matter of sextets taking into account the degeneracies.

The first quartet corresponds to the fundamental level. The second and third to the first and second torsionally excited levels. The fourth quartet corresponds to the first wagging excited level. This assignment rests on the intensities given in Table 2. The dipole moment variations due to a wagging transition must be indeed expected to be much larger than those due to a torsional transition.

It is seen that the first excited torsional levels agree fairly well with the value deduced from experiment [14], whereas the wagging level appears to be too low. In particular, the first excited wagging level is found at 830 cm^{-1} instead of 720 cm^{-1} [14].

This discrepancy could be attributed to the interactions between the wagging and bending motions of the amine hydrogen atoms. If the bending angle is plotted versus the wagging angle a large dependency is indeed detected. The bending angle exhibits the largest value close to 120° (sp^2 hybridization) when the amine group is forced to be in the molecular plane. On the contrary, the bending angle presents the smallest values (sp^3 hybridization) when the amine group adopts a pyramidal conformation [16].

The splittings between the torsional fundamental sublevels for constant and variable B_θ are seen to be 0.353 and 0.435 cm^{-1} in relatively good agreement with the experimental value of 0.249 cm^{-1} given by Onashi et al.[11].

Table 1. Energy levels (in cm^{-1}) for the torsion and wagging vibration modes in Methylamine obtained with the constant and variable (B) kinetic parameters.

Levels		Symmetry	Energy in cm^{-1}	Vibrational mode			Exp.[14]
			B const.	B varia.	ν_{15}	ν_9	
0		A_1	609.697	602.555			
1	-1	E_1	610.051	602.990	0	0	600
	-2	B_2	609.899	603.057			
2	-3	E_2	610.142	603.243			
3	-4	E_2	864.987	859.860			
4	-5	E_1	865.294	860.631	1	0	870
5		A_1	872.070	866.709			
	-6	B_2	872.750	868.414			
6		A_1	1045.610	1041.845			
	-7	B_2	1046.093	1042.972	2	0	1010
7	-8	E_1	1086.093	1083.324			
8	-9	E_2	1086.965	1083.921			
9	-10	E_2	1220.800	1218.555			
10	-11	E_1	1220.937	1018.804	3	0	1310
11		B_1	1363.315	1361.840			
	-12	A_2	1363.459	1362.047			
12		B_2	1375.089	1373.934			
	-13	A_1	1376.628	1375.643	4	0	
13		A_1	1391.518	1409.130			
14	-14	E_1	1395.773	1415.389			
15	-15	E_2	1404.130	1428.379	0	1	1315
	-16	B_2	1409.621	1436.863			
16	-17	E_2	1558.542	1558.314	4	0	
17	-18	E_1	1559.592	1559.464			
18		B_1	1608.333	1627.357			
19	-19	E_2	1607.474	1627.357	1	1	
20	-20	E_1	1625.599	1658.956			
	-21	A_2	1657.308	1699.178			

In Table 2, the calculated frequencies and intensities are given. Unfortunately, the FIR spectrum of methylamine is too crowded to permit a reliable comparison. The first torsional frequency 257.3 cm^{-1}, however, appears to be in very good agreement with the experimental value 262.7 cm^{-1} [11].

Table 2. Far infrared frequencies (in cm^{-1}) and relative intensities for the c type torsional and wagging bands in methylamine obtained from ab initio calculations with the variable kinetic parameters.

Assignments $\nu\nu'$	$\rightarrow$ $\nu\nu'$	Symmetries	Frequencies	Intensities
00	10			
		$E_1 \rightarrow E_2$	256.87	1.10^{-4}
		$E_2 \rightarrow E_1$	257.39	1.10^{-4}
10	20			
		$E_1 \rightarrow E_2$	221.67	–
		$E_2 \rightarrow E_1$	221.71	–
00	01			
		$B_2 \rightarrow A_1$	806.07	0.0858
		$E_2 \rightarrow E_1$	812.15	0.0531
		$E_1 \rightarrow E_2$	825.39	0.0543
		$A_1 \rightarrow B_2$	834.31	0.0837
10	11			
		$A_2 \rightarrow B_1$	758.94	0.0213
		$E_2 \rightarrow E_1$	771.68	0.0206
		$E_1 \rightarrow E_2$	799.10	0.0197
		$B_1 \rightarrow A_2$	832.47	0.0206

3.2. Amine Hydrogen Wagging and Bending in Methylamine

In order to verify the interaction between the amine hydrogen atoms bending and wagging modes, the energy levels corresponding to these motions are calculated discarding the torsion. The three-dimensional problem will be considered in a next future. For this purpose, let us take as before as origin for the wagging angle the molecular plane of methylamine in a planar conformation. The bending coordinate is the H-N-H angle.

The Hamiltonian operator restricted to these two motions is similar to the previous one (4) in which the θ variable has to be replaced by the β one. This operator is easily seen to be invariant under the following dynamical operations:

1) A change of sign of the wagging angle:

$$\hat{U}_\alpha f(\alpha,\beta) = f(-\alpha,\beta) \tag{10}$$

2) A change of sign of the bending angle:

$$\hat{U}_\beta f(\alpha,\beta) = f(\alpha,-\beta) \tag{11}$$

Operation 1) is closely related with the full optimization of the molecular geometry. In particular, the conformation of the methyl group adopts the energy minimum for any values of α and β, in such a way that it may be considered as planar.

As a result, the r-NRG for these motions may be written as:

$$[U_\alpha^I \times U_\beta^I] = G_4 \sim C_{2v} \tag{12}$$

which is a group of order four isomorphic with the symmetry point group C_{2v}, with the irreducible representations A_1, A_2, B_1 and B_2.

In this expression, the subgroups U_α^I and U_β^I are defined from the operations (10) and (11), respectively.

In these conditions, the potential energy function for these two motions takes the symmetry adapted analytical form:

$$V(\alpha,\beta) = \sum_K \sum_L \cos(K\alpha)\cos(L\beta) \tag{13}$$

The energy of methylamine was determined for a set of 49 wagging and bending angles using the same approach: RHF/MP2 with 6-311G++(3df,3dp) basis set, and with full optimization of the geometry with respect to the other coordinates including the torsion. For the bending the following values were considered: 91.27.30°, 96.2730°, 101.2730°, 106.2730°, 111.2730°, 116.2730° and 121.27.30°, i.e., each 5.0° from -15.0° to 15.0° arround the minimum found at 106.2730°. For each of these bending values a different optimum wagging angle was found. This was included in the set of wagging angles used in the calculations: 0.0°, 15.0°, 30.0°, 45.0°, 60.0°, and 70.0°.

These electronic energy values were fitted to expression (13), as well as the kinetic parameters obtained from the optimum geometries. For solving the Schrödinger equation, the solutions were developed on 41 × 41 trigonometric functions for the wagging and bending, respectively. The energy levels are given in Table 3.

Table 3. Energy levels (in cm^{-1}) for the wagging and bending vibration modes in Methylamine.

Levels	Symmetry	Energy in cm^{-1}	Vibrational mode	
			ν_9	ν_4
0	A_1	1230.34	0	0
-1	B_1	1230.34		
-2	B_2	1231.20		
1	A_2	1231.20		
-3	B_1	1969.86	1	0
2	A_1	1969.86		
3	A_2	2000.25		
-4	B_2	2000.25		
4	A_1	2524.90	2	0
-5	B_1	2524.90		
-6	B_2	2724.62		
5	A_2	2724.62		
-7	B_1	2859.01	0	1
6	A_1	2859.01		
7	A_2	2881.62		
-8	B_2	2881.63		

In this table, it is seen that the levels appear clustered into quartets as to be expected from a four well potential energy surface. The first quartet corresponds to the fundamental level. The first and second excited quartets may be attributed to the wagging mode, whereas the third one to the bending mode. This assignment rests on the theoretical intensities given in Table 4. No strong intensities were obtained between the first and third levels, nor between the second and the fourth ones. In addition, the two wagging transitions present a quasi harmonic behavior.

Table 4. Far infrared frequencies (in cm^{-1}) and relative intensities for the **c** type wagging and bending bands in methylamine obtained from ab initio calculations.

Assignments		Symmetries	Frequencies	Intensities
$\nu\nu'$ $\rightarrow$	$\nu\nu'$			
0 0	1 0			
		$A_1 \rightarrow B_2$	769.91	0.2398
		$B_1 \rightarrow A_2$	769.91	0.2397
		$B_2 \rightarrow A_1$	738.67	0.2589
		$A_2 \rightarrow B_1$	738.67	0.2589
10	20			
		$A_1 \rightarrow B_2$	754.76	0.0053
		$B_1 \rightarrow A_2$	754.76	0.0053
		$A_2 \rightarrow B_1$	524.65	0.0134
		$B_2 \rightarrow A_1$	524.65	0.0134
00	01			
		$B_1 \rightarrow A_2$	1651.29	0.0255
		$A_1 \rightarrow B_2$	1651.29	0.0255
		$B_2 \rightarrow A_1$	1627.81	0.0370
		$A_2 \rightarrow B_1$	1627.81	0.0370

It is seen that the first excited level is found at 770 cm^{-1} above the fundamental one in better agreement, but still slightly too high when compared with the experimental value 720 cm^{-1} [14].

The splitting between the wagging fundamental sublevels is 0.756 cm^{-1} in some agreement with an hypothetical experimental value of 0.206 cm^{-1} given by Honashi et al.[11].

3.3. Double Torsion in Dimethylamine

Let now consider the double methyl torsion in dimethylamine, let us remark that the two methyl groups are superimposable by reflection, see Fig. 2. The Hamiltonian operator is then seen to be invariant under the following dynamical operations [10]:

1) A threefold rotation of each of the methyl group:

$$\hat{C}_3 f(\theta) = f(\theta + \frac{2\pi}{3}) \tag{14}$$

2) An exchange-double switch of the two rotation angles:

$$\hat{W}\hat{V}f(\theta_1,\theta_2) = f(-\theta_2,-\theta_1) \tag{15}$$

With such a definition, the r-NRG for the double internal rotation in dimethylamine is a group of order 18:

$$[C_3^I \times C_3'^I] \times [WV]^I = G_{18} \tag{16}$$

The character table of such a group is given in Refs.[17,18].

In particular, the following symmetry adapted expression is found for the totally symmetric potential energy function:

$$\begin{aligned} V(\theta_1,\theta_2) = &\sum_{K,L=0} A_{KL}[\cos 3K\theta_1 \cos 3L\theta_2 + \cos 3L\theta_1 \cos \theta 3K\theta_2] + \\ &\sum_{K,L=1} B_{KL}[\sin 3K\theta_1 \sin 3L\theta_2 + \sin 3L\theta_1 \cos \theta 3K\theta_2] + \\ &\sum_{K=0,L=1} C_{KL}[\cos 3K\theta_1 \sin 3L\theta_2 - \sin 3L\theta_1 \cos \theta 3K\theta_2] \end{aligned} \tag{17}$$

Let us remark that when the third set of terms of this equation is neglected this expression coincides with that for planar acetone of G_{36} symmetry [4]. Since the coefficients of these terms are generally small, both descriptions are considered in the following.

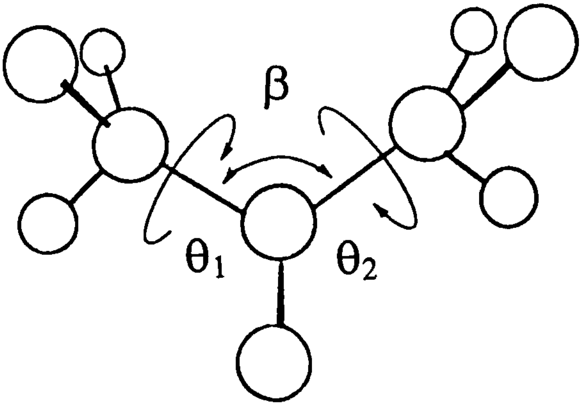

Figure 2. Structure of dimethylamine. The θ_1 and θ_2, torsional angles, and the β bending angle.

The electronic energy of dimethylamine was determined for ten conformations at the RHF/MP2 level with the 6-311G(df,p) basis set. The symmetry criterion was applied to select the conformations for the torsional coordinates. The conformation, in which one of the hydrogen of each methyl group lies on the CNC molecular plane and pointing outwards, was taken as the origin for the rotations. In this condition, the selected geometries were (0^o ,0^o), (60^o,0^o), (60^o,60^o), (30^o,0^o), (0^o,30^o), (60^o,30^o) (30^o,30^o), (30^o,-30^o) and (-30^o,30^o).

In the most stable conformation, the methyl hydrogen atoms do no lie anymore in the CNC plane but at 3.3^o and -3.3^o. The wagging and bending angles were found to be equal to 55^o and 111.6^o, respectively.

The relative energy values with respect to the most stable conformation were fitted to expression (17) taking the energy minimum as origin for the potential. The kinetic parameters were determined from the optimized geometries by using equation (1), and fitted to the same expression (17).

For solving the Schrödinger equation, the solutions were developed on 37 × 37 trigonometric functions for each torsion mode. In Table 5, the energy levels calculated into the two models, G_{18} and G_{36}, are given.

In this table it is seen that the energy levels are clustered into quartets. In fact it is a matter of a ninefold multiplicity taking into account the degeneracies of the G and E representations in accordance to the nine potential energy wells. The G_{36} model furnishes sligthly too high levels.

The first quartet corresponds to the fundamental level. The second and fourth to antisymmetric torsionally excited levels. The third, fifth and the last to symmetric torsionally excited levels. The antisymmetric torsion modes correspond to a gearing rotation along the principal diagonal of the potential energy surface. They are active in Raman and somewhat in infrared spectra. The symmetric modes correspond to an antigearing rotation along the secondary diagonal and are active in infrared.

Table 5. Dimethylamine energy levels (in cm^{-1})

			$V_3(G_{36})$		$V_3(G_{18})$
0	0	A_1	240.392	A_1	237.541
		G	240.392	G	237.541
		E_1	240.392	E_1	237.541
		E_3	240.392	E_3	237.541
1	0	A_3	461.562	A_2	458.767
		G	461.561	G	458.766
		E_2	461.560	E_2	458.765
		E_3	461.560	E_3	458.765
0	1	A_2	491.478	A_1	490.330
		G	491.477	G	490.329
		E_1	491.476	E_1	490.328
		E_4	491.474	E_3	490.328
2	0	A_1	677.741	A_1	675.153
		G	677.759	G	675.170
		E_1	677.778	E_1	675.188
		E_3	677.778	E_3	675.188
1	1	A_1	701.276	A_2	700.143
		G	701.304	G	700.171
		E_2	701.332	E_2	700.198
		E_4	701.332	E_3	700.198
0	2	A_1	739.400	A_1	738.909
		G	739.409	G	738.918
		E_1	739.418	E_1	738.927
		E_3	739.418	E_3	738.927
3	0	A_1	887.090	A_2	884.838
		G	886.907	G	884.663
		E_2	886.729	E_2	884.493
		E_3	886.729	E_3	884.493
0	3	A_2	982.308	A_1	982.045
		G	982.287	G	982.024
		E_1	982.266	E_1	982.003
		E_4	982.266	E_3	982.003

In Tables 6a and 6b, the frequencies and intensities are given for the two torsional modes toghether with the experimental data. It is a matter of **a**- and **b-c** hybrid type bands with sharp Q branches. A very good agreement is observed [19]. The relative position of the ν_{12} and ν_{24} fundamental frequencies, however, shows a small error: 31.6 cm^{-1} instead of 36.9 cm^{-1}.

Table 6a. Calculated frequencies (in cm^{-1}) and relative intensities for the symmetric ν_{12} torsion mode (double antigearing rotation) in dimethylamine.

assign.	freq.	int.	exp.[a] [19]	
0 0 → 0 1				
A_1-A_1	252.789	3.690		
G-G	252.788	7.379	256.3	vs
E_1-E_1	252.787	1.845		
E_3-E_3	252.787	1.845		
0 1 → 0 2				
A_1-A_1	248.579	2.038		
G-G	248.589	4.077	250.8	s
E_1-E_1	248.599	1.019		
E_3-E_3	248.599	1.019		
0 2 → 0 3				
A_1-A_1	243.136	0.834		
G-G	243.106	1.657	245.3	ms
E_1-E_1	243.076	0.417		
E_3-E_3	243.076	0.417		
1 0 → 1 1				
A_2-A_2	241.376	0.926		
G-G	241.405	1.854	239.8	s
E_2-E_2	241.433	0.464		
E_3-E_3	241.433	0.464		

[a] vs = very strong; s = strong; ms = medium strong

Table 6b. Calculated frequencies (in cm^{-1}) and relative intensities for the symmetric ν_{24} torsion mode (double gearing rotation) in dimethylamine.

assign.	freq.	int.	exp.[a]	
0 0 → 1 0				
A_1-A_2	221.226	0.101		
G-G	221.225	0.203	219.4	ms
E_1-E_2	221.224	0.051		
E_3-E_3	221.224	0.051		
1 0 → 2 0				
A_2-A_1	216.386	0.023		
G-G	216.404	0.046	213.0	w
E_2-E_1	216.423	0.012		
E_3-E_3	216.423	0.012		

[a] ms = medium strong; w = weak.

3.4. Double Torsion + Bending in Dimethylamine

Since the introduction of the COC angle bending mode in dimethylether [20] appears to correct the gap between the symmetric and antisymmetric torsion modes, the symmetric bending of the CNC angle was introduced explicitly in the calculations. The non-bonding interactions between the hydrogen atoms during the methyl torsion could be indeed important. The three-dimensional vibration Hamiltonian of dimethylamine may be written as:

$$\begin{aligned} H(\theta_1,\theta_2,\beta) = &-\frac{\partial}{\partial\theta_1}B_{11}\frac{\partial}{\partial\theta_1} - \frac{\partial}{\partial\theta_2}B_{22}\frac{\partial}{\partial\theta_2} - \frac{\partial}{\partial\beta}B_{33}\frac{\partial}{\partial\beta} \\ &-\frac{\partial}{\partial\theta_1}B_{12}\frac{\partial}{\partial\theta_2} - \frac{\partial}{\partial\theta_2}B_{12}\frac{\partial}{\partial\theta_1} - \frac{\partial}{\partial\theta_1}B_{13}\frac{\partial}{\partial\beta} - \frac{\partial}{\partial\beta}B_{13}\frac{\partial}{\partial\theta_1} \\ &-\frac{\partial}{\partial\theta_2}B_{23}\frac{\partial}{\partial\beta} - \frac{\partial}{\partial\beta}B_{23}\frac{\partial}{\partial\theta_2} + V(\theta_1,\theta_2,\beta) \end{aligned} \tag{18}$$

where $B_{ij}(\theta_1,\theta_2,\beta)$ represents the kinetic energy parameters and $V(\theta_1,\theta_2,\beta)$ the three-dimensional potential energy function.

It is easily seen that this three-dimensional Hamiltonian operator is invariant under the same operations that those of the two-dimensional problem, since the bending mode is totally symmetric. The r-NRG for double methyl torsion and bending in dimethylamine will be the G_{18}.

The three-dimensional potential energy function was determined from the electronic energies of 150 selected conformations. Calculations were performed at the RHF/MP2 level with the 6-311G(d,p) basis set. All the structures were fully optimized taking into account in some way the interactions with the remaining vibration modes.

The same symmetry criterion used before was applied to select the conformations for the torsional coordinates. In addition, five values of the CNC angle around the equilibium, were also selected for describing the variation of the energy with the bending. These angle values were -5.0°,-3.0°. 0.0° 3.0° and 5.0°. The relative energy values were fitted to the expression for the potential.

In the most stable conformation, the methyl hydrogen atoms do no lie anymore on the CNC plane but stand at 4.0° and -4.0°. In the same way, the CNC angle was found to be 111.37°.

The kinetic parameters were determined as before using the Harthcock and Laane procedure [1,2], but now the dependence on the remaining vibrational coordinates was not taken into account because the previous calculations showed that they were very small [18].

The Schrödinger equation was solved by developing the solutions onto 37 × 37 trigonometric functions and 10 harmonic oscillator ones. This basis length implies a Hamiltonian matrix of order 13,690. The symmetry properties of the G_{18} group permit, however, to factorize this matrix into eight boxes of dimension: $A_1(910)$, $A_2(780)$, $G(3120)$, $E_1(1560)$, $E_2(1320)$ and $E_3(1440)$. Some of them are degenerate, so that only six matrices have to be diagonalized.

In Table 7, the energy levels for the double methyl torsion and bending are given. It is seen that as before the levels are clustered into quartets. In the second column of this table, the bending levels are collected. In Table 8, the frequencies of the torsional bands for the bending fundamental in which the v"= 0 are given.

The torsional frequencies obtained in these three-dimensional calculations may be compared with those of the previous example calculated in two dimensions, as well as with the experimental data [19] . It is clear that the introduction of the bending mode displaces the whole spectrum to higher wave-numbers, but modifies the relative position of the symmetric ν_{12} and antisymmetric ν_{24} torsion modes. There are no changes in the assignment, but now the gap between the two modes is 37.9 cm_1 in better agreement with the experimental value of 36.9 cm^{-1}. The bending levels are found to be too high.

Table 7. Energy levels (in cm^{-1}) for the double methyl torsion and CNC bending in dimethylamine.

v	v'	v"		calc.	v	v'	v"		calc.
0	0	0	A_1	442.54	0	0	1	A_1	854.45
			G	442.40				G	854.45
			E_1	442.54				E_1	854.45
			E_3	442.54				E_3	854.45
1	0	0	A_2	659.40	1	0	1	A_2	1071.69
			G	659.40				G	1071.66
			E_2	659.40				E_2	1071.64
			E_3	659.40				E_3	1071.64
0	1	0	A_1	697.98	0	1	1	A_2	1108.87
			G	697.97				G	1108.82
			E_1	697.97				E_1	1108.76
			E_3	697.97				E_3	1108.76
2	0	0	A_1	873.90	2	0	1	A_1	1280.16
			G	873.91	2	0	1	G	1280.86
			E_1	873.93				E_1	1281.64
			E_3	873.93				E_3	1281.64
1	1	0	A_2	902.75	1	1	1	A_2	1321.56
			G	902.77				G	1321.83
			E_2	902.80				E_2	132.16
			E_3	902.80				E_3	132.16
0	2	0	A_1	949.75	0	2	1	A_1	1361.91
			G	949.76				G	1361.92
			E_1	949.77				E_1	1361.94
			E_3	949.77				E_3	1361.94
3	0	0	A_2	1085.46					
			G	1085.35					
			E_2	1085.24					
			E_3	1085.24					
0	3	0	A_1	1196.76					
			G	1196.73					
			E_1	1196.69					
			E_3	1196.70					

Table 8. Frequencies (in cm^{-1}) for the symmetric ν_{12} (antigearing) and antsymmetric ν_{24} (gearing)torsional modes in dimethylamine.

v	v'	v"		v	v'	v"		calc.	obs.[19]	cal-obs
antigearing mode										
0	0	0	→	0	1	0	$A_1 \to A_1$	258.12		
							$G \to G$	258.12	256.3	1.8
							$E_1 \to E_1$	258.12		
							$E_3 \to E_3$	258.12		
0	1	0	→	0	2	0	$A_1 \to A_1$	254.34		
							$G \to G$	254.35	250.8	3.5
							$E_1 \to E_1$	254.36		
							$E_3 \to E_3$	254.36		
0	2	0	→	0	3	0	$A_1 \to A_1$	249.46		
							$G \to G$	249.42	245.3	4.1
							$E_1 \to E_1$	249.38		
							$E_3 \to E_3$	249.38		
1	0	0	→	1	1	0	$A_2 \to A_2$	246.33		
							$G \to G$	246.35	239.8	6.5
							$E_2 \to E_2$	246.37		
							$E_2 \to E_2$	246.37		
gearing mode										
0	0	0	→	1	0	0	$A_1 \to A_2$	220.18		
							$G \to G$	220.18	219.4	0.6
							$E_1 \to E_2$	220.18		
							$E_3 \to E_3$	220.18		
1	0	0	→	2	0	0	$A_2 \to A_2$	217.64		
							$G \to G$	217.65	213.0	4.6
							$E_2 \to E_1$	217.67		
							$E_3 \to E_3$	217.67		

4. CONCLUSIONS

The ab initio calculations appear to reproduce relatively well the torsional energy levels as well as the far infrared torsional spectra of methylamine and dimethylamine. The wagging and bending energy levels appear to be too high and the corresponding infrared spectra shift to higher wave-numbers. In addition, the interaction between the wagging and/or bending with the torsion seems to be relatively weak. In the case of methylamine, three-dimensional calculations taking into account simultaneously torsion, wagging and symmetric bending seem to be necessary.

Anyway the present approach appears to be a powerful tool, which could help in the assignment of large-amplitude bands as well as in the prediction of the spectrum.

ACKNOWLEDGEMENTS

Y.G.S. and M.L.S. wish to thank the *"Comisión Interministerial de Ciencias y Tecnología"* of Spain for financial support through grant nº PB93-0185, M.V. would like to thank the CSIC (Spain) and CONACYT (Mexico) for a sabbatical fellowship.

References

[1] D.G. Lister, J.N. MacDonald and N.L.Owen, in "*Internal Rotation an Inversion*", Academic Press, London, 1978.

[2] H.C. Longuet-Higgins, Mol. Phys.,**6**, 445 (1963).

[3] Y.G. Smeyers, Adv. Quantum Chem.,**24**, 1-77, (1992)

[4] Y.G. Smeyers, M.L. Senent, V. Botella and D.C. Moule, J.Chem. Phys., **98**, 2754 (1993)

[5] M.A. Harthcock and J. Laane, J. Chem. Phys., **89**, 4231 (1985).

[6] Y.G. Smeyers, A. Hernández-Laguna and P.Galera-Gómez, An. Quim. (Madrid), **76**, 67 (1980).

[7] J.M. Hollas, in "*High Resolution Spectroscopy*", Butterworths, London, 1982.

[8] N. Onashi and J.T. Hougen, J. Mol. Spectrosc., **121**, 484 (1987).

[9] Y.G. Smeyers, M. Villa and E. Ortiz, J. Math. Chem., **18**, 209-216(1985).

[10] J. Maruani, Y.G. Smeyers and A. Hernández-Laguna, J. Chem. Phys., J. Chem. Phys., **74**,3123 (1982).

[11] N. Ohashi, K. Takagi, J.T. Hougen, W.B. Olson and W.J. Lafferty, J. Mol Spectrosc.,**126**, 443 (1987); ib. **132**, 242 (1988).

[12] N. Ohashi, S. Shimada, W.B. Olson, and K. Kawagushi, J. Mol. Spectrosc., **152**, 298 (1992).

[13] M. Kreglewski and F. Winther, J. Mol. Spectrosc. **156**, 261 (1992).

[14] M. Kreglewski, in "Structure and Conformation of Non-Rigid Molecules", (J. Laane et al Eds.), NATO-ASI Series, pp 29-43, Kluwer, Dordrecht, 1993.

[15] M.J. Firsch, G.W. Trucks, M. Head-Gordon, P.M.W. Gill, M.W. Wong, J.B. Foresman, B.G. Johnson, H. B. Schlegel, M.A. Robb, E.R. Repongle, R. Gomperts, J.L. Andres, K. Raghvachari, J.S. Binkley, C. González, R.L. Martin, D.J. Fox, D,J. Defrees, J. Baker, J.J.P. Stewart and J.A. Pople (Gaussian, Inc. Pittsburg PA, 1992).

[16] Y.G. Smeyers, M. Villa and M.L. Senent, J. Mol. Spectrosc, **177**, 66-73 (1996)

[17] Y.G. Smeyers and A. Niño, J. Comput. Chem.m, **8**,380 (1987).

[18] M.L. Senent and Y.G. Smeyers, J. Chem. Phys.,**105**, 2789 (1996).

[19] J.R. Durig, M.G. Griffin an P. Groner, J. Phys. Chem., **81**, 554 (1977).

[20] M.L. Senent, D.C. Moule and Y.G. Smeyers., J. Chem. Phys.,**102**, 5952 (1995).

Gauge Invariance and Multipole Moments

R.G.Woolley

Department of Chemistry and Physics,
Nottingham Trent University, Clifton Lane,
Nottingham NG11 8NS, U.K.

Abstract

Some arguments that imply limitations on the concept of molecular multipole moments due to the requirements of gauge invariance are presented. The discussion is based on a pair of polarization field vectors which are natural generalizations of multipole series. A class of transformations that mix some of the components of the polarization field vectors, so spoiling a separation into `electric′ and `magnetic′ types, is identified. The results are related to the gauge-invariant transition amplitudes.

1. Introduction
2. Polarization fields and the interaction potential
3. The charge-current density and polarization fields
4. Discussion

References

ADVANCES IN QUANTUM CHEMISTRY, VOLUME 32

Copyright ©1999 by Academic Press. All rights of reproduction in any form reserved.

0065-3276/99 $30.00

1. Introduction

An important guiding principle in theoretical work is to express the equations describing physical observables in such a way as to make explicit their *invariances* under specified transformations, for example changes of coordinates - or more generally changes of reference frames under Galilean or Lorentz transformations, gauge transformations and so on. Only in rather special cases is it possible to carry out calculations in a *manifestly* invariant fashion. Thus it is usually the case that to carry out a particular calculation some *choice* of coordinates is required; of course this choice should not affect the result. Such a choice is only a matter of convenience, but may also seem 'natural' or 'physical'. It is easy to think of situations where a physical quantity is expressed, in general, as a sum of distinct terms all of which except one can be made to vanish by a choice of 'coordinates', so that the physical quantity is numerically equal to this one term. It is possible for the appeal of 'physical' choices to be deemed to be more important than the requirements of more abstract fundamentals e.g. through a particular choice of coordinates or preferred reference frame being singled out as being 'physically significant'. Two examples show different aspects of this idea.

According to the usual second-order perturbation theory for an atom or molecule in a static magnetic field, the magnetic susceptibility, χ, can be written as the sum of two terms,

$$\chi = \chi_d[A] + \chi_p[A] \tag{1}$$

conventionally known as the 'diamagnetic' and (Van Vleck) 'paramagnetic' contributions. The two terms are not separately gauge invariant and so can be varied at will by making gauge transformations of the vector potential **A**, but their sum χ *is* invariant, and χ is a physical observable. In the particular case of an atom it is possible to choose the vector potential in such a way (using the nucleus as the origin for the coordinates) that χ_p vanishes, so that χ and χ_d are numerically equal. In a pioneering variational calculation of χ_d, Kirkwood was able to demonstrate a relation between the magnetic susceptibility and the electric polarizability, α, for an atom. The spirit of Kirkwood's calculation can be seen in the literature devoted to atom and bond contributions to χ_d and χ_p for molecules that involves the processing of experimentally determined χ values [1]. On the other hand, if gauge invariance is demanded, Kirkwood's relationship for an N-electron system must be

$$\chi = - C (N\alpha)^{1/2} \tag{2}$$

where C depends on only fundamental constants, i.e. one between α and χ, rather than χ_d, because the former are both gauge-invariant, while χ_d is not [2].

Next, consider a charged parallel plate capacitor; an observer in a reference frame that is at rest relative to the capacitor (the laboratory frame) will describe it as the source of a static electric field ($\mathbf{E} = \mathbf{E}_1$; $\mathbf{B} = \mathbf{B}_1 = \mathbf{0}$) determined purely by a scalar potential. An observer moving uniformly relative to the capacitor sees a magnetic field ($\mathbf{B}_2$) in addition to an electric field ($\mathbf{E}_2$) because this observer sees a current flowing in opposite directions in the plates; thus the notion of 'an electric field' is not Lorentz invariant. The charge density ρ and the current density $\mathbf{j}$ together transform as a 4-vector j_μ; the first reference frame has $j_0 = \rho$ as the only non-zero component, but this is no longer true for the moving frame [3]. These observations about different reference frames are related by the fact that $\mathbf{E}.\mathbf{E} - c^2 \mathbf{B}.\mathbf{B}$ is a Lorentz invariant and both observers agree as to its value (similarly for $\mathbf{j}.\mathbf{j} - c^2\rho^2$). Obviously the laboratory frame is the natural choice to make to describe the physics of a capacitor, and it would be extreme to require manifest invariance in such a discussion.

Molecular multipole moments are widely used in the perturbation theory of molecule-radiation interactions, routinely calculated in standard computational codes and subject to experimental determinations; and yet as shown by Barron and Gray [4], the multipolar interaction between molecules and electromagnetic fields can be made explicit directly by the *choice* of a particular form of gauge. Definitions of multipoles are conventional - not least because the origin about which the multipole expansion is made is arbitrary - and a choice must be made; different choices can be identified with different gauges. This raises the question - in what circumstances can multipoles be physical observables ? In a recent paper we described how the electric polarization field $\mathbf{P}(\mathbf{x})$ for a collection of charges, which is a natural generalization of a multipole series of electric type, is intimately involved with the issue of gauge invariance [5]. A gauge condition that selects a particular vector potential, $\mathbf{A}(\mathbf{x})$, for the electromagnetic field can be expressed as an integral over the polarization field $\mathbf{P}(\mathbf{x})$, and a specific choice for $\mathbf{P}(\mathbf{x})$ [6] yields the multipolar gauge specified in [4]. In this note we wish to analyse further the arbitrariness in the polarization field, $\mathbf{P}(\mathbf{x})$, and its relationship to atomic/molecular multipole moments, and their possible roles as observables. The main idea exposed here is that the conventional multipole definitions e.g. the electric dipole approximation, equation (26) below, involve a choice that is strictly analogous to the choice of an atomic nucleus for the calculation of a magnetic susceptibility χ and should be interpreted in the same way.

2 Polarization fields and the interaction potential

The electric and magnetic polarization fields $\{\mathbf{P}(\mathbf{x}), \mathbf{M}(\mathbf{x})\}$ are invoked to describe the electrodynamic properties of charged particles; they enter the theory through a representation of the lagrangian interaction potential for a closed system of electric charges and the electromagnetic field

$$V = \int d^3x\ \mathbf{P}(\mathbf{x}).\mathbf{E}(\mathbf{x}) + \int d^3x\ \mathbf{M}(\mathbf{x}).\mathbf{B}(\mathbf{x}) \tag{3}$$

The remaining parts of the lagrangian L describe the free field and free particles, and are not needed here. The requirements of V are that under lagrangian variation of the fields (for fixed particle variables) it should contribute the appropriate terms to the Maxwell equations, and that variation of the particle variables (for a fixed electromagnetic field) gives the Lorentz force on the particles.

Much of the discussion below applies to both classical and quantum systems of charges and electromagnetic fields; for simplicity we give classical formulae for the polarization fields and the charge-current density to which they are closely related. The changes required by quantization (observables to be represented by hermitian operators etc.) are well-known and need not be detailed. In classical electrodynamics it is conventional to make a distinction between free charges and the polarization fields of bounded charge distributions. In the quantum theory this distinction is made through the solutions of the Schrödinger equation for the charges which are used as reference states in the perturbation theory of e.g. the optical properties of atoms and molecules. The complete sets of states introduced to describe `virtual' processes span the discrete (bound) and continuous (unbound) spectrum of a molecule, and the operators describing the molecule-field interactions need to be defined for the whole set. Thus one can in principle refer to the polarization fields of a single charge described by quantum theory; of course a multipole expansion associated with the $k \to 0$ limit (see below) is inappropriate in such a case.

As is well known, explicit expressions for the polarization fields can be given such that equation (3) has the requisite properties; these expressions, involving multipole series or line integrals, are by no means unique. That this must be so can be seen from at least two levels of theory. We noted earlier that the notion of an electric field (or a magnetic field) is not invariant with respect to Lorentz transformations; under such transformations however V should be an invariant scalar and this implies a definite transformation law for $\{\mathbf{P}(\mathbf{x}), \mathbf{M}(\mathbf{x})\}$ that mixes them, and mirrors that for $\{\mathbf{E}(\mathbf{x}), \mathbf{B}(\mathbf{x})\}$; classically both pairs can be shown to be components of skew-symmetric second-rank tensors [7]. Although we cannot expect Lorentz invariance in a molecular quantum theory, this does point to limitations of an attempt at a physical interpretation based on electric field interactions mediated via **P**(**x**), as opposed to magnetic interactions mediated via **M**(**x**).

Now specify a cartesian coordinate system with orthogonal unit vectors satisfying $\hat{e}_x \wedge \hat{e}_y = \hat{e}_z$ in the laboratory reference frame. It is convenient to introduce a momentum representation for the fields through fourier transformation between **x** and **k**; in physical applications the momentum vector **k** can often be identified with the wavevector of a photon. We choose the z-axis to be along the direction of **k** (i.e. $\mathbf{k} = k\,\hat{e}_z$). A vector field **U**(**k**) may be decomposed into its longitudinal and transverse components

$$U(\mathbf{k})^{\parallel} = \hat{e}_z . \mathbf{U}(\mathbf{k}) \tag{4a}$$

$$\mathbf{U}(\mathbf{k})^{\perp} = \| \hat{e}_x . \mathbf{U}(\mathbf{k}),\ \hat{e}_y . \mathbf{U}(\mathbf{k}) \| \tag{4b}$$

where the notation in (4b) gives the components of the two-dimensional vector $\mathbf{U}^{\perp}$. A static electric field is derivable from a scalar potential (cf the discussion in §1),

$$\mathbf{E}(\mathbf{x}) = -\,\nabla\,\phi(\mathbf{x}) \tag{5}$$

so that only the longitudinal component, $P(\mathbf{x})^{\parallel}$, appears in the potential V for such a case in this reference frame. The electric field associated with electromagnetic radiation is transverse and so couples to $\mathbf{P}(\mathbf{x})^{\perp}$. The magnetic field is always transverse ($\nabla . \mathbf{B}(\mathbf{x}) = 0$), so only couples to the transverse components, $\mathbf{M}(\mathbf{x})^{\perp}$, of the magnetization.

Even if we eschew the Lorentz transformation requirements for **P**(**x**) and **M**(**x**), which would break the longitudinal/transverse component separation just described, there is still a class of transformations that mixes their *transverse* components. If we define new polarization fields {**P**′, **M**′} by the relations [5]

$$\mathbf{P}(\mathbf{x})' = \mathbf{P}(\mathbf{x}) + \nabla \wedge \mathbf{G}(\mathbf{x}) \tag{6a}$$

$$\mathbf{M}(\mathbf{x})' = \mathbf{M}(\mathbf{x}) - d\mathbf{G}(\mathbf{x})/dt \tag{6b}$$

with **G**(**x**) having appropriate derivatives, we can use equation (6) in (3) to construct a new lagrangian potential V′; then from the Maxwell equations it is easily seen [8] that

$$V' = V - dF/dt \tag{7}$$

where

$$F = \int d^3\mathbf{x}\ \mathbf{G}(\mathbf{x}).\mathbf{B}(\mathbf{x}). \tag{8}$$

We have assumed that the time dependence of **G**(**x**) arises purely from its dependence on the dynamical variables of the particles (only); otherwise **G**(**x**) is not further specified. Thus (7) contributes an extra term

$$S' = -\int_{t_1}^{t_2} dt \left(\frac{dF}{dt}\right) = F(t_1) - F(t_2) \tag{9}$$

to the action integral. According to The Principle of Least Action V and V′ generate the same motion provided only that δS′ = 0, and this simply requires that F be *integrable* so that its values at the endpoints (t_1, t_2) are definite.

In the lagrangian formulation of quantum theory, S′ only enters as a phase factor in propagators, but disappears from squared modulus expressions such as transition probabilities [9]. This already suggests the invariance of the physical predictions of the theory against different choices of the field **G**(**x**). One can also see this directly in the Hamiltonian formulation of quantum theory. If F is hermitian with respect to some inner product,

$$\Omega = \exp(iF/\hbar) \tag{10}$$

is a unitary operator and intertwines the Hamiltonians related to V and V′,

$$\Omega H' = H\Omega \tag{11}$$

so that both generate the same motion. All we learn from this discussion then is that the arbitrary field **G**(**x**), which mixes the transverse components of the polarization fields {**P**(**x**), **M**(**x**)}, must make F *hermitian*; this is a very weak constraint on the explicit determination of the polarization fields.

In a previous paper [5] we wrote the polarization field as a linear functional of the charge density ρ(**x**)

$$\mathbf{P}(\mathbf{x}) = \int d^3\mathbf{x}'\,\mathbf{p}(\mathbf{x};\mathbf{x}')\,\rho(\mathbf{x}') \tag{12}$$

with $\mathbf{p}(\mathbf{x};\mathbf{x}')$ any vector field such that

$$\nabla_{\mathbf{x}}.\mathbf{p}(\mathbf{x};\mathbf{x}') = -\delta^3(\mathbf{x}-\mathbf{x}') \tag{13}$$

it being imagined that $\mathbf{p}(\mathbf{x};\mathbf{x}')$ has no time dependence and is independent of the particles. The foregoing discussion suggests however that (12) still represents a particular choice for the electric polarization field. For example, $\mathbf{G}(\mathbf{x})$ can be any hermitian combination of the lagrangian dynamical variables (positions *and* velocities) for the particles, and it can have any dependence on their electric charge parameters; non-linear charge terms simply end up in $\delta S'$, and so do not disturb the Lorentz Force Law. This means, in effect, that the *transverse* part of $\mathbf{p}(\mathbf{x};\mathbf{x}')$ (annihilated by $\mathbf{Div}_{\mathbf{x}}$) can be much more general than previously suggested. This discussion leads apparently towards a characterization of the polarization fields as such monstrosities that it is doubtful whether the expressions `electric polarization' and `magnetization' have any meaning ! What is needed of course is a calculational procedure that is invariant against the *transverse* transformations generated by the arbitrary field $\mathbf{G}(\mathbf{x})$ (see §4).

3. The charge-current density and polarization fields

A system of particles with charges $\{e_i, i = 1,....N\}$ and masses $\{m_i, i = 1,....N\}$ has position and momentum variables $\{\mathbf{x}_i, \mathbf{p}_i, i = 1,....N\}$, defined in the laboratory frame; we assume that all particle velocities are small compared to the speed of light so that Galilean (`non-relativistic') kinematics apply. Under these conditions the charge density $\rho(\mathbf{k})$ and current density $\mathbf{j}(\mathbf{k})$ are,

$$\rho(\mathbf{k}) = \sum_i e_i \, e^{i\mathbf{k}.\mathbf{x}_i}, \tag{14a}$$

$$\mathbf{j}(\mathbf{k}) = \sum_i \frac{e_i}{m_i}\mathbf{p}_i \, e^{i\mathbf{k}.\mathbf{x}_i}. \tag{14b}$$

The components of the polarization fields can be expressed in terms of the charge and current densities by the relations

$$\rho(\mathbf{k}) = i\, k\, P(\mathbf{k})^{\parallel} \tag{15a}$$

$$j(\mathbf{k})^{\parallel} = [H_0, P(\mathbf{k})^{\parallel}] \tag{15b}$$

$$\mathrm{j}(\mathbf{k})^{\perp} = [\mathrm{H}_{\mathrm{o}}, \mathbf{P}(\mathbf{k})^{\perp}] + \mathrm{k}\ \hat{\mathbf{o}}_{\mathrm{y}}\ \mathbf{M}(\mathbf{k})^{\perp} \tag{15c}$$

where $\hat{\mathbf{o}}_{\mathrm{y}}$ is the usual Pauli matrix [10] and H_{o} is the Hamiltonian for the particles; the last term in (15c) is $\mathbf{k} \wedge \mathbf{M}(\mathbf{k})$ in three-dimensional notation but is written here with the factor k explicit for use below. The bracket $[\mathrm{H}_{\mathrm{o}},\Omega]$ determines the time derivative of Ω due to the motion of the particles

$$\frac{d\Omega}{dt} = [\mathrm{H}_{\mathrm{o}},\Omega] \equiv \sum_{\mathrm{i}} \left(\frac{\partial \mathrm{H}_{\mathrm{o}}}{\partial \mathrm{p}_{\mathrm{i}}} \frac{\partial \Omega}{\partial \mathrm{x}_{\mathrm{i}}} - \frac{\partial \mathrm{H}_{\mathrm{o}}}{\partial \mathrm{x}_{\mathrm{i}}} \frac{\partial \Omega}{\partial \mathrm{p}_{\mathrm{i}}} \right). \tag{16}$$

For $\mathrm{k} \neq 0$, equation (15a) may be inverted to yield

$$\mathrm{P}(\mathbf{k})^{\parallel} = -\ (\mathrm{i}/\mathrm{k})\ \rho(\mathbf{k}); \tag{17}$$

substituting this in (15b) yields,

$$\mathrm{i\ k\ j}(\mathbf{k})^{\parallel} = [\mathrm{H}_{\mathrm{o}}, \rho(\mathbf{k})] \equiv d\rho(\mathbf{k})/dt \tag{18}$$

which is the equation of continuity required by charge conservation. The asymmetric nature of the relationship between the polarization fields and the charge and current densities of the particles should be noted. While a given pair of polarization fields $\{\mathbf{P}(\mathbf{x}), \mathbf{M}(\mathbf{x})\}$ generates a definite charge-current density, the converse is not true because equation (15c) is under-determined.

It is instructive to examine the behaviour of these equations about $\mathrm{k} = 0$; this is the 'long wavelength' limit that we conventionally associate with the electric dipole and quadrupole moments, and the magnetic dipole moment. At $\mathrm{k} = 0$ we have $\rho(0) = \sum_{\mathrm{i}} e_{\mathrm{i}} \equiv \mathrm{q}$, the net charge in the system, so that

$$\lim_{\mathrm{k} \to 0} \mathrm{i\ k\ P}(\mathbf{k})^{\parallel} = \mathrm{q}. \tag{19}$$

For an overall *neutral* system, $\mathrm{q} = 0$, $\mathrm{P}(\mathbf{k})^{\parallel}$ is regular and the limit is well-defined, explicitly from (14a) and (17),

$$\lim_{\mathrm{k} \to 0} \mathrm{P}(\mathbf{k})^{\parallel} = -\lim_{\mathrm{k} \to 0} \frac{\mathrm{i}}{\mathrm{k}} \sum_{\mathrm{i}} e_{\mathrm{i}} \left(1 + \mathbf{ik.x}_{i} - \ldots\right)$$

$$= \hat{\mathbf{e}}_{\mathrm{z}}.\mathbf{d} \tag{20}$$

where $\mathbf{d} = \sum_{\mathrm{i}} e_{\mathrm{i}} \mathbf{x}_{\mathrm{i}}$ is the electric dipole moment for the system. For $\mathrm{q} \neq 0$, $\mathrm{P}(\mathbf{k})^{\parallel}$

has a pole at k = 0 with residue 2πq, which is independent of the dynamical variables. Hence considering the limit k → 0 for (15b), and evaluating the time derivative *before* taking the limit since we want the limit of **j**, this contribution has a vanishing time derivative, and the expected result for the continuity equation follows from the z-component of the time derivative of the dipole moment. If we continue the expansion upto terms linear in k we have

$$\mathbf{P}(\mathbf{k})^{|} \approx -\frac{\mathrm{iq}}{\mathrm{k}} + \hat{\mathbf{e}}_z.\mathbf{d} + \mathrm{ik}\ \hat{\mathbf{e}}_z\hat{\mathbf{e}}_z{:}\overset{\leftrightarrow}{\mathbf{Q}} \qquad (21)$$

with

$$\overset{\leftrightarrow}{\mathbf{Q}} = \frac{1}{2}\sum\nolimits_{\mathrm{i}} e_{\mathrm{i}}\mathbf{x}_{\mathrm{i}}\mathbf{x}_{\mathrm{i}} \qquad (22)$$

the electric quadrupole moment dyadic, and higher order terms in the expansion yield the components along $\hat{\mathbf{e}}_z$ of higher order multipole tensors. $\mathbf{P}(\mathbf{k})^{\parallel}$ couples to a *static* electric field and causes shifts in energy levels that are accessible in spectroscopic experiments (Stark effect theory) which therefore give information about the multipole moment components displayed in (21).

This argument however cannot be carried through in the same way for (15c); , for small k the left-hand side yields simply

$$\mathbf{j}(\mathbf{k}) \approx \sum\nolimits_{\mathrm{i}} \frac{e_{\mathrm{i}}}{m_{\mathrm{i}}}\mathbf{p}_{\mathrm{i}\alpha}(1 + i\mathbf{k}.\mathbf{x}_{\mathrm{i}}), \qquad \alpha = \mathrm{x,y}. \qquad (23)$$

Considering first the k = 0 limit of (23) this must be equal to the *sum* of the two rhs terms in (15c) evaluated at k = 0 and, so far, there is *no* requirement for one of them to vanish. We consider in turn the three possibilities: one or other of these two terms vanishes in the limit, and finally neither term vanishes. The term k $\hat{\mathbf{o}}_y$ $\mathbf{M}(\mathbf{k})^{\perp}$ will only vanish at k = 0 *if* $\mathbf{M}(\mathbf{k})^{\perp}$ is *chosen* to be regular at k = 0; if we make this choice we know from the velocity-dipole formula that

$$[\mathrm{H_o},\mathbf{d}] = \sum\nolimits_{\mathrm{i}} e_{\mathrm{i}}\ (\mathrm{d}\mathbf{x}_{\mathrm{i}}/\mathrm{dt}) = \sum\nolimits_{\mathrm{i}}(e_{\mathrm{i}}/m_{\mathrm{i}})\ \mathbf{p}_{\mathrm{i}} \qquad (24)$$

and this yields,

$$\mathbf{P}(0)^{\perp}{}_{\alpha} = \mathrm{d}_{\alpha} + \Delta_{\alpha}, \ \alpha = \mathrm{x,y} \qquad (25)$$

where **Δ** is any vector quantity that commutes with the Hamiltonian $\mathrm{H_o}$ (e.g. the constant vector **a**q that arises from displacing all coordinates $\{\mathbf{x}_i\}$ by the constant amount **a**, or any vector function of the constants of the motion of the system). This is the conventional choice since it avoids discussion of the 'magnetization' in the k = 0 limit, and if $\boldsymbol{\Delta}$ commutes with H_0 it shares the same eigenfunctions and so has no off-diagonal matrix elements if the eigenstates of H_0 are used as the perturbation theory reference states (V, equation (3), is off-diagonal for the atomic/molecular states since it is linear in the photon annihilation and creation operators). The matrix elements of $\mathbf{j}(0)^{\perp}$ are then expressible entirely in terms of those of the electric dipole moment operator **d**.

It is usual to interpret this result in terms of a physical interaction between the electric dipole moment and a (uniform) transverse electric field associated with radiation,

$$V = -\,\mathbf{d}.\mathbf{E}^{\perp} \tag{26}$$

and to declare that this result has the great advantage of being 'gauge invariant'. To the extent that gauge transformations are associated with the field potentials $\{\phi, \mathbf{A}\}$ this is obviously true. It is evident however that this result depends on making certain *choices* and as noted earlier (§1), putting V in the form (26) can be viewed as making a specific choice of gauge.

Suppose instead we require the operator $\boldsymbol{\Delta}$ in (25) to have the property that it forces

$$[H_o, \mathbf{P}(0)^{\perp}] = 0 \tag{27}$$

which includes the possibility that $\mathbf{P}^{\perp} = 0$. Then the matrix elements of the first term in V, equation (3), all vanish in the basis of eigenstates of H_0 and the interaction must apparently be mediated by the 'magnetization' and the magnetic field of the radiation; thus for example we can satisfy (15c) trivially if we drop the transverse electric polarization from V and put

$$\mathbf{M}(\mathbf{k}) = \frac{1}{k}\sum_i \frac{e_i}{m_i}\,\hat{\mathbf{e}}_z \wedge \mathbf{p}_i \quad \text{for } k \to 0 \tag{28}$$

More importantly if we augment (25) by a contribution $\boldsymbol{\Delta}'$ for which $[H, \boldsymbol{\Delta}']$ is nonzero, then at k = 0 this bracket is related to the singularity properties of $\mathbf{M}(0)^{\perp}$ through equation (15c) which yields the condition

$$-\,[H_o, \boldsymbol{\Delta}'] = \lim_{k \to 0}\left(k\;\hat{\boldsymbol{\sigma}}_y\;\mathbf{M}(\mathbf{k})^{\perp}\right) \tag{29}$$

and so contributions from both the electric polarization and the magnetization in V are required, even in what is conventionally called the `electric dipole approximation'.

This argument shows that there cannot be a definite expansion in powers of k, analogous to equation (21), for the transverse polarization fields. What has been customarily done is as follows: an explicit form for the transverse part of the electric polarization field is proposed to complete (21) e.g. by analogy with classical dielectric theory in terms of electric multipoles [11], or using line-integrals [5,6], and then (15c) is `solved' for the corresponding magnetization field. Of course we know from elementary mathematics that solving one equation in two unknowns gives a `solution' containing an arbitrary parameter or function. From a different point of view, equation (26) is simply a choice of a scalar potential in the sense of Barron & Gray [4] and so it is wrong to suppose that using the electric dipole interaction eliminates the need to deal with questions of gauge invariance.

4. Discussion

The foregoing discussion can be compared with that for the magnetic susceptibility summarized in §1; there a particular choice of gauge forces $\chi_p[\mathbf{A}]$ for an atom to vanish so that the observable susceptibility χ can be calculated purely in terms of the diamagnetic term. Here we have seen a similar calculational simplification achieved by reducing the interaction V, equation (3) to one term, equation (26), with a special choice of gauge. As we have seen the longitudinal component of the electric polarization field has a well-defined expansion in powers of k and electric multipole moment components, equation (21). Formally there is a pole in $P(\mathbf{k})^{\parallel}$ at $k = 0$ for an ionic system; in real physical situations there is a minimum value to k imposed by the size of the apparatus, and no serious difficulties arise for the interaction energy with static electric fields. The transverse components of the polarization fields however cannot be defined unambiguously; in the absence of an independent theory of polarization fields, one of the fields can be chosen freely and then the other must be fixed from equation (15c). Thus the concept of electric and magnetic multipoles has to be sharply constrained in discussion of the interaction between electromagnetic radiation and atoms and molecules. Having made some choice, calculations of absorption, emission, scattering rates can be made by the usual perturbation methods [12] but one is left with the question of whether the results of such calculations are independent of the choice of the transverse polarization fields.

We have recently studied the question of gauge invariance in non-relativistic quantum electrodynamics in a general setting [5]. The principal results we need here are these. Let |i> and |f> be two distinct states of the reference system (atom/molecule + field), with energies E_i and E_f. A physical transition amplitude $\Re_{if}$ between these two states contains the energy conservation delta function $\delta(E_i - E_f)$. Absorption and emission of a photon can be described in first-order perturbation theory and one can show that

$$^{(1)}\Re_{if}[\mathbf{P}^{\perp}] \propto \langle i|V_1[\mathbf{P}^{\perp}]|f\rangle \equiv \langle i|V_1[\mathbf{0}]|f\rangle. \qquad (30)$$

Here, square brackets indicate functional dependence, and $V_1[\mathbf{P}^{\perp}]$ is the molecule-field interaction operator linear in the electronic charge e for a given transverse polarization field $\mathbf{P}^{\perp}$ (essentially equation (3)). $V_1[\mathbf{0}]$ corresponds to the usual $\mathbf{p}.\mathbf{A}$ terms in the Coulomb gauge theory (Div $\mathbf{A} = 0$). It is related directly to the discussion presented here since, for example, the cross-section for absorption of a photon with wavevector $\mathbf{k}$ and polarization direction $\hat{\mathbf{e}}_\alpha$ (α = x,y) that causes an atomic transition n → m is obtained from the Coulomb gauge theory as proportional to,

$$|\langle n|\mathbf{j}(\mathbf{k}).\hat{\mathbf{e}}_\alpha|m\rangle|^2 \quad (E_n - E_m = hkc) \qquad (31)$$

where the current is given precisely by equation (14b) [12].

Second-order perturbation theory (linear response) yields the Kramers-Heisenberg formula for scattering of a photon. This involves using the potential $V_1[\mathbf{P}^{\perp}]$ in second-order perturbation theory, together with the first-order perturbation theory average of the interaction $V_2[\mathbf{P}^{\perp}]$ proportional to e^2 - see [5] for details of the general form of these interaction potentials. The second-order amplitude $^{(2)}\Re_{if}[\mathbf{P}^{\perp}]$ for a general polarization field thus has a structure completely analogous to the magnetic susceptibility, equation (1), with two terms that can be varied at will by changing $\mathbf{P}^{\perp}$. Corresponding to (30) however one has for the second-order amplitude

$$^{(2)}\Re_{if}[\mathbf{P}^{\perp}] - {}^{(2)}\Re_{if}[\mathbf{0}] = (E_i - E_f)\, \Delta[\mathbf{P}^{\perp}]_{if} \qquad (32)$$

and on the energy shell, the rhs vanishes, confirming the *invariance* of the second-order amplitude against changes in the polarization field $\mathbf{P}^{\perp}$ [5]. We note that the amplitude $^{(2)}\Re_{if}[\mathbf{0}]$ for the scattering of a photon $(\mathbf{k},\hat{\mathbf{e}}_\alpha)$ to a final state $(\mathbf{k}',\hat{\mathbf{e}}'_\alpha)$ can be expressed in terms of matrix elements of $\mathbf{j}(\mathbf{k}).\hat{\mathbf{e}}_\alpha$ and $\mathbf{j}(-\mathbf{k}').\hat{\mathbf{e}}'_\alpha$ [13]. All the discussion in §3 is applicable directly to (31), and to the Kramers-Heisenberg formula.

The results (30),(32) confirm that the important physical quantities like the Einstein A & B coefficients, light scattering cross-sections, the Stokes parameters that describe the polarization characteristics important for birefringence, are quantities that are invariant against changes in the (transverse) polarization field. Remembering the discussion of the magnetic susceptibility we started with, we conclude that no one choice e.g. in terms of a specific definition of electric and magnetic multipole moment operators is any more significant physically than any other choice, and this statement refers equally to the choice $\mathbf{P}^{\perp} = 0$, equation (31) (the Coulomb gauge theory). From this perspective the long-running discussion about the relative merits of different gauges that can be traced back to the first discussions of the Lamb shift fifty years ago [11], ('velocity gauge', equation (31), 'length gauge', equation (26) - see e.g. a recent example [14]) can only be about computational details in specific calculations. The general gauge invariance of non-linear optical responses (expressed by hyperpolarizabilities) needs to be demonstrated; it seems very plausible however that the same limitations on the concept of multipole moments will apply to such calculations.

References

(1) W. Haberditzl: in *Theory and Applications of Molecular Diamagnetism*, Ed. L.N.Mulay & E.A.Boudreaux, Wiley Interscience (1976)

(2) R. G. Woolley: Chem.Phys.Lett., **51**, 279 (1977).

(3) P. Lorrain and D. R. Corson: *Electromagnetic Fields and Waves*, 2nd edition, W.H.Freeman (1970).

(4) L. D. Barron and C. G. Gray: J.Phys.A: Math.Nucl.Gen.Phys. **6**, 59 (1973).

(5) R. G. Woolley: Mol.Phys. **88**, 291 (1996)

(6) R. G. Woolley: J.Phys.B: Atom. Molec.Phys. **7**, 488 (1974)

(7) W. P. Healy: J.Phys.A: Math.Gen. **11**, 1899 (1978)

(8) R. G. Woolley and J. E. Cordle: Chem.Phys.Lett., **22**, 411 (1973)

(9) R. P. Feynman and F. L. Vernon Jr.: Annals of Physics, **24**, 118 (1963)

(10) D. M. Brink and G. R. Satchler, G.R.: *Angular Momentum*, O.U.P., 23 (1968)

(11) E. A. Power and S. Zienau: Phil.Trans.Roy.Soc.(London) **251**, 427 (1959)

(12) E. A. Power: *Introductory Quantum Electrodynamics*, p.87 Longmans, Green & Co. Ltd. (1964)

(13) W. P. Healy: Phys.Rev.A, **16**, 1568 (1977)

(14) S. J. van Enk, J. Zhang and P. Lambropoulos: J.Phys.B: At.Mol.Opt.Phys. **30**, L17 (1997)

VERTICAL ELECTRON TRANSITIONS IN RYDBERG RADICALS

I. Martin, C. Lavín and Y. Pérez-Delgado

Departamento de Química Física; Facultad de Ciencias;
47005 Valladolid, Spain

J. Karwowski

Instytut Fizyki, Uniwersytet Mikolaja Kopernika;
Grudziądzka 5, 87-100 Toruń, Poland

G. H. F. Diercksen

Max Planck Institut für Astrophysik;
D-85740 Garching bei München, Germany

Abstract

Oscillator strengths and Einstein emission coefficients for several Rydberg radicals are reported. The Quantum Defect Orbital (QDO) method has been employed, and comparison is made with the results of more complex theorical procedures.

1 Introduction

2 Method of calculation

3 Numerical examples

4 Concluding remarks

5 Acknowledgments

References

ADVANCES IN QUANTUM CHEMISTRY, VOLUME 32
Copyright © 1999 by Academic Press. All rights of reproduction in any form reserved.
0065-3276/99 $30.00

1. Introduction

Rydberg states are named after the Swedish physicist J. R. Rydberg (1) who first established that most highly excited states of atoms can be understood in much the same way as the excited states of the hydrogen atom, that is, as due to orbitals with increasing principal quantum number, n. For highly enough states, the Rydberg electron may be considered as nearly independent of the core. The same characteristics may be attributed to highly excited states in molecules, with differences arising from vibration and rotation of the molecular core ion, which gives rise to the differences in the atomic and molecular high-resolution optical spectra. Vibration and rotation lead to a great many levels and there are interactions between these levels. In the simplest approximation, there is a Rydberg series converging to every rotational- vibrational level of the core ion. For sufficiently high n, these means that the electronic levels are more closely spaced than vibrational (and even rotational) levels of the core. These effects are dealt with the multichanel quantum defect theory (MQDT) (see, e.g., 2-4).

But it can be established that atoms and molecules in high Rydberg states are similar in many ways (5). Each consists of a core ion and an electron at a large mean distance from the core. For many purposes, the core can be appoximated by a point charge. The coarse energy-level structure is given by Rydberg's formula (1):

$$E_n = -\frac{13.6}{(n-\delta_l)^2}\ \text{eV} \qquad (1)$$

Small deviations result from the interaction of the Rydberg electron with the structured core; they are expressed as quantum defects, δ_l, which are functions of the orbital angular momentum l. Rydberg series of molecular energy levels are known, although they are not as extensive as those observed in atoms.

At present, there is a renewed interest in high-energy states which is stimulated by general advances in space research. This is producing a wealth of "raw" spectral data which is leading to a close interaction between observers, astrophysical modelers, and molecular physicists and chemists. In diagnosing astrophysical observations, the availability of reliable theoretical transition probabilities is essential, since they can allow the determination of molecular abundances, electron temperature and densities, among other properties.

In comparison with the large variety of work so far being done on atomic Rydberg states, there are, up do date, few studies on highly excited molecular states. Significant advances have arisen in the last decade thanks to the new laser spectroscopy techniques that make the interpretation of the complex molecular spectra easier. Yet, there is a great demand of theoretical transition probability data by the experimentalists (6).

A feature that quite often helps simplify the calculations is the empirical fact that the observation of long Rydberg series in absorption is associated with small (if any) changes in the geometry of the molecular core ion, relative to the ground state of the ion. This situation corresponds to an almost vertical alignment of the potential energy surfaces for the Rydberg states. It appears then, reasonable, to assume simply, from the Frank-Condon principle, that Rydberg transitions will appear with appreciably intensity in absorption from low vibrational levels of the ground state (7). In fact, it has been observed that in most cases the main bands correspond to transitions between the fundamental vibrational states, $v = 0$, of different electronic states (8).

A particulary interesting class of molecules in this context is that of "Rydberg molecules" (9), for which the ground electronic state is unstable but all the excited states have Rydberg character. They possess long lifetimes compared to rotational or vibrational periods, and their corresponding core ion is quite stable. Several Rydberg molecules have been observed in regions of astrophysical importance (10). They also offer a more general chemical interest, as some of them have been detected as short-lived intermediates in chemical reactions (11).

The first polyatomic Rydberg molecule thoroughly studied experimentally by Herzberg and his co-workers (12) was H_3. Since then, not many more polyatomic Rydberg molecules have been identified. However, because of the large proton affinity of some of the second-row hydrides, some of which have been observed in interstellar regions (13), the corresponding cations are expected to be stable (9). The addition of an electron to those, a favorable process in the interstellar regions (14), would yield the corresponding Rydberg radicals. The spectra of most of these radicals have not been obtained in the laboratory. The theoretical determination of these spectra becomes a clear requisite for diagnosing astrophysical observations, as well as for establishing the mechanisms of important chemical reactions that take place on the Earth. This is one of the reasons why we have been interested in their theoretical study.

The prediction of molecular Rydberg spectra, as well as the analysis of the available laboratory data, has constituted a challenge on the theory. A number of ab initio calculations have been carried out on transition probabilities of Rydberg molecules, such as the frequently quoted Hartree-Fock (HF) study of H_3 by King and Morokuma (15), the self-consistent-field frozen-core calculation with floating-spherical-Slater-type orbitals (FSSO) on the second-row Rydberg hydrides by Raynor and Herschbach (16), and other works to which we shall refer when discussing a specific Rydberg radical. A recent large-scale configuration interaction (CI) calculation on H_3 by Diercksen et al. (17) revealed the serious problem of the energy ordering of the high Rydberg levels to be basis-dependent. On the other hand, the great computational effort required when advanced ab initio methodologies are applied to the prediction of molecular Rydberg spectral intensities, lead us a few years ago (18) to apply the Quantum Defect Orbital (QDO) formalism (19) (which has little relation with the aforementioned MQDT (2-4)) to calculate transition probabilities in molecular Rydberg states, given its proved adequacy to study these properties in atomic Rydberg states (20). The Einstein coefficients and oscillator strengths obtained in our pilot QDO study of H_3 (18) were in a strikingly good agreement with the results of rather more complex theoretical procedures (15, 16). Nevertheless, we later modified the description originally given for the angular part of the molecular Rydberg quantum defect orbitals (21). The modified QDO theory has led to improved f-values for H_3 (22), and to seemingly correct transition probabilities for other Rydberg radicals (21, 23, 24).

In the next section, the modified version of the QDO formalism will be briefly described.

2. Method of calculation

In the QDO method the molecular Rydberg electron is described by an orbital $\psi(r,\vartheta,\varphi)_{nl\mu\nu}$ which is a solution of the one-electron Schrödinger equation:

$$\left[-\frac{1}{2}\Delta+V(r,\vartheta,\varphi)_M\right]\psi(r,\vartheta,\varphi)_{nl\mu\nu}=E_{nl\mu}\ \psi(r,\vartheta,\varphi)_{nl\mu\nu} \tag{2}$$

where V_M is an effective potential of the molecular core,

$$\psi(r,\vartheta,\varphi)_{nl\mu\nu}=\frac{1}{r}R(r)_{nl\mu}\Xi(\vartheta,\varphi)_{l\mu\nu} \tag{3}$$

n and l are, respectively, the principal and the orbital angular momentum quantum numbers, and μ and ν label different wavefunctions corresponding to the same (n, l) pair. The radial part of the wavefunction is obtained from the equation

$$\left[-\frac{d^2}{2dr^2}+\frac{l(l+1)}{2r^2}+V(r)_a\right]R(r)_a=E_a\ R(r)_a \tag{4}$$

where a stands for (n, l, μ). The effective central field potential is defined as

$$V(r)_a = \frac{(c-\delta_a)(2l+c-\delta_a+1)}{2r^2} - \frac{1}{r} \tag{5}$$

Solutions of this equation are related to the Kummer functions. The parameter δ_a, is the quantum defect and c is an integer chosen to ensure the normalizability of the orbitals and their correct nodal pattern.

The quantum defect δ_a, corresponding to a given state, is related to its energy through the following equation

$$E_a = T - \frac{1}{2(n_a - \delta_a)^2}, \tag{6}$$

where T is the ionization energy. Since experimental energies are usually only known for few transitions and since their assignment is frequently uncertain, in many cases transition energies are taken from theoretical calculations or even from extrapolation formulae.

The second parameter, c, determines the number of radial nodes. The number of nodes in the radial function is equal to

$$\tilde{n} = n - l - c - 1 \tag{7}$$

Therefore,

$$c \leq n - l - 1 \tag{8}$$

On the other hand, the radial orbitals are normalizable only if (19)

$$c > \delta - l - \frac{3}{2} \tag{9}$$

In the case of spherically symmetric systems, the pairs of indices μ, ν correspond to the magnetic quantum numbers $m = -l, -l+1, \ldots, l$ and $\Xi(\vartheta, \varphi)_{l\mu\nu}$ are equal to the spherical harmonics $Y(\vartheta, \varphi)_{lm}$. In the case of molecules the angular part of the QDO wavefunction may be expressed as a symmetry-adapted combination of the spherical harmonics. Index μ in this case identifies the

The absorption oscillator strengths may be expresed as

$$f(a \rightarrow b) = \frac{2}{3}(\mathrm{E_b} - \mathrm{E_a})\,\mathrm{Q}\,\{a \rightarrow b\}\,|\,\mathrm{R_{ab}}\,|^2 \qquad (10)$$

where Q $\{a \rightarrow b\}$, referred to as the *angular factors*, result from the angular integration. Values for the angular factors corresponding to different symmetry groups have been reported (21-24). The radial transition integrals are defined as

$$\mathrm{R_{ab}} = \langle \mathrm{R_a}(r)\,|r|\,\mathrm{R_b}(r)\rangle \qquad (11)$$

The Einstein probabilities for spontaneus emission are related to the absorption oscillator strengths through the well-known expresion,

$$\mathrm{A_{ba}} = 6.6702 \times 10^{15}\,\tilde{\lambda}^{-2}\,(\mathrm{g_a} / \mathrm{g_b})\,f_{\mathrm{ab}}\,, \qquad (12)$$

where the wavelength for the transition, $\tilde{\lambda}$, is in Angstroms, and $\mathrm{A_{ba}}$ is expresed in seconds^{-1}. $\mathrm{g_a}$ and $\mathrm{g_b}$ are, respectively, the statistical weights of the initial and final states in the absorption process.

The emission oscillator strengths are given by

$$\mathrm{f_{ba}} = -\,(\mathrm{g_a} / \mathrm{g_b}\,)\,\mathrm{f_{ab}} \qquad (13)$$

The radial transition moment integrals may be expressed in the following closed analytic form:

$$\mathrm{R}_{ab} = \frac{1}{4Z_{net}}(t_a t_b)^{1/2} \sum_{i=0}^{\tilde{n}_a} \sum_{j=0}^{\tilde{n}_b} A(a,b)_{\mathrm{i}}\, A(b,a)_{\mathrm{j}}\, \Gamma(\lambda_a + \lambda_b + i + j + 4), \qquad (14)$$

where $\tilde{n}_a = n_a - l_a - c_a - 1, \quad t_a = \frac{\Gamma\left(n_a^* + \lambda_a + 1\right)}{\Gamma\left(n_a^* - \lambda_a\right)}, \quad n_a^* = n_a - \delta_a,$ and

$$A(a,b)_{\mathrm{i}} = \left(\frac{2n_b^*}{n_a^* + n_b^*}\right)^{\lambda_a + i + 2} \binom{\lambda_a - n_a^* + i}{i} \Gamma\left(2\lambda_a + i + 2\right)^{-1} \qquad (15)$$

As one can see, the transition moments are given by simple functions of the quantum numbers and the quantum defects of the two states involved in the transition.

3. Numerical examples

A few representative oscillator strengths and/or Einstein emission coefficients so far obtained with the procedure described above will now be reported.

In table I we collect emission oscillator strengths for several transitions of H_3, calculated with the initially employed QDO formalism (18) and with the modified one (22). As comparative data we include the HF f-values obtained by King and Morokuma (15) and by Martin (25).

As one can see, the overall quality of the results obtained with the modified QDO method is slightly better than the ones obtained with the simplified approach (18). The reference data, i. e., the ionization energy and the energy levels have been taken from a large-scale multireference configuration interaction (MRCI) calculation by Petsalakis et al. (26), which are probably the most accurate ab initio energy levels available. We extrapolated higher Rydberg levels making use of the well-known regularities of the quantum defects along a given Rydberg series (22).

A revelant Rydberg radical is NH_4, for which the experimental spectrum has long been kown, but for which the assignment of one of the most prominent series of bands, the Schüler system, has been the subjet of much controversy. Herzberg suggested (9, 27, 28) that the Schüler bands are the exact analoge of the D lines of sodium (the atom isoelectronic with NH_4). In view of the observed sizable spin doubling, Herzberg originally assumed that the $^2T_2$ (3p) state should be involved, and that it should be the lower state of the transition. According to Herzberg's reasoning (27), the upper state of the main Schüler band could be any of the two states that strongly combine with the $^2T_2$ (3p) state, and, on the basis of the similarity with the $^2P(3p)$-$^2D(3d)$ transition in sodium, he suggested this to be the $^2E(3d)$ state. Thus, the main Schüler band would correspond to the $^2E(3d)$ - $^2T_2$ (3p) transition, although Herzberg remarked (27) that a more definite assignment would have to await the results of the appropriate theoretical work.

Only some of the theoretical studies concerned with the assignment of the NH_4 spectrum report energy levels, ionization energies and transition probabilities (16, 29, 30). Perhaps the most complete studies are those by Havriliak and King (29), based on the first-order Rayleigh-Schrödinger perturbation theory (RSPT/ 1) and by Havriliak et al. (30), who extended the perturbation theory to second order (RSPT/ 2).

Table I : Oscillator strengths for selected Rydberg transitions in H_3. All quantities are multiplied by -10^3.

Transition	QDO[a]	QDO[b]	HF[c]	HF[d]
$1^2A'_1$ (2s) → $1^2E'$(2p)	330	200	260	260
$2^2A'_1$ (3s) → $1^2E'$(2p)	9.76	9.8	11	10.2
$4^2A'_1$ (4s) → $1^2E'$(2p)	2.50	6.5	4.0	3.29
$6^2A'_1$ (5s) → $1^2E'$(2p)	1.04	0.21		
$3^2A'_1$ (3d) → $1^2E'$(2p)	5 4.0	22	38	60.6
$5^2A'_1$ (4d) → $1^2E'$(2p)	19.2	6.3	14	14.4
$7^2A'_1$ (5d) → $1^2E'$(2p)	9.06	2.8		
$3^2E'$ (3d) → $1^2E'$(2p)	174	140	150	158
$5^2E'$ (4d) → $1^2E'$(2p)	59.3	49	54	51.8
$7^2E'$ (5d) → $1^2E'$(2p)	27.4	37		
$1^2E''$ (3d) → $1^2E'$(2p)	82.4	82	51	73.2
$2^2E''$ (4d) → $1^2E'$(2p)	29.1	24	18	24.9
$3^2E''$ (5d) → $1^2E'$(2p)	13.6	5.2		
$2^2E'$ (3p) → $1^2A'_1$ (2s)	272	400	350	339
$4^2E'$ (4p) → $1^2A'_1$ (2s)	32.5	49		38.2
$6^2E'$ (5p) → $1^2A'_1$ (2s)	10.8	18		
$1^2A''_2$ (2p) → $1^2A'_1$ (2s)	29.9	38	48	4
$2^2A''_2$ (3p) → $1^2A'_1$ (2s	103	100	100	107
$3^2A''_2$ (4p) → $1^2A'_1$ (2s)	26.9	26	2	27.9
$4^2A''_2$ (5p) → $1^2A'_1$ (2s)	11.4	12		
$2^2A'_1$ (3s) → $1^2A''_2$(2p)	18.8	22	28	30.3
$4^2A'_1$ (4s) → $1^2A''_2$(2p)	4.06	4.8	6.7	6.32
$6^2A'_1$ (5s) → $1^2A''_2$(2p)	1.60	1.9		
$3^2A'_1$ (3d) → $1^2A''_2$(2p)	254	180	250	260
$5^2A'_1$ (4d) → $1^2A''_2$(2p	53.0	52		49.3
$7^2A'_1$ (5d) → $1^2A''_2$(2p)	20.5	22		
$1^2E''$ (3d) → $1^2A''_2$(2p)	192	230	17	195

Table I (continued).

$2^2E''$ (4d) → $1^2A''_2$ (2p)	39.2	58	34	36.4
$3^2E''$ (5d) → $1^2A''_2$ (2p)	15.1	24		

[a] Martin et al. (22).
[b] Martin et al. (18).
[c] Martin (25).
[d] King and Morokuma (15).

In table II we collect Einstein emmision coefficients for several relevant transitions (including the main Schüler band candidates) of NH_4. To extract quantum defects we have adopted the energies of Havriliak et al. (30) and performed a few extrapolations. Except for a few cases, the agreement between the QDO values and the comparative data is rather good. It seems that the FSSO approach (16), in general, overestimates transition probabilities for all but the lowest energy transitions.

All theoretical studies, including our work (21), predict that the ^2E (3d)-$^2T_2$ (3p) transition is very strong (in agreement with the experimental results and Herzberg's tentative assignment (27) for the main Schüler band). However, this band appears in the spectrum between 6635 Å and 6637 Å, far from the wavelengths predicted by Havriliak and King (29) and Havriliak et al. (30). Havriliak and King (29) suggested that the main Schüler band terminates in the ground vibrational state of $^2A_1$ (3s), since this would resolve the conflict between spectroscopic and molecular-beam lifetimes (31-33) and would bring the frecuencies in line with the theory. On the grounds of more recent comments by Herzberg (9), by some other authors, and our calculations, an assignmemt of the main Schüler band to the $^2T_2$ (3p)-$^2A_1$ (3s) transition seems to be most plausible. An observed satellite Schüler band at about 6270 Å and of much lower intensity than the main band, may be assigned to the ^2E(4d)-$^2T_2$ (3p) transition, for which the RSPT/ 2 wavelength (30) is 6693 Å and the QDO Einstein coefficient is 0.33 × 10^7 / s.

Table II : Wavelengths $\tilde{\lambda}$ (in Å) and Einstein emision coefficients A (in units of 10^7/s) for NH_4 transitions.

Transition	QDO[a]		RSTP/1[b]		RSPT/2[c]		FSSO[d]	
	$\tilde{\lambda}$	A	$\tilde{\lambda}$	A	$\tilde{\lambda}$	A	$\tilde{\lambda}$	A
2^2A_1 (4s) $\rightarrow 1^2T_2$ (3p)	13115	2.09	14108	1.95	13115	2.40	12785	2.33
3^2A_1 (5s) $\rightarrow 1^2T_2$ (3p)	6928	0.53	7603	0.60	6928	0.79	7078	2.64
4^2A_1 (6s) $\rightarrow 1^2T_2$ (3p)	5751	0.24					6081	2.50
1^2E (3d) $\rightarrow 1^2T_2$ (3p)	11025	2.47	12288	5.09	11025	10.10	12228	2.58
2^2E (4d) $\rightarrow 1^2T_2$ (3p)	6693	0.33	7385	0.37	6693	0.2	7300	0.63
3^2E (5d) $\rightarrow 1^2T_2$ (3p)	5659	0.13						
4^2E (6d) $\rightarrow 1^2T_2$ (3p)	5241	0.069					5685	1.26
2^2T_2 (3d) $\rightarrow 1^2T_2$ (3p)	15094	1.01	13548	2.78	15094	1.52	13477	1.89
4^2T_2 (4d) $\rightarrow 1^2T_2$ (3p)	7383	0.0142	7637	0.0007	7383	0.0025		
6^2T_2 (5d) $\rightarrow 1^2T_2$ (3p)	5902	0.0239						
8^2T_2 (6d) $\rightarrow 1^2T_2$ (3p)	5347	0.0128					5737	1.46
1^2T_2 (3p) $\rightarrow 1^2A_1$ (3s)	6592	4.08	8572	3.30	6592		8380	3.62
3^2T_2 (4p) $\rightarrow 1^2A_1$ (3s)	3700	0.37	4481	0.17	3700	0.18		
3^2T_2 (4p) $\rightarrow 2^2A_1$ (4s)	23641	0.52	28066	0.43	23641	0.70		

[a] Martin et al. (21).
[b] Havriliak and King (29).
[c] Havriliak et al. (30).
[d] Raynor and Herschbasch (16).

Another second-row Rydberg radical that we have studied with the modified QDO procedure is the fluoronium radical (21), for which, to our knowledge, no spectra have so far been recorded. The most advanced theoretical studies on this radical are the large-scale CI calculations by Petsalakis et al. (34, 35). In our calculations on H_2F both the ionization energy and the reference energy levels for calculating quantum defects have been taken from these authors (34). Again, an extrapolation of higher energy states have been carried out in our study. Wavelenghts and Einstein emission coefficients are collected in table III.

Table III : Wavelengths $\tilde{\lambda}$ (in Å) and Einstein emission coefficients A (in units of 10^7/s) for H_2F transitions.

Transition	QDO[a]		MRD-CI[b]		FSSO[c]	
	$\tilde{\lambda}$	A	$\tilde{\lambda}$	A	$\tilde{\lambda}$	A
1^2B_2 (3p) →1^2A_1 (3s)	5040	5.90	5040	8.41	5904	6.64
2^2B_2 (4p) →1^2A_1 (3s)	2767	0.276	2767	0.67		
$^2B_2$ (5p) →1^2A_1 (3s)	2401	0.057				
$^2B_2$ (6p) →1^2A_1 (3s)	2263	0.020				
$^2B_2$ (7p) →1^2A_1 (3s)	2195	0.0096				
$^2B_2$ (8p) →1^2A_1 (3s)	2157	0.0053				
1^2B_1 (3p) →1^2A_1 (3s)	3668	13.2	3668	12.1	4344	9.12
3^2B_1 (4p) →1^2A_1 (3s)	2610	2.64	2610			
$^2B_1$ (5p) →1^2A_1 (3s)	2348	1.01				
$^2B_1$ (6p) →1^2A_1 (3s)	2239	0.496				
$^2B_1$ (7p) →1^2A_1 (3s)	2182	0.282				
$^2B_1$ (8p) →1^2A_1 (3s)	2148	0.177				
2^2A_1 (3p) →1^2A_1 (3s)	3573	13.9	3573	11.1	4307	9.32
6^2A_1 (4p) →1^2A_1 (3s)	2556	3.88	2556	4.06		
$^2A_1$ (5p) →1^2A_1 (3s)	2328	1.61				
$^2A_1$ (6p) →1^2A_1 (3s)	2229	0.829				
$^2A_1$ (7p) →1^2A_1 (3s)	2176	0.419				
$^2A_1$ (8p) →1^2A_1 (3s)	2145	0.308				
2^2B_2 (4p) →3^2A_1 (4s)	19991	0.66	19991	0.63		
3^2B_1 (4p) →3^2A_1 (4s)	13931	1.25	13931	1.47		
6^2A_1 (4p) →3^2A_1 (4s)	12523	1.2	12523	1.51		
1^2A_2 (3d) →1^2B_2 (3p)	5876	3.71	5876	4.81	6657	3.4
4^2A_1 (3d) →1^2B_2 (3p)	5876	4.97	5876	6.68	6780	4.43
3^2B_2 (3d) →1^2B_2 (3p)	5821	3.74	5821	2.31	6892	1.63
1^2A_2 (3d) →1^2B_1 (3p)	10419	1.50	10419	1.98	11190	1.44
2^2B_1 (3d) →1^2B_1 (3p)	9919	1.67	9919	2.02	10328	1.48
5^2A_1 (3d) →1^2B_1 (3p)	9611	2.38	9611	2.25	10329	1.54

Table III (continued).

3^2B_2 (3d) →2^2A_1 (3p)	11070	1.34	11070	1.72	12153	1.11
2^2B_1 (3d) →2^2A_1 (3p)	10688	1.45	10688	1.83	10541	0.68
5^2A_1 (3d) →2^2A_1 (3p)	10332	2.10	10332	2.03	10542	1.59
2^2A_2 (4d) →1^2B_2 (3p)	4540	1.30			4866	1.68
8^2A_1 (4d) →1^2B_2 (3p)	4454	1.72			4898	2.31
4^2B_2 (4d) →1^2B_2 (3p)	4625	1.03			4964	0.49
4^2B_1 (4d) →1^2B_1 (3p)	6652	0.48			6715	0.64
9^2A_1 (4d) →1^2B_1 (3p)	6907	0.59			6714	0.66
4^2B_1 (4d) →2^2A_1 (3p)	6990	0.39			6804	0.69
9^2A_1 (4d) →2^2A_1 (3p)	7271	0.48			6804	0.6
3^2A_2 (5d) →1^2B_2 (3p)	4090	0.60			4353	0.89
12^2A_1 (5d) →1^2B_2 (3p)	4053	0.74			4365	0.84
6^2B_2 (5d) →1^2B_2 (3p)	4125	0.48			4392	0.72
13^2A_1 (5d) →2^2A_1 (3p)	6158	0.23			5911	0.50
3^2A_1 (4s) →1^2B_2 (3p)	8856	1.45	8856	1.62	9377	0.74
7^2A_1 (5s) →1^2B_2(3p)	5008	0.40			5408	0.69
11^2A_1 (6s) →1^2B_2 (3p)	4267	0.21			4553	0.57

[a] Martin et al. (21).
[b] Petsalakis et al. (34).
[c] Raynor and Herschbach (16).

Inspection of the table reveals that the QDO results are of more than reasonable quality when compared to those derived from much more sophisticated procedures.

Very recently, we have also calculated transition probabilities for the Rydberg radical CH_5, isoelectronic with NH_4 and H_2F, and also expected to be of astrophysical and general chemical importance. Its parent ion, CH_5^+, has been produced in the laboratory with the same technique as other Rydberg radical cations, such as NH_4^+ and H_3O^+ (36). The ground state geometrical structure of the CH_5 radical has been the subjet of several theoretical studies (see, e.g., 37), all yielding a C_s symmetry as the most stable one. We have assumed the Rydberg states to possess the same symmetry, for the reasons given in the Introduction. The only work that, to our knowledge, has dealt with the calculation of Rydberg states and electronic transition probabilities for this radical is the one by Raynor and

Herschbach (16). It is, thus, from these authors (16) from whom we have taken the ionization energy and quantum defects required in our calculations, although, once more, an extrapolation of higher electronic states belonging to different Rydberg series has been carried out.

A few of the oscillator strengths and Einstein coefficients that we have obtained are collected in tables IV and V, corresponding to transitions between states of different symmetry. The available FSSO values (16) have also been included, and it is apparent that, when comparison is possible, the QDO results and those by Raynor and Herschbach (16) conform quite well with each other.

Table IV : Oscillator strengths (multiplied by 10^3), wavelengths (in Å) and Einstein emission coefficients (in units of 10^7/s) for 3s → np transitions in CH_5.

Transition	QDO[a]			FSSO[b]		
	f	$\tilde{\lambda}$	A	f	$\tilde{\lambda}$	A
$1^2A'$ (3s) → $2\,^2A'$ (3p)	269	8547	2.45	306	8547	2.80
$1^2A'$ (3s) → $8^2A'$ (4p)	7.84	4435	0.26			
$1^2A'$ (3s) → $^2A'$ (5p)	1.54	3787	0.07			
$1^2A'$ (3s) → $^2A'$ (6p)	0.55	3531	0.03			
$1^2A'$ (3s) → $3^2A'$ (3p)	283	8070	2.90	279	8070	2.85
$1^2A'$ (3s) → $9^2A'$ (4p)	11.3	4392	0.39			
$1^2A'$ (3s) → $^2A'$ (5p)	2.54	3773	0.12			
$1^2A'$ (3s) → $^2A'$ (6p)	0.98	3524	0.05			
$1^2A'$ (3s) → $1^2A''$ (3p)	298	7558	3.48	313	7558	3.66
$1^2A'$ (3s) → $4^2A''$ (4p)	13.8	4365	0.48			
$1^2A'$ (3s) → $^2A''$ (5p)	3.28	3763	0.15			
$1^2A'$ (3s) → $^2A''$ (6p)	1.30	3520	0.07			

[a] This work.

[b] Raynor and Herschbach (16).

Table V : Oscillator strengths (multiplied by 10^3), wavelengths (in Å) and Einstein emission coefficients (in units of 10^7/s) for 3p → nd transitions in CH_5.

Transition	QDO[a]			FSSO[b]		
	f	$\tilde{\lambda}$	A	f	$\tilde{\lambda}$	A
$1^2A''$ (3p) → $2^2A''$ (3d)	204	17096	0.47			
$1^2A''$ (3p) → $5^2A''$ (4d)	0.9	8665	0.008			
$1^2A''$ (3p) → $^2A''$ (5d)	0.03	7022	0.0005			
$1^2A''$ (3p) → $^2A''$ (6d)	0.00	6376	$1.6\ 10^{-5}$			
$1^2A''$ (3p) → $6^2A'$ (3d)	292	15810	0.78	221	15810	0.59
$1^2A''$ (3p) → $12^2A'$ (4d)	6.23	8426	0.058			
$1^2A''$ (3p) → $^2A'$ (5d)	1.02	6941	0.014			
$1^2A''$ (3p) → $^2A'$ (6d)	0.32	6338	0.0053			
$1^2A''$ (3p) → $3^2A''$ (3d)	229	14973	0.68	242	14973	0.72
$1^2A''$ (3p) → $6^2A''$ (4d)	7.37	8318	0.071			
$1^2A''$ (3p) → $^2A''$ (5d)	1.47	6904	0.020			
$1^2A''$ (3p) → $^2A''$ (6d)	0.53	6320	0.009			

[a] This work.

[b] Raynor and Herschbach (16).

4. Concluding remarks

We consider the QDO method to be a useful tool for estimating transition probablities between molecular Rydberg states. A drawback of our method is its empirical character in that it requires the quantum defects for the states involved in transitions as an input. However, the well established correspondence between the energy levels of a Rydberg molecule and those of its united atom limit (9), as well as the regular behavior of the quantum defects along a Rydberg series are very helpful in their estimations.

The QDO method supplies also simple analytic wavefunctions to describe Rydberg electrons. Possible applications of those wavefunctions to studying various properties of the Rydberg states (as, e. g., their behavior in external fields), have been hardly explored. It is our next goal to apply the QDO formalism not only to transition probabilities but also to other spectral properties of Rydberg molecules.

5. Acknowledgements

It is a pleasure to thank V. H. Smith Jr. for stimulating discussions. I. M. would like to thank G. H. F. D. for his kind hospitality during her visits to the Max-Planck-Institut für Astrophysik in Garching. This work has been partly supported by the D.G.C.Y.T. of the Spanish Ministry of Education within Projects No. PB91-0207-C02-01 and PB94-1314-C03-03, and by the Polish K. B. N.

References

(1) J.R. Rydberg, Kgl. Sven. Vendesk. Akad. Handl. 23 Sections 15 and 16 (1889).
(2) J.A. Dagata, G.L. Findley, S.P. McGlynn, J.P. Connerade, M.A. Baig, Phys. Rev. A 34, 2485 (1981).
(3) S. Ross in "AIP Conference Proceedings 255"; M. Garcia-Sucre, G. Raseev, S.C. Ross, Eds.; American Institute of Physics: New York, 1991.
(4) I.D. Petsalakis, G. Theodorakopoulos, M.S. Child, J. Phys. B : At. Mol. Opt. Phys. 28, 5179 (1995).
(5) R.S. Freund, in "Rydberg States in Atoms and Molecules", R.F. Stebbings, F.D. Dunning, Eds.; Cambridge Univ.Press: Cabridge, 1983.
(6) H. Helm, Phys. Rev. Lett. 56 , 42 (1986).
(7) A.B.F. Duncan, "Rydberg Series in Atoms and Molecules"; Academic Press: New York, (1971).
(8) D.S. Ginter, M.L. Ginter, J. Mol. Spectrosc. 82 , 152 (1980).
(9) G. Herzberg, Ann. Rev. Phys. Chem. 38 , 27 (1987), and references therein.
(10) B.E. Turner, Symp. Int. Astron. Union 150 , 181 (1992).
(11) M.E. Jacox, J. Phys. Chem. Ref. Data 17 , 269 (1988); *ibid* 19 , 1387 (1990).
(12) G. Herzberg, J. Chem. Phys. 70 , 4806 (1979).
(13) W.W. Duley and D.A. Williams, "Interestellar Chemistry"; Academic Press: London, 1984.
(14) M. Guelin, in "Molecules in Physics, Chemistry and Biology", J. Maruani, Ed.; Kluwer: Dordrecht, 1988.
(15) H.F. King, K. Morokuma, J. Chem. Phys. 71 , 3213 (1979).
(16) S. Raynor, D.R. Herschbach, J. Phys. Chem. 86 , 3592 (1982).
(17) G.H.F. Diercksen, W. Duch, J. Karwowski, Chem, Phys. Lett. 168 , 69 (1990).

(18) I. Martin, J Karwowski, G.H.F. Diercksen, C. Lavin, Int. J. Quant. Chem. S27 723 (1993).
(19) G. Simons, J. Chem. Phys. 60 , 645 (1974); G. Simons, I. Martin, J. Chem. Phys. 62 , 4799 (1975).
(20) C. Lavin, I. Martin, M.J. Vallejo, Int. J. Quant. Chem. S26 , 455 (1992), and references therein.
(21) I. Martin, C. Lavin, A.M. Velasco, M.O. Martin, J. Karwowski, G.H.F. Diercksen, Chem. Phys. 202 , 307 (1996).
(22) I. Martin, C. Lavin, J. Karwowski, Chem. Phys. Lett. 255 , 89 (1996).
(23) A.M. Velasco, I. Martin, C. Lavin, Chem. Phys. Lett. 264 , 579 (1997).
(24) C. Lavin, I. Martin in Adv. Quant. Chem., vol 28; Academic Press: New York (1997), p.205
(25) R.L. Martin, J. Chem. Phys. 71 , 3541 (1979).
(26) I.D. Petsalakis, G. Theodorakopoulos, J.S. Wright, J. Chem. Phys. 89 , 6850 (1988).
(27) G. Herzberg, Dicuss. Faraday Soc. 71 , 165 (1981).
(28) G. Herzberg, J. Mol. Struct. 113 , 1 (1984).
(29) S. Havriliak, H.F. King, J. Am. Chem. Soc. 105 , 4 (1983).
(30) S. Havriliak, T.R. Furlani, H.F. King, Can. J. Phys. 62 , 1336 (1984).
(31) G.I. Gellene. D.A. Cleary, R.F. Porter, J. Chem. Phys. 77 , 3471 (1982).
(32) M.N.R. Ashfold, R.N. Dixon, R.S. Stickland, Chem. Phys. 88 , 463 (1984).
(33) M.N.R. Ashfold, C.L. Bennett, R.N. Dixon, Chem. Phys. 93 , 293 (1985).
(34) I.D. Petsalakis, Theodorakopoulos, J.S. Wright, I.P. Hamilton, J. Chem. Phys. 88 , 7633 (1988).
(35) I.D. Petsalakis, Theodorakopoulos, J.S. Wright, I.P. Hamilton, J. Chem. Phys. 89, 6841 (1988).
(36) B.W. Williams, R.F. Porter, J. Chem. Phys. 73 , 5598 (1980).
(37) D.W. Boo, Y.T. Lee, J. Chem. Phys. 103, 520 (1995).

Time-dependent quantum treatment of two-colour multiphoton ionization using a strong laser pulse and high-order harmonic radiation

V. Véniard, R. Taïeb and A. Maquet

Laboratoire de Chimie Physique-Matière et Rayonnement (*)
Université Pierre et Marie Curie
11, Rue Pierre et Marie Curie, 75231 PARIS Cedex 05 FRANCE

Abstract : Recent advances achieved in the numerical resolution of the Time-Dependent Schrödinger Equation (TDSE), have made possible to address difficult problems in the analysis of highly non-linear processes taking place when an atom is submitted to an ultra-intense laser pulse. We discuss the main properties of the photoelectron spectra obtained when a high frequency harmonic field is also present in addition to the laser field. This class of processes is believed to serve as a basis to explore new secnarios to achieve a coherent control of atomic photoionization.

Table of Content :

1. Introduction
2. Theoretical Model
3. Numerical Calculations
4. Results and Discussion
5. References

1. INTRODUCTION

The possibility to use laser radiations to achieve the so-called "coherent control" of molecular dissociation or of atomic photoionization has been predicted since the advent of laser sources in the early sixties. It was expected that, thanks to the coherence and monochromaticity properties of the laser light, one could selectively choose a dissociation channel and the spatial orientation of ejection of the fragments (either ions or electrons or even neutrals) in an elementary chemical process. However, earlier attempts, based on simple photoabsorption processes, have been unsuccessful and it is only recently that experiments have been shown to enable one to achieve such a goal in some selected systems. Amongst the various scenarios which have been explored, one of the most promising is based on the realization of quantum interferences in so-called "two-colour" photodissociation or

---

(*) Unité de Recherche Associée au CNRS, URA 176

ADVANCES IN QUANTUM CHEMISTRY, VOLUME 32
Copyright ©1999 by Academic Press. All rights of reproduction in any form reserved.
0065-3276/99 $30.00

photoionization processes [1], [2]. The underlying idea is to use two distinct radiation sources with commensurable frequencies in such a way as to reach the chosen final state of the system via two distinct quantum paths. Changing the relative phase between the two fields can lead to the realization of constructive quantum interferences which can help to enhance the relative weight of a quantum path against others, thus leading to the control of the reaction channel. See the references [3] and [4] for recent theoretical works along these lines on photodissociation and atomic photoionization.

This latter class of scenarios has been shown to be amenable to experimental realizations for some simple test-case systems such as diatomic molecules for photodissociation and rare gases for atomic photoionization, in rather long radiation pulses [1], [2]. However, the questions of the quantum dynamics of more complex systems and/or on shorter time scales are still open problems. Indeed, in the case of atomic photoionization the available sources of intense radiation in the infrared and visible domains are pulsed lasers with pulse durations within the sub-picosecond (and even femtosecond) ranges. One of the major consequence of this fact is that, for the theoretical treatment, it is no longer correct to rely on the simplified picture of a constant amplitude field and on perturbative approaches. The object of the present paper is to report on recent advances made in the numerical treatment of the Time-Dependent Schrödinger Equation (TDSE), with application to two-colour atomic photoionization within a radiation pulse containing simultaneously the fundamental of a laser and one of its high-order harmonics, [5]. The process under consideration exploits the advances made in the implementation of powerful sources of coherent radiation in the X-UV frequency domain, which are based on the recent discovery of the generation of high-order harmonics of an IR laser. These harmonics are generated when a laser beam is focused on a jet of rare-gas atoms, [6]. In this perspective, it is worth to mention that such high harmonic sources, with photon energies up to $\omega_H \approx 150\, eV$, have been recently operated.

2. THEORETICAL MODEL

An isolated atom submitted to an intense infrared laser pulse can be ionized via multiphoton absorption. Moreover, at higher intensities, the atom can absorb more photons than strictly necessary for being ionized, thus giving rise to the so-called "Above-Threshold Ionization" (ATI) process. The signature of ATI is the presence, in the photoelectron spectrum, of equally spaced lines separated by the laser photon energy ω_L, see Figs. 1 and 2b. On the other hand, if the atom is exposed to a pulse of harmonic radiation alone, with frequency $\omega_H > E_{Ionization}$, it can be ionized via a standard (single-photon) ionization process, see Fig. 2a. We note that, in applications, harmonics generated in atomic gases (which are centro-symmetric systems) have frequencies which are odd multiples of the laser one,

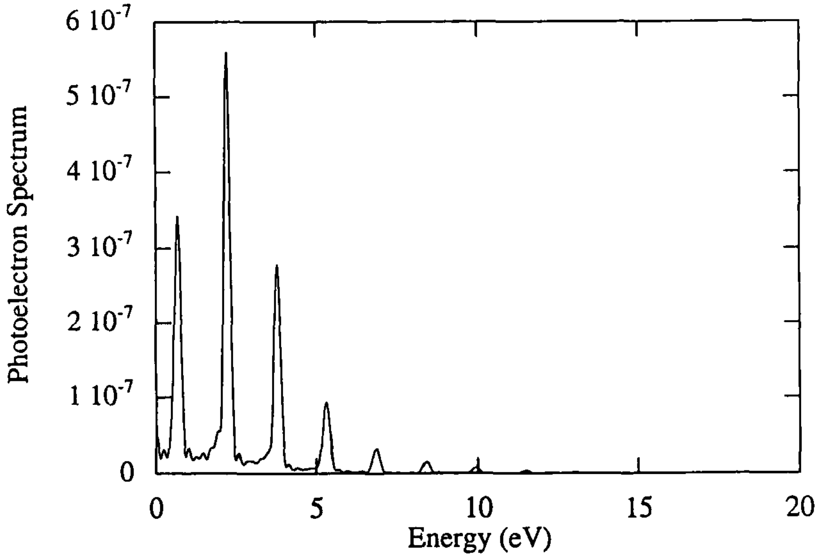

Fig. 1. Typical ATI photoelectron spectrum obtained from hydrogen *1s* with an infrared laser radiation pulse (see text). Here, the spectrum is derived from the occupation density of the atomic positive energy states, as computed after the laser pulse.

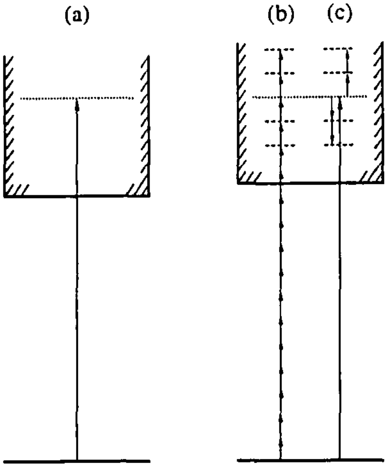

Fig. 2. Energy diagrams schematically representing photoionization processes from the atomic ground state : (a) single-photon ionization resulting from the absorption of one high-frequency UV photon (here it is the 13th harmonic of an IR laser); (b) ATI multiphoton ionization occurring in the presence of an intense IR laser; (c) two-colour ionization occurring in the simultaneous presence of the IR laser and of the UV harmonic

namely one has : $\omega_H = (2n+1)\omega_L$, $n = 1, 2, 3, \dots$ This feature makes possible the realization of quantum interferences which can take place in photoionization if the laser and one of its harmonics are simultaneously present. The reason is that any final continuum state of the atom, with energy compatible with the energy conservation law, can then be reached via several (in any case, at least two) quantum paths, as schematically indicated when comparing the Figures 1b and 1c. In order to discuss the main features of this class of processes we have considered the test case of an hydrogen atom, initially in its ground state $1s$, which is submitted to a pulse of radiation containing two (or several, see refs. [7]) distinct fields, as explained next.

There is first the fundamental of a strong infrared laser. For the sake of illustration, we have chosen the case of a Ti:sapphire laser operated at $\omega_L = 1.55$ eV, i.e. $\omega_L = 0.057$ $a.u.$, which is representative of the recently operated "femtosecond" sources. We have considered intensities I_L around 10^{13} W/cm^2, which are typical. Note that, although such intensities are very high by laboratory standards, they remain quite moderate when compared to the "atomic" intensity, $I_0 = 3.5\ 10^{16}$ W/cm^2, which is associated to the field strength experienced by an electron on the first Bohr orbit in hydrogen, namely : $F_0 = 5.1\ 10^9$ V/cm. At intensities $I_L \approx 10^{13}$ W/cm^2 the atom can experience multiphoton ionization and even ATI, as shown in Fig. 1, which displays the simulation of a photoelectron spectrum for a peak intensity $I_L = 2.\ 10^{13}$ W/cm^2. Here, the pulse shape is assumed to be trapezoidal with linear turn-on and turn-off durations of one laser period ($T_L = 110$ $a.u.$, *i.e.* $T_L = 2.6\,fs$), the total duration of the pulse being $8T_L$.

The second source of radiation is one of the high-order harmonics of the fundamental. For the sake of illustration, we have chosen the 13th harmonic, so that $\omega_H = 13\omega_L > E_{Ionization}$ and we have assumed that this high frequency field has the same pulse duration and polarization orientation than the laser's. Then, by suitably changing the relative intensities of the two fields, one can explore different regimes in which the photoionization process is dominated either by the atom-harmonic interaction (Fig. 2a) or by the atom-laser interaction (Fig. 2b) or by a two-colour process (Fig. 2c). In order to compute the corresponding photoelectron spectra, we have written original codes intended to numerically solve the Time-Dependent Schrödinger Equation (TDSE) and to perform the spectral analysis of the atomic wave function after the laser pulse.

3. NUMERICAL COMPUTATION

The TDSE to be solved reads in atomic units :

$$i\partial\Psi(r,t)/\partial t = [H_{at} + H_L(t) + H_H(t)]\ \Psi(r,t),$$

where H_{at} is the three-dimensional hamiltonian for hydrogen and the time-dependent atom-field interaction hamiltonians are respectively :

$$H_L(t) = -zF_L(t)\sin(\omega_L t)$$

for the atom-laser interaction and :

$$H_H(t) = -zF_H(t)\sin(\omega_H t + \phi)$$

for the atom-harmonic interaction. Here the two fields are assumed to be linearly polarized along the z-axis and they are supposed to be single-mode and spatially homogeneous. The phase ϕ has been introduced in order to account for the phase-shift between the laser and its harmonic. Note that the interaction hamiltonians are represented here under the electric-dipole ***E.r*** form but that we have checked that one obtains the same results when using the ***A.p*** gauge. The numerical integration has been performed by using a technique similar to the one previously proposed by Kulander *et al.* [8]. More specifically, after a partial wave decomposition of the wave function, its radial components for each angular momenta are computed on a grid between $r = 0$ and $r_{max} = 1250$ *a.u.* with steps $\delta r = 0.25$ *a.u.* When performing the computation in the ***A.p*** gauge we had to include up to $l_{max} = 20$ angular momenta in order to get converged results. We note that the number of angular momenta needed to ensure the same accuracy when using the ***E.r*** gauge is around $l_{max} = 100$, see ref. [9] for a recent discussion of this particular feature of this class of calculations. The time propagation of the solution has been carried out via a standard Peaceman-Rachford algorithm. We mention that, as we have considered rather short laser pulses, the box was wide enough to render negligible the effects of spurious reflections of the fast components of the electronic wave function on the boundary.

The photoelectron spectra have been obtained from the atomic wave function after the pulse via a spectral analysis technique. To this end, we have used a Lorentzian-like window operator of the form, [10] :

$$W(E_k,\gamma) = \gamma^4/[(H_{at} - E_k)^4 + \gamma^4]$$

where the parameter γ, here chosen so that : $2\gamma = 0.025\ eV$, indicates the energy resolution of our analysis. Then the occupation density of a given atomic state with energy E_k, pertaining either to the discrete or continuous spectrum, is defined as :

$$P(E_k) = <\Psi(t)|W(E_k,\gamma)|\Psi(t)>.$$

We turn now to the presentation of some typical results of our analysis applied to the discussion of two-colour photoionization in strong laser fields.

4. RESULTS AND DISCUSSION

The most direct way to demonstrate the importance of the above-mentioned phenomena is to compare the photoelectron spectra simulated with the laser alone and with the two colours (laser + harmonic). For a given laser pulse shape and peak intensity, it appears that adding a moderately intense harmonic field, (well within the capabilities of the currently developed harmonic sources), can dramatically modify the photoelectron spectra. This is shown in the Figures 3a and 3b where we present the occupation densities of the continuum states after the radiation pulse for two different laser peak intensities. Note that when the 13th harmonic field is present it has a peak intensity of $3.0\ 10^8\ W/cm^2$. In Fig. 3a, the laser peak intensity ($10^{13}\ W/cm^2$) is such that ATI (thin line), starts to be significant even for such a short pulse. Adding the rather weak harmonic field strongly modifies the spectrum (thick line), as many more equally spaced photoelectron peaks are present at higher kinetic energies. This tendency is further amplified if the laser peak intensity is doubled ($2.\ 10^{13}\ W/cm^2$), as shown in Fig. 3b. However, a new interesting feature does appear in the spectrum : the low energy range is now dominated by ATI, while the already seen two-colour process dominates the high energy range. Between these extremes, (i.e. around the peak #5), ATI and two-colour ionization are in fact competing processes and quantum interferences can take place, see Figs. 2b-2c. Then, the relative phase between the laser and its harmonic can play a determinant role. This point is addressed next.

Changing the phase difference ϕ between the laser and its harmonic, everything else being kept fixed, can indeed considerably modify the magnitudes of some of the photoelectron peaks. This is shown in the Figure 4, where the changes in the magnitudes of two selected photoelectron peaks are reported for several typical values of the phase difference. The laser intensity is now $1.75\ 10^{13}\ W/cm^2$. One of the main outcomes of our simulations is to clearly show the occurrence of constructive and destructive interferences with a contrast factor being close to two in the present conditions, thus providing a clear example of a partial coherent control in atomic photoionization.

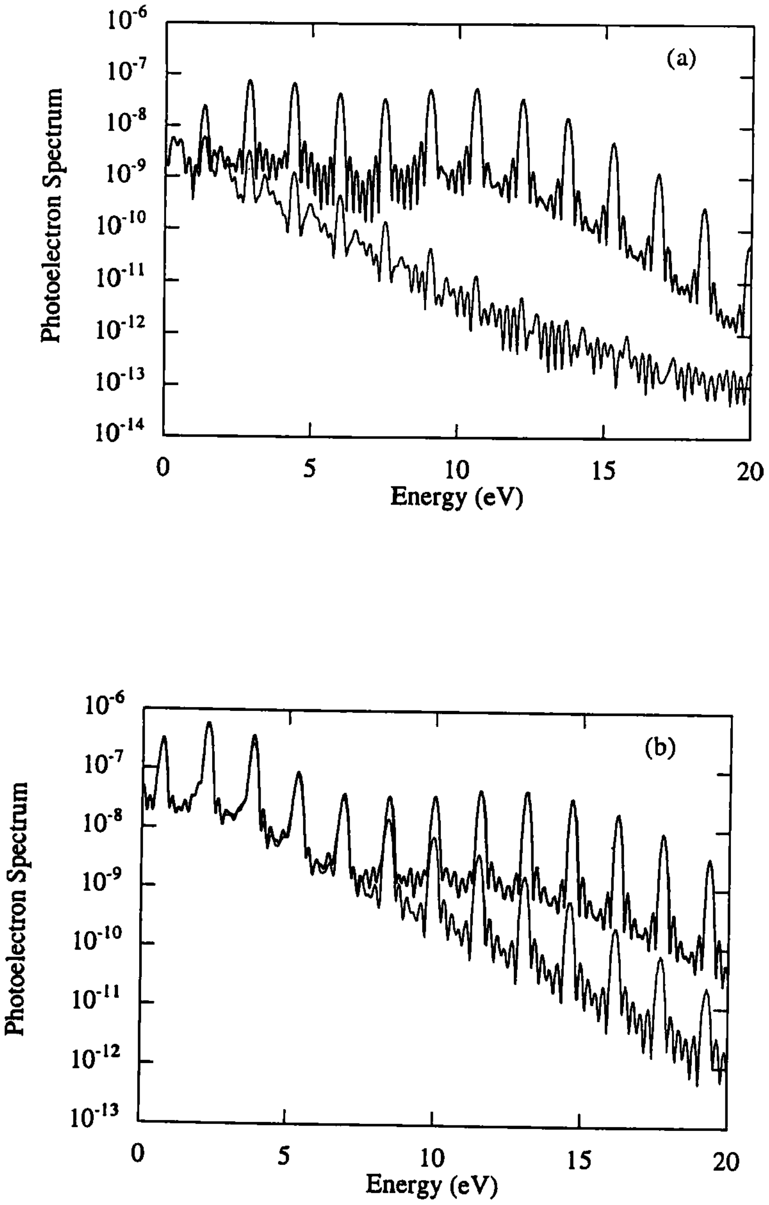

Fig. 3. Comparison of (single-colour) ATI spectra (thin lines) obtained with a Ti: sapphire laser with two-colour photoionization spectra (thick lines) in the presence of the 13th harmonic of the laser frequency ($I_H = 3.0\ 10^8$ W/cm^2.). (a) $I_L = 1.0\ 10^{13}$ W/cm^2; (b) $I_L = 2.0\ 10^{13}$ W/cm^2.

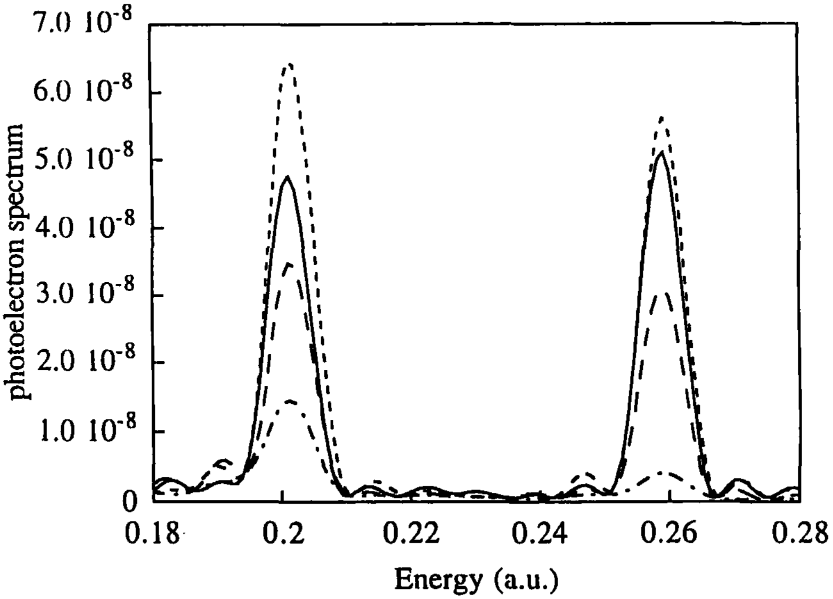

Fig. 4. Dependence of two photoelectron peaks on the phase difference between the laser and its 13th harmonic. Dot-dashed line : ATI spectrum (laser alone); long-dashed line : $\phi = 0$; full line : $\phi = \pi/2$; dashed line : $\phi = \pi$.

To conclude, let us mention that preliminary two-colour (and in fact N-colour, N > 2) experiments are currently under way, [11]. Our numerical codes implemented to solve the TDSE and to perform the spectral analysis of the wave function, are helpful tools to explore the main features of this new class of processes which seem to open the possibility to better control basic photoionization processes.

Akcnowledgements. The Laboratoire de Chimie Physique-Matière et Rayonnement is a Unité de Recherche Associée au CNRS. This work has been partially supported by the EC Contract # ERB CHRX 940470. Parts of the computations have been performed at the CCR Jussieu, Paris and at the Institut du Développement et des Ressources en Informatique Scientifique (IDRIS).

5. REFERENCES

[1] L. Zhu, V. Kleinman, X. Li, S.P. Lu, K. Trentelman and R.J. Gordon, Science, **270**, 77 (1995).

[2] Ce Chen and D.S. Elliott, Phys. Rev. Lett. **65**, 1737 (1990). Recent references include : D.W. Schumacher, F. Weihe, H.G. Muller and P.H. Bucksbaum, Phys. Rev. Lett. **73**, 1344 (1994); S. Watanabe, K. Kondo, Y. Nabekawa, A. Sagisaka and Y. Kobayashi, Phys. Rev. Lett. **73**, 2692 (1994).

[3] M. Schapiro and P. Brumer, J. Chem. Phys. **84**, 4103 (1986); A.D. Bandrauk, J.M. Gauthier and J.F. McCann, J. Chem. Phys. **100**, 340 (1994); E. Charron, A. Giusti-Suzor and F.H. Mies, Phys. Rev. A **49**, R641 (1994); see also the review articles by M. Schapiro and P. Brumer, Int. Rev. Phys. Chem. **13**, 187 (1994) and by A. Giusti-Suzor, F.H. Mies, L.F. DiMauro, E. Charron and B. Yang, J. Phys. B **28**, 309 (1995).

[4] K.C. Schafer and K.J. Kulander, Phys. Rev. A **45**, 8026 (1992); R.A. Blank and M. Schapiro, Phys. Rev. A **52**, 4278 (1995); M. Protopapas and P.L. Knight, J. Phys. B **28**, 4459 (1995).

[5] V. Véniard, R. Taïeb and A. Maquet, Phys. Rev. Lett. **74**, 4161 (1995), R. Taïeb, V. Véniard and A. Maquet, J. Opt. Soc. Am. B **13**, 363 (1996).

[6] A. L'Huillier, L.A. Lompré, G. Mainfray and C. Manus in *Atoms in Strong Fields*, edited by M. Gavrila, Adv. Atom. Molec. Opt. Phys. Suppl. **1** (Academic Press, San Diego, 1992), pp. 139; a recent reference is : R. Zerne, C. Altucci, M. Bellini, M.B. Gaarde, T.W. Hänsch, A. L'Huillier, C. Lynga and C.-G. Wahlström, Phys. Rev. Lett. **79**, 1006 (1997).

[7] V. Véniard, R. Taïeb and A. Maquet, Phys. Rev.A **54**, 721 (1996); Comments At. Mol. Phys. **33**, 53 (1996).

[8] K.C. Kulander, K.J. Schafer and J.L. Krause in *Atoms in Strong Fields*, edited by M. Gavrila, Adv. Atom. Molec. Opt. Phys. Suppl. **1** (Academic Press, San Diego, 1992), pp. 247.

[9] E. Cormier and P. Lambropoulos, J. Phys. B **29**, 1667 (1996).

[10] K.J. Schafer, Comp. Phys. Commun. **63**, 427 (1991).

[11] J.M. Schins *et al.* J. Opt. Soc. Am. B **13**, 197 (1996); T.E. Glover *et al.* Phys. Rev. Lett. **76**, 2468 (1996)

Methods Involving Complex Coordinates Applied to Atoms

Mirosław Bylicki

Instytut Fizyki
Uniwersytet Mikołaja Kopernika
ul. Grudziądzka 5/7, 87-100 Toruń, Poland

Abstract

A review of recent developments of methods involving complex coordinates and their applications to autoionizing states of free atoms as well as to atoms in external fields is presented.

1. Introduction
2. Problems and methods
3. Basis sets
4. Recent computations
5. Summary
6. Acknowledgments
References

ADVANCES IN QUANTUM CHEMISTRY, VOLUME 32
Copyright © 1999 by Academic Press. All rights of reproduction in any form reserved.
0065-3276/99 $30.00

1. Introduction

The Aquilar, Balslev, Combes and Simon (ABCS) theorems concerning spectrum of analytically dilated (complex rotated) Hamiltonians were published in the early seventies (1–3). They caused an explosive development of techniques using complex coordinates and their applications, which have been reviewed in numerous articles (4–13).

Some of these computational methods emerged directly from the ABCS theorems. Some others are related to this theory just by the idea of using complex coordinates, which was first put forth by Dykhne and Chaplik (14). In all of them the practical meaning of employing complex coordinates is the transformation of the unbound resonance wave function into a square-integrable one. Thus the methods are applicable to various phenomena of atomic, molecular, solid state, surface physics, which can be formulated in terms of quasistationary states, thus including autoionization and predissociation, dc- and ac-field induced ionization (12), multiphoton dissociations (15), scattering (10, 16), trapping of atoms and molecules on solid surfaces (17), tunneling in low-dimensional structures (18).

In this article a part of the implementations of complex-coordinate methods is briefly reviewed. We consider only recent applications to free atoms (ions) or atoms interacting with an external field. Mainly recent papers of the nineties are quoted here. However, earlier review and precursory articles are also cited.

In section 2 the most often asked physical questions concerning resonant phenomena in atoms are recollected, together with methods capable of answering them by implementation of complex coordinates. Problems connected with basis sets used within the complex-coordinate methods are described in section 3. Finally, in section 4, recent applications to atoms are listed.

2. Problems and methods

2.1. Position and width

What is the position and width of an investigated resonance? In order to answer this fundamental question, one can use complex coordinates within computational methods that had been originally developed for bound states. The real part of a complex energy, ϵ, that one obtains for the resonance, constitutes its position, i.e., the actual real energy. The imaginary part gives the width of the resonance, $\Gamma = -2Im(\epsilon)$, so it determines the lifetime of the state, $\tau = \frac{\hbar}{\Gamma}$.

2.1.1. Variational methods

The complex coordinate rotation (CCR) or complex scaling method (5,6,10,19) is directly based on the ABCS theory (1–3), therefore Reinhardt (5) also called it the *direct approach.* A complex rotated Hamiltonian, $\hat{H}(\theta)$, is obtained from the electron Hamiltonian of the atom, $\hat{H}$, by replacing the radial coordinates r by $re^{i\theta}$, where θ is a real parameter. The eigenproblem of this non-Hermitian operator is solved variationally in a basis of square-integrable functions. The matrix representation of $H(\theta)$ is obtained by simple scaling of matrices T and V representing the kinetic and Coulomb potential part of the unrotated Hamiltonian $\hat{H}$,

$$H(\theta) = e^{-i2\theta}T + e^{-i\theta}V. \tag{1}$$

Those complex eigenvalues of $H(\theta)$ which do not depend on θ for some well defined range of θ, are associated with resonances.

Most of the actual realizations of the CCR method diagonalize the matrix $H(\theta)$. However, there are some versions of the CCR method which do not diagonalize $H(\theta)$, but some other matrices related to it. Sommerfeld *et al.* (20) diagonalizes the matrix $e^{i\theta}H(\theta) = e^{-i\theta}T + V$, so that the complex arithmetic is connected only with the matrix T, which is very sparse in comparison to V. The resulting eigenvalues are multiplied by $e^{-i\theta}$ to obtain the eigenvalues of $H(\theta)$. In the Hermitian representation of the CCR method, introduced by Moiseyev (21) and modified by Bylicki (22), the eigenproblem of a Hermitian operator defined in terms of the Hermitian and non-Hermitian parts of $\hat{H}(\theta)$ is solved; no complex arithmetic is involved. However, a disadvantage of this method is that it is addressed to a single resonance, whose approximate energy has to be known in advance.

An alternative approach emerges from the critical analysis of the convergence property of the CCR method carried out by Rescigno, McCurdy and Orel (23), Junker and Huang (24), and Nicolaides and Beck (25). In this approach, the Hamiltonian is not scaled. Complex basis functions are used instead. Moreover, different basis are applied for the bound and unbound parts of the system. The complex-eigenvalue Schrödinger equation (CESE) method of Nicolaides and coworkers (11–13), starts from the general form of the wave function corresponding to the resonance (25–27)

$$\Psi = a\Phi_o + \sum_j b_j X_j. \tag{2}$$

The localized part Φ_o describes the resonance in the first approximation as a bound state. The remaining part contains all the open channels

$$X_j = A[\chi_j^{core}(x_1, ..., x_{N-1}) g_j(x_N)], \tag{3}$$

each described by an unbound Gamow orbital, g_j, associated with a bound state of the $(N-1)$-electron core, χ_j^{core}. Asymptotically the g_j functions describing the detaching electron are oscillating outgoing waves. This property of the resonance state asymptotic behaviour is fundamental for the CESE method. On one hand, it requires that the resonance energy should be a complex number (26). On the other hand, it shows that the resonance wave function can be made square integrable just by regularizing the g_i functions. As a result of using complex scaling $r \rightarrow re^{i\theta}$ as a technique of regularizing them (14), the Gamow orbitals are expressed in a basis of back-rotated square-integrable orbitals (28,23).

The complex stabilization method of Junker (7), although it was introduced in a different way, gives practically the same computational prescription as the CESE method, as far as the way of using complex coordinates is considered. Another approach of this type, resembling the CESE method as well as the complex stabilization method, is the saddle-point complex-rotation technique of Chung and Davis (29). These methods provide clear physical insight into the resonance wave function. They differ in the way the localized part of the wave function is expanded in basis sets and how it is optimized.

2.1.2. Non-variational methods

Recently Lindroth (30) has introduced the concept of complex coordinates into nonvariational methods. The idea of Lindroth is to produce a basis set of one-particle complex rotated functions as solutions of the one-particle complex-rotated problem, and then to apply this basis within a bound-state method for a many-particle system. In this way the complex rotation has been combined with the many-body perturbation theory (30) and with the coupled cluster method (31). Apart from the fact that the resulting energy is complex and its real and imaginary part can be interpreted as the position and width of a resonance under consideration, the use of complex coordinates has the advantage that singularities caused by the degeneracy on the real axis between the resonance and the adjacent continuum are not present in the complex energy plane.

An interesting problem of behaviour of the resonance levels along isoelectronic sequences can be investigated by the Z-dependent perturbation theory. Manning and Sanders (32,33) combined the complex rotation method with the Z-dependent perturbation theory. Expansion of the complex eigenvalue corresponding to the resonance as a power series in $\frac{1}{Z}$ simultaneously yields values of both the resonance position and width for all members of an isoelectronic sequence.

The CCR computations for a many-electron system become very expensive due to the extremely large size of the basis sets. In special cases like Rydberg systems in external electromagnetic fields, this difficulty can be avoided by implementing the R-matrix method (34–36). The configuration space is divided into an inner and outer regions chosen so that, on one hand, the many-electron core is contained in the inner region and, on the other hand, the field terms are negligible there. In the outer region, outside a multielectron core, the one-electron complex-rotated problem is solved. The inner region solutions for the outer electron are at the boundary surface (where both the inner- and outer-region solutions must match) expressed as linear combination of Coulomb functions, parametrized with quantum defects representing the influence of the many electron core and deduced from field-free spectral measurements. (In this sense the method is semiempirical).

Actually, in the opinion of the author, the R-matrix complex-rotation method, presented above, should be considered as an implementation of the idea proposed by Nicolaides and Beck (37) and then by Simon (38), and known as the exterior complex-scaling. This interpretation is natural due to the fact that the R-matrix method and the exterior complex-scaling share the idea of dividing the configuration space into internal and external parts.

2.2. Partial widths

The total width of the resonance is directly given by the resonance complex energy. In the case where many channels of autodetachment are open, the question of partial widths for the decay into individual channels arises. This always requires analysis of the wave function. The problem of obtaining partial widths from complex coordinate computation has been discussed by Noro and Taylor (39) and Bačić and Simons (40), and recently by Moiseyev (10). However, these considerations do not seem to have found a practical application. Interchannel coupling for a real, multichannel, multielectron problem has been solved in a practical way within the CESE method by Nicolaides and Mercouris (41). According to this theory the partial widths, γ_j, and partial shifts to the real energy, δ_j, are computed to all orders via the simple formula

$$\delta_j - \frac{i}{2}\gamma_j = \frac{b_j}{a}\langle\Phi_o|H|X_j\rangle \tag{4}$$

where all the symbols are the same as in Eq(2). This formula has been applied successfully to the computation of partial widths with interchannel coupling in multiply excited autoionizing states (42–46).

2.3. Atoms in static electric or magnetic field

The complex-coordinate methods can be applied to atoms in external fields (5, 12, 47). From a technical point of view, in the CCR method the electric and square magnetic terms of the Hamiltonian need to be scaled by factor $e^{i\theta}$ and $e^{i2\theta}$, respectively. From a mathematical point of view, the ABCS theory does not apply to this case. The application of the CCR method to the Stark problem has been justified by Herbst and Simon (48).

The CESE method is applicable directly. Nicolaides and Themelis (49) considering the asymptotic behaviour of the LoSurdo-Stark resonance states, showed that the wave function is regularizable by the complex rotation transformation and that the complex energy of the resonance can be obtained as a solution of the CESE. In the case of a magnetic field, the asymptotic behaviour of the resonance wave function is governed by the atom potential, hence the results for field-free atoms (26) remain valid.

First applications were done for the hydrogen atom in an electric field (47) and in a magnetic field (50,51). Among recent computations for many-electron atoms, one should mention the R-matrix CCR calculations for Rydberg states in a magnetic field (34–36,52) as well as in an electric field (36). Investigation of multiply excited states in electric fields, initiated twenty years ago by Wendoloski and Reinhardt (53) for H^-, has been continued in the nineties by Ho (54–60), using the CCR method for two-electron atoms, and by the group of Nicolaides (12), using the CESE approach to many electron atoms. The investigation of the Zeeman problem for multiply excited states has been started very recently by Bylicki, Themelis and Nicolaides (61,62).

2.4. Interaction with photons

Rescigno and McKoy (63) have presented a prescription for computing photoabsorption cross sections by the complex rotation method. The cross section for absorption of photons, $\hbar\omega$, by an atom or molecule in an initial state Ψ_o of energy E_o, can be computed as

$$\sigma(\omega) = A\omega Im\{\sum_i \frac{\langle\Psi_o(\theta)|\mu(\theta)|\Psi_i\rangle\langle\Psi_i|\mu(\theta)|\Psi_o\rangle}{E_i - E_o - \hbar\omega}\} \qquad (5)$$

where the dipole operator, μ, as well as the initial state Ψ_o are complex rotated by the $r \rightarrow re^{i\theta}$ replacement. The summation is performed over all final states obtained by the complex rotation method. Some of them are bound or resonance states. The others constitute a discrete representation of the continuum. Thus the cross section takes into account direct photoionization as well as autodetachment preceded by photoexcitation to a resonance state. In many recent works this theory has been developed and applied (35,52,64–68) to compute photoionization cross sections for atoms, including partial cross sections and double photoionization cross sections.

Multiphoton processes taking place in atoms in strong laser fields can be investigated by the non-Hermitian Floquet formalism (69–71,12). This time-independent theory is based on the equivalence of the time-dependent Schrödinger description to a time-independent field-dressed-atom picture, under assumption of monochromaticity, periodicity and adiabaticity (69,72). Implementation of complex coordinates within the Floquet formalism allows direct determination of the complex energy associated with the decaying state. The real part provides the position of the level changed with respect to the field-free case by the ac Stark shift. The imaginary part, $\frac{\Gamma}{2}$, is related to the multiphoton detachment rate.

Recently Yao and Chu have developed complex-scaling grid techniques which can be used to discretize the time-independent Floquet Hamiltonian (73,74). The methods are applied to multielectron atoms represented by a one-electron potential (73–76). Ben-Tal, Moiseyev and coworkers also developed an approach combining complex-coordinates with the Floquet formalism and applied it to model Hamiltonians (77–82). They also considered non-periodic time-dependent Hamiltonians (81).

Unlike the above mentioned methods, another Floquet-theorem-based approach, the many-electron many-photon theory (MEMPT) of Mercouris and Nicolaides (71,72) does not involve complex rotated Hamiltonians. The complex coordinate rotation is used only to regularize that part of the wave functions which describes unbound electrons (see the CESE method). This allows efficient description of bound or quasi-bound states, involved in a problem under consideration, by MCHF solutions and therefore enables *ab initio* application to many-electron systems (71,72,83–87).

The localization of multiphoton ionization resonance wave functions in ac fields has been recently discussed, from a mathematical point of view, by Moiseyev (88,89). He showed (88) that upon complex scaling the resonance wave functions, obtained for a general (not necessarily time-periodic) Hamiltonian in the acceleration frame or the velocity gauge, are square integrable functions. In the case of the length gauge, he used (89) the exterior complex scaling procedure (37,38) to regularize the resonance wave function at any given time.

2.5. Electric properties

The Stark shifts to the energy levels of atoms put into an external dc or ac field can be expanded in a Taylor series:

$$\Delta(F) = -\frac{1}{2!}\alpha F^2 - \frac{1}{4!}\gamma F^4 - \dots , \tag{6}$$

for static field or

$$\Delta(\omega, F) = -\frac{1}{2!}\alpha(\omega)\frac{1}{2}F^2 - \frac{1}{4!}\gamma(\omega)\frac{3}{8}F^4 - \dots , \tag{7}$$

for linearly polarized monochromatic light of frequency ω, averaged over the field cycle (90,91). The linear, α, and nonlinear, γ, polarizabilities can be obtained by fitting the formulas Eqs.(6,7) to the energy shift values, $\Delta(F)$, computed by means of methods described above, for different values of the field strength, F. This approach has been applied by Nicolaides and coworkers to ground and excited states of many-electron atoms (49,90–97).

3. Basis sets

Transformation of the Hamiltonian by the $r \rightarrow re^{i\theta}$ replacement causes analogous rotation of coordinates in the eigenfunctions of the Hamiltonian. Thus an eigenfunction corresponding to a resonance, which before trasformation had asymptotic character of an oscillating outgoing wave nonvanishing at infinity, becomes square-integrable, provided that the rotation parameter θ is in the proper range (5–7, 10). This nice property allows us to use square-integrable basis sets, when performing computations for autoionizing resonances. Unfortunately, simultaneously with the desirable square-integrability of the asymptotic part, the rotation transformation changes the smooth radial part of the wave function describing bound parts of the system, into strongly oscillating functions (5, 24). Representing these oscillations in a typical basis set of real functions appropriate for unrotated bound states is a difficult task requiring very large expansions (23–25). Small basis sets would not be capable of producing reliable results stable against variation of θ, even if their nonlinear parameters were optimized.

The Hylleraas expansion is well known to be an efficient tool for obtaining accurate results for two-electron systems. The complex-rotation transformation does not effect the angular properties of this expansion; Its capability of representing the angular electron correlation effects to the infinite order is preserved. Computations for helium-like atoms employing the Hylleraas-type expansion have been performed for two decades and have given numerous accurate results (6, 98–111).

Another way of taking into account the r_{12}-dependence of the two-electron wave function is to use perimetric coordinates defined as combinations of r_1, r_2, and r_{12} (112). Richter and Wintgen (113) and Wintgen and coworkers (65, 114–116) have used complete sets of Sturmian functions to expand each degree of freedom represented by the perimetric coordinates. The orthonormalization and recursion properties of the Laquerre polynomials, in terms of which the Sturmian functions are defined, guarantee that most of the matrix elements between basis functions vanish and the nonvanishing elements can be calculated algebraically using fast and accurate integer aritmetic (114). This leads to the sparse and banded structure of the matrix representation of the Hamiltonian, which allows using large basis sets and efficient diagonalization of the Hamiltonian matrix.

Methods involving r_{ij}-correlated trial functions have also been developed for three-electron bound systems (117). One of them, the superposition of correlated configuration method of Woźnicki (118), has been recently combined with the complex rotation method and succesfully applied to He^- autoionizing resonances (22, 119–121).

However, application of r_{ij}-correlated basis sets is confined to two- and three-electron atoms. In general, the most often used are configuration expansions constructed in terms of one-particle functions. The Slater-type orbitals are commonly used for atoms (54–61,99–103,122–127). Occasionally Gaussian functions are applied (20).

Since the entire wave function is distorted by the CCR method, the experience coming from bound state computations cannot help in choosing or preparing basis functions. The only thing one can do is to cover densely with the basis set the most important part of the configuration space (121). This can be achieved by appropriate distribution of the basis function parameters, e.g., by systematically increasing powers of the radial coordinates in the Hylleraas expansion, or by choosing the orbital exponents to form regular sequences (121, 128).

In this context, the idea of discrete numerical basis sets, introduced by Salomonson and Öster (129) for the bound-state problem and combined with the complex-rotation method by Lindroth (30), is very interesting. One-particle basis functions are defined on a discrete grid inside a spherical box containing the system under cosideration. The functions are evaluated by diagonalizing the discretized one-particle complex-rotated Hamiltonian. Such basis sets are then used to compute autoionizing state parameters by means of bound-state methods (30, 31, 66).

Unlike the CCR method, the complex stabilization technique of Junker (7) as well as the CESE approach of Nicolaides (11, 12) do not rotate the wave function into the complex plane except for the escape coordinate of the detaching particle. This particle is represented in a basis of square-integrable orbitals, back-rotated by the replacement $r \rightarrow re^{-i\theta}$. Highly developed bound-state techniques can be employed to obtain optimized bound parts of the total resonant wave function, i.e., the localized part of the wave function and the bound states of the ionized system in terms of which the asymptotic part of the total wave function is constructed (Eq.(2)). Hence the orbital basis for the bound parts may consist of numerical orbitals obtained from an MCHF computation (12, 13), and/or analytical orbitals optimized in the configuration interaction (12, 13), or saddle-point (29) calculation. The linear coefficients obtained in such preparatory computations can be kept fixed in order to minimize the size of the complex matrix which has to be diagonalized (13), or they can be set free to relax by the full matrix diagonalization (125). This state-specific approach (13) allows efficient applications to many-electron atoms within basis sets of a reasonable size.

The use of complex coordinates either in the Hamiltonian or in the trial functions leads to complex symmetric matrices, which are often large due to the necessity of employing large basis. Some effective algorithms and computer codes have been recently developed (130–132) for diagonalizing such matrices.

Let us point out that one can take advantage of using large basis sets. They allow for obtaining the positions and widths of many resonances at once. For instance, in the big computation of Bürger, Wintgen, and Rost (114), in which a basis of 24497 functions was used, extremely accurate results for about one hundred of ^1S resonances of He were obtained.

4. Recent computations

Recently, many accurate results have been obtained for few-electron atoms by means of methods involving complex coordinates. They are briefly listed here. Unfortunately, there is no space in present article to discuss them in comparison to other theoretical and experimental resuls.

4.1. Two-electron atoms

4.1.1. H^-

Recent computations of Ho and Bhatia for the resonant spectrum of H^- were mostly devoted to shape resonances. In (110) they computed the position and width of the well known $^1P^o$ shape resonance lying above the $N = 2$ hydrogen threshold, and $^3P^o$ and $^1D^e$ resonances above the $N = 3$ threshold. Further shape resonances lying above this threshold were reported by Bhatia and Ho (109) and Ho (122). The resonances lying above the $N = 4$ and $N = 5$ thresholds were investigated by Ho in (123) and (124), respectively.

Ho also computed series of high-lying Feshbach-type resonances converging to the $N = 3,..,9$ hydrogen threshols (133). Several tens of resonances were reported. Chen (134) applied a basis set of B-spline functions within the saddle-point complex rotation method to compute parameters of twelve $^{1,3}S^e$, $^{1,3}P^o$, and $^1D^e$ low lying Feshbach resonances.

Two-electron ionization ladders of the $^1P^o$, $^1D^e$, and $^3P^e$ autoionizing states, leading to the double ionization threshold were investigated by Chrysos, Komninos and Nicolaides (42), Themelis and Nicolaides (45) and Themelis and Nicolaides (46), respectively. The positions, total widths and partial widths of the resonances were calculated.

Themelis and Nicolaides (135) computed the dc-field-induced tunneling rate for the H^- ground state. Static electric field effects on the $2p^2\ ^3P^e$ bound state and the doubly-excited $^3P^o$ resonances below the $N = 2$ threshold were investigated by Ho (56). The widths of the $2p^2\ ^3P^e$ and $2s2p\ ^3P^o$ states coupled by external ac and dc fields were computed by Mercouris and Nicolaides (84).

The doubly excited $^1S^e$, $^1P^o$, $^1D^e$, $^1F^o$ and $^1G^e$ resonances in the static electric field were studied by Ho (57–59) and Ho and Callaway (60).

Static and dynamic polarizabilities and hyperpolarizabilities were computed by Nicolaides, Mercouris and Piangos (90) for the ground state, and by Nicolaides and Mercouris (91) for the $2p^2\ ^3P^e$ bound state.

Above threshold ionization of H^- in the presence of a dc field was studied by Mercouris and Nicolaides (83) using the MEMPT method. Telnov and Chu (76) used the complex-scaling generalized pseudospectral method to investigate the above threshold detachment of H^- modeled by a one-electron potential. The double photoionization cross section was computed by Nicolaides, Haritos and Mercouris (87).

Investigations of doubly excited states of many-electron atoms in strong static and uniform magnetic fields have been initiated by Bylicki, Themelis and Nicolaides (61). The authors considered the H^- ${}^1S^e$, ${}^1D^e$ and ${}^3P^e$ states lying in the field-free situation below the $N = 2$ threshold. Very recently, the ${}^1P^o$ resonances lying in the vicinity of the $N = 2$ threshold also were investigated by Bylicki and Nicolaides (62). One of these states, the ${}^1P^o$ shape resonance, also was investigated by Ho (136). An interesting phenomenon of field stabilization of some autoionizing states has been predicted.

4.1.2. Helium

Richter and Wintgen (113) and Burgers, Wintgen and Rost (114) used the complex rotation methods with large basis sets of Sturmian functions of perimetric coordinates to compute to high accuracy the series of singlet as well as triplet S^e states up to the $N = 10$ threshold. They report on about one hundred ${}^1S$ resonances and about ninety triplets. Wintgen and Delande (65) and Domke *et al.* (65, 115, 116) also applied very large Sturmian basis sets for extensive CCR computations for series of ${}^1P^o$ resonanses converging to the He^+ thresholds up to $N = 9$. Interferences between series converging to different ionization thresholds were discussed (116).

A particular class of S^e states with both electrons located on the same side of the nucleus, considered by Richter and Wintgen (113), was also investigated by Prunele (137) by the method of o(4,2) operator replacements generalized by the method of complex scaling, which gave rather qualitative results in comparison with the very accurate results of Richter and Wintgen.

Hylleraas-type basis sets of moderate size were used by Ho to perform accurate computation for ${}^1P^o$ (102, 103, 138) and for ${}^3P^o$ (101, 138), and by Ho and Bhatia (98) for singlet as well as triplet P^e resonances.

Tunneling rates and energy shifts induced by static electric fields for He $1s^2\ {}^1S$ ground state were computed by Themelis and Nicolaides (135,139). Ho (54, 55) computed strong electric-field effects on the doubly-excited $2s^2\ {}^1S^e$, $2s2p\ {}^1P^o$, $2p^2\ {}^1D^e$, $2p^2\ {}^3P^e$ and $2s2p\ {}^3P^o$ resonances.

The double photoionization cross section has been computed by Nicolaides, Haritos, and Mercouris (87).

4.1.3. Helium-like ions

Other helium-like systems also were investigated. Ho (99) considered doubly excited states of C^{4+} between the $N = 2$ and $N = 3$ C^{5+} thresholds. He computed both resonance positions and total widths for odd parity states of total angular momentum $L = 0,..,5$ and for even parity states of $L = 1,..,4$. Ho also computed the doubly excited autoionizing states of S XV ion converging on the $N = 2$ to $N = 4$ thresholds of S XVI ion (100). He gave positions and widths of 77 resonances of $L = 0,..,6$.

Doubly excited ${}^{1,3}P^e$ and ${}^{1,3}D^o$ Feshbach resonances in heliumlike systems, Z=2–10, have been investigated by Ho and Bhatia (98, 111). Their CCR computations predicted positions and widths of ${}^{1,3}P^e$ resonances lying below the $N = 3, 4$, and 5 thresholds of hydrogenic systems (98, 111), and ${}^{1,3}D^o$ resonances lying below the $N = 3$ and 4 thresholds (111).

Manning and Sanders (33) used the Z-dependent perturbation theory combined with the complex rotation method to calculate the resonance position and width for the $2s2p$ ${}^{1,3}P^o$ autoionizing states of all members of the helium isoelectronic sequence.

4.2. Three-electron atoms

4.2.1. He^-

The lowest resonance of He^-, $1s2s^2$ ${}^2S^e$ state, is one of the most investigated by using different methods. The CCR method was for the first time successfully applied to this state by Bylicki (22). Using a 184-term r_{ij} correlated expansion gave the position and width of this resonance in very good agreement with the experimental data of Cvejanović, Comer and Read (140). However, it was in disagreement with other theoretical results.

Two-electron ionization ladders of ${}^2S^e$ and ${}^4P^e$ resonances converging to the $1s$ He^+ threshold were investigated by the state specific CESE approach by Chrysos, Aspromallis, Komninos and Nicolaides (43) and by Themelis and Nicolaides (46), respectively. The authors considered partial widths of these resonances.

The ${}^4P^e$ spectrum of He^- has also been treated by Bylicki (121) using an r_{ij} correlated basis set within the CCR method. Apart from the resonances reported by Themelis and Nicolaides (46), sixteen other doubly excited *Feshbach* as well as *shape* resonances have been discovered in the energy region up to the $1s7p$ ${}^3P^o$ helium threshold.

Triply-excited states of He^- ion consitute a challenging subject for investigation demanding taking into account electron correlation effects and an infinite number of open channels of autoionization. Application of a basis set of r_{ij}-correlated functions within the CCR method (119, 120) gave accurate results for the positions and widths of the $2s^22p$ ${}^2P^o$, $2s2p^2$ ${}^2D^e$, ${}^4P^e$, ${}^2P^e$, and $2p^3\ ^2D^o$ intrashell resonances. The most interesting result of that work is the statement that the $2s2p^2\ ^2D^e$ resonance level definitely lies below the $2s2p\ ^3P^o$ autoionizing state of He. Thus it is real and of the Feshbach type. The $2s2p^2\ ^4P^e$ resonance, one of those considered by Bylicki and Nicolaides (119,120), was also investigated by Chung (141). He performed a single open channel complex coordinate computation which resulted in a slightly lower value for the width of the resonance, indicating that the $1s2p\ ^3P^o$ open channel, assumed by Chung as the only one, is the most important one but the infinite number of other open channels, including that one associated with the two-electron ionisation threshold, are not completely negligible. They were taken into account in (119,120).

Chrysos, Aspromallis, Komninos and Nicolaides (43) considered the partial and total widths, with interchannel coupling for $1s(nl)^2\ ^2S^e$ resonances of n=3,4. Partial widths of $1s3s3p\ ^4P^o$ and $1s3p^2\ ^4P^e$ states for Z=2–5 and 10, were investigated by Davis and Chung (142) in the single-channel approximation, without the interchannel coupling, and by Themelis and Nicolaides (44) with interchannel coupling. The effect of interchannel coupling on the partial widths in the case of the $^4P^o$ state has been found considerable. On the contrary, interchannel coupling has no significant effect on the total widths.

4.2.2. Li

Energies and widths of fifteen $^2P^o$ resonances lying between the $Li^+\ 2^1P$ and 2^3S thresholds have been computed by Wu and Chung (143) using the saddle-point complex-rotation method.

The triply-excited states of lithium atom were studied by Chung and Gou (125,126). They computed the energies and the total as well as partial widths of a dozen or so of triply excited states.

Themelis and Nicolaides have calculated the dc-field-induced tunneling rates and energy shifts of the ground $1s^22s\ ^2S^e$ state (135, 139) and the excited $1s^22p\ ^2P^o$, $1s^23s\ ^2S^e$, $3p\ ^2P^o$, $3d\ ^2D^e$ bound states (96,139). They have also computed scalar and tensor polarizabilities and hyperpolarizabilities of these states (93,94,96).

Halley, Delande, and Taylor (34) used the combined R-matrix complex-coordinate technique to compute the diamagnetic Rydberg spectrum of resonances.

4.2.3. H^{2-}

The doubly-negative hydrogen ion is an extremely interesting and challenging system. Existence of a bound state for such a system was excluded twenty years ago by Beck and Nicolaides (144). However it could exist in a triply excited autoionizing resonance state. Recently Sommerfeld, Riss, Meyer, and

Cederbaum *et al* (20) have performed a CCR computation in a basis of Gaussian functions. They have found that the $2p^3\ {}^4S^o$ resonance exists at the energy of -0.072 *au*, with a half width of 0.032 *au*. This result is waiting to be confirmed by an independent computation (128).

4.2.4. Lithium-like ions

Gou and Chung (127) used the saddle-point complex-rotation method to investigate triply excited resonances of Be^+ and C^{3+}. They computed the energies and the total widths of seven resonances. They also considered partial widths in one open channel approximation.

4.3. Four-electron atoms

4.3.1. Beryllium

The $1s^22p^2\ {}^1S$ resonance of beryllium has been studied by Lindroth and Martensson-Pendrill (31), who used a combined coupled-cluster complex-rotation method. Scalar and tensor polarizabilities and hyperpolarizabilities of the $1s^22s2p\ {}^3P^o$ and ${}^1P^o$, $1s^22p^2\ {}^3P^e$ and $1s^22p^2\ {}^1D^e$ excited valence states of Be were computed by Themelis and Nicolaides (97).

4.3.2. Li^-

The Li^- ${}^1P^o$ resonances were studied in photodetachment cross section computation of Lindroth (66). The ground state of Li^- in electric fields was considered (92,135). Themelis and Nicolaides (135) computed tunneling rates and energy shifts induced by dc fields. The dynamic polarizability and hyperpolarizability of the Li^- ground state were computed by Nicolaides, Mercouris and Aspromallis (92)

4.4. Other atoms and ions

Rydberg states of Ba and Sr in an external magnetic field have been considered by Halley, Delande, and Taylor (35), by means of the R-matrix complex rotation method. Seipp and Taylor (36) used the same method for the Stark and Stark-Zeeman problem of Rydberg states of Na. Themelis and Nicolaides (96) investigated the $1s^22s^22p^63s\ {}^2S$, $3p\ {}^2P^o$, $4s\ {}^2S$, and $3d\ {}^2D$ bound states of Na. They used the CESE method to compute tunneling rates and scalar and tensor polarizabilities and hyperpolarizabilities. Medikeri, Nair, and Mishra (145,146) considered ${}^2P^o$ *shape* resonances in Be^-, Mg^- and Ca^- in two-particle-one-hole-Tamm-Dancoff approximation. Photodetachment rate for Cl^- described by one-electron model was computed by Yao and Chu (73) using the complex-scaling Fourier-grid technique within the Floquet formalism. Harmonic generation under laser field in a Xe atom, represented by a model potential, was studied by the complex-scaled adiabatic-switch method (78).

4.5. Exotic systems

The CCR method has been applied to exotic atoms. Among those, the resonances of negative positronium ion have been mostly investigated by Ho (147) and Ho and Bhatia (104–107). Positron-atom scattering resonances have been considered by Ho (108, 148). Hu and Bhatia (149) have studied resonances in muonic systems.

5. Summary

For a quarter of century the methods involving complex-coordinates have been continouosly applied to nonstationary processes of atomic physics. They seem to be the ones most often used for such phenomena. Due to the implementation of new efficient algorithms and due to progress in computer performance, they bring more and more accurate and extensive results. They are applied in new contexts, like multiphoton double electron ionization (86, 87), harmonic generation (78, 79, 82), triply-excited autoionizing states (120, 126, 20), doubly excited-resonances in strong magnetic fields (61, 62), searching for "quantum chaos" (64, 52).

So far most of the computations have been performed for few-electron atoms or for medium atoms modeled by one-electron potentials. However, there are methods, like the state specific CESE and MEMPT approach (13), which can be applied to larger systems. Also combination of complex-rotation technique with the many body perturbation theory (30) or coupled cluster method (31), which are addressed to large systems, seems to be promising in this context.

6. Acknowledgements

Support received from the Polish State Committee for Scientific Research (grant PB962/P03/95/08) is gratefully acknowledged.

References

(1) J. Aquilar and J. M. Combes, Commun. Math. Phys. **22**, 269-79 (1971).
(2) E. Balslev and J. M. Combes, Commun. Math. Phys. **22**, 280-94 (1971).
(3) B. Simon, Ann. Math. **97**, 247-74 (1973).

(4) see the complex-rotation devoted issue of Int. J. Quantum Chem. **14**, No. 4 (1978).

(5) W. P. Reinhardt, Ann. Rev. Phys. Chem. **33**, 223-55 (1982).

(6) Y. K. Ho, Phys. Rep. **99**, 1-68 (1983).

(7) B. R. Junker, Adv. At. Mol. Phys. **18** 207-63 (1982); in *Autoionization: Recent Developments and Applications* edited by A. Temkin (Plenum, New York, 1985) p. 103-33.

(8) P. O. Löwdin, Adv. Quant. Chem. **19**, 77 (1988).

(9) Lecture Notes in Physics *Resonances — The Unifying Route Towards the Formulation of Dynamical Processes*, edited by E. Brändas and N. Elander (Springer, Berlin, 1989) Vol. **325**, many articles of this volume summarize formal developments concerning complex scaling and applications to resonances in various domains, including atomic physics.

(10) N. Moiseyev, Israel J. Chem. **31**, 311-22 (1991).

(11) C. A. Nicolaides, in *Applied Many-Body Methods in Spectroscopy and Electronic Structure*, edited by D. Mukherjee (Plenum, New York, 1992) p. 233.

(12) C. A. Nicolaides, Th. Mercouris, Y. Komninos, and I. D. Petsalakis, Int. J. Quantum Chem. **51**, 529-37 (1994).

(13) C. A. Nicolaides, Int. J. Quantum Chem. **60**, 119-129 (1996).

(14) A. M. Dykhne and A. V. Chaplik, Sov. Phys.-JETP **13**, 1002 (1961).

(15) C. A. Nicolaides, Th. Mercouris, and I. D. Petsalakis, Chem. Phys. Lett. **212**, 685-90 (1993).

(16) U. Peskin and N. Moiseyev, J. Chem. Phys. **97**, 6443-50 (1992).

(17) N. Moiseyev, in Lecture Notes in Physics, edited by E. Brändas and N. Elander (Springer, Berlin, 1989), Vol. **325**, pp. 459-74.

(18) M. Bylicki, W. Jaskólski, and R. Oszwałdowski, J. Phys.: Condens. Matter **8**, 6393-403 (1996); W. Jaskólski and M. Bylicki, Vacuum **48** 235-9 (1997).

(19) E. Brändas and P. Froelich, Phys. Rev. A **16**, 2207-10 (1977).

(20) T. Sommerfeld, U. V. Riss, H.-D. Meyer, and L. S. Cederbaum, Phys. Rev. Lett. **77**, 470-3 (1996); Phys. Rev. A **55**, 1903-10 (1997).

(21) N. Moiseyev, Chem. Phys. Lett. **99**, 364-7 (1983).

(22) M. Bylicki, J. Phys. B: At. Mol. Opt. Phys. **24** 413-21 (1991).

(23) T. N. Rescigno, C. W. McCurdy, and A. E. Orel, Phys. Rev. A **17**, 1931-8 (1978).

(24) B. R. Junker and C. L. Huang, Phys. Rev. A **18**, 313-23 (1978).

(25) C. A. Nicolaides and D. R. Beck, Int. J. Quantum Chem. **14**, 457-513 (1978).

(26) Y. Komninos and C.A. Nicolaides, Chem. Phys. Lett. **78**, 347-50 (1981).

(27) C. A. Nicolaides, Y. Komninos, and Th. Mercouris, Int. J. Quantum Chem. Symp. **15**, 355-67 (1981).

(28) Th. Mercouris and C. A. Nicolaides, Z. Phys. D **5**, 1-7 (1987).
(29) K. T. Chung and B. F. Davis, Phys. Rev. A **26**, 3278-82 (1982).
(30) E. Lindroth, Phys. Rev. A **49** 4473-80 (1994).
(31) E. Lindroth, and A.-M. Martensson-Pendrill, Phys. Rev. A **53**, 3151-6 (1996).
(32) L. W. Manning and F. C. Sanders, Condensed Matter Theories. **7**, Proceedings of the Fifteenth International Workshop, edited by A. N. Proto and J. L. Aliaga (Plenum, New York, 1992) pp. 179-88.
(33) L. W. Manning and F. C. Sanders, Phys. Rev. A **44**, 7206-13 (1991).
(34) M. H. Halley, D. Delande, and K. T. Taylor, J. Phys. B: At. Mol. Opt. Phys. **25**, L525-32 (1992).
(35) M. H. Halley, D. Delande, and K. T. Taylor, J. Phys. B: At. Mol. Opt. Phys. **26**, 1775-90 (1993).
(36) I. Seipp and K. T. Taylor, J. Phys. B: At. Mol. Opt. Phys. **27**, 2785-99 (1994).
(37) C. A. Nicolaides and D. R. Beck, Phys. Lett. **65**A, 11-12 (1978).
(38) B. Simon, Phys. Lett. **71**A, 211-4 (1979).
(39) T. Noro and H.S. Taylor, J. Phys. B: At.Mol. Phys. **13**, L377-81 (1980).
(40) Z. Bačić and J. Simons, Int. J. Quantum Chem. **21**, 727-39 (1982).
(41) C. A. Nicolaides and Th. Mercouris, Phys. Rev. A **32**, 3247 (1985).
(42) M. Chrysos, Y. Komninos, and C. A. Nicolaides, J. Phys. B: At. Mol. Opt. Phys. **25**, 1977-84 (1992).
(43) M. Chrysos, G. Aspromallis, Y. Komninos, and C. A. Nicolaides, Phys. Rev. A **46**, 5789-94 (1992).
(44) S.I. Themelis and C.A. Nicolaides, Phys. Rev. A **49**, 1618-22 (1994).
(45) S. I. Themelis and C. A. Nicolaides, Phys. Rev. A **49**, 596-8 (1994).
(46) S. I. Themelis and C. A. Nicolaides, J. Phys. B: At. Mol. Opt. Phys. **28**, L379-85 (1995).
(47) C. Cerjan, R. Hedges, C. Holt, W. P. Reinhardt, K. Scheibner, and J. J. Wendoloski, Int. J. Quantum Chem. **14**, 393-418 (1978).
(48) I. W. Herbst and B. Simon, Commun. Math. Phys. **80**, 181-216 (1981); and references therein.
(49) C. A. Nicolaides and S. I. Themelis, Phys. Rev. A **45**, 349-57 (1992).
(50) S.-I Chu, Chem. Phys. Lett. **58**, 462-6 (1978).
(51) S. K. Bhattacharya and S.-I Chu, J. Phys. B: At. Mol. Phys. **16**, L471 (1983).
(52) J. Main and G. Wunner, J. Phys. B: At. Mol. Opt. Phys. **27**, 2835-48 (1994).
(53) J. J. Wendoloski and W. P. Reinhardt, Phys. Rev. A **17**, 195-220 (1978).
(54) Y. K. Ho, Chin. J. Phys. **34**, 1136-44 (1996).
(55) Y. K. Ho, Z. Phys. D **38**, 191-6 (1996).
(56) Y. K. Ho, J. Phys. B: At. Mol. Opt. Phys. **28**, 4025-36 (1995).

(57) Y. K. Ho, Phys. Rev. A **52**, 2062-9 (1995).
(58) Y. K. Ho, Phys. Rev. A **52**, 375-81 (1995).
(59) Y. K. Ho, Chin. J. Phys. **33**, 229-45 (1995).
(60) Y. K. Ho and J. Callaway, Phys. Rev. A **50**, 4941-4 (1994).
(61) M. Bylicki, S. I. Themelis, and C. A. Nicolaides, J. Phys. B: At. Mol. Opt. Phys. **27**, 2741-51 (1994).
(62) M. Bylicki and C. A. Nicolaides, unpublished.
(63) T. N. Rescigno and V. McKoy, Phys. Rev. A **12**, 522-5 (1975).
(64) J. Main and G. Wunner, Phys. Rev. Lett. **69**, 586-9 (1992).
(65) D. Wintgen and D. Delande, J. Phys. B **26**, L399-405 (1993).
(66) E. Lindroth, Phys. Rev. A **52** 2737-49 (1995).
(67) S. Han and W. P. Reinhardt, J. Phys. B: At. Mol. Opt. Phys. **28**, 3347-67 (1995).
(68) S. Han and W. P. Reinhardt, J. Phys. B: At. Mol. Opt. Phys. **28**, 3369-90 (1995).
(69) S.-I Chu and W. P. Reinhardt, Phys. Rev. Lett. **39**, 1195-8 (1977).
(70) S.-I Chu, Adv. Chem. Phys. **73**, 739 (1989).
(71) Th. Mercouris and C. A. Nicolaides, J. Phys. B: At. Mol. Opt. Phys. **21**, L285-90 (1988).
(72) Th. Mercouris and C. A. Nicolaides, J. Phys. B: At. Mol. Opt. Phys. **23**, 2037-53 (1990).
(73) G. Yao and S.-I Chu Phys. Rev. A **45** 6735-43 (1992).
(74) G. Yao and S.-I Chu, Chem. Phys. Lett. **204**, 381-8 (1993).
(75) J. Wang, S.-I Chu and C. Laughlin, Phys. Rev. A**50**, 3208-15 (1994).
(76) D. A. Telnov and S.-I Chu Phys. Rev. A **50**, 4099-108 (1994).
(77) N. Ben-Tal, N. Moiseyev, C. Leforestier, and R. Kosloff, J. Chem. Phys. **94**, 7311-8 (1991).
(78) N. Ben-Tal, N. Moiseyev, and R. Kosloff, Phys. Rev. A **48**, 2437-42 (1993).
(79) N. Ben-Tal, N. Moiseyev, and A. Beswick, J. Phys. B: At. Mol. Opt. Phys. **26**, 3017-24 (1993).
(80) N. Ben-Tal, N. Moiseyev, and R. Kosloff, J. Chem. Phys. **98**, 9610-17 (1993).
(81) U. Peskin and N. Moiseyev, J. Chem. Phys. **99**, 4590-6 (1993).
(82) N. Ben-Tal, N. Moiseyev, R. Kosloff, and C. Cerjan, J. Phys. B: At. Mol. Opt. Phys. **26**, 1445-61 (1993).
(83) Th. Mercouris and C. A. Nicolaides, J. Phys. B: At. Mol. Opt. Phys. **24**, L57-61 (1991).
(84) Th. Mercouris and C. A. Nicolaides, J. Phys. B: At. Mol. Opt. Phys. **24**, L557-63 (1991).
(85) T. Mercouris and C. A. Nicolaides, Phys. Rev. A **45**, 2116-17 (1992).
(86) Th. Mercouris and C. A. Nicolaides, Phys. Rev. A **48**, 628-33 (1993).

(87) C. A. Nicolaides, C. Haritos, and Th. Mercouris, Phys. Rev. A **55**, 2830-41 (1997).

(88) N. Moiseyev, J. Chem. Phys. **101**, 9716-8 (1994).

(89) N. Moiseyev, Int. J. Quantum Chem. **63**, 279-85 (1997).

(90) C. A. Nicolaides, Th. Mercouris, and N. Piangos, J. Phys. B **23**, L669-75 (1990).

(91) C. A. Nicolaides and Th. Mercouris, Phys. Rev. A **44**, 7827-9 (1991).

(92) C. A. Nicolaides, Th. Mercouris, and G. Aspromallis, J. Opt. Sc. Am. B **7**, 494 (1990).

(93) S. I. Themelis and C. A. Nicolaides, Phys. Rev. A **46**, R21-4 (1992).

(94) C. A. Nicolaides and S. I. Themelis, J. Phys. B: At. Mol. Opt. Phys. **26**, 2217-24 (1993).

(95) C. A. Nicolaides and S. I. Themelis, J. Phys. B: At. Mol. Opt. Phys. **26**, L387-91 (1993).

(96) S. I. Themelis and C. A. Nicolaides, Phys. Rev. A **51**, 2801-7 (1995).

(97) S. I. Themelis and C. A. Nicolaides, Phys. Rev. A **52**, 2439-41 (1995).

(98) Y. K. Ho and A. K. Bhatia, Phys. Rev. A **47**, 2628-33 (1993).

(99) Y. K. Ho, Physica Scripta **50**, 654-60 (1994).

(100) Y. K. Ho, Physica Scripta **44**, 559-61 (1991).

(101) Y. K. Ho, Phys. Rev. A **48**, 3598-605 (1993).

(102) Y. K. Ho, Z. Phys. D **21**, 191-6 (1991).

(103) Y. K. Ho, Phys. Rev. A **44**, 4154-61 (1991).

(104) Y. K. Ho and A. K. Bhatia, Phys. Rev. A **47**, 1497-9 (1993).

(105) A. K. Bhatia and Y. K. Ho, Phys. Rev. A **48**, 264-7 (1993).

(106) Y. K. Ho and A. K. Bhatia, Phys. Rev. A **50**, 2155-60 (1994).

(107) Y. K. Ho and A. K. Bhatia, Phys. Rev. A **45**, 6268-71 (1992).

(108) Y. K. Ho, Phys. Rev. A **53**, 3165-8 (1996).

(109) A. K. Bhatia and Y. K. Ho, Phys. Rev. A **50**, 4886-90 (1994).

(110) Y. K. Ho and A. K. Bhatia, Phys. Rev. A **48**, 3720-4 (1993).

(111) Y. K. Ho and A. K. Bhatia, J. Phys. B **30**, 3597-3609 (1997).

(112) A. S. Coolidge and H. M. James, Phys. Rev. **51**, 855-9 (1937).

(113) K. Richter and D. Wintgen, J.Phys. B: At. Mol. Opt. Phys. **24**, L565-571 (1991).

(114) A. Bürgers, D. Wintgen, and J.-M. Rost, J. Phys. B: At. Mol. Opt. Phys. **28**,1 3163-83 (1995).

(115) M. Domke, K. Schulz, G. Remmers, A. Gutierrez, G. Kaindl, amd D. Wintgen, Phys. Rev. A **51**, R4309-12 (1995).

(116) M. Domke, K. Schulz, G. Remmers, G. Kaindl, and D. Wintgen, Phys. Rev. A **53**, 1424-38 (1996).

(117) for references see M. Bylicki and G. Pestka, J. Phys. B: At. Mol. Opt. Phys. **29** L353-7 (1996).

(118) W. Woźnicki, in *Theory of Electronic Shell in Atoms and Molecules* edited by A. Jucys (Mintis, Vilnius, 1971) p. 103-6.
(119) M. Bylicki and C. A. Nicolaides, Phys. Rev. A **48**, 3589-94 (1993).
(120) M. Bylicki and C. A. Nicolaides, Phys. Rev. A **51**, 204-10 (1995).
(121) M. Bylicki, J. Phys. B: At. Mol. Opt. Phys. **30**, 189-201 (1997).
(122) Y. K. Ho, Phys. Lett. A **189**, 374-8 (1994).
(123) Y. K. Ho, Phys. Rev. A **49**, 3659-63 (1994).
(124) Y. K. Ho, Phys. Rev. A **50**, 4877-85 (1994).
(125) K. T. Chung and B.-C. Gou Phys. Rev. A **52**, 3669-76 (1995).
(126) K. T. Chung and B.-C. Gou Phys. Rev. A **53**, 2189-93 (1996).
(127) B.-C. Gou and K. T. Chung J. Phys. B: At. Mol. Opt. Phys. **29**, 6103-11 (1996).
(128) M. Bylicki and C. A. Nicolaides, unpublished.
(129) S. Salomonson and P. Öster, Phys. Rev. **40**, 5559-67 (1989).
(130) D. Delande, A. Bommier and J. C. Gay, Phys. Rev. Lett. **66**, 141-4 (1991).
(131) S. Dallwig, N. Fahrer, and C. Schlier, Chem. Phys. Lett. **191**, 69-76 (1992).
(132) I. Bar-On and V. Ryaboy, in *Proceedings of the Seventh SIAM Conference on Parallel Processing for Scientific Computing*, edited by D. H. Bailey, P. E. Bjorstad, J. R. Gilbert, M. V. Mascagni, R. S. Schreiber, H. D. Simon, V. J. Torczon, and L. T. Watson (SIAM, Philadelphia, 1995) p. 571-2.
(133) Y. K. Ho, Phys. Rev. A **45**, 148-53 (1992).
(134) M.-K. Chen, J. Phys. B: At. Mol. Opt. Phys. **30**, 1669-76 (1997).
(135) S. I. Themelis and C. A. Nicolaides, Phys. Rev. A **49**, 3089-91 (1994).
(136) Y. K. Ho, Phys. Lett. A **230**, 190-6 (1997).
(137) de Prunele, E. Phys. Rev. A **46**, 2344-50 (1992).
(138) Y. K. Ho, Chin. J. Phys. **34**, 9-23 (1996).
(139) C. A. Nicolaides and S. I. Themelis, Phys. Rev. A **47**, 3122-7 (1993).
(140) S. Cvejanović, J. Comer, and F. H. Read, J. Phys B: At. Mol. Phys. **7**, 468-77 (1974).
(141) K. T. Chung, Phys. Rev. A **51**, 844-6 (1995).
(142) B. F. Davis and K. T. Chung, Phys. Rev. A **41**, 5844-55 (1990).
(143) L. Wu and K. T. Chung, J. Phys. B: At. Mol. Opt. Phys. **30**, 1173-8 (1997).
(144) D. R. Beck and C. A. Nicolaides, Chem. Phys. Lett. **59**, 525-8 (1978).
(145) M. N. Medikeri, J. Nair, and M. K. Mishra, J. Chem. Phys. **100**, 2044-51 (1994).
(146) M. N. Medikeri, J. Nair, and M. K. Mishra, J. Chem. Phys. **99**, 1869-74 (1993).
(147) Y. K. Ho, Hyperfine Interactions **89**, 401-6 (1994).
(148) Y. K. Ho, Hyperfine Interactions **73**, 109-30 (1992).
(149) C.-Y. Hu and A. K. Bhatia, Muon Catalyzed Fusion **6**, 439-44 (1991).

Recent Advances in the Description of Solvent Effects with the Polarizable Continuum Model

Claudio Amovilli [a], Vincenzo Barone[b], Roberto Cammi[c],
Eric Cancès[d], Maurizio Cossi[b], Benedetta Mennucci[a],
Christian S. Pomelli[e] and Jacopo Tomasi[a]*

[a] Dipartimento di Chimica e Chimica Industriale
Universitá di Pisa, Italy
[b] Dipartimento di Chimica, Universitá Federico II, Napoli, Italy
[c] Dipartimento di Chimica Generale ed Inorganica
Universitá di Parma, Italy
[d] CERMICS, Ecole Nationale des Ponts et Caussées, Paris, France
[e] Scuola Normale Superiore, Pisa, Italy

---

*Corresponding author; email: tomasi@dcci.unipi.it

ADVANCES IN QUANTUM CHEMISTRY, VOLUME 32
Copyright ©1999 by Academic Press. All rights of reproduction in any form reserved.
0065-3276/99 $30.00

Contents

1 Introduction. 3

2 Basic classification of continuous effective Hamiltonian methods. 3

3 Basic aspects of the PCM method. 4

4 The formulation of PCM: recent advances. 7
- 4.1 Dispersion and repulsion in the HF formalism of PCM. 7
- 4.2 Different formulations of the electrostatic problem. 10
- 4.3 COSMO-PCM. 12
- 4.4 IEF-PCM. 13
- 4.5 PCM-QINTn. 16

5 Cavity errors and their corrections. 18

6 Analytical geometry derivatives. 20

7 Molecular response functions. 23

8 Further extensions and variants of PCM for the definition of the cavity 27
- 8.1 The united atom topological model (UATM). 27
- 8.2 Variable tessellation of the cavity surface 28
- 8.3 Cavity surface tessellation not based on atomic spheres 29

9 Final remarks 31

1 Introduction.

With the acronym PCM (polarizable continuum model) we indicate a set of methods addressed to the study of solvation problems at the Quantum Mechanical level with the use of continuum solvent distributions.

We shall not try to expose here the evolution of continuous methods since the first proposals [1] or the first formulation at a QM level, semiempirical [2, 3, 4], or *ab initio* [5, 6, 7] . There are several reviews giving detailed expositions [8, 9, 10, 11].

The attention will be exclusively focussed on recent advances, partly still unpublished, in the PCM methods; the exposition of the basic strategies and of the elaborations of the method given in the past for numerous specific problems will be limited to the strict necessary. Moreover, our account will be limited just to a part of what has been recently done, being the space limited and the number of items large.

2 Basic classification of continuous effective Hamiltonian methods.

In this section we shall be extremely concise, in order to reserve more space to recent advances. PCM belongs to the family of methods in which the attention is focussed on a limited portion of matter, the 'solute' (one or more molecules) while the remaining, and larger, portion of the solution, called here the 'solvent', is treated at a lower level of accuracy.

PCM is a quantum mechanical (QM) method in which use is made of an effective Hamiltonian for the solute M, and the corresponding Schrödinger equation is generally (but not compulsory) treated at the ab initio level.

PCM makes use of continuous solvent distributions to describe the solute-solvent interaction potential. Later we shall see that PCM manages to treat not only the well known model based on a uniform isotropic dielectric description of the solvent, whose interactions are limited to the electrostatic terms, but also more complex models including interactions of different physical origin and other solvent distribution functions.

PCM formulates the basic electrostatic problem with the aid of an apparent surface charge (ASC) spread on the surface of a cavity in the solvent where M is accommodated. There are several methods to treat the same electrostatic problem, we quote here a classification drawn from an exhaustive review on this subject to which reference is made for more details [8].

1. apparent surface charge methods (ASC);

2. multipole expansion methods (MPE);
3. generalized Born approximation methods (GB);
4. image charge methods (IC);
5. finite difference methods (FD);
6. finite elements methods (FE).

The methods today more in use in computational chemistry belong to the ASC, MPE, GB and FD families. For every type of method there are now QM versions, many thus far limited to infinite isotropic distributions. Several of those methods may introduce, via the effective Hamiltonian or with less formal procedures, solute-solvent interaction effects of non electrostatic origin.

We quote here as examples the SCRF set of methods due to Rivail and coworkers [7] (for a review also see ref. [9]) which belong to the MPE family, and the AMSOL methods due to Cramer and Truhlar [12] (for a review also see [10]) belonging to the GB family.

These are the QM methods that with PCM cover the largest part of the chemical applications thus far published.

Some FD and FE methods have had, and still have, a great success with formulations given at the classical level [13]. There are now QM versions still at the first stages of their development, while some FE-PCM models we have developed in the past years are now transformed into ASC versions, as it will be shown later.

We have introduced this classification among continuous methods at the beginning of our exposition as the technical details about the specific model exploited to describe the electrostatic interactions are the most used features in characterizing and discussing continuum solvation methods. To be more effective in presenting extensions of the basic procedure it is convenient to go a step back.

3 Basic aspects of the PCM method.

The starting point in the implementation of QM versions of the continuum solvation model is the following Schrödinger equation:

$$\left[\hat{H}^0_M + \hat{V}_{int}(\rho_M)\right] \Psi = E\Psi \tag{1}$$

Here $\hat{H}^0$ is the Hamiltonian of the solute M *in vacuo* (M can be either a single molecule or two, or more, interacting molecules eventually supplemented by some solvent molecules, if one considers it convenient). $V_{int}(\rho_M)$ is the solute-solvent interaction functionally depending on the solute total (i.e. nuclear and electronic) charge distribution. More details about V_{int} will be given later; here it is important to stress that it is always described in terms of a continuous distribution of the 'solvent' S (i.e. of the very large number of solvent molecules excluding the few eventually included in M) characterized by suitable response functions.

The basic energetic quantity is a free energy, G^S, which is conveniently written as a sum of different contributions, each due to a specific solute-solvent interaction:

$$G^S = G_{el} + G_{ster} + G_{dis} + G_{Mm} \tag{2}$$

This partition parallels that usually exploited in the analysis of the energy of clusters, $M \cdot S_n$, even if changes due to the different complexity of the problem and to the use of averaged distributions of solvent molecules are required.

To make our analysis of G^S more clear we report here a compact formulation of the energy of a cluster at fixed nuclear geometry

$$E(M \cdot S_n) = \sum_K^{n+1} E_K^0 + \Delta E_{ES} + \Delta E_{POL} + \Delta E_{REP} + \Delta E_{DIS} \tag{3}$$

Here E_K^0 is the energy of each of the $n+1$ molecules of the cluster when not interacting with the others. ΔE_{ES} is a linear term collecting all the pair coulombic interactions among the partners, ΔE_{POL} is the non linear electrostatic contribution due to the mutual polarizations of the partners, and ΔE_{REP} and ΔE_{DIS} are the contributions due to Pauli repulsion and dispersion interactions among partners (both not limited to pair contributions).

The differences between eq.(3) and eq.(2) are first due to the fact that in (2) an effective Hamiltonian of M is exploited, and thus the specific terms due to S molecules disappear or are replaced by response functions of an averaged distribution. This change leads to the use of a free energy G instead of an internal energy E. Moreover, into G_{el} we collect what remains of $\sum_K^{n+1} E_K^0$, i.e. $E^0(M)$ with ΔE_{ES} and ΔE_{POL}, and ΔE_{REP} is replaced by G_{ster}, which is divided into two parts, to be treated separately:

$$G_{ster} = G_{rep} + G_{cav} \tag{4}$$

Here G_{cav} is the reversible work needed to modify the distribution of the pure solvent in order to create a cavity within it such as to accommodate M in the best way, while G_{rep} describes the Pauli repulsion contributions between M and the solvent molecules within the framework of a continuous distribution which takes into account the existence of the cavity.

G_{dis} parallels ΔE_{DIS}: once again, in the former case the solvent distribution takes into account the existence of a cavity.

Expression (2) contains a term, G_{Mm}, not present in (3). The reason is that in dealing with free energies we also have to consider entropic contributions. A formal derivation will not be reported here: in short, it consists in a formal definition of the partition function of the whole solution, in its factorization into M and S components, in the introduction of the continuous distribution of the solvent, and then in the use of standard formulations of statistical mechanics to get free energy (Gibbs or Helmholtz) contributions for the M portion. The formal treatment can be found e.g. in the Ben-Naim's books [14, 15], and the application to our model in ref.[8].

The subscript Mm emphasizes the fact that the main contribution to G_{Mm} comes out from thermal motion of M. The calculation of this contribution is further simplified when one limits the analysis to the solvation energy ΔG_{sol}. By defining the latter as

$$\Delta G_{sol} = G^S - G^0 \tag{5}$$

where G^0 is the free energy of the system with an unperturbed pure solvent and M in the gas phase, one arrives at

$$\Delta G_{sol} = \Delta G_{el} + G_{cav} + G_{rep} + G_{dis} + \Delta G_{Mm} \tag{6}$$

where the appropriate reference states for M in both the systems are separately defined (see again Ben-Naim). The ΔG_{Mm} term is thus reduced to

$$\begin{aligned} \Delta G_{Mm} = &\ RT \ln \left(\frac{q_{rot,g} q_{vib,g}}{q_{rot,s} q_{vib,s}} \right) - RT \ln \left(\frac{n_{M,g} \Lambda_{M,g}}{n_{M,s} \Lambda_{M,s}} \right) \\ &= \Delta(ZPE) + \Delta G_{vib} + \Delta G_{rot} \end{aligned} \tag{7}$$

a quantity composed by a difference in the zero-point vibrational energies, an entropic contribution due to molecular vibrations (to be computed with standard QM methods) and a difference in the rotational contribution to the entropy, which in continuum models requires the introduction of a parameter describing the friction of the rotation of M as a rigid body (an easy task, when the solute is not too floppy, allowing the separation of the partition function of M we have used in eq.(7)).

The partition of G^S (eqs. 2 and 4) can be accompanied by a parallel partition of V_{int}, eventually supplemented by a separation between terms which are dependent and independent on the charge distribution of M

$$V_{int}(\rho_M) = V_{el} + V_{ster} + V_{dis} = V'_{int}(\rho_M) + V''_{int} \tag{8}$$

Since in $V'_{int}(\rho_M)$ there is a functional dependence on ρ_M, the variational solution of eq.(1) requires the minimization of the free energy functional [16]:

$$\mathrm{G} = \frac{\langle\Phi|\, \hat{H}^0 + \frac{1}{2}\hat{V}'_{int}(\rho_M) + V''_{int}\, |\Phi\rangle}{\langle\Phi|\Phi\rangle} \tag{9}$$

where Φ is a trial wave function.

The factor 1/2 in the kernel of eq.(9) is related to the linearity in the dependence of $V'_{int}(\rho_M)$ on ρ_M: we have not used thus far models requiring to go beyond linearity which would have meant to use generalized factors equal to $1/(1+q)$ with $q > 1$.

The recent advances we have mentioned in the title and in the introduction just start from the basic formulation resumed in eq.(9). We dispense ourselves with the exposition of further details on the original version of PCM method and on the numerous extensions given in the past to treat a number of problems going beyond the basic model. They can be found in the already quoted review [8], supplemented by another review [17] just printed, and by a score of other more recent papers published after the preparation of these two reviews.

We shall continue our exposition inserting at the appropriate places the real subject of this report, namely the recent advances.

4 The formulation of PCM: recent advances.

The usual starting point in the formulation of a QM molecular problem is given by the HF theory applied within the approximation of clamped nuclei. Using an expansion on a discrete basis set and adopting a matrix formulation, the minimization of G (eq.7) can be reduced to the solution of the following Fock equation

$$\mathbf{F'C} = \mathbf{SC}\boldsymbol{\varepsilon} \tag{10}$$

where $\mathbf{C}$, $\mathbf{S}$, and $\boldsymbol{\varepsilon}$ represent the standard matrices of the molecular orbital coefficients, of the overlap and of the one-electron orbital energies, exactly as *in vacuo*, while the Fock matrix $\mathbf{F}'$ is modified with respect to calculation *in vacuo*. The recent advances in PCM we are exposing here just start from the definition of this matrix.

4.1 Dispersion and repulsion in the HF formalism of PCM.

In the detailed expression of the Fock matrix $\mathbf{F}'$ given below, we have introduced three terms not present in the original 1995 formulation [16], which are due to repulsion and dispersion contributions to the system free energy G^S:

$$\mathbf{F}' = \mathbf{h}' + \mathbf{G}'(\mathbf{P}) \tag{11}$$

with

$$\begin{aligned} \mathbf{h}' &= \mathbf{h}^0 + \tfrac{1}{2}(\mathbf{j} + \mathbf{y}) + \mathbf{h}_{rep} + \mathbf{h}_{dis} \\ \mathbf{G}'(\mathbf{P}) &= \mathbf{G}^0(\mathbf{P}) + \mathbf{X}_{el}(\mathbf{P}) + \mathbf{X}_{dis}(\mathbf{P}) \end{aligned} \tag{12}$$

By exploiting the definition given in section 3, the expression for the corresponding free energy can be easily written as:

$$G = tr\mathbf{P}\mathbf{h}' + \frac{1}{2}tr\mathbf{P}\mathbf{G}'(\mathbf{P}) + V_{NN} + \frac{1}{2}U_{NN} \tag{13}$$

where the two terms V_{NN} and U_{NN} collect the solute-solute and the solute-solvent nuclear repulsion interactions, respectively.

The meaning of the matrices reported in the eqs.(12) is the following: $\mathbf{h}^0$ and $\mathbf{G}^0(\mathbf{P})$ are the usual one- and two-electron matrices used in the HF problem for *M in vacuo*; here we have indicated that the two-electron matrix comes from a contraction of the supermatrix **I** of the two-electron integrals involving the one-electron charge density matrix **P**.

Regarding the additional solvent-induced matrices, here we anticipate, but without giving any detail, some of the features exploited by the PCM method to describe solute-solvent electrostatic interactions which will be better described later. **j** and **y** are two one-electron matrices collecting the electrostatic interactions between each solute electronic elementary charge distribution $\chi_\mu\chi_\nu$ and the nuclei-induced ASCs, and between solute nuclear charges and the electron-induced ASCs, respectively, while $\mathbf{X}_{el}(\mathbf{P})$ is the matrix defining the same kind of interactions but, this time, between the solute electrons and the ASCs they generate.

Passing now to the new terms of eq.(12), i.e. those not present in the original PCM version, we note that the first, namely $\mathbf{h}_{rep}$, describes the contribution of solute-solvent repulsion on the solute energy, according to the formulation given by Amovilli and Mennucci [18].

In the derivation of this term the solvent distribution is assumed to be uniform (but it is possible to extend the method to non uniform distributions, to describe e.g. dielectric saturation effects for cations [19], and electrostriction effects for supercritical liquids [20, 21]), and the response function is modeled in terms of a matrix partitioning approach to the calculation of intermolecular potentials [22]. With the aid of a formal re-elaboration of the whole model, and by introducing a few reasonable approximations, the related matrix is reduced to the following form:

$$\mathbf{h}_{rep} = \alpha\left[\mathbf{S} - \mathbf{S}^{(in)}\right] \tag{14}$$

where α is a parameter depending on the density and on the number of valence electron pairs of the solvent molecules, $\mathbf{S}$ is the overlap matrix while $\mathbf{S}^{(in)}$ is based on the value of the normal component of the solute electric field produced by each elementary charge distribution $\chi_\mu\chi_\nu$ at the cavity surface Σ:

$$\mathrm{S}_{\mu\nu}^{(in)} = -\frac{1}{4\pi}\oint_\Sigma E_{\mu\nu}(\vec{r})d\vec{r} \tag{15}$$

We remark that the integral in eq.(15) is computed by exploiting the same partition of the cavity surface into tesserae used in all PCM programs to compute the electrostatic term according to the basic philosophy of the ASC approach (see next sections for more details about this point).

Further details can be found in the source paper [18].

Both the remaining new terms of eq.(12), namely $\mathbf{h}_{dis}$ and $\mathbf{X}_{dis}(\mathbf{P})$, describe the contribution of solute-solvent dispersion to the solute energy. The formulation given in ref. [18] derives from Amovilli's elaboration [23] of the dispersion response theory [24] for solvation models exploiting cavities. The original formulation has been re-elaborated to obtain a simplified expression explicitly containing the solute ground state electronic density. The other required energetic quantities reduce to the solvent ionization potential, I_S, and an averaged transition energy for the solute, ω_M.

The term deriving from this elaboration of the theory is divided into two sets, one depending on the solute charge density matrix and the other not depending on it. The formal expressions of the matrix elements are:

$$\begin{aligned}(\mathrm{h}_{dis})_{\mu\nu} &= -\frac{\beta}{2}\sum_{\kappa\lambda}\{\mu\kappa|\lambda\nu\}\mathrm{S}_{\kappa\lambda}^{-1} \\ (\mathrm{X}_{dis})_{\mu\nu} &= \frac{\beta}{2}\sum_{\kappa\lambda}\{\mu\kappa|\lambda\nu\}\mathrm{P}_{\kappa\lambda}\end{aligned} \tag{16}$$

where β is a factor depending on I_S, ω_M, and on the zero frequency refractive index of the solvent. $\{\mu\kappa|\lambda\nu\}$ collects integrals defined in terms of the potential $V_{\mu\nu}$ as well as the outward component of the electric field $E_{\mu\nu}$ referred to the solute elementary charge distribution $\chi_\mu\chi_\nu$, both computed at the cavity surface; namely we have:

$$\{\mu\kappa|\lambda\nu\} = \frac{1}{2}\oint_\Sigma d\vec{r} \quad [V_{\mu\kappa}(\vec{r})E_{\lambda\nu}(\vec{r}) + V_{\lambda\nu}(\vec{r})E_{\mu\kappa}(\vec{r})] \tag{17}$$

The PCM partition of the cavity into tesserae is here exploited once again.

To get reliable values of G_{dis} one has to use very large basis sets, and sometimes the whole calculation becomes rapidly prohibitive. In these cases, Amovilli and Mennucci have found it convenient to split the basis set into two parts, one used to define the density matrix $\mathbf{P}$ (and all the other $\mathbf{P}$-dependent contributions to G), and the other, orthogonalized to the first, used only for dispersion.

Further details about the latter point, and about the whole procedure, here only briefly summarized, can be found in the source paper [18].

Going back to eqs.(11) and (12), it is evident that their full use gives as output a collective value of $G_{el}+G_{rep}+G_{dis}$. The three separate components can be easily recovered from the calculation.

It is also possible to drop out the matrices $\mathbf{h}_{rep}$, $\mathbf{h}_{dis}$, and $\mathbf{X}_{dis}$ and to proceed with a direct calculation of G_{el} only, using for G_{rep} and G_{dis} procedures not based on the solution of the Fock equation. This is the standard (default) option in the PCM programs distributed thus far. These QM-independent methods used to compute G_{rep} and G_{dis} have been elaborated by Floris *et al.* [25, 26, 27].

4.2 Different formulations of the electrostatic problem.

In defining the matrices of eq.(12), we have not said that the PCM method to compute G_{el} now in use introduces a partition of the ASCs into two sets according to the nature of the source generating them: electrons and nuclei of M. This partition was originally proposed by Sakurai's group and exploited in a semiempirical version of PCM [28]. We have adapted it to make more effective the calculation of *ab initio* analytical derivatives of G with respect to nuclear coordinates [29, 30, 31], a subject on which there are recent progresses from our group.

By using this partition the set of linear equations expressing the apparent charges $\mathbf{q}$ are completely defined in terms of some specific properties of the solute and on basic electrostatic relationships imposed by the model.

We give here, for the first time, a formal unifying expression of these equations which is valid for both the original and the two complementary PCM approaches we have recently implemented and tested:

$$\begin{aligned} \mathbf{q}^e &= -\mathbf{A}\mathbf{O}^{-1}\mathbf{p}^e \\ \mathbf{q}^N &= -\mathbf{A}\mathbf{O}^{-1}\mathbf{p}^N \end{aligned} \tag{18}$$

Here $\mathbf{q}^x$ (with $x = e$ or N) is a row vector with as many elements as the number T of tesserae and $\mathbf{A}$ a square diagonal matrix with elements equal to the area of tesserae, $A_{kk} = a_k$.

Both the square $\mathbf{O}$ matrix and the column vector $\mathbf{p}^x$ change according to the specific approach we are taking into account.

To define $\mathbf{O}$ and $\mathbf{p}$ for the three different approaches it is convenient to make explicit reference to the basic equation for a solute M into a cavity C

surrounded by an infinite dielectric with a given function for the permittivity ϵ:

$$\begin{cases} L_i V = 4\pi\rho_M & \text{in } C \\ L_e V = 0 & \text{outside } C \\ [V] = 0 & \text{on } \Sigma \\ [\partial_L V] = 0 & \text{on } \Sigma \end{cases} \qquad (19)$$

Here V is the electrostatic potential due to the presence of ρ_M located inside the cavity, Σ the cavity surface and the operator L_i the Laplacian operator: $L_i = -\Delta$.

The operator L_e has a different form according to the model we are using to describe the system. We report here the expression for three important cases, namely the linear infinite isotropic dielectric, the linear infinite anisotropic dielectric (with homogeneous tensorial permittivity $\boldsymbol{\epsilon}$), and the infinite ionic solutions in the linearized Poisson-Boltzmann formulation:

$$\begin{array}{ll} L_e V = -\epsilon\Delta V & \text{for isotropic dielectrics} \\ L_e V = -div(\boldsymbol{\epsilon}\cdot\nabla V) & \text{for anisotropic dielectrics} \\ L_e V = -\epsilon\Delta V + \epsilon\kappa^2 V & \text{for ionic solutions} \end{array} \qquad (20)$$

The jump condition $[V] = 0$ means that V is continuous across the cavity interface Σ, i.e. $V_e - V_i = 0$ on Σ, where the subscript e and i indicate positions in the external and internal space with respect to Σ, respectively. The second jump condition $[\partial_L V] = 0$ regards the gradient of the potential, i.e. the electric field; its explicit expression changes according to the solution model. In the case of a linear isotropic homogeneous model it takes the well-known form:

$$\left(\frac{\partial V}{\partial n}\right)_i - \epsilon\left(\frac{\partial V}{\partial n}\right)_e = 0 \qquad (21)$$

where n is the outward pointing unit vector perpendicular to the cavity.

In the following exposition we shall call 'standard PCM' the method based on the use of eq.(21). Within this formalism the Green functions of the operators L_i and L_e assume the form:

$$\begin{array}{l} G_i(x,y) = 1/\left(|x-y|\right) \\ G_e(x,y) = 1/\left(\epsilon\,|x-y|\right) \end{array} \qquad (22)$$

while the basic eq.(18) becomes:

$$\begin{array}{rl} \mathbf{q}^e = & -\mathbf{A}\mathbf{D}^{-1}\mathbf{E}_n^e \\ \mathbf{q}^N = & -\mathbf{A}\mathbf{D}^{-1}\mathbf{E}_n^N \end{array} \qquad (23)$$

where $\mathbf{E}_n^x$ collects the components of the solute electric field having its source in ρ_M^x, and the matrix $\mathbf{D}$ has elements given by:

$$\begin{array}{l} D_{kk} = 4\pi[\epsilon/(\epsilon-1) - (1-\sqrt{a_k/4\pi R_k^2})/2] \\ D_{kl} = a_l[(s_k - s_l)\cdot n(s_k)]/|s_k - s_l|^3 \end{array} \qquad (24)$$

s_k and s_l are vectors defining the position of tesserae k and l, respectively, while R_k is the radius of the sphere which tessera k belongs to. The diagonal term of $\mathbf{D}$, which collects the contribution of the reaction field induced by the charge placed on tessera k on itself, is derived by the Gauss formula for an infinite charged plane with a correction term accounting for the curvature of the convex tessera.

The charges $\{\mathrm{q}^x\}$ defined in eq.(23) are the quantities determining the previously defined matrices $\mathbf{y}$, $\mathbf{j}$, and $\mathbf{X}_{el}$ appearing in the Fock operator (11). Their explicit expressions can be found elsewhere, e.g. in [16]

The Fock eq.(10) is solved with the same iterative procedure of the problem *in vacuo*; the only difference introduced by the presence of the continuum dielectric is that, at each SCF cycle, one has to simultaneously solve the standard quantum mechanical problem and the additional electrostatic problem of the evaluation of the interaction matrices, and hence of the apparent charges. The latter are obtained from eq.(23) through a self-consistent technique which has to be nested to that determining the solute wave function, in fact $\mathbf{E}_n^c$ has to be recomputed at each SCF cycle; as a consequence, in each cycle, and *a fortiori* at the convergency, solute and solvent distribution charges are mutually equilibrated.

By exploiting the expressions given in eqs.(9) and (13) the final value of the related electrostatic free energy contribution is easily written as:

$$\begin{aligned} G_{el} &= \langle\Psi|\,\hat{H}^0\,|\Psi\rangle + \langle\Psi|\,\tfrac{1}{2}\hat{V}_{el}\,|\Psi\rangle + \tfrac{1}{2}U_{NN} + V_{NN} \\ &= tr\mathbf{P}\left[\mathbf{h}^0 + \tfrac{1}{2}(\mathbf{j}+\mathbf{y})\right] + \tfrac{1}{2}tr\mathbf{P}\left[\mathbf{G}^0(\mathbf{P}) + \mathbf{X}_{el}(\mathbf{P})\right] + \left[\tfrac{1}{2}U_{NN} + V_{NN}\right] \end{aligned} \tag{25}$$

where the term U_{NN} represents the interaction energy between solute nuclei and the solvent reaction field component described by the nuclear-induced set of apparent charges $\mathbf{q}^N$.

4.3 COSMO-PCM.

The first of the two recent PCM versions quoted above, namely that we shall call COSMO-PCM, has been implemented by Barone and Cossi [32]. It formally derives from the computational model proposed by Klamt and Schüürman [33], which consists in defining apparent charges $\{q\}$ by first exploiting a liquid conductor model (i.e. $\epsilon = \infty$), and then introducing a correction factor f^c multiplying each ASC in order to make the obtained formulas coherent with the isotropic dielectric model.

The jump conditions of system (19) are here replaced by the condition:

$$V(x) = 0 \quad \text{if } x \in \Sigma \tag{26}$$

In this formalism eq.(18) becomes:

$$\begin{aligned} \mathbf{q}^e &= -f^c\mathbf{A}\mathbf{B}^{-1}\mathbf{V}^e \\ \mathbf{q}^N &= -f^c\mathbf{A}\mathbf{B}^{-1}\mathbf{V}^N \end{aligned} \tag{27}$$

where $\mathbf{V}^x$ collects the components of the solute potential having its source in ρ^x_M, and $\mathbf{B}$ elements are defined as follows:

$$\begin{aligned} B_{kk} &= 1.07a_k\sqrt{4\pi/a_k} \\ B_{kl} &= a_l/|s_k - s_l| \end{aligned} \tag{28}$$

The numerical factor 1.07 (originally introduced by Klamt) corresponds to that one analytically derives for the simple model of a homogeneously charged spherical surface partitioned into equivalent segments by the vertices of a regular polyhedron inscribed in it.

There have been some debates among people using the COSMO approach [33, 34]: there are no formal reasons asking for a constant factor f^c equal for all tesserae; anyway, the examination of simple models for which there are analytical solutions (point multipoles within a regular cavity) suggests a constant value of the type $(\epsilon - 1)/(\epsilon + k)$ with k ranging from 0 to 2. In the present implementation we have selected $k = 0$ and then $f^c = (\epsilon - 1)/\epsilon$.

The values of the ASCs obtained with the aid of eq.(27) are inserted in the interaction matrices $\mathbf{j}$, $\mathbf{y}$ and $\mathbf{X}_{el}(\mathbf{P})$ exactly as in standard PCM and the following Fock equation solved with standard iterative methods.

COSMO is of course an approximate method working better when the bulk dielectric constant ϵ is large.

From a computational point of view, there are some advantages in using COSMO-PCM: one is just given by the simplest expression of the symmetric $\mathbf{B}$ matrix when compared to the non-symmetric $\mathbf{D}$. However there are no significant changes in the computational times passing from standard PCM to COSMO-PCM, at least for the calculation of solvation energies at a given geometry of M. Later we shall compare other features of the methods we are presenting here that can address potential users to the most convenient choice.

We stress that COSMO is an independent method of which there are now several versions, both at the semiempirical and at the *ab initio* QM level. In particular, with the acronym COSMO-PCM we indicate a version which exploits all the features present in standard PCM.

4.4 IEF-PCM.

The third approach we are presenting here is more general and encompasses standard PCM and COSMO-PCM as special cases. We shall call this approach

IEF-PCM, emphasizing that IEF (the acronym stays for Integral Equation Formulation) is an independent method that has been included into PCM but that can be adapted to other ASC solvation procedures. The mathematical foundations have been given by Cancès and Mennucci [35]; we shall limit ourselves to the computational implementation. In IEF the Green functions of the operators L_i and L_e, these latter expressed for the three cases we have introduced with eq.(20) [35],

$$G_i(x,y) = \frac{1}{|x-y|} \tag{29}$$

and

$$\begin{cases} G_e(x,y) = 1/\left(\epsilon|x-y|\right) & \text{for isotropic diel.} \\ G_e(x,y) = \left[det(\boldsymbol{\epsilon})\left(\boldsymbol{\epsilon}^{-1}\left(x-y\right)\right)\cdot\left(x-y\right)\right]^{-\frac{1}{2}} & \text{for anisotropic diel.} \\ G_e(x,y) = \exp\left(-k|x-y|\right)/\left(\epsilon|x-y|\right) & \text{for ionic solutions} \end{cases} \tag{30}$$

are used to define a new set of operators defined as follows:

$$\begin{aligned} \left(S_i\cdot u\right)(x) &= \int_\Sigma G_i(x,y)u(y)dy && x\in C \\ \left(D_i\cdot u\right)(x) &= \int_\Sigma \partial_y G_i(x,y)u(y)dy && x\in C \\ \left(D_i^*\cdot u\right)(x) &= \int_\Sigma \partial_x G_i(x,y)u(y)dy && x\in C \\ \left(S_e\cdot u\right)(x) &= \int_\Sigma G_e(x,y)u(y)dy && x\notin C \\ \left(D_e\cdot u\right)(x) &= \int_\Sigma \partial_y G_e(x,y)u(y)dy && x\notin C \end{aligned} \tag{31}$$

Here $\partial_y G_i(x,y) = \nabla_y G_i(x,y)\cdot n(y)$, $\partial_x G_i(x,y) = \nabla_x G_i(x,y)\cdot n(x)$, and $\partial_y G_e(x,y) = (\boldsymbol{\epsilon}\cdot\nabla_y G_i(x,y))\cdot n(y)$ for the anisotropic medium, where the tensor $\boldsymbol{\epsilon}$ goes to the scalar function ϵ for the case of the linear isotropic solutions.

The approach we have sketched here can be extended to other models of solution but we limit ourselves to cases for which we have written and tested the computational codes, with some worked out examples.

The first result to be stressed is that, with the IEF approach, it is possible to reduce to an ASC form problems which are generally treated by resorting to 3D numerical techniques. Dielectrics with a tensorial permittivity $\boldsymbol{\epsilon}$ have been thus far treated by a combined Boundary Element - Finite Element Method (BEM/FEM) [36] and ionic solutions using Finite Difference (FD) approaches.

Both FEM and FD methods require a 3D scanning of the outer space with techniques (see e.g. [8, 37]) by far more expensive than the BEM one used in the ASC approaches.

On the contrary, by applying the IEF method, we have only to define the apparent charges $\mathbf{q}^x$ spread on the cavity surface also for dielectric with a tensorial permittivity or for the ionic solutions, exactly as for the simple isotropic case. The basic relationships (18) can be written in the following form:

$$\mathbf{q}^x = -\mathbf{A}\mathbf{C}^{-1}\mathbf{g}^x \tag{32}$$

where $x = e$ or N.

The matrix $\mathbf{C}$ and the row vector $\mathbf{g}$ have the following expressions:

$$\mathbf{C} = \left(\frac{1}{2}\mathbf{A} - \mathbf{D}_e\right)\mathbf{A}^{-1}\mathbf{S}_i + \mathbf{S}_e\mathbf{A}^{-1}\left(\frac{1}{2}\mathbf{A} + \mathbf{D}_i^*\right) \tag{33}$$

$$\mathbf{g}^x = \left(\frac{1}{2}\mathbf{A} - \mathbf{D}_e\right)\mathbf{V}^x - \mathbf{S}_e\mathbf{E}_n^x \tag{34}$$

In $\mathbf{g}$ there are both the normal components of the electric field ($\mathbf{E}_n^x$) we have used for the standard PCM and the electric potential ($\mathbf{V}^x$) we have used for COSMO-PCM.

The $\mathbf{D}_i$ matrix can be associated to the $\mathbf{D}$ matrix of PCM whose elements give the normal components of the field the ASCs induce on the center of the tesserae, while the $\mathbf{S}_i$ matrix is strictly related to the $\mathbf{B}$ matrix of COSMO giving the potential of the apparent charges on the center of the tesserae.

The explicit expressions of their elements is equal for all the three different systems and are given by

$$\begin{cases} \{D_i\}_{kk} = & -1.07\sqrt{4\pi a_k}/(2R_k) \\ \{D_i\}_{kl} = & a_k a_l\left[(\vec{s}_k - \vec{s}_l)\cdot\vec{n}\,(s_k)\right]/\left|\vec{s}_k - \vec{s}_l\right|^3 \end{cases} \tag{35}$$

$$\begin{cases} \{S_i\}_{kk} = & 1.07 a_k\sqrt{4\pi a_k} \\ \{S_i\}_{kl} = & a_k a_l/\left|\vec{s}_k - \vec{s}_l\right| \end{cases} \tag{36}$$

On the contrary, the definition of the elements of $\mathbf{D}_e$ and $\mathbf{S}_e$ depends on the model chosen for the solvent. In the isotropic case $\mathbf{D}_i = \mathbf{D}_e$ and $\mathbf{S}_e = \mathbf{S}_e/\epsilon$. In the anisotropic case we have for the non diagonal elements:

$$\{\mathbf{D}_e\}_{kl} = \frac{a_k a_l}{\sqrt{det(\epsilon)}}\frac{(\vec{s}_k - \vec{s}_l)\cdot\vec{n}\,(\vec{s}_k)}{\left[(\epsilon^{-1}(\vec{s}_k - \vec{s}_l))\cdot(\vec{s}_k - \vec{s}_l)\right]^{\frac{3}{2}}} \tag{37}$$

$$\{\mathbf{S}_e\}_{kl} = \frac{a_k a_l}{\sqrt{det(\epsilon)}}\left[\left(\epsilon^{-1}(\vec{s}_k - \vec{s}_l)\right)\cdot(\vec{s}_k - \vec{s}_l)\right]^{\frac{1}{2}} \tag{38}$$

while for the diagonal elements $\{\mathbf{D}_e\}_{kk}$ and $\{\mathbf{S}_e\}_{kk}$ we have preferred not to introduce approximate correction factors, as those used in eqs.(35) and (36) but to resort to a numerical integration using a gaussian quadrature.

The charges $\mathbf{q}^x$ (eq.(32)) are inserted into the HF expression (10) and, from this point, the program runs as the standard PCM version.

We have here a more complex formulation, requiring the evaluation of a larger number of matrices. Remark, however, that the size of these matrices is left unchanged ($T \times T$) as in standard PCM and that $\mathbf{C}$, eq.(33), has to be computed only once, at the beginning of the calculation. Only $\mathbf{V}$ and $\mathbf{E}_n$ vectors must be updated during each SCF cycle.

For brevity's sake we do not report the demonstration of the formal equivalence between IEF and either PCM or COSMO, when the dielectric constant is put equal to a constant value ϵ or to $\epsilon = \infty$, respectively [38]; in both cases this formal equivalence does not mean that calculations run in parallel using e.g. standard PCM or IEF-PCM for the isotropic model: there are differences which ultimately lead to consider the use of IEF-PCM more effective (as measured by the computational costs) when an higher accuracy in the results is required. These topics will be treated later under the headings of 'Cavity errors', and 'Calculation of molecular response functions' (sections 5 and 7, respectively).

4.5 PCM-QINTn.

The inversion of the $\mathbf{D}$ matrix used in PCM (see eq.23) can represent a computational bottleneck. This inversion may be avoided making use of an expansion interpolation procedure which maintains the quality of the results at a lower computational cost. The matrix $(\mathbf{DA}^{-1})$ is rewritten in terms of other matrices in the following way:

$$\mathbf{DA}^{-1} = \frac{4\pi\epsilon}{\epsilon - 1}(\mathbf{L} + \mathbf{1} - \mathbf{M}) \tag{39}$$

with

$$\begin{aligned} L_{kl} = &\ 0 \\ L_{kk} = &\ \tfrac{\epsilon-1}{2\epsilon}\left(1 - \sqrt{\tfrac{a_k}{4\pi R_k^2}}\right) \end{aligned} \tag{40}$$

and

$$\begin{aligned} M_{kk} = &\ \tfrac{\epsilon-1}{4\pi\epsilon} a_k \tfrac{(\vec{r}_k - \vec{r}_l)\cdot\hat{n}_k}{|\vec{r}_k - \vec{r}_l|^3} \\ M_{kk} = &\ 0 \end{aligned} \tag{41}$$

We have changed th names of the matrices with respect to the original formulation of Pomelli and Tomasi [39] to have a consistent terminology along the present paper. By invoking a recursive formulation of the $\mathbf{q}$ charges, with partial closure [40], we may write

$$\mathbf{q}^{(\infty,n)} = \mathbf{K}_n \mathbf{q}^{(0)} \tag{42}$$

where $\mathbf{q}^{(0)}$ are the ASCs obtained at the zero-order step of the HF procedure, and $\mathbf{q}^{(\infty,n)}$ the charges obtained by applying $\mathbf{K}_n$ (the correct value is given by $n = \infty$).

$\mathbf{K}_n$ is thus defined

$$\mathbf{K}_n = (\mathbf{1} - \mathbf{L})^{-1} \left[\sum_{m=0}^{n} \left(-\mathbf{M}(\mathbf{1} - \mathbf{L})^{-1} \right)^m \right] \tag{43}$$

where the inversion is limited to the diagonal matrix only.

This procedure has been called PCM-CLSn (the acronym CLS reflects the partial closure of the iterative formulas we have exploited).

Even more efficient is the expression exploiting an interpolation between $\mathbf{K}_{n-1}$ and $\mathbf{K}_n$, namely

$$\mathbf{Q}_n = (1 - \lambda_n)\mathbf{K}_n + \lambda_n \mathbf{K}_{n-1} \tag{44}$$

and

$$\mathbf{q}^{(n)} = \mathbf{Q}_n \mathbf{q}^{(0)} \tag{45}$$

There is a formal relation between the different matrices defined above, namely we have:

$$\mathbf{K}_\infty = \mathbf{Q}_\infty = \mathbf{A}\mathbf{D}^{-1} \tag{46}$$

This method, called PCM-QINTn, has been applied to standard PCM with separation of $\mathbf{q}$ into electron- and nuclei-induced sets $\mathbf{q}^e$ and $\mathbf{q}^N$.

To get good results it is sufficient to keep a low value of n. QINT2 (i.e. $\mathbf{K}_2$) gives ΔG values exhibiting differences with respect to standard PCM of less than 0.1% (the regression coefficient for 40 molecules, neutral and charged, is r=0.999996) with reduction of computational times by a factor 3 for solutes having ≈600 tesserae; the comparison is even more favorable for larger solutes.

As it will be discussed later, PCM-QINTn also gives good derivatives of the free energy. The method has been thus far implemented for standard PCM only.

To summarize in few words this quite large section, we may say that we have extended HF expressions to dispersion and repulsion contributions (section 4.1), formulated two new versions of PCM (sections 4.3 and 4.4) which accompany the standard one and add more flexibility to the computational tools among which to choose for specific applications. We have detailed these new methods, COSMO-PCM and IEF-PCM, for the electrostatic contribution to G^S, but it must be remarked that other features, as QINTn and the direct calculation of G_{rep} and G_{dis}, can be exploited too. This extension of QINT has not been tested yet. Regarding the inclusion of V_{rep} and V_{dis} in the Fock operator, this means to modify to same extent the resulting wavefunctions, and then the $\mathbf{E}_n^e$ or $\mathbf{V}^e$ vectors defining $\mathbf{q}^e$; hence also V_{el} is somewhat affected by these interactions terms [41].

5 Cavity errors and their corrections.

The use of apparent surface charges allows to quantify some 'errors', of both numerical and physical origin, related to the computational procedures analyzed above.

According to Gauss theorem, the integral value of the apparent surface charges, $Q_\sigma^N = \sum_k q_k^N$ and $Q_\sigma^e = \sum_k q_k^e$, should be related by a simple expression to the solute charges $Q_M^N = \sum_\alpha Z_\alpha$ and $Q_M^e = n_e$ (n_e is the number of electrons of M):

$$Q_\sigma^x(theo) = -\frac{\epsilon - 1}{\epsilon} Q_M^x \tag{47}$$

In the computational practice this relationship is not numerically satisfied, and we may define errors in the apparent charge as follows:

$$\Delta_\sigma^x = Q_\sigma^x(theo) - Q_\sigma^x(comp) \tag{48}$$

There are two sources of error that we shall call 'discretization' and 'tail' errors, respectively. The discretization error is due to the use of the BEM procedures to solve the electrostatic problem. Both the partition of the continuous apparent surface distribution into discrete elements (the point-charges $\mathbf{q}^x$) and the use of the latter to define the self-polarization of the charges themselves (i.e. the operation performed via the matrix $\mathbf{O}^{-1}$ of eqs.18) give origin to errors of numerical origin that can be reduced by introducing correction factors in the diagonal elements of the involved matrices (as we have done e.g. in eq.(24) for $\mathbf{D}$ and in eq.(28) for $\mathbf{B}$) either by resorting to more complex surface integration techniques. Actually, the global numerical error has little to do with the error introduced by replacing surface integration with summations over a discrete number of points: the smoothness of the partition of the cavity surface we use is by far sufficient to get values precise enough for these surface integrals. We have tested it by pushing the partition of the cavity to a very large number of tesserae (960 tesserae per sphere, instead of the default value of 60). By contrast, this error depends on the nature of the interaction operator exploited by the method, being larger for the operators related to the electric field (standard PCM) and smaller for the operators related to the electric potential (COSMO and IEF).

The second error has a physical origin. In all continuum solvation methods it is assumed that the whole charge of M lies inside the cavity. This is not true for the electronic component which fades exponentially, and it is surely quite different from zero on the cavity surface to ensure the proper balance between attractive and and repulsive forces between solute and solvent. When the separation in $\mathbf{q}^e$ and $\mathbf{q}^N$ charges is introduced it is possible to learn something more by comparing Δ_σ^e and Δ_σ^N errors. They are of opposite sign, and Δ_σ^N is due to discretization errors only (the nuclear charge is in fact completely within the cavity) while Δ_σ^e is due to both errors. In former PCM versions [6, 42], called here iterative PCM, there was no separation between the two sets of charges; and the global error was corrected by introducing a simple procedure, called re-normalization, in which each q_k value was multiplied by an appropriate factor such as to satisfy the Gauss' relation (47) (re-normalization technique N1 [6]).

Re-normalization techniques have been also employed for the direct PCM, called here standard PCM, in which the separation between $\mathbf{q}^e$ and $\mathbf{q}^N$ charges is exploited.

In this case, the errors are larger, because there is no authomatic compensation between positive and negative contributions to the discretization error; however a simple re-normalization procedure, called here N2, and based on the considerations given above about the different nature of errors Δ_σ^N and Δ_σ^e, is sufficient for almost all the standard calculations [16].

However, there are also non standard calculations, such as calculations with very diffuse basis sets (especially for anions), and calculations of derivatives of G with respect to external electric fields. We shall give later more details about the derivatives of G with respect to external electric fields, a subject on which there are recent progresses in PCM, and here we mention this subject simply to justify our effort of having a better definition of the correction for tail errors.

First we have improved the re-normalization procedure by adding a constant multiplicative correction factor for the discretization error - drawn from Δ_σ^N - and a second correction changing for each tessera and based on the value of electronic solute density $\rho_M^e(s_k)$ at the center of the tessera [43]. In such a way the tail error is compensated with a weight proportional to the actual value of the electronic tail at the specific site. This re-normalization procedure (called N3) is a bit more expensive than N2, but more efficient.

However, it is not efficient enough for very hard cases, such as the calculation of high order polarizabilities, and recently we have decided to exploit a more sophisticated approach in which the electronic charge lying on the outer space is explicitly taken into account. This method leads to the definition of a second set of apparent surface charges $\mathbf{q}^e_{eff}$ which are not affected by discretization errors and can be used in PCM without changing the dimension of the $\mathbf{D}$ matrix. The details on the derivation of this correction procedure, called here N4, can be found in the source paper [44]: it is able, in our opinion, to completely correct tail errors. A comparison among N2, N3 and N4 procedures can be found in a recent paper [43].

Also COSMO and IEF are affected by both discretization and tail errors. The entity of the errors are however lower, at least by an order of magnitude, than those found in standard PCM. The reason is due to the use of operators related to the electric potential instead of the electric field, as standard electrostatics would require. So, when N2 or N3 are sufficient, COSMO-PCM and IEF-PCM can be used without corrections. Moreover, for more 'difficult' cases, where a N3 procedure was found to be necessary in the standard PCM, a by far simpler N2 correction is sufficient for COSMO and IEF. This lowering in the level of the correction can even reverse the trend in the computational times in favor of the IEF method, if compared to the standard PCM. This is particularly true in computing hyperpolarizabilites [38], for the reason we shall explain later. We have no COSMO hyperpolarizabilities calculations to compare.

6 Analytical geometry derivatives.

Among the various types of G derivatives that can be computed with the PCM program, a special importance is taken by the derivatives with respect to nuclear coordinates. Without analytical expressions of the energy gradient it is not possible to perform studies of geometry optimizations for molecules of medium size, and without analitycal formulation of the Hessian both the characterization of the saddle points and the determination of vibrational frequencies become quite expensive.

We started to introduce analytical derivatives with respect to nuclear coordinates into PCM in 1994, and so the results we obtained, documented by several papers (see e.g. [29, 30, 31]), cannot be grouped under the heading 'Recent developments'.

There are however recent progresses in this field too. They can be divided in two groups: exploitation of the new PCM versions we have presented in the preceding pages and improvements for the standard PCM.

The derivative of G with respect to the nuclear parameter α will be written here in an abbreviated form: $G^\alpha = \frac{\partial G}{\partial \alpha}$:

$$G^\alpha = G^\alpha_{el} + G^\alpha_{cav} + G^\alpha_{dis} + G^\alpha_{rep} \tag{49}$$

In PCM all the four derivatives can be computed.

The non electrostatic terms mostly rely on partial derivatives of the cavity surface. In the model we have used here the radii R_k of the spheres defining the cavity are kept fixed: these radii can be considered variable parameters when the derivatives regard other quantities, like temperature or pression [29]. Still keeping the R_k values constant, there may be changes in G^α regarding cavity parameters, as the portion of the surface Σ_k of each sphere exposed to the solvent, and the area a_k of some tesserae (also the number of tesserae and of spheres may change during the evolution of the α parameter) [31]. These partial derivatives are sufficient to compute G^α_{cav}, and both G^α_{dis} and G^α_{rep} in the Floris-Tomasi version [26, 45]. G^α_{rep} and G^α_{dis} in the Amovilli and Mennucci version [18] are treated with G^α_{el} via derivatives of the Fock matrix $\mathbf{F}^\alpha$.

We recall that in standard PCM we exploit the GEPOL definition of the cavity and of its tessellation [46, 47, 48] with a more accurate definition of the area of those tesserae which are cut by other spheres (the so-called Gauss-Bonnet partition, GEPOL-GB [31]). Other definitions of the molecular cavity and its tessellation will be given later.

We report here the expression of the first derivative only; the parallel expression for the second derivative $G^{\alpha\beta}$ can be found in the reference paper [30]:

$$\mathbf{G}^\alpha_{HF} = tr\mathbf{P}\mathbf{h}'^\alpha + \frac{1}{2}tr\mathbf{P}\mathbf{G}'^\alpha - tr\mathbf{S}^\alpha\mathbf{W} + \frac{1}{2}U^\alpha_{NN} + V^\alpha_{NN} \tag{50}$$

where

$$\mathbf{W} = \mathbf{P}\mathbf{F}'\mathbf{P} \tag{51}$$

and the elements of the matrices bearing α as superscript are the partial derivatives with respect to α of the elements of the original matrices. The detailed expression of these integrals can be found elsewhere; in a recent paper [49] we have presented a revised synopsis correcting some typographical errors present in the source paper [30] (these errors were not present in the computational codes).

What resumed here is sufficient to discuss some points leading us to the presentation of some recent advances in PCM related to the search of critical points on the PES.

The search of critical points ($\nabla G = 0$) leading to the definition of equilibrium geometry or saddle points is always a computer demanding task, and so it is compelling to reduce computational times at every step of the procedure.

To compute G at a fixed geometry with standard PCM we are arrived now to a ratio of about 1.2 with respect to the same calculation of E^0 *in vacuo* for molecules of medium size up to 50 atoms (the ratio rises to 1.5 for small solutes). The same ratio holds for a single point calculation of G^α when compared to $E^{0\alpha}$.

A computational bottleneck is given by the inversion of the **D** matrix (eq.23) and this is a reason to keep the dimension T of this matrix low. For calculations at fixed geometries divergences near the minimum rarely occour (they may appear when sizeable portions of the potential energy surface are sampled), on the contrary events of this type, interrupting the search of the critical point, are more probably when the number T of tesserae is larger. Divergences are here connected to the occurrence of very small tesserae.

These considerations have led us to consider some variants in the calculation of G^α_{el} which we summarize here.

1. Definition and use of a united atom topological model (UATM) for the construction of the cavity [50]. The UATM reduces the number of spheres and then of tesserae. The frequency of divergence cases in the inversion of **D** is greatly reduced. The quality of the description of the solvent effects, measured by a difference between experimental and computed ΔG_{sol} values, is increased with respect to standard cavities.

   The UATM version for calculating G^α also has an option to permit the use of a fixed cavity. There is no great reduction in computational times, but the occurrence of divergences is further noticeably reduced. This version is now implemented in both standard and COSMO-PCM versions.

   More details about UATM will be given in section 8.1.

2. G^α with COSMO-PCM (with or without UATM). The mathematical structure of COSMO allows to the introduction of noticeable simplifications in the calculations of G^α [32, 33]. By rearranging the COSMO formulas one arrives at

   $$G^\alpha_{el} = E^{0\alpha} + \Delta G^\alpha_{el} = E^{0\alpha} + \sum_k q_k V^\alpha_M + \frac{1}{2}\frac{\epsilon}{\epsilon - 1}\sum_k\sum_l \left(\mathbf{A}^{-1}\mathbf{B}\right)_{kl} q_k q_l \quad (52)$$

   where the derivatives of the apparent charge cancel out.

   By using UATM cavities the time necessary to compute G^α_{el} becomes almost equal to that necessary for $E^{0\alpha}$ (the ratio of times is about 1.2).

   This method has been also implemented for DFT versions of PCM and is now inserted in the package we are preparing for Gaussian.

3. Use of QINT formulas. As we have already said both PCM-CLSn [40] and PCM-QINTn [39] methods avoid the inversion of the **O** matrix.

> Apparently, CLSn does not give good derivatives because the renormalization procedures are too large. We have found good results with QINT, and within the number of tests so far performed we have not found cases of divergence in the search of optimuum geometries.
>
> The method has been implemented for standard PCM only, but there are no formal obstacles to use it into COSMO or IEF methods.

There are also some other ideas about possible ways to make the calculation of the gradient and of the Hessian more effective, but we limit ourselves to expose topics for which there is a working computer code. The field is in evolution but surely progresses towards computational methods with computational costs and range of applicability comparable to those used for molecules *in vacuo* are within reach. In our opinion the most difficult point is to find search algorithms for critical points able to treat in a more efficient way some small roughness in the PES introduced by the tessellation of the cavity surface.

7 Molecular response functions.

The solvent affects the solute properties at a variable extent not easy to be quantified without the use of accurate calculations. In the past years we have computed and analyzed solvent effects on a variety of molecular properties, but here we shall limit ourselves to response properties only, in a restricted technical meaning of this term.

With molecular response property we mean here the change in some properties of a molecule when subject to an external field of electric or magnetic type.

Actually, all the solutes are subject to an external electric field, namely the solvent reaction field: here we shall consider an additional field acting in parallel with the reaction field.

These remarks are necessary to put our models, and our calculations in the appropriate context.

Let us consider an example, i.e. the electric (hyper)polarizabilities, $\gamma^{(n)}$, where n is the order in the power expansion of the property). If the molecule M is *in vacuo* the definition of these molecular response functions is straightforward; on the contrary, when M is in a medium, things are more complex.

From the experimental data one gets values of the related bulk properties, namely the susceptibilities $\chi^{(n)}$. From the latter one may derive information about the (hyper)polarizabilities $\gamma^{(n)}$ by taking into account the relation between the two different fields involved in the definition of the two quantities, namely the macroscopic uniform external field and the local microscopic field, respectively. This relation can be defined in terms of suitable local-field corrections f_x^C having origin in the polarizing field acting on any particular molecule due to the influence of surrounding molecules. These correction functions assume simple forms when the cavity is spherical and the medium is isotropic: in these cases it is common practice to exploit the well known Lorentz and/or Onsager factors of which we do not report here the explicit expression.

The relationship between $\chi^{(n)}$ and $\gamma^{(n)}$ is given by the following expressions, according to the eventual frequency dependence of the applied external field:

$$\begin{array}{l}\chi^{(1)} = N f_x^C(\omega_b)\gamma^{(1)}(-\omega_b;\omega_b) \\ \chi^{(n)}(\omega_b;\omega_1,\omega_2\ldots\omega_n) = N f_x^C(\omega_b)\prod_k^n f_x^C(\omega_k)\gamma^{(n)}(-\omega_b;\omega_1,\omega_2\ldots\omega_n)\ n \geq 2\end{array} \tag{53}$$

What we are computing with PCM are the microscopic $\gamma^{(n)}$ values. In addition, and this is one of the recent progresses we are examining, we can also use PCM to get values of the local field corrections in the case of cavity of general molecular shape. The latter is a subject of remarkable importance to relate calculations and experiments, for which, at the best of our knowledge, there are no other computationally effective recipes.

Moreover, the calculation of $\gamma^{(n)}$ can be partitioned into several contributions: for studies *in vacuo* the partition is generally done in terms of electronic and vibrational contributions. Here we consider it convenient to make reference to the *in vacuo* case, adding a further term, the geometry relaxation contribution, measuring the effects on the electronic polarizability due to the changes in the equilibrium geometry induced by the solvent.

The PCM calculation are performed by using the CPHF formalism [51] for the static case, and to the TD-CPHF formalism for the frequency dependent case [52]. There are also calculations at higher levels of the QM theory which have not been fully analyzed. The formulas are quite complex, and we refer the interested readers to the two source papers. What is worth remarking here is that (hyper)polarizability values are quite sensitive to the cavity errors. In passing from $\gamma^{(1)}$ (i.e. α, the polarizability tensor) to $\gamma^{(2)}$ (i.e. β, the first hyperpolarizability) and to $\gamma^{(3)}$ (i.e. γ, the second hyperpolarizability) the problem of cavity errors become worse and worse.

The reason is simple; the computation of the various (hyper)polarizability elements requires the knowledge of the one-electron density matrix derivatives with respect to the external field Cartesian components E_v, with $v = x, y, z$; in fact, by expanding the molecular dipole in terms of powers of the external field, we can derive:

$$\begin{aligned}\alpha_{rs} &= -tr\mathbf{m}_r\mathbf{P}^s \\ \beta_{rst} &= -tr\mathbf{m}_r\mathbf{P}^{st} \\ \gamma_{rstu} &= -tr\mathbf{m}_r\mathbf{P}^{stu}\end{aligned} \tag{54}$$

where $\mathbf{P}^{stu} = \partial^3\mathbf{P}/\partial E_s\partial E_t\partial E_u$ and $\mathbf{m}_r$ is the rth component of the dipole moment matrix. The derivative distributions $\mathbf{P}^s$, $\mathbf{P}^{st}$ ... are obtained by solving separate HF equations, each taking into account the effects of the corresponding external field components. It can be easily shown that by increasing the order of derivation, i.e. the power in the dipole expansion in terms of the external field, the tail errors become larger and larger, even of several orders of magnitude with respect to the zero-order calculation.

This remark has relevance also on the computational accuracy. Polarizability functions require large basis sets, with an high contribution from diffuse functions, which greatly emphasize the presence of electronic tails outside the molecular cavity. This fact has led us to abandon the N2 normalization procedure, no longer sufficient, in favor of N4, even if more costly from a computational point of view. However, even at this more refined level, numerical errors remain relatively large. In particular, we have found that the formal equivalence which should exist between the direct iterative procedure and the so-called (2n+1) scheme is not satisfied. In brief, the (2n+1) rule states that knowledge of the wave function through order n allows one to calculate the energy through order (2n+1); passing to the energy derivatives, this means that for both the first and second hyperpolarizabilities the order of the required wave function derivatives is lower by one compared to the standard iterative scheme.

The IEF-PCM approach works by far better. The tail errors are strongly reduced and, eventually, they can be completely corrected by a simple renormalization process (i.e. N2); as a consequence the (2n+1) procedure can be applied, and, in conclusion, computational times are by far shorter with IEF than with standard PCM.

The computational scheme we have planned and we are using for studies on specific systems is the following:

1. calculations *in vacuo* both for the electronic and vibrational components of the $\gamma^{(n)}$ at fixed geometry;
2. calculations in solution for the electronic component of the $\gamma^{(n)}$ at fixed geometry;
3. geometry optimization in solution and then calculation of both electronic and vibrational components of the (hyper)polarizabilities.

The number of accurate studies is quite limited (especially in solution, but also *in vacuo*) and the number of 'surprises' we have found (both for static and frequency dependent cases) is large; an adequate scrutiny of the results we have obtained will require some time before publication. At the same time there is a rapid evolution in the elaboration of computational procedures; from HF we are now passing to DFT formulations, and to higher-order QM levels, also considering non linear approaches (Cammi, unpublished results). In addition, the possible application of IEF to anisotropic dielectrics will be accompanied by the elaboration of more complex models of the medium, such as that composed by a metallic body and a liquid dielectric, with the solute M on the surface of the metal; anyway, these are subjects to be treated in another report on 'recent progresses' which we hope to write not too far in the future.

Passing now to the local field functions, f_x^C, we remark that PCM can give numerical values of the field inside the cavity when an external field is applied to the system composed by the unperturbed solvent with a void cavity of the correct shape to accommodate M [53]. Actually, it is also possible to do more, for example to decompose the local field according to a power expansion, or to numerically couple solvent reaction field and the internal field deriving from the external field. On the other hand, it is also possible to rework the CPHF equations including an explicit dependence of G on the external field via an additional set of ASCs, named here $\mathbf{q}^E$ which depend on the external field $\vec{E}$. The ratio between the $\gamma^{(n)}$ values computed with and without this further set of charges gives the 'cavity field factor' (remark that Onsager's and Lorentz's factors actually combine cavity field and reaction field effects and thus they cannot be properly used in combination of the $\gamma^{(n)}$ values obtained in solution, for which the effects of the reaction field has been already taken into account [53]). The first numerical tests show that for molecules of small-medium size the computed values of the local field factors are almost identical to those calculated with the Onsager model applied to a spherical cavity; remarkable changes are present when the cavity deviates from sphericity.

With this new implementation which explicitly introduces the effects of the local fields in the PCM-CPHF procedure, we think to have almost completely settled the problem for static hyperpolarizabilities; at the present moment we are on the verge of doing the same for dynamical analogs which require an additional local field function $f^C(\omega_b)$ corresponding to the frequency of the leaving wave (see eq.53).

The implementation of PCM methods to compute magnetic response properties has started later but has rapidly reached computational effectiveness. Cammi [54] has elaborated the formalism for the magnetic susceptibility $\boldsymbol{\chi}$ and the magnetic shielding $\boldsymbol{\sigma}^N$. Both quantities can be expressed as second derivatives of the free energy G with respect to Cartesian components of the magnetic field ($\vec{B}$) and of the magnetic moment of nucleus N ($\vec{\mu}^N$):

$$\begin{aligned} \chi_{rs} &= \partial^2 G / \partial B_r \partial B_s \\ \sigma_{rs}^N &= \partial^2 G / \partial B_r \partial \mu_s^N \end{aligned} \qquad (55)$$

The Fock operator of eq.(10) has to be thus modified:

$$\mathbf{F}'' = \mathbf{h}'' + \mathbf{G}' \tag{56}$$

with

$$\mathbf{h}'' = \mathbf{h}' + \mathbf{h}^{(10)} + \mathbf{h}^{(01)} + \mathbf{h}^{(11)} + \mathbf{h}^{(20)} \tag{57}$$

The new operators introduced here depends on both $\vec{B}$ and $\vec{\mu}$ (see the source paper for more details).

The properties of interest are given by the second derivatives $G^{\alpha\beta}$ computed with a CPHF formalism parallely to what reported for the electric response functions (the derivative parameters are here the components of $\vec{B}$ and $\vec{\mu}$, instead of the external electric field $\vec{E}$). It would be too long to report here the development of the theory, which assumes different forms in the various algorithms in use, according to the selection of the gauge and to the eventual dependence of the basis set on the magnetic field $\vec{B}$.

The formulas have been elaborated for the four computational methods more in use in the calculation of NMR properties: GIAO [55], CSGT [56], IGLO [57], and LORG [58], and implemented for GIAO and CSGT.

The results thus far obtained agree with the experimental evidence. We cannot say which formulation is more convenient for routine PCM calculations nor to present results about related problems, such as the description of local magnetic field effects or the calculations of other properties of interest for the NMR spectroscopy.

Our studies on molecular response properties have been limited to the standard PCM, with the exception of the application of the IEF formalism to electric (hyper)polarizabilities. Molecular response functions are quite sensitive to the details of the calculation, by far more than energy, and can be used to test in a deeper way the various extensions of PCM we have exposed in the previous pages; an example of this use of molecular response, addressed to the inclusion into HF equation of dispersion and repulsion terms, can be found in [41]. Similar tests have been planned, but not yet performed, for other recent extensions or modifications of PCM we shall expose in the next section.

8 Further extensions and variants of PCM for the definition of the cavity

8.1 The united atom topological model (UATM).

We have already introduced this variant of PCM in treating nuclear geometry derivatives. We give here more details about this PCM version that probably will become the recommended one for routine calculations.

In standard PCM the cavity is defined in terms of the union of van der Waals (vdW) spheres, one for each atom of M, with radii multiplied by a constant factor (typically equal to 1.2), eventually supplemented by additional spheres to take into account the small portions of the outer space from which the solvent is excluded (the resulting cavity surface corresponds to the so-called solvent excluding surface Σ_e) [46]. All the proposed sets of van der Waals radii have been tested, with some modifications, both for neutral and charged solutes [59, 50] but none is able to reproduce the subtleties of the differential solvation energies occurring in some sets of related compounds. We decided to perform an extensive survey of solvation energies for which there are experimental values, with the goal of getting a set of vdW radii well fitting the experimental data. We realized that it is easier to reach this goal if the H atoms are included in the sphere of the heavy atom to which they are bonded. We have also found that fine details in differential solvation energies (some never reproduced by other solvation methods, of both continuous and discrete type) can be well reproduced by modulating the basic united atom sphere with some corrections based on the topological connections of the heavy atom [50].

The mean unsigned error for ΔG_{sol} of a generous number of neutral solutes in water is about 0.16 kcal/mole. Analogous values have been found for both COSMO-PCM and IEF-PCM. Passing to charged solutes the mean unsigned error is larger (1.0 kcal/mole for standard PCM) but in percentage to the ΔG_{sol} values it is lower than the experimental bar error.

This good performance is related to the basis set (e.g. 6-31G(d)) and to the N4 renormalization of HF calculations we exploited to fix the atomic parameters (all the second and third row atoms, supplemented by Br and I treated with pseudopotentials). In changing basis set and/or the QM procedure, analogous (or even better) performances have been obtained by introducing minor numerical changes in the definition of the corrections of UATM radii; anyway, the original set of parameters still continues to give excellent results even when applied to other basis sets, when a simpler (N2) renormalization procedure is used, and when the HF description is replaced by a MP2 or by a DFT formulation using hybrid B3LYP functional [32].

We have already commented the advantages of using UATM for the calculation of energy derivatives.

8.2 Variable tessellation of the cavity surface

We have recalled that in PCM molecular cavities there can be additional spheres inserted to describe solvent excluded space. The radii of such spheres can have very different values, but they are generally small. In the GEPOL procedure [46, 47, 48] elaborated first for PCM and then used for other methods all the spheres are partitioned in the same way, i.e. according to the partition of each spherical surface given by an inscribed pentakisdodecahedron. GEPOL also introduces a threshold to eliminate too small additional spheres; anyway, in order to get an accurate description of Σ_e, one has to keep also spheres of small size.

We have thus elaborated a variety of partitions of the spherical surfaces using polyhedra starting from some basic forms (tetrahedron, octahedron, dodecahedron, etc.) and progressively increasing the number of faces. The analysis of the results on the free energy obtained by using this set of new tessellations for the main (i.e. atomic) spheres shows that the pentakisdodecahedron actually is a good choice: it corresponds to an almost complete saturation of the tessera size effects. With a larger number of tesserae there is no appreciable changes in G, while by reducing the number there are remarkable deviations. This conclusion does not hold for the additional spheres: there is a beneficial to use a variable tessellation guided by the area of each tessera which must be kept as more constant as possible. The advantages are related not only to the reduction of the number of tesserae, and then of the dimension of the **O** matrix (see eq. 18), but also to the elimination of a part of the roughness in the description of the PES of the system we have lamented in discussing energy derivatives (Pomelli and Tomasi, unpublished results).

8.3 Cavity surface tessellation not based on atomic spheres

The GEPOL procedure we have mentioned becomes very expensive and leads to a too large number of tesserae when applied to solutes containing a large number of atoms. We started a couple of years ago the development of an alternative model, mostly addressed to large molecules (i.e. from 500 atoms upwards) but also applicable to smaller solutes [60]. The main field of application is not addressed to full QM *ab initio* calculations, but rather to molecular mechanic (MM) or hybrid QM/MM description of the solute [61] which we are now developing.

In this method, called DEFPOL, the cavity surface is defined starting form a single cavity of regular shape (the present version is limited to a sphere, covering all molecules having a closed structure topology, but formulas have been extended to the case of a torus, more suitable for systems characterized by structures with a hole). The sphere is then deformed to an ellipsoid according to the inertia axes of the molecule M, and enlarged to have all M atoms inside. The resulting surface is partitioned into tesserae (there are available different partitions all based on curvilinear triangles) and each tessera is examined and shifted to touch with all the three vertices the 'obstruction function' (i.e. the union of atomic van der Waals spheres); it can be also be splitted into smaller tesserae when the distance of its center with respect to the obstruction function is too large. This is in short the basic strategy, which is then complemented by several refining features.

The efficiency in dealing solvation energies ΔG_{sol} (all the contributions included) for large molecule is impressive: the gains in computational times with respect to GEPOL cavities are of the order of a magnitude for solutes with about 100 atoms, and increase further in passing to larger solutes, until to solute sizes (some enzymes) for which the memory demand of GEPOL cannot be satisfied by our computers. All the comparisons with the standard version of PCM have been thus far performed with formulations at the MM level (Pomelli and Tomasi, paper in elaboration). We also have now codes for *ab initio* HF calculations, and the results for small-medium molecules are in line with those obtained with standard methods, both for time and accuracy. We have not fully implemented the code of geometry derivatives, for which we have provisionally adapted a mathematical strategy differing from that described in section 6, which we shall also use for the PCM-QINT procedure we have shortly summarized in the same section.

The number of tesserae for large solutes (e.g. enzymes) can be by far smaller than with GEPOL: for example for the HIV protease the DEFPOL value is of the order of 1000 while the GEPOL analog is larger than 40000. In very large molecules the areas of DEFPOL tesserae are noticeably larger than in normal GEPOL-PCM and this fact could make it interesting to explore the use of other techniques of integration. We have already explored for tesserae of normal size the use of BEM techniques not limited to the first-level formulation, in which the value of the apparent charges at the representative point of each tessera is defined in terms of a single point function. In passing to higher levels of BEM formulations one may sample the surface functions better, but still leaving unchanged the dimension of the **O** matrix. We have used these more refined techniques in the earlier stages of the implementation of IEF, with a final choice of the simpler first level formulation as almost equally accurate and less time demanding, but probably there will be some gain in precision when the same techniques are applied to large DEFPOL tesserae.

These are, however, subjects to be treated in a future report of PCM progresses.

9 Final remarks

To complete this account it would have been convenient to report and to analyze some numerical results. Reasons of space forbid us to do it. We have stressed at the maximum the limits established by the Editors in the effort of making this review comprehensible, if not completely self-containing.

Numerical results can be found in the recent papers we have quoted: they represent the natural issue of our efforts, addressed to the elaboration of computational methods.

Reasons of space also obliged us to summarize some items in a few sentences, or even less, and to completely omit others, which should be at least mentioned; in the following sentences we shall try to give a brief summary of these omitted items.

There has been progress in the definition of the cavitation energy term: Floris and Tani are writing reports on that. The PCM method can be applied to a variety of QM levels of the theory: we mentioned a few, from MP2 to DFT, and we report here the most recent, the implementation given by Amovilli and Mennucci of the CASSCF method. The latter has been used to recast the MO wavefunction in terms of VB structures, and then applied to the study of reaction mechanisms. The formal aspects of the theory of linear response solutes within the PCM formalism, elaborated by Cammi, will be followed by implementations of other computational codes. Systematic studies on the hyperfine ESR coupling parameters have been performed by Barone and Cossi in collaboration with Nadia Rega; the same studies also regard a point of general interest: at what extent it is possible to replace with a continuum description solvent molecules which could play a direct role in determining the actual value of the physical observable under scrutiny. We have not yet numerical results on other topics on which we have a past experience, renovated now, namely the elaboration and use of tools for the interpretation of solvent effects on chemical reactions and for the description of dynamical effects in photochemical reactions. Chiara Cappelli is working on the first subject and there will be contributions to the second subject both by some authors of the present account and by Maurizio Persico and Paola Cattaneo who are exploiting their large experience in the accurate description of the dynamics of photochemical events.

To conclude, we hope that readers will share with us the feeling that ASC methods treating solvent effects open the possibility to introduce a large part of the quantum chemistry methods in the realm of solutions, with a computational cost comparable with that needed for isolated molecules. We also think that this report shows that PCM has a structure flexible enough to allow many other modifications, improvements and extensions. To do it a larger cooperative effort is required. We are willing to share with interested persons our experience. The codes for the advances reviewed here will be presented to Gaussian for distribution; other similar– but not identical – codes for a part of what said here have been prepared by Mennucci for GAMESS and are distributed with the last release of this package.

References

[1] J.G. Kirkwood; *J. Chem. Phys.* **2**, 351 (1934).

[2] D. Rinaldi and J.L. Rivail; Theor. Chim. Acta **32**, 57 (1973).

[3] J.L. Rivail and D. Rinaldi; Chem. Phys. **18**, 233 (1976).

[4] O. Tapia and G. Goschinski; *Mol.Phys.* **29**, 1653 (1975).

[5] B.T. Thole and P.Th. van Duijnen; *Theor. Chim. Acta* **55**, 211 (1980).

[6] S. Miertuš, E. Scrocco and J. Tomasi; *Chem. Phys.* **55**, 117 (1981).

[7] D. Rinaldi, M.F. Ruiz–López and J.L. Rivail; *J. Chem. Phys.* **78**, 834 (1983).

[8] J. Tomasi and M. Persico; *Chem. Rev.* **94**, 2027 (1994).

[9] J.L. Rivail and D. Rinaldi, in *Computational Chemistry, Review of Current Trends*, J. Leszczynski, Ed, World Scientific Publishing, 1995.

[10] C.J. Cramer D.G. and Truhlar, in *Solvent Effects and Chemical Reactivity*, O. Tapia and J. Bertrán Eds, Kluver, Dordrecht, 1995.

[11] M. Orozco, C. Alhambra, X. Barril, J.M. López, M.A. Busquets and F.J. Luque; *J. Mol. Model.* **2**, 1 (1996).

[12] (a) C.J. Cramer and D.G. Truhlar,*J. Am. Chem. Soc.* **113**, 8305 (1991); (b) D.A. Liotard, G.D. Hawkins, G.C. Lynch, C.J. Cramer and D.G. Truhlar, *J. Comp. Chem.* **16**, 422 (1994).

[13] B.H. Honig, K.A. Sharp and A.S. Yang; *J. Phys. Chem.* **97**, 1101 (1993).

[14] A. Ben–Naim *Water and Aqueous Solutions*, Plenum Press, New York, 1974.

[15] A. Ben–Naim *Solvation Thermodynamics*, Plenum Press, New York, 1987.

[16] R. Cammi and J. Tomasi; *J. Comp. Chem.* **16**, 1449 (1995).

[17] R. Cammi, M. Cossi, B. Mennucci and J. Tomasi, in *Theoretical Aspects of Biochemical Reactivity*, G. Náray-Szabó and A. Warshel Eds., Kluwer Academic Pub., 1997.

[18] C. Amovilli and B. Mennucci; *J. Phys. Chem.B* **101**, 1051 (1997).

[19] M. Cossi, B. Mennucci and J. Tomasi; *Chem. Phys. Lett.* **228**, 165 (1994).

[20] C.S. Pomelli and J. Tomasi; *J. Phys. Chem.A* **101**, 3561 (1997).

[21] H. Luo and S. Tucker; *J. Phys. Chem.B* **101**, 1063 (1997).

[22] C. Amovilli and R. McWeeny; *Chem. Phys.* **140**, 343 (1990).

[23] C. Amovilli; *Chem. Phys. Lett.* **229**, 244 (1994).

[24] (a) R. McWeeny;*Croat. Chem. Acta* **57**, 865 (1984); (b) P. Claverie in *Molecules in Physics, Chemistry and Biology*, J. Maruani, Ed, Kluwer, Dordrecht 1988; vol.2, p. 303.

[25] F. M. Floris and J. Tomasi; *J. Comp. Chem.* **10**, 616 (1989).

[26] F.M. Floris, J. Tomasi and J.L. Pascual-Ahuir; *J. Comp. Chem.* **12**, 784 (1991).

[27] F.M. Floris, A. Tani and J. Tomasi; *Chem. Phys. Lett.* **169**, 11 (1993).

[28] (a) H. Hoshi, M. Sakurai, Y. Inoue and R. Chûjô; *J. Chem. Phys.* **87**, 1107 (1987); (b) T. Furuki, M. Sakurai and Y. Inoue; *J. Comp. Chem.* **16**, 378 (1995).

[29] R. Cammi and J. Tomasi; *J. Chem. Phys.* **100**, 7495 (1994).

[30] R. Cammi and J. Tomasi; *J. Chem. Phys.* **101**, 3888 (1994).

[31] M .Cossi, B. Mennucci and R. Cammi; *J. Comp. Chem.* **17**, 57 (1996).

[32] V. Barone and M. Cossi; *J. Phys. Chem.* (submitted).

[33] A. Klamt and G. Schüürman; *J. Chem. Soc. Perkin Trans.* **2**, 799 (1993).

[34] T.N. Truong and E.V. Stefanovich; *Chem. Phys. Lett.* **240**, 253 (1995).

[35] (a) E. Cancès and B. Mennucci; J. Math. Chem. (submitted). (b) E. Cancès, B. Mennucci and J. Tomasi; *J. Chem. Phys.* (in press).

[36] B. Mennucci, M. Cossi and J. Tomasi; *J. Chem. Phys.* **102**, 6837 (1995).

[37] M.E. Davis and J. A. McCammon; *Chem. Rev.* **90**, 509 (1990).

[38] B. Mennucci, E. Cancès and J. Tomasi *J. Phys. Chem.* (submitted).

[39] C.S. Pomelli and J. Tomasi; *Theor. Chem. Acc.* **96**, 39 (1997).

[40] E.L. Coitiño, J. Tomasi and R. Cammi; *J. Comp. Chem.* **16**, 20 (1995).

[41] B. Mennucci, C. Amovilli and J. Tomasi; *J. Chem. Phys.* (submitted).

[42] R. Bonaccorsi, R. Cimiraglia and J. Tomasi; *J. Comp. Chem.* **4**, 567 (1983).

[43] M. Cossi, B. Mennucci, J. Pitarch and J. Tomasi; *J. Comp. Chem.* (submitted).

[44] B. Mennucci and J. Tomasi; *J. Chem. Phys.* **106**, 5151 (1997).

[45] M. Cossi, R. Cammi and J. Tomasi; *Int. J. Quant. Chem. Symp.* **29**, 695 (1995).

[46] J.L. Pascual-Ahuir, E. Silla, J. Tomasi and R. Bonaccorsi; *J. Comp. Chem.* **8**, 778 (1987).

[47] J.L. Pascual-Ahuir and E. Silla; *J. Comp. Chem.* **11**, 1047 (1990).

[48] J.L. Pascual-Ahuir, E. Silla and I. Tuñón ; *J. Comp. Chem.* **15**, 1127 (1994).

[49] V. Barone, M. Cossi and J. Tomasi (submitted).

[50] V. Barone, M. Cossi and J. Tomasi, *J. Chem. Phys.* (in press).

[51] R. Cammi, M. Cossi and J. Tomasi; *J. Chem. Phys.* **104**, 4611 (1996).

[52] R. Cammi, M. Cossi, B. Mennucci and J. Tomasi; *J. Chem. Phys.* **105**, 10556 (1996).

[53] R. Cammi, B. Mennucci and J. Tomasi, *Chem. Phys. Lett.* (submitted).

[54] R. Cammi, *J. Chem. Phys.* (submitted).

[55] K. Wolinski, J.F. Hinton and P. Pulay; *J. Am. Chem. Soc.* **112**, 825 (1990).

[56] (a) T.A. Keith and R.F.W. Bader; *Chem. Phys. Lett.* **210**, 154 (1993). (b) J.R. Cheeseman, G.W. Trucks, T.A. Keith, M.J. Frisch; *J. Chem. Phys.* **104**, 5497 (1996)

[57] (a) W. Kutzelnigg; *Isr. J. Chem.* **19**, 193 (1980); (b) M. Schindler and W. Kutzelnigg; *J. Chem. Phys.*,**76**, 1919 (1982).

[58] A.E. Hansen and T.D. Bouman; *J. Chem. Phys.* **82**, 5035 (1985).

[59] M. Bachs, F.J. Luque and M. Orozco; *J. Comp. Chem.* **15**, 237 (1994).

[60] R. Cammi, M. Cossi, B. Mennucci, C.S. Pomelli and J. Tomasi; *J. Comp. Chem.* **60**, 1165 (1996).

[61] (a) J. Gao; *Rev. Comp. Chem.* **7**, 119 (1996). (b) J. Tomasi and C.S. Pomelli, in *Encyclopedia of Computational Chemistry*, John Wiley & Sons, in press.

New *ab initio* VB interaction potential for molecular dynamics simulation of liquid water.

M. RAIMONDI, A. FAMULARI, E. GIANINETTI, M. SIRONI, R. SPECCHIO, AND I. VANDONI

Dipartimento di Chimica Fisica ed Elettrochimica and Centro CNR CSRSRC,
Università di Milano, via Golgi 19, 20133 Milano, Italy.

Abstract

SCF-MI (Self Consistent Field for Molecular Interactions) and non orthogonal CI were used to determine a water-water interaction potential, from which BSSE is excluded in an *a priori* fashion. The new potential has been employed in molecular dynamics simulation of liquid water at 25°C. The simulations were performed using MOTECC suite of programs. The results were compared with experimental data for water in the liquid phase, and good accordance was found, both in radial distribution functions and thermodynamic properties, as well as in geometric parameters.

I. Introduction 2
II. The water-water interaction potential 3
III. BSSE free *ab initio* intermolecular interaction potentials 5
IV. Results and discussion
V. *Ab initio* calculations 9
VI. Molecular dynamics simulation 11
VII. Simulation results 12
VIII. IR and Raman spectra 17
IX. Conclusions 20
References

ADVANCES IN QUANTUM CHEMISTRY, VOLUME 32
Copyright © 1999 by Academic Press. All rights of reproduction in any form reserved.
0065-3276/99 $30.00

I. Introduction

Statistical classical mechanics states that, in principle, it is possible to deduce macroscopic system properties from its time evolution in the phase space. This requires nuclear potential energy as a function of the atomic coordinates of the system to be known. To determine the shape of the potential energy, models are considered which acceptably reproduce the greatest number of experimental physical properties of the system. The parameters included in the analytical expression of the potential are chosen so as to be consistent with experimental data (semiempirical potentials) or with the energy value calculated by means of *ab initio* methods.

Models of this kind are employed in molecular dynamics simulations, to determine static and dynamic properties of a given system; this permits to verify the consistency and reliability of the model, to explain the molecular origin of physical characteristics of a system or to calculate properties for which no experimental data are available. Great interest has been devoted, for example, to the study of the structure and dynamics of liquid water, ice and solutions. Liquid water simulations are used to represent the hydrogen bond network in the liquid phase and to explain some unusual and not yet understood properties of water, such as its high thermal capacity, in terms of its structure. Still more important is the elucidation of the molecular origin of dynamic phenomenons such as the solvations of ions in water and the interaction of macromolecules with the solvent.

Rahman and Stillinger (1971) have applied to the study of liquid water a model potential, named ST2, which could anticipate the existence of the so called "high frequency sound" years before this collective excitation of water molecules was observed, by means of inelastic neutron scattering experiments (Texeira, Bellisent-Funel, Chen and Dorner,(1985). Lie and Clementi (1986) obtained a notable model potential for water from extensive *ab initio* calculations.

This statistical classical mechanics approach gives rise to a series of problems. It is questionable whether a computational method which assumes the validity of classical mechanics can reproduce the physical properties of a system. It is well known, in fact, that the study of intramolecular vibrations requires a quantum mechanical approach.

Two routes are available to obtain such quantum mechanical description: a simulation can be realised with the *path integral molecular dynamics* method (PIMD), recently applied to liquid water (Billeter, King and van Gunsteren, 1994), or a classical dynamics simulation can be realised, with an *a posteriori* corrections of the results (Berens, Mackay, White and Wilson, 1983; Berens and Wilson, 1981). The latter choice has been made for the calculation of gaseous CO spectra in liquid argon (Berens and Wilson, 1981).

Moreover, the phase space volume considered in the course of a simulation is truncated and some properties cannot be obtained with the desired accuracy. The molecular dynamics simulation evaluates the properties that are a consequence of the motion of an isolated particle more accurately than those which originate from collective phenomenons. The former, in fact, can be averaged among all the system molecules as well as over different time intervals. Thermodynamical properties are thus determined less accurately than the internal molecular geometry or the molecular dipole moment.

In the present work a model potential for water will be described which, once inserted in a molecular dynamics simulation, excluding the value of the internal pressure, satisfyingly reproduces the physical properties of the system at ambient temperature and density. A general *ab initio* VB approach, based on the SCF-MI (Self Consistent Field for Molecular Interactions) procedure (Gianinetti *et al.*, 1996), was used to determine the water-water pair interaction potential, from which BSSE is excluded in an *a priori* fashion. The recent generalisation of the SCF-MI method (Gianinetti *et al.*, 1997) allowed to compute without BSSE also non-additive many body contributions to the total polarisation interaction energy. The simulations were performed using MOTECC suite of programs (Sciortino, Corongiu and Clementi, 1994). The results were compared with previous simulations and with experimental data for water in the liquid phase.

We underline that this scheme allows a complete elimination of BSSE in an *a priori* fashion, a fact which seems of vital importance to generate a satisfyingly reliable *ab initio* potential.

II. The water-water interaction potential

In this paragraph a short summary of NCC (Niesar, Corongiu, Clementi, Kneller and Bhattacharya, 1990), a polarizable and flexible water-water interaction model first proposed by Niesar, Corongiu, Clementi, Kneller and Bhattacharya, (1990), will be presented.

According to this approach, the interaction energy among water molecules in the liquid phase can be expressed in terms of a many-body potential (Niesar, Corongiu, Clementi, Kneller and Bhattacharya, (1990):

$$U = V + V_{pol}$$

(1).

The term V contains two contributions arising from intermolecular and intramolecular motions and is defined as:

$$V = \sum_{i<j} V_{ij}\left(r_{\alpha\beta}, a_k\right) + \sum_{i} V_{INTRA}\left(q_{i\alpha}\right)$$

(2)

where i and j define all the molecules of the system, $r_{\alpha\beta}$ are the intermolecular distances and $q_{i\alpha}$ are the internal coordinates of the molecule. Coupling between intermolecular and intramolecular motions are considered negligible, so that the parameters a_k can be regarded as constants. In the following discussion an analytical form for the additive portion of the potential will be considered, which derives from the point charge model originally proposed by Bernal and Fowler (1933). According to this model, positive charges q are located at the position of the two hydrogen atoms of each water molecule (1, 2, 3 and 4), and a negative charge -2q is positioned at a point P along the C_{2v} symmetry axis of the molecule (7, 8) at a fixed distance from the oxygen atom (5, 6) (see Fig. 1). The analytical expression of the pairwise additive part of the potential is therefore (Niesar, Corongiu, Clementi, Kneller and Bhattacharya, (1990):

$$\begin{aligned}
V_{\mathrm{INTER}}(r_{\alpha\beta}) &= q^2\left(\frac{1}{r_{13}}+\frac{1}{r_{14}}+\frac{1}{r_{23}}+\frac{1}{r_{24}}\right)+\frac{4q^2}{r_{78}}-2q^2\left(\frac{1}{r_{81}}+\frac{1}{r_{82}}+\frac{1}{r_{73}}+\frac{1}{r_{74}}\right)+\\
&+A_{OO}\,e^{-B_{OO}\,r_{56}}+A_{HH}\left(e^{-B_{HH}\,r_{13}}+e^{-B_{HH}\,r_{14}}+e^{-B_{HH}\,r_{23}}+e^{-B_{HH}\,r_{24}}\right)+A_{OH}\left(e^{-B_{OH}\,r_{53}}+\right.\\
&\left.+e^{-B_{OH}\,r_{53}}+e^{-B_{OH}\,r_{61}}+e^{-B_{OH}\,r_{62}}\right)+A'_{OH}\left(e^{-B'_{OH}\,r_{53}}+e^{-B'_{OH}\,r_{54}}+e^{-B'_{OH}\,r_{61}}+e^{-B'_{OH}\,r_{62}}\right)+\\
&A_{PH}\left(e^{-B_{PH}\,r_{73}}+e^{-B_{PH}\,r_{74}}+e^{-B_{PH}\,r_{81}}+e^{-B_{PH}\,r_{82}}\right)+A_{PO}\left(e^{-B_{PO}\,r_{76}}+e^{-B_{PO}\,r_{85}}\right)
\end{aligned} \qquad (3).$$

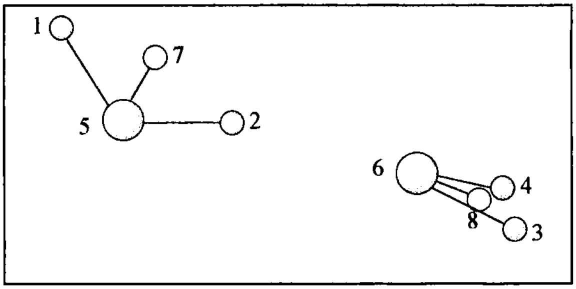

Fig. 1. Water dimer atom labels.

The geometry of the rigid water molecule corresponds to that of an isolated water molecule in the gas phase (OH bond length = 0.9572 Å; HOH angle = 104.52°) (Benedict, Gailar and Plyler, 1956). The terms A_{PH} and A_{PO} in Eq. (3) are needed to correct the model potential behaviour at short distances.

As regards intramolecular motions, the *ab initio* D-MBPT(∞) potential is employed (Bartlett, Shavitt and Purvis, 1979), which is expressed, up to the quartic terms, as a function of the three internal coordinates of water, and is obtained from many body perturbation theory.

The term V_{pol} in Eq. (1) is a polarisation contribution which includes the many-body non-additive effects. It has been demonstrated (Clementi and Corongiu, 1983) that the many-body corrections are necessary for an accurate quantitative prediction of the system properties. These effects are included by ascribing to each molecule a dipole moment and a bond polarizability, according to the classical model (Böttcher, 1973). Within this scheme the polarisation energy can be expressed as:

$$V_{pol} = -\frac{1}{2}\sum_{i}^{N_m}\sum_{\lambda}^{N_d} \vec{\mu}_{i_\lambda} \vec{E}_{i_\lambda} \tag{4}$$

where:

$$\vec{\mu}_{i_\lambda} = \vec{\alpha}_{i_\lambda} \vec{E}_{i_\lambda} \tag{5}$$

and:

N_m is the total number of system molecules;

N_d is the number of induced dipole moments per molecule;

$\vec{\mu}_{i_\lambda}$ is the induced dipole moment on the λ-th bond of the i-th molecule;

$\vec{\alpha}_{i_\lambda}$ is the polarizability of the λ-th bond of the i-th molecule;

$\vec{E}_{i_\lambda}$ is the total electric field acting on the λ-th bond of the i-th molecule;

Aiming to obtain a non-empirical potential to be used for liquid water simulations, the parameters of the NCC model described above are determined by fitting to extensive *ab initio* calculations, which will be presented in a following section.

III. BSSE free *ab initio* intermolecular interaction potential

A general *ab initio* VB wavefunction consisting of single and double excitations out of the SCF-MI determinant, are used to determine an *ab initio* interaction potential apt to the dynamics simulation of liquid water. A short summary of the theory involved will be presented. For a more detailed account see (Gianinetti *et al.*, 1996; Famulari, 1997; Specchio, 1997). The chosen scheme permits to eliminate BSSE in an *a priori* fashion, both at the SCF and at the correlated level.

The BSSE is a well known inconvenience which strongly affects the intermolecular potential investigations of weakly interacting systems, such as van der Waals or hydrogen bonded systems. In such systems, it is common that the BSSE is of the same order of magnitude of the interaction energy involved. The most frequently employed *a posteriori* method to correct this error is the counterpoise technique (Boys and Bernardi, 1970). Nevertheless, many authors have emphasised that the method introduced by Boys and Bernardi does not realise a clear and precise determination of the BSSE magnitude (van Duijneveldt, van Duijneveldt-van de Rijdt and van Lenthe, 1994). In addition, it is worth emphasising that the SCF-MI "*a priori*" strategy to avoid BSSE is *always* correct and not only for full CI wavefunctions as in the case of the CP *a posteriori* procedure (van Duijneveldt, van Duijneveldt-van de Rijdt and van Lenthe, 1994). Furthermore, the addition of the partner's functions introduces other spurious contributions - the "secondary superposition error" - owing to the improper modification of multipole moments and polarizabilities of the monomers. This becomes particularly important in the case of anisotropic potentials where these new errors in the wavefunction introduced by the CP procedure can contribute to alter the shape of the PES and the resulting physical picture.

Recently, the SCF-MI algorithm (Gianinetti *et al.*, 1996) has been implemented (Famulari *et al.*, 1997a) into the GAMESS suite of programs (Schmidt *et al.*, 1993). Within this scheme the one determinant wavefunction of the supersystem AB is written as

$$\begin{aligned}\Psi_{AB} = (N!)^{-\frac{1}{2}} \mathcal{A}\Big[\Phi_1^A(1)\overline{\Phi}_1^A(2)\ldots\overline{\Phi}_{N_A}^A(2N_A)\Phi_1^B(2N_A+1)\overline{\Phi}_1^B(2N_A+2)\ldots \\ \ldots\overline{\Phi}_{N_B}^B(2N_A+2N_B)\Big]\end{aligned} \qquad (6)$$

where the molecular orbitals of each fragment are free to overlap with each other. The orbitals of fragment A ($\Phi_1^A\ldots\Phi_{N_A}^A$) and the orbitals of fragment B ($\Phi_1^B\ldots\Phi_{N_B}^B$) are expanded in two different subsets of the total basis set $\chi = \{\chi_k\}_{k=1}^{M}$, $\chi^A = \{\chi_p^A\}_{p=1}^{M_A}$ centred on A and $\chi^B = \{\chi_q^B\}_{q=1}^{M_B}$ centred on B:

$$\begin{aligned}\Phi_i^A &= \sum_{p=1}^{M_A} \chi_p^A T_{pi}^A \qquad & i = 1\ldots N_A \\ \Phi_j^B &= \sum_{q=1}^{M_B} \chi_q^B T_{qj}^B \qquad & j = 1\ldots N_B\end{aligned} \qquad (7a)$$

with $N=2N_A+2N_B$ and $M=M_A+M_B$, or in matrix form

$$\mathbf{\Phi}^A = \boldsymbol{\chi}^A\mathbf{T}^A \qquad \mathbf{\Phi}^B = \boldsymbol{\chi}^B\mathbf{T}^B \qquad (7b).$$

These restrictions obviously permit the complete elimination of BSSE in an *a priori* fashion, by assuming and maintaining the orbital coefficient variation matrix in block diagonal form:

$$\delta\mathbf{T} = \begin{bmatrix} \delta\mathbf{T}_A & \mathbf{0} \\ \mathbf{0} & \delta\mathbf{T}_B \end{bmatrix} \tag{8}$$

From these premises it follows that the general stationary condition is equivalent to the coupled secular problems:

$$\begin{cases} \mathbf{F}'_A\mathbf{T}_A = \mathbf{S}'_A\mathbf{T}_A\mathbf{L}_A \\ \mathbf{T}_A^+\mathbf{S}'_A\mathbf{T}_A = \mathbf{I}_A \end{cases} \qquad \begin{cases} \mathbf{F}'_B\mathbf{T}_B = \mathbf{S}'_B\mathbf{T}_B\mathbf{L}_B \\ \mathbf{T}_B^+\mathbf{S}'_B\mathbf{T}_B = \mathbf{I}_B \end{cases} \tag{9}$$

where the effective Fock and overlap matrixes **F'** and **S'** possess the correct asymptotic behaviour. By means of a general variational approach, the interaction energy is expressed as:

$$\Delta E_{SCF-MI} = E^{AB}_{SCF-MI} - E^{A}_{SCF} - E^{B}_{SCF}$$

To take the correlation contribution to water dimer interaction energy into account, a very compact multi-structure VB - non-orthogonal CI - calculation is carried out. With this aim, a method to obtain virtual orbitals corresponding to the SCF-MI wavefunction which furnishes an energetic contribution of the same accuracy as very extended CI calculations, was developed. In order to avoid that BSSE switches on, both the occupied Φ_a^A - Φ_b^B and virtual Φ_{a*}^A - Φ_{b*}^B SCF-MI orbitals are constrained to the restrictions

$$\Phi_a^A = \sum_{p=1}^{M_A}\chi_p^A T_{pa}^A\,,\quad \Phi_b^B = \sum_{q=1}^{M_B}\chi_q^B T_{qb}^B\,,\quad \Phi_{a^*}^A = \sum_{p=1}^{M_A}\chi_p^A T_{pa^*}^A\,,\quad \Phi_{b^*}^B = \sum_{q=1}^{M_B}\chi_q^B T_{qb^*}^B \tag{10}$$

The above constraints imply the *non-orthogonality* of the orbitals.

The resulting wavefunction is assumed to have a general Valence Bond form:

$$\Psi_{AB} = C_0\Psi_{AB}^0 + \sum_{a=1}^{Na}\sum_{b=1}^{Nb} C_{ab}\Psi_{ab}^{a*b*} + \sum_{a=1}^{Na} C_a\Psi_a^{a*} + \sum_{b=1}^{Nb} C_b\Psi_b^{b*} \tag{11}$$

It represents the configuration interaction between the SCF-MI wavefunction

$$\Psi_{AB}^0 = |\Phi_1^A\overline{\Phi}_1^A\Phi_2^A\overline{\Phi}_2^A..\overline{\Phi}_{Na}^A\Phi_1^B\overline{\Phi}_1^B\Phi_2^B\overline{\Phi}_2^B..\overline{\Phi}_{Nb}^B >$$

(12),

the singly excited *localised* configuration state functions

$$\Psi_{a}^{a*} = |\Phi_{1}^{A}\overline{\Phi}_{1}^{A}..\Phi_{a}^{A}\Phi_{a*}^{A}..\overline{\Phi}_{Na}^{A}\Phi_{1}^{B}\overline{\Phi}_{1}^{B}..\Phi_{b}^{B}\overline{\Phi}_{b}^{B}..\overline{\Phi}_{Nb}^{B}\Theta_{0,0;1}^{2} >$$

$$\Psi_{b}^{b*} = |\Phi_{1}^{A}\overline{\Phi}_{1}^{A}..\Phi_{a}^{A}\overline{\Phi}_{a}^{A}..\overline{\Phi}_{Na}^{A}\Phi_{1}^{B}\overline{\Phi}_{1}^{B}..\Phi_{b}^{B}\Phi_{b*}^{B}..\overline{\Phi}_{Nb}^{B}\Theta_{0,0;1}^{2} >$$

and the doubly excited *localised* configuration state functions

$$\Psi_{ab}^{a*b*} = |\Phi_{1}^{A}\overline{\Phi}_{1}^{A}..\Phi_{a}^{A}\Phi_{a*}^{A}..\overline{\Phi}_{Na}^{A}\Phi_{1}^{B}\overline{\Phi}_{1}^{B}..\Phi_{b}^{B}\Phi_{b*}^{B}..\overline{\Phi}_{Nb}^{B}\Theta_{0,0;2}^{4} >$$

(13)

obtained by simultaneous single excitation localised on A and B, where the singlet spin function for the two or four electrons involved in the single or double excitation are:

$$\Theta_{0,0;1}^{2} \text{ and } \Theta_{00}^{4} = C_1\Theta_{0,0;1}^{4} + C_2\Theta_{0,0;2}^{4}$$

(14).

The virtual orbitals Φ_{a*}^{A} and Φ_{b*}^{B} are determined according to the approximation that they maximise separately the dispersion contribution of each of the two configuration wavefunctions

$$\Psi'_{AB} = C_0\Psi_{AB}^{0} + C_{ab}\Psi_{ab}^{a*b*}$$

(15),

where "a" labels one specific occupied MO of fragment A and "b" one specific occupied MO of fragment B. The dimension of the virtual space so generated is given by the product of the *active* occupied MOs of fragments A and B, respectively.

The associated virtual orbitals are determined at the variation-perturbation level of theory by minimisation of the second order expression of the energy:

$$E^{(2)} = H_{00} + \sum_{a=1}^{N_A}\sum_{b=1}^{N_B} \frac{\left[H_{(0,ab)} - H_{00}S_{(0,ab)}\right]^2}{H_{00}S_{(ab,ab)} - H_{(ab,ab)}}$$

by satisfying the conditions

$$\frac{\partial E^{(2)}}{\partial \Phi_{a*}^{A}} = 0 \qquad \frac{\partial E^{(2)}}{\partial \Phi_{b*}^{B}} = 0$$

(16).

The minimisation strategy is the specialisation to the case of a SCF-MI zero order wavefunction of the algorithm previously described by Raimondi *et al.* (1996) in the context of the Spin Coupled theory. Acceleration of the minimisation procedure now includes the approximate evaluation of the Hessian as described by Clarke *et al.* (1997). It should be underlined that in this scheme the *a priori* exclusion of BSSE is still operative, as the virtual orbitals are expanded on the two distinct subsets centred on A and B, see Eq. (10).

The virtual orbitals obtained by means of the perturbation theory approximation are then employed to construct a full set of all the singly- and doubly-excited configurations which provide the final VB-like wavefunction Eq. (11). Finally, the multi structure VB (non-orthogonal CI) problem is set up and solved variationally according to standard VB techniques, see Raimondi *et al.* (1977) and Cooper *et al.*, (1987).

In the present case, for each water molecule we considered an *active* space of four MOs with one MO (oxygen $1s^2$ electrons) kept *frozen*. The resulting dimension of the *virtual* space of each fragment is sixteen, corresponding to four virtual orbitals for each occupied MO. This implies a set of 32 *vertical* singly excited configurations. By adding all the corresponding *vertical* doubly excited spatial configurations the final VB-like wavefunction was generated. By taking the dimension of the spin space into account, the size of the resulting VB matrix is 545.

IV. Results and discussion

V. *Ab initio* calculations

The water dimer interaction energy was investigated at the Hartree-Fock and correlated level using SCF-MI and the VB-like wavefuntion described above. The 7s4p2d/4s2p basis set proposed by Millot and Stone (1992) was employed in both cases. This basis set reproduces well the Hartree Fock limit results obtained by Famulari *et al.* (1997b). Optimal geometry, calculated employing the VB-like wavefunction Eq. (11), is in good accordance with the experimental data (see Table I and Fig. 2). The binding energy value of -4.67 Kcal/mol falls within the experimental range (see Table II).

TABLE I

Optimised geometrical parameters for the water dimer system (see Fig. 2).

	VB Present work	Exp. (a)	SAPT MBPT4 (b)	MP4 (c)
R o-o(Å)	3.00	2.98±0.03	2.953	2.949
β°	134.5	122.0±10	124	124.8
Φ°	2.5	0.0±10	6.8	5.35

(a) Dyke, Mack and Muenter (1977);
(b) Mas and Szalewicz (1996);
(c) van Duijneveldt-van de Rijdt and van Duijneveldt (1992).

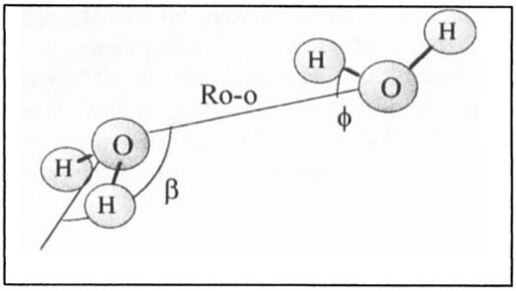

Fig. 2. Intermolecular coordinates in the water dimer system.

TABLE II

Water dimer binding energy.

Oxygen (a)	Hydrogen (a)	Total	ΔE_{VB} Present work Kcal/mol	ΔE_{Exp} (b) Kcal/mol	ΔE_{Exp} (c) Kcal/mol
7s4p2d	4s2p	102	-4.67	-5.2±0.7	-5.44±0.7

(a) Millot and Stone (1992);
(b) Mas and Szalewicz (1996);
(c) Curtiss, Frurip and Blander (1979).

All the parameters which appear in the NCC potential expression are determined by the present VB *ab initio* calculations. In this way a new non empirical potential used in the simulation of liquid water was obtained. The calculations include the determination of the interaction energy relative to 225 configurations of the water dimer and of the non additive three-body contributions relative to 28 trimer configurations.

As regard the calculations on the trimer, the quantity in question is expressed as follows:

$$\begin{aligned}&\Delta E_{\text{non-additive}}(1,2,3) = \Delta E(1,2,3) - \Delta E(1,2) - \Delta E(1,3) - \Delta E(2,3) = \\ &E(1,2,3) - E(1,2) - E(1,3) - E(2,3) + E(1) + E(2) + E(3)\end{aligned} \tag{18}$$

where E(1,2,3) is the Hartree-Fock energy of the (1,2,3) cluster. Also in this case, the interaction energy is BSSE free, as the calculations are performed by employing the n-body extension (Gianinetti, Vandoni, Famulari and Raimondi, 1997; Famulari, 1997) of the SCF-MI method. As it has been shown elsewhere (Habitz, Bagus, Siegbahn and Clementi, 1983), the main contribution to the three-body non-additivity derives from induction effects, while corrections due to electronic correlation are mostly additive. For this reason, such contributions are determined at the Hartree-Fock level and fitted to provide the parameters in Eq. (1) defining the many body non-additive polarisation contributions to the new *ab initio* VB NCC-like potential. Geometries are generated starting from the minimum energy configuration of the trimer by varying the relative O-O distances of the three molecules, with the hydrogens moving rigidly and maintaining their relative positions with respect the plane of the oxygen's.

The calculations on the water dimer are performed at the VB level, with single and double excitations, according to the scheme already discussed. Inclusion of the intermolecular correlation is thus guaranteed. The 225 points of the PES computed for the water dimer included 13 configurations corresponding to the "closed" or "cyclic" structures. The energies corresponding to other 22 "open" configurations, near the minimum, were also calculated. It is to be noted that, although the "bifurcated" structures are attractive, they do not correspond to a local minimum, as sometimes reported (Muggiest, Robins and Bassez-Muguet, 1991).

VI. Molecular dynamics simulation

The molecular dynamics simulation is performed using the MOTECC suite of programs (Sciortino, Corongiu and Clementi, 1994) in the context of microcanonical statistical ensemble. The system considered is a cube with periodic boundary conditions, which contains 343 water molecules. Compatibility of this data with the water experimental density of 0.998 g/cm^3 requires a cube with a side length of 21.7446 Å. In accordance with the polarizable model, a spherical cutoff with radium equal to half of the simulation cube side is imposed, together with a switching function to suppress energy drift.

The interaction of a single molecule with molecules whose oxygen atoms are outside the cutoff sphere are not calculated directly from Eq. (1), but by means of Ewald sum for Coulomb interactions. The equations of motion are integrated with a Gear prediction-correction algorithm at the sixth order. During the initial equilibration time, velocities are scaled every ten steps in order to fulfil the relation:

$$< \frac{1}{2}\sum_{i}^{N} m_i v_i^2 >= \frac{3}{2} N k_B T \qquad (19)$$

where T is the temperature imposed on the system (this relation is used for all translational, rotational and vibrational degrees of freedom, so that there will be a temperature relative to each degree of freedom).

Each step is 2.0 10^{-16} s long. In fact, the prediction-correction algorithm is more accurate for small time steps, and moreover, molecular vibrational frequencies are above 10^{14} s^{-1}.

The equilibration period is 25000 time steps, that is 5ps long. During the following 10 ps, corresponding to 50000 steps, atomic position and velocities and dipole moments of the molecules are evaluated every 10 steps, and stored for the subsequent analysis of the system properties.

VII. Simulation results

During the 10 ps of simulation time, temperature was equal to 299±5.95 K. The potential energy of the system of -40.56±0.22 kJ/mol is to be compared with the experimental value for the vaporisation enthalpy of liquid water at 298 K, which is -41.5 kJ/mol. The computed molecular dipole moment in the liquid is 2.48±0.01 D, to be compared with the experimental value of 2.4-2.6, see Table IV, and a value of 1.83 D predicted by the model potential for the isolated molecule.

The contributions to the total energy of the molecule obtained during the simulation are shown in Table III.

TABLE III

Contributions to the total potential energy of the liquid water.

	E (kJ/mol)
V_{KIN}	11.19±0.22
V_{INTRA}	4.93±0.20
$V_{TWO\text{-}BODY}$	-36.01±0.24
V_{POL}	-9.48±0.20
V_{TOT}	-29.378±0.010

It should be noticed that, in contrast with previous simulation results by Niesar, Corongiu, Clementi, Kneller and Bhattacharya, 1990 - NCC-flex -, the main contribution to the total potential energy comes from the two-body term, the many-body polarisation term contributing to the total potential energy only for the 23%.

Some of the properties calculated during the simulation are reported in Table IV.

TABLE IV

Contributions to the total potential energy of the liquid water.

	ΔU (kJ/mol)	Press. (atm.)	μ (D)	ε	C_V (cal/mol K)
PPC (a)	-41.4	-	2.51	77	-
PSPC (b)	-38.0	-	-	-	-
SPC/E (c)	-41.5	400	-	-	-
SPC/E(PIMD) (d)	-44.56	-	-	-	-
RER(pair) (e)	-41.6	-98	-	-	-
RER(pol) (e)	-41.2	-197	-	-	-
ST2 (f)	-38.20	3000	-	-	-
MCYL (g)	-35.40±0.6	7900	2.259	26±14	26.5
NCC-flex (h)	-44.88±0.25	-2160±364	3.08	-	(17.6) (i)
Present work (two body only)	-38.89±0.21	553±131	-	-	18.7
Present work (many-body included)	-40.56±0.22	724±156	2.48±0.01	54±10	22.2
Exp.	-41.5 (j)	~1	2.4-2.6	80	17.9 (k)

(a) Svishchev, Kusakik, Wang and Boyd (1996);
(b) Ahlstrom, Wallqvist, Engstrom and Jonsson (1989);
(c) Berendsen, Grigera and Straatsma (1987);
(d) Billeter, King and Van Gunsteren (1994);
(e) Wallqvist and Berne (1993);
(f) Rahman and Stilliger (1971);
(g) Lie and Clementi (1986);
(h) Corongiu (1992);
(i) Niesar, Corongiu, Clementi, Kneller and Bhattacharya, (1990);
(j) Jorgensen, Chandrasekhar, Madura, Impey and Klein (1983);
(k) Kell, G. S. (1971).

As it can be seen in Table IV, all the results of the simulation computed using the present *ab initio* VB potential turn out encouraging. Even the computed internal pressure, although incompatible with the experimental data, is greatly improved with respect to the corresponding MCYL (two body only) or NCC-flex (many-body) results obtained by Lie and Clementi (1986) and by Corongiu (1992). Addition of the many body terms gives a computed internal pressure of about 700 atm to be compared with a value of about 500 atm obtained with the two body only potential. The fact that the calculated values of the internal pressure can change much after small changes in the potential surface has been the subject of a thorough discussion by Niesar, Corongiu, Huang, Dupuis and Clementi, (1989); the variation of about 200 atm obtained in the present work when including the effect of many-body polarisation interactions, can be assumed as a very encouraging result confirming the consistency of the new *ab initio* VB potential.

In Table V the calculated geometry of the water molecule in liquid and gas phase is reported.

TABLE V

Calculated geometric parameters of water molecule in gas and liquid phase compared with the experimental values.

	Gas phase		Liquid phase		
	<ROH> (Å)	HOH (deg)	<ROH> (Å)	HOH (deg)	<RHH> (Å)
Present work	0.9576	104.59	0.972	102.75	1.52
Exp. (a,b)	0.9572	104.52	0.966±0.006	(102.8) (c)	1.510±0.01

(a) Benedict, Gailar and Plyler (1956);
(b) Thiessen and Narten (1982);
(c) Calculated from <ROH> and <RHH>.

Fig. 3-6 and Tables VI-VIII show the experimental and computed site-site pair correlation functions $g_{OO}(r)$, $g_{OH}(r)$ and $g_{HH}(r)$. The relative position and intensities of peaks are reported in Tables VI-VIII.

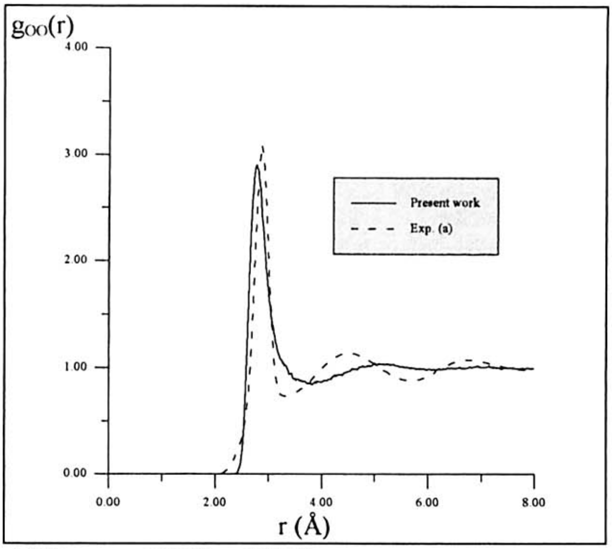

(a) Soper and Phillips (1986).

Fig. 3. Site-site pair correlation functions $g_{OO}(r)$.

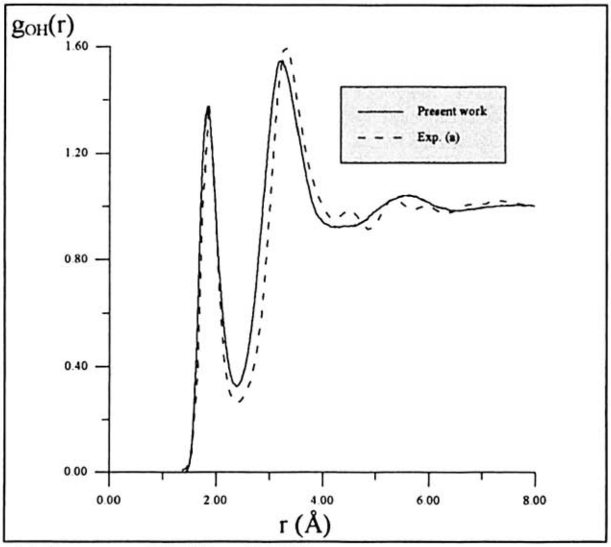

(a) Soper and Phillips (1986).

Fig. 4. Site-site pair correlation functions $g_{OH}(r)$.

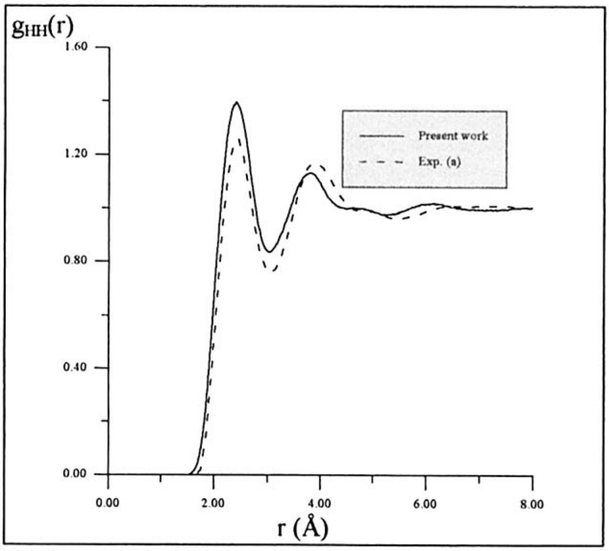

(a) Soper and Phillips (1986).

Fig. 5. Site-site pair correlation functions $g_{HH}(r)$.

TABLE VI

Position and intensities (in parenthesis) of the peaks of $g_{OO}(r)$.

	1st Max (Å)	1st min (Å)	2nd Max (Å)	2nd min (Å)
Present work	2.77 (2.93)	3.68 (0.88)	4.77 (1.04)	-
Exp.(neutron diffr.) (a)	2.89 (3.09)	3.32 (0.73)	4.53 (1.14)	5.6 (0.88)
Exp.(X ray diffr.) (b)	2.83 (2.31)	3.45 (0.85)	4.53 (1.12)	5.6 (0.86)

(a) Soper and Phillips (1986);
(b) Narten and Levy (1971).

TABLE VII

Position and intensities (in parenthesis) of the peaks of $g_{OH}(r)$.

	1st Max (Å)	1st min (Å)	2nd Max (Å)	2nd min (Å)
Present work	1.83 (1.37)	2.40 (0.33)	3.24 (1.55)	4.23 (0.92)
Exp.(neutron diffr.) (a)	1.85 (1.38)	2.35 (0.26)	3.35 (1.60)	4.25 (0.95)
Exp.(X ray diffr.) (b)	1.90 (0.80)	2.45 (0.50)	3.35 (1.70)	-

(a) Soper and Phillips (1986);
(b) Narten and Levy (1971).

TABLE VIII

Position and intensities (in parenthesis) of the peaks of $g_{HH}(r)$.

	1st Max (Å)	1st min (Å)	2nd Max (Å)	2nd min (Å)
Present work	2.40 (1.40)	3.03 (0.83)	3.81 (1.13)	-
Exp.(neutron diffr.) (a)	2.45 (1.26)	3.05 (0.76)	3.85 (1.17)	5.45 (0.96)
Exp.(X ray diffr.) (b)	2.35 (1.04)	3.00 (0.47)	4.00 (1.08)	-

(a) Soper and Phillips (1986);
(b) Narten and Levy (1971).

The number of the first neighbours around a central water molecule, calculated by integration of the correlation function $g_{OO}(r)$ up to the position of the first minimum, is 5.5. This result is consistent with a local tetrahedron with addition of contributions from some interstitial coordination. The computed $g_{OO}(r)$ shows a long range structure which decays faster than the experimentally based function. In particular, the second peak results lower. This can be ascribed to a variety of factors, including an incomplete determination of the two body potential, due to basis and configuration spaces not large enough. In addition, it is possible that the many-body contribution to the potential, approximated with a three-body term only, could be responsible of this loss in structure for the simulated liquid.

The correlation functions $g_{OH}(r)$ and $g_{HH}(r)$ are in good accordance with experimental data. By integrating $g_{OH}(r)$ up to the first minimum a value of 1.92 is obtained. This means that each water molecule forms 3.84 hydrogen bonds with its first neighbours, allowing to conclude that at room temperature, the four nearest water molecules are preferentially oriented in a tetrahedron configuration.

The comparison between the simulation which includes only two-body effects and the one obtained including many body terms (see Table IV) shows a perfect equivalence as regards the calculated properties of the liquid phase. The many body contribution plays a fundamental role only in the position of the second peak of the site-site pair correlation function $g_{OO}(r)$, which shows a greater accordance with the experimental.

VIII. IR and Raman spectra

IR and Raman spectra are calculated by means of autocorrelation function of the dipole moment and of the polarizability tensor of the system. The characteristics of the spectra, shown in Fig. 6 and 7, are reported in Table IX.

TABLE IX

IR and Raman band of liquid water.

Vibrational band (cm^{-1})	Infra-Red Exp. (a)	Infra-Red Present work	High Frequency Raman Exp. (a)	High Frequency Raman Present work
Hindered translation ν_{T2}		Weak band $\nu \approx 65$		
Hindered translation ν_T	Band appears as shoulder of ν_L band $\nu \approx 193$	Band appears as shoulder of ν_L band $\nu \approx 190$		
Libration ν_L	Very broad band extending from 300 cm^{-1} to 900 cm^{-1} with principal maximum at: $\nu \approx 685$	Very broad band extending from 300 cm^{-1} to 900 cm^{-1} with principal maximum at: $\nu \approx 651$		
H-O-H bending ν_2	$\nu \approx 1645$	$\nu \approx 1726$	$\nu \approx 1640$	$\nu \approx 1726$
Association ν_A	$\nu \approx 2125$	$\nu \approx 2185$		
O-H stretching ν_S	Very broad band with two principal maxima and a shoulder: $\nu \approx 3280$ $\nu \approx 3490$ $\nu \approx 3920$	Very broad band with two principal maxima: $\nu \approx 3615$ $\nu \approx 3746$	Very broad band with principal maximum at: $\nu \approx 3439$	Very broad band with principal maximum at: $\nu \approx 3583$

(a) Eisenberg and Kauzmann (1969).

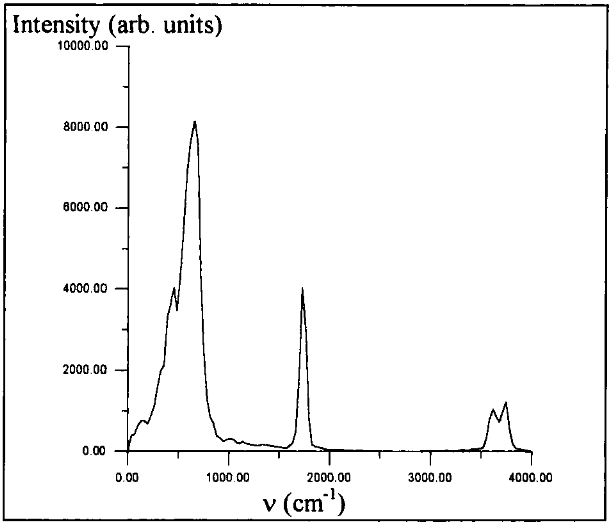

Fig. 6. Calculated IR spectra.

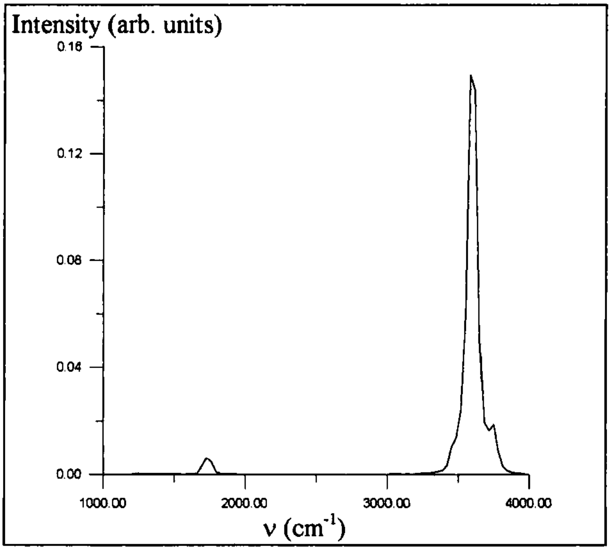

Fig. 7. Calculated Raman spectra.

The shift in the intramolecular frequencies on passing from gaseous to liquid phase are reported in Table X.

TABLE X

Shift on intramolecular frequencies between liquid and gaseous phase.

	Exp. (a) (cm^{-1})	Present work (cm^{-1})
H-O-H bending	50	41
Symmetric stretching	-167	-231
Antisymmetric stretching	-266	-209

(a) Eisenberg and Kauzmann (1969).

IX. Conclusions

On the basis of the results of the dynamics simulation of liquid water it turns out that the VB like wavefunction based on the SCF-MI *non-orthogonal* occupied and virtual orbitals, describes accurately the intermolecular potential of water. Exclusion of BSSE in an *a priori* fashion is ensured and geometry relaxation effects are naturally taken into account.

The new *ab initio* results were used to determine a BSSE free water-water interaction potential which was employed in molecular dynamics simulation of the liquid phase at room temperature.

Extensive calculation were performed on water dimer and trimer and the parametrization of a new NCC-like (Niesar, Corongiu, Clementi, Kneller and Bhattacharya, 1990) potential was accomplished. The results showed good accordance with the experimental data relative to radial distribution functions, thermodynamic properties and geometric parameters. The computed IR and Raman frequencies shifts also agree with the experimental values. The prediction of the internal pressure shows a great improvement in the computed value and an increased stability.

It should be noticed that although non-additive many-body contributions are likely to be necessary for an accurate reproduction of the experimental data, two body terms appear strongly dominant.

The aim of the present work was to perform a first test of the reliability of the general VB approach. The next step will be to investigate the effect of the temperature and system density variations. In particular we want to set a challenge to the present procedure to correctly describe the physical behaviour of water at the critical point, where a fundamental variation of the hydrogen bond is observed (Soper, Bruni and Ricci, 1997). Preliminary results already obtained are encouraging.

Future improvements, aimed to establish the actual importance of many-body contributions, will concentrate on the extension of the basis set employed.

More configurations in the VB step will also be added and improvements of the simulation attempted.

References

Ahlstrom, P., Wallqvist, A., Engstrom, S., and Jonsson, B. (1989). *Mol. Phys.* **68**, 563.

Bartlett, R. J., Shavitt, I., Purvis III, G. D. (1979). *J. Chem. Phys.* **71**, 281.

Benedict, W. S., Gailar, N., and Plyler, E. K. (1956). *J. Chem. Phys.* **24**, 1139.

Berendsen, H. J. C., Grigera, J. R., and Straatsma, T. P. (1987). *J. Phys. Chem.*, **91**, 6296.

Berens, P. H., and Wilson, K. R. (1981). *J. Chem. Phys.* **74**, 4872.

Berens, P. H., Mackay, D. H. J., White, G. M., and Wilson, K. R. (1983). *J. Chem. Phys.* **79**, 2375.

Bernal, J. D., and Fowler, F. D. (1933). *J. Chem. Phys.* **1**, 515.

Billeter, S. R., King, P. M., and van Gunsteren, W. F. (1994). *J. Chem. Phys.* **100**, 6692.

Böttcher, C. F. J. (1973). "Theory of electric polarisation". Elsevier, Amsterdam. Vol. 1.

Boys, S. F., and Bernardi, F. (1970). *Mol.Phys.* **19**, 553.

Clarke, N., Raimondi, M., Sironi, M., Gerratt, J., and Cooper, D. L. *Theor. Chim. Acta* in the press

Clementi, E., and Corongiu, G. (1983). *Int. J. Quantum Chem Symp.* **10**, 31.

Cooper, D. L., Gerratt, J., and Raimondi, M. (1987). *Adv. Chem. Phys.* **69**, 319.

Corongiu, G. (1992). *Int. J. Quantum Chem.* **44**, 1209.

Curtiss, L. A., Frurip, D. J., and Blander, M. (1979). *J. Chem. Phys.* **71**, 2703.

Dyke, T. R., Mack,K. M., and Muenter, J. S. (1977) *J. Chem. Phys.* **66**, 498.

Eisenberg, D., and Kauzmann, W. (1969). "The structure and properties of water". Oxford University Press, London.

Famulari, A. (1997). Ph.D. Thesis, Universita' di Milano.

Famulari, A., Gianinetti, E., Raimondi, M., and Sironi, M. (1997a). Submitted.

Famulari, A., Gianinetti, E., Raimondi, M., and Sironi, M. (1997b). Submitted.

Gianinetti, E., Raimondi, M., and Tornaghi, E. (1996). *Int. J. Quantum Chem.* **60**, 157.

Gianinetti, E., Vandoni, I., Famulari, A., and Raimondi, M. *Adv. Quantum Chem.* Present volume.

Habitz, P., Bagus, P., Siegbahn, P., and Clementi, E. (1983) *Int. J. Quantum Chem.* **23**, 1803.

Jorgensen, W. L., Chandrasekhar, J., Madura, J., Impey, R.W., and Klein, M.L. (1983). *J. Chem. Phys.*79, 926.

Kell, G. S. (1971). "Water: a comprehensive treatise". Vol. 1, 363. Franks, F., Ed. Plenum, New York.

Lie, G. C., and Clementi, E. (1986). *Phys. Rev. A* **33**, 2679.

Mas, E. M., and Szalewicz, K. (1996). *J. Chem. Phys.* **104**, 7606.

Millot, C., and Stone, A. J. (1992). *Mol. Phys.* **77**, 439.

Muguet, F. F., Robinson, G. W., and Bassez-Muguet, M. P. (1991). *Int. J. Quantum Chem.* **39**, 449.

Narten, A. H., and Levy, H. A. (1971). *J. Chem. Phys.* **55**, 2263.

Niesar, U., Corongiu, G., Clementi, E., Kneller, G. R., and Bhattacharya, D. K. (1990). *J. Phys. Chem.* **94**, 7949.

Niesar, U., Corongiu, G., Huang, M-J., Dupuis, M., and Clementi, E., (1989). *Int. J. Quantum Chem. Symp.* **23**, 421.

Rahman, A., and Stilliger, F. H. (1971). *J. Chem. Phys.* **55**, 3336.

Raimondi, M., Campion, W., and Karplus, M. (1977). *Mol. Phys.* **34**, 1483.

Raimondi, M., Sironi, M., Gerratt, J., and Cooper, D. L. (1996) *Int. J. Quantum Chem.* **60**, 225.

Schmidt, M. W., Baldridge, K. K., Boatz, J. A., Elbert, S. T., Gordon, M. S., Jensen, J. H., Koseki, S., Matsunaga, N., Nguyen, K. A., Su, S. J., Windus, T. L., Dupuis, M., Montgomery, J. A. (1993). *J. Comput. Chem.* **14**, 1347.

Sciortino, F., and Corongiu, G. (1994). "Modern Techniques in Computational Chemistry: MOTECC-94.". Clementi, E., Ed. ESCOM, Leiden, The Netherlands.

Soper, A. K., and Phillips, M.G. (1986). *Chem. Phys.* **107**, 47.

Soper, A. K., Bruni, F., and Ricci, M. A. (1997). *J. Chem. Phys.* **106**, 247.

Specchio, R., (1997). Degree Thesis, Universita' di Milano.

Svishchev, I. M., Kusakik, P. G., Wang, J., and Boyd, R. J. (1996). *J. Chem. Phys.*, **105**, 4742.

Texeira, J., Bellisent-Funel, M. C., Chen, S. H., and Dorner, B. (1985). *Phys. Rev. Lett.* **54**, 2681.

Thiessen, W. E., and Narten, A. H., (1982). *J. Chem. Phys.*, **77**, 2656.

van Duijneveldt, F. B., van Duijneveldt-van de Rijdt, J. G. C. M., and van Lenthe, J. H. (1994). *Chem. Rev.* **94**, 1873.

van Duijneveldt-van de Rijdt, J. G. C. M., and van Duijneveldt, F. B. (1992). *J. Chem. Phys.* **97**, 5019.

Wallqvist, A., and Berne, B. J. (1993). *J. Phys. Chem.* **97**, 13841.

Systematic Sequences of Even-Tempered Gaussian Primitives for Diatomic Molecules in Solution: A Preliminary Study using Continuum Solvation Models

G.J.A. Keith[†], P.J. Grout[†] and S. Wilson[‡]
[†]*Physical and Theoretical Chemistry Laboratory*
University of Oxford, South Parks Road
Oxford, OX1 3QZ, UK
[‡]*Rutherford Appleton Laboratory, Chilton*
Oxfordshire, OX11 OQX, UK

Abstract

The convergence of the matrix Hartree-Fock energy, with increasing basis set size, for the isoelectronic series N_2, BF, CO, NO^+ is examined for three continuum solvation models using systematic sequences of even-tempered basis sets of s- and p-type primitive Gaussian functions. For the quantum Onsager model, the polarized continuum model and the isodensity polarized continuum model, trends in the energy differences, dipole moments and cavity sizes are investigated for systematically extended basis sets.

Contents

1. Introduction
2. Continuum Models
3. Systematic sequences of even-tempered Gaussian primitive functions
4. Results

ADVANCES IN QUANTUM CHEMISTRY, VOLUME 32
Copyright ©1999 by Academic Press. All rights of reproduction in any form reserved.
0065-3276/99 $30.00

5. Discussion
6. Conclusions
Acknowledgment
References

1 Introduction

Traditionally, *ab initio* electronic structure calculations have been carried out for isolated molecular species[1]-[4]. However, most chemistry takes place in solution, and therefore, recent years have seen a growing interest in the problem of describing molecules in solution[5]-[9]; a problem which has increasingly assumed both theoretical and practical importance. Physical models for the description of solvation processes in equilibrium are often considered in three stages: (*i*) the formation of a cavity in the solvent, (*ii*) the introduction of the solute molecule into the cavity, which is accompanied by electrostatic and orientational polarization together with dispersion interactions between the solute molecule and the solvent, (*iii*) hydrogen bonding, or the formation of complexes, between the solute and the solvent molecules.

The methods employed in the *ab initio* quantum mechanical description of isolated molecules range from independent particle models, such as the Hartree-Fock ansatz, to sophisticated treatments of electron correlation effects[1]-[4] [10]. An almost universal feature of the practical realization of these methods is the use of finite basis set expansions and the use of Gaussian basis sets is ubiquitous[11]-[17]. However, it is widely recognized that the error associated with the truncation of the basis set is often a dominant source of error in such calculations and, therefore, recent years have seen a growing interest in the systematic refinement of the algebraic approximation; that is, the use of finite analytic basis set expansions. In particular, basis sets have been designed for diatomic molecules which can support an accuracy approaching the sub-$\mu Hartree$ level in matrix Hartree-Fock calculations[18]-[25]. These basis sets have then been used in studies of polyatomic molecules[26] and refined for high precision electron correlation calculations[27]-[28].

In this paper, a study is made of the effects that the choice of basis set can have on calculated total energies in solution and in the gas phase, on the energy differences between solution and gas phase for three different continuum models, on the dipole moments and on the cavity sizes of the isoelectronic series N_2, BF, CO, NO^+. For these diatomic molecules exact gas phase Hartree-Fock energies at their equilibrium geometries (N_2 : r_e = 2.068 $Bohr, BF$: r_e = 2.386 $Bohr, CO$: r_e = 2.132 $Bohr, NO^+$: r_e = 2.010 $Bohr$) are available from finite difference calculations[29]. In the present work, gas phase and solute calculations are carried out within the matrix Hartree-Fock model at these geometries. The solvation models used are continuum models, for which the underlying assumptions are: (*i*) the solvent is a uniform dielectric, (*ii*) the charge distribution in the solute induces polarization in the solvent, (*iii*) polarization produces an electric field in the cavity affecting the solute, (*iv*) the solute interaction with individual solvent molecules is neglected. The models differ in the definition of the cavity shape and in the manner in which the reaction field is approximated. An initial series of calculations employed some of the "standard" basis sets of Gaussian functions developed by Pople and his coworkers[30]-[39]; in particular, the sets designated "*STO*-3*G*", "3-21*G*", "6-21*G*" and "6-31*G**". A systematic study of the effects of basis set truncation on calculated energies in solution and in the gas phase was made by generating sequences of even-tempered primitive Gaussian functions.

The purpose of the present work is to investigate the convergence characteristics of calculations for solvated systems using continuum models when the solute is described by a matrix Hartree-Fock wave function and systematically constructed even-tempered basis sets of Gaussian primitive functions are employed. Specifically, no attempt has been made to achieve high accuracy but rather the emphasis has been on the trends in molecular properties with increasing basis set size.

In Section 2 below, we give an outline of each of the continuum models used. The development of systematic sequences of primitive, even-tempered Gaussian functions is briefly described in section 3. In Sections 4 the results obtained in the present work are given beginning with a preliminary study using some 'standard' basis sets and then employing sequences of even-tempered basis sets of primitive Gaussian functions. In section 5, the results are discussed and then, in section 6, the conclusions are presented.

All of the calculations reported in this paper were performed with the GAUSSIAN94 suite of programs[40].

2 Continuum models

The continuum models employed in the present study are extensively documented in the literature[5]-[9], [41]-[43]. Here we review the salient features which are pertinent to the present study.

The solvated molecule is described by an effective, fixed nuclei Hamiltonian which may be written

$$\hat{H}\left(\mathbf{r};\mathbf{R}\right) = \hat{H}_0\left(\mathbf{r};\mathbf{R}\right) + \hat{V}_{int} \tag{1}$$

This operator depends on $\mathbf{r}$, the coordinates of the electrons and, parametrically, on $\mathbf{R}$, the coordinates of the nuclei. $\hat{H}_0\left(\mathbf{r};\mathbf{R}\right)$ is the usual electronic Hamiltonian in vacuo and V_{int} is the potential arising from the interaction between the solvent molecule and the dielectric continuum. In general, the definition of V_{int} implies a knowledge of the thermally averaged distribution function of the solvent molecules, g_S, and, therefore

$$\hat{V}_{int} = \hat{V}_{int}\left(\mathbf{r},\mathbf{R},g_S\right) \tag{2}$$

The precise form of $\hat{V}_{int}$ depends on the choice of model.

For a molecule with a dipole moment, the interaction is given by

$$\hat{V}_{int} = \Gamma\ \langle\phi\,|\hat{\mu}|\,\phi\rangle\ \hat{\mu} \tag{3}$$

where $\hat{\mu}$ is the dipole moment operator, $\langle\phi\,|\hat{\mu}|\,\phi\rangle$ is the self-consistent reaction field expectation value of the dipole moment of the solute molecule and Γ is a factor which depends on the size and the shape of the solute cavity. In this work, higher multipole moments of the charge distribution of the solute are neglected.

2.1 Quantum Onsager Model

The quantum Onsager model, which has also been termed the Self-Consistent Reaction Field (SCRF) method, is the simplest of the continuum models used in solvation studies. In this model, which dates from the work of Kirkwood[44] and Onsager[45] in the 1930s, the solvent is represented by a continuous uniform dielectric with a static dielectric constant, ϵ, surrounding a solute in a spherical cavity[46] - [48].

A dipole in the solute molecule will interact with the dielectric medium which will then relax to electrostatically stabilize the solute. Because the solvent lacks structure, this model not appropriate for solvents having important specific interactions with the solute, such as hydrogen bonds. However, it does allow the geometry and dipole moment of the solute molecule reflect the interaction with the dielectric medium.

For a neutral molecule in the spherical cavity assumed in the quantum Onsager model, the factor Γ, defined in equation (3) above, takes the following form

$$\Gamma = \frac{\epsilon - 1}{(2\epsilon + 1)\, a_0^3} \tag{4}$$

where a_0 is the cavity radius. For ionic solute molecules, the factor Γ must be modified to maintain gauge invariance. For positively charged ions with charge Q and with n_e electrons it can be shown that

$$\Gamma = \Gamma \frac{n_e}{n_e + Q} \tag{5}$$

and the ionic solvation term has to be added to the electrostatic solvation energy.

The electron distribution varies with basis set, thereby also changing the molecular size. The molecular volume was calculated for the molecule in the gas phase for each basis set. Wong, Wiberg and Frisch[49] found that there was a strong correlation between the calculated 0.001 $electrons/Bohr^3$ density envelope (DE) and the experimentally measured molar volume (V_m), in that the ratio V_{DE}/V_m, where V_{DE} is the volume enclosed by the density envelope, is close to $\frac{3}{4}$ for a wide range of organic molecules. Thus their procedure is to compute the 0.001 $electrons/Bohr^3$ density envelope of a solute and scale it by a factor of $\frac{4}{3}$, from which the cavity radius (a_0) was determined by assuming the molecule was spherical with radius r, and then defining $a_0 = r + 0.5$Å to account for the nearest approach of solvent molecules.

2.2 Polarized Continuum Model

In the polarized continuum model [50]-[52] the cavity is defined by a set of overlapping spherical atoms each having the appropriate van der Waals radii. By placing spheres at the atom centres, a more realistic cavity shape for extended molecules can be produced. Tomasi and co-workers[53] suggest that the appropriate radii are 20% greater than the standard van der Waals radii. Again, the dielectric constant was set to that of water at room temperature.

For this more complex cavity, the electrostatic interaction energy between the solute charge distribution and the reaction field is calculated numerically. In the present study, the charge distribution was approximated by a distributed set of 150 fractional point charges on the cavity surface.

2.3 Isodensity Polarised Continuum Model

A weakness of the Polarised Continuum Model is the arbitrary choice of radii in defining the cavity. The Isodensity Polarised Continuum Model was developed[54] to avoid this problem.

In the Isodensity Polarised Continuum Model the cavity is based on an isosurface of the total electron density calculated at the level of theory being employed. Only the electron density describing the isosurface is required to fully specify this model instead of the set of radii for the spheres used in the Polarised Continuum Model. The cavity is derived entirely from the electronic environment. In the present study, the isosurface was defined by the 0.001 $electrons/Bohr^3$ density envelope.

The isodensity surface is varied in each iteration of the self-consistent field calculation. In each iteration the solute density is updated, and consequently, the isodensity surface used for the cavity is relaxed to the isodensity surface of the solvated molecule. However, it is important to realize that this process is not fully self-consistent with respect to the isodensity surface, since there are no direct terms in the Hamiltonian that couple the isodensity surface to the solute.

3 Systematic sequences of even-tempered Gaussian primitive functions

An efficient scheme for generating the large and flexible primitive Gaussian basis sets required for accurate calculations is provided by the even-tempered prescription in which the exponents, $\zeta_{kN\ell}$, are taken to form a geometric progression:-

$$\ln \zeta_{kN\ell} = \ln \alpha_{N\ell} + k \ln \beta_{N\ell}, \ k = 1, 2, ..., N \tag{6}$$

This approach, which was suggested by McWeeny[55] and explored by Reeves and Harrison[56], [57] in the early 1960s, was thoroughly investigated by Ruedenberg and his coworkers[58]-[64] in the 1970s.

Even-tempered basis sets can be systematically increased (or decreased) in size by following the empirical prescription of Schmidt and Ruedenberg[65] in which the parameters $\alpha_{N\ell}$ and $\beta_{N\ell}$ depend on the number of functions, N, in the basis set. The following empirical formulae lead to a sequence of basis sets which become complete in the limit of large N

$$\ln \ln \beta_{N\ell} = b_\ell \ln N + b'_\ell \tag{7}$$

$$\ln \alpha_{N\ell} = a_\ell \ln(\beta_{N\ell} - 1) + a'_\ell \tag{8}$$

Schmidt and Ruedenberg[65] optimized the constants a_ℓ, a'_ℓ, b_ℓ and b'_ℓ, for individual atomic species. However, for the large and flexible even-tempered basis sets required for calculations of high precision it has been recognized that the precise values of these constants is not critical and, building on the concept of a universal basis set[66] - [72], a universal systematic sequence of even-tempered Gaussian basis sets has been investigated[71], [74].

The basis sets employed in the present work contained $2N$ s-type functions and N p- functions. The, so-called "regularized", coefficients a_s, b_s, a'_s, b'_s, a_p, b_p, a'_p, b'_p used in eqns. (7) and (8) to generate the parameters $\alpha_{N\ell}$ and $\beta_{N\ell}$ for these even-tempered basis sets were taken from Schmidt and Ruedenberg[65] for each atom considered.

4 Results

4.1 A study using some "standard" basis sets

The gas phase matrix Hartree-Fock energies of each of the molecules N_2, CO, BF and NO^+ at their respective equilibrium geometries were calculated for each of the basis sets designated "*STO-3G*", "3-21*G*", "6-21*G*" and "6-31*G**" [30]-[39]. The results are presented in Table 1. The basis set truncation errors associated with the total energies presented in Table 1 can be determined by comparison with the exact Hartree-Fock energies which have been determined[26] for the four systems studies here using finite difference techniques[75]-[80]. For the N_2, CO, BF and NO^+ systems the exact Hartree-Fock energies are -108.993826, -112.790907, -124.168779 and

−128.977741 Hartree, respectively. For the "STO-3G" basis set, the basis set truncation errors are 2233, 1566, 1813 and 1792 *milliHartree* for the N_2, CO, BF and NO^+ systems, respectively, whilst for the "3-21G" basis set the corresponding errors are 693, 698, 737 and 841 *milliHartree* and for the "6-21G" basis set they are 223, 218, 230 and 298 *milliHartree*. For the largest "standard" basis set considered, the "6-31G^*" set, the basis set truncation errors are reduced to 51, 54, 66 and 70 *milliHartree* for the N_2, CO, BF and NO^+ systems.

For each of the three continuum models defined in section 2, the energy of each of the four diatomic molecules in water, with static dielectric constant, ϵ, equal to 81.0, was calculated. The resulting total matrix Hartree-Fock energies are given in Table 2. Also in this table, the difference between the energy determined in solution and in the gas phase is given in brackets [...] and, where appropriate, the cavity radius is given in parenthesis (...).

It should be noted that although the gas phase energies are converging with increasing basis set, the same is not true of the energy differences.

Table 1

Gas phase total matrix Hartree-Fock energies for N_2, BF, CO, NO^+ from calculations using some "standard" basis sets[†].

Molecule	STO-3G	3-21G	6-21G	6-31$G*$
N_2	−106.760851	−108.300538	−108.770681	−108.943065
CO	−111.224580	−112.093298	−112.572456	−112.737321
BF	−122.356157	−123.431783	−123.938555	−124.103179
NO^+	−127.186200	−128.136808	−128.679570	−128.907636

[†] All energies are given in *Hartree*

Table 2

Total Hartree-Fock energies for the N_2, BF, CO, NO^+ molecules in the three continuum models. Differences between the continuum model and the gas phase energies are given in brackets [...] and cavity radii in parentheses (...)†.

Onsager Model

	STO-3G	3-21G	6-21G	6-31G*
N_2	-106.760851	-108.300538	-108.770681	-108.943065
	[0]	[0]	[0]	[0]
	(4.80)	(4.97)	(4.78)	(5.12)
CO	-111.224600	-112.093393	-112.572548	-112.737389
	[-0.020]	[-0.096]	[-0.092]	[-0.068]
	(4.88)	(5.12)	(5.14)	(5.14)
BF	-122.356984	-123.432197	-123.938886	-124.103570
	[-0.827]	[-0.415]	[-0.331]	[-0.391]
	(4.90)	(4.99)	(5.33)	(5.41)
NO^+	-127.186345	-128.137613	-128.680310	-128.908059
	[-0.145]	[-0.805]	[-0.741]	[-0.423]
	(4.57)	(4.69)	(4.80)	(4.86)

Polarised Continuum Model

	STO-3G	3-21G	6-21G	6-31G*
N_2	-106.760851	-108.300538	-108.770681	-108.943065
	[0]	[0]	[0]	[0]
CO	-111.229828	-112.098693	-112.577733	-112.737990
	[-5.249]	[-5.394]	[-5.277]	[-0.969]
BF	-122.363638	-123.436921	-123.943525	-124.103884
	[7.481]	[0.414]	[-4.970]	[0.706]
NO^+	-127.352537	-128.301919	-128.844633	-129.069521
	[-166.337]	[-165.111]	[-165.063]	[-161.885]

Table 2 (cont.)

Isodensity Polarised Continuum Model

	STO-3G	3-21G	6-21G	6-31G*
N_2	-106.760851 [0]	-108.300538 [0]	-108.770681 [0]	-108.943065 [0]
CO	-111.227904 [-3.324]	-112.096636 [-3.338]	-112.575739 [-3.283]	-112.739117 [-1.796]
BF	-122.362096 [-5.939]	-123.437416 [-5.633]	-123.944091 [-5.536]	-124.106909 [-3.730]
NO^+	-127.339202 [-153.002]	-128.283409 [-146.601]	-128.826234 [-146.664]	-129.048675 [-141.039]

[†] Energies are given in *Hartree*, energy differences in *milliHartree* and the cavity radii in *Bohr*

4.2 Systematic sequences of even-tempered basis sets of Gaussian primitive functions in calculations using continuum models

For the solvation models considered in this work there is no interaction between the solute and the solvent for systems not having a dipole moment and, therefore, for the N_2 molecule the total matrix Hartree-Fock energy for each of the continuum models is equal to that of the gas phase system. The convergence of the matrix Hartree-Fock energy for the gas phase N_2 molecule for systematic sequences of even-tempered basis sets has been studied previously[21]. It has been demonstrated[81] that a sufficiently large and flexible universal even-tempered basis set of Gaussian primitive functions can support a total matrix Hartree-Fock energy of -108.9938234 *Hartree* for a nuclear separation of 2.068 *Bohr*. This differs from the finite difference Hartree-Fock energy by 2.3 μ*Hartree*. The N_2 ground state will not be considered further in the present work.

The calculated matrix Hartree-Fock energies for the ground state of the CO molecule with a nuclear separation of 2.132 *Bohr* are presented in Table 3 for the sequence of regularized even-tempered basis sets in the gas phase and in each of the three continuum models described in section 2. In this Table, N defines the size of the basis set; each set in the sequence containing $2N$ s-type functions and N p-type functions. E^{gas} is the gas phase matrix Hartree-Fock energy. E^{ons}, E^{pcm} and E^{ipcm} are the total matrix Hartree-

Fock energies for the quantum Onsager, polarized continuum and isodensity polarized continuum models, respectively. The following energy differences are also given in Table 3

$$\Delta E^{ons} = E^{ons} - E^{gas} \tag{9}$$

$$\Delta E^{pcm} = E^{pcm} - E^{gas} \tag{10}$$

and

$$\Delta E^{ipcm} = E^{ipcm} - E^{gas} \tag{11}$$

together with the radius of the spherical cavity used in the quantum Onsager model, a_0 and the cavity volume in the isodensity polarized continuum models, V_c^{ipcm}.

It has been demonstrated[81] that a sufficiently large and flexible universal even-tempered basis set of Gaussian primitive functions can support a total matrix Hartree-Fock energy for the gas phase CO molecule of -112.7909045 $Hartree$ for a nuclear separation of 2.132 $Bohr$. This differs from the finite difference Hartree-Fock energy by 2.8 $\mu Hartree$.

The calculated matrix Hartree-Fock energies for the ground states of the BF molecule and the NO^+ ion, with nuclear separations of 2.386 $Bohr$ and 2.010 $Bohr$, are presented in Tables 4 and 5, respectively. It has been demonstrated[81] that a sufficiently large and flexible universal even-tempered basis set of Gaussian primitive functions can support a total matrix Hartree-Fock energies of -124.1687612 and -128.9777375 $Hartree$ for gas phase BF and NO^+, respectively for nuclear separations of 2.386 and 2.010 $Bohr$. These energies differs from the corresponding finite difference Hartree-Fock energies by 18 and 3.2 $\mu Hartree$, respectively.

Table 3

Calculated total matrix Hartree-Fock energies for the ground state of the CO molecule with a nuclear separation of 2.132 *Bohr* using a systematic sequence of even-tempered Gaussian primitive functions in the gas phase and in three continuum models. See text for details.

N	$E^{gas}+112$ *Hartrees*	$E^{ons}+112$ *Hartrees*	ΔE^{ons} *mHartrees*	a_0 *Bohr*	$E^{pcm}+112$ *Hartrees*	ΔE^{pcm} *mHartrees*	$E^{ipcm}+112$ *Hartrees*	ΔE^{ipcm} *mHartrees*	V_c^{ipcm} $Bohr^3$
3	−0.364398	−0.364722	−0.324	4.84	−0.372736	−8.338	−0.368692	−4.294	212.81
4	−0.640796	−0.640963	−0.168	5.31	−0.646903	−6.108	−0.644196	−3.401	238.36
5	−0.695894	−0.696050	−0.155	5.31	−0.701577	−5.682	−0.699116	−3.221	243.40
6	−0.710223	−0.710383	−0.161	5.27	−0.715937	−5.714	−0.713465	−3.243	243.07
7	−0.714847	−0.715012	−0.165	5.24	−0.720370	−5.522	−0.718087	−3.239	243.84
8	−0.716126	−0.716276	−0.149	5.41	−0.721494	−5.368	−0.719366	−3.239	244.43
9	−0.716858	−0.717037	−0.179	5.14	−0.722204	−5.346	−0.720117	−3.259	244.51
10	−0.717471	−0.717637	−0.166	5.26	−0.722847	−5.376	−0.720754	−3.283	244.40
11	−0.717678	−0.717836	−0.158	5.33	−0.723066	−5.388	−0.720972	−3.294	244.34
12	−0.717602	−0.717786	−0.184	5.09	−0.722984	−5.382	−0.720895	−3.292	244.36
13	−0.717602	−0.717765	−0.164	5.27	−0.722980	−5.378	−0.720892	−3.290	244.40
14	−0.717829	−0.717997	−0.169	5.24	−0.723212	−5.383	−0.721116	−3.287	244.40
15	−0.718134	−0.718293	−0.159	5.33	−0.723521	−5.388	−0.721421	−3.287	244.37
16	−0.718290	−0.718453	−0.163	5.29	−0.723677	−5.387	−0.721580	−3.290	244.35
17	−0.718264	−0.718441	−0.177	5.16	−0.723648	−5.384	−0.721558	−3.293	244.38
18	−0.718168	−0.718347	−0.179	5.14	−0.723551	−5.383	−0.721464	−3.295	244.46

Table 4

Calculated total matrix Hartree-Fock energies for the ground state of the *BF* molecule with a nuclear separation of 2.386 *Bohr* using a systematic sequence of even-tempered Gaussian primitive functions in the gas phase and in three continuum models. See text for details.

N	$E^{gas}+124$ *Hartrees*	$E^{ons}+124$ *Hartrees*	ΔE^{ons} *mHartrees*	a_0 *Bohr*	$E^{pcm}+124$ *Hartrees*	ΔE^{pcm} *mHartrees*	$E^{ipcm}+124$ *Hartrees*	ΔE^{ipcm} *mHartrees*	V_c^{ipcm} *Bohr*^{3}
3	+0.263398	+0.263178	−0.220	5.24	+0.257022	−6.376	+0.257024	−6.374	241.99
4	−0.033622	−0.033737	−0.116	5.46	−0.038609	−4.987	−0.038649	−5.027	271.81
5	−0.103027	−0.103121	−0.095	5.27	−0.107609	−4.583	−0.107580	−4.553	280.24
6	−0.120675	−0.120754	−0.080	5.44	−0.125345	−4.670	−0.125143	−4.468	279.80
7	−0.124013	−0.124099	−0.085	5.27	−0.128695	−4.682	−0.128576	−4.563	278.14
8	−0.125001	−0.125073	−0.072	5.48	−0.129656	−4.655	−0.129678	−4.677	277.66
9	−0.126282	−0.126366	−0.084	5.24	−0.130855	−4.573	−0.130984	−4.702	278.19
10	−0.127098	−0.127172	−0.074	5.46	−0.131587	−4.488	−0.131757	−4.659	278.73
11	−0.127188	−0.127265	−0.077	5.39	−0.131649	−4.461	−0.131800	−4.612	278.84
12	−0.127010	−0.127086	−0.076	5.39	−0.131502	−4.492	−0.131611	−4.601	278.62
13	−0.127029	−0..127105	−0.076	5.37	−0.131559	−4.530	−0.131649	−4.620	278.31
14	−0.127238	−0.127312	−0.074	5.43	−0.131774	−4.536	−0.131884	−4.646	278.12
15	−0.127441	−0.127517	−0.076	5.39	−0.131957	−4.516	−0.132101	−4.661	278.12
16	−0.127533	−0.127605	−0.073	5.46	−0.132026	−4.493	−0.132194	−4.661	278.26
17	−0.127540	−0.127614	−0.074	5.43	−0.132024	−4.484	−0.132192	−4.652	278.44
18	−0.127538	−0.127607	−0.069	5.52	−0.132025	−4.487	−0.132181	−4.643	278.55

Table 5

Calculated total matrix Hartree-Fock energies for the ground state of the NO^+ molecule with a nuclear separation of 2.010 *Bohr* using a systematic sequence of even-tempered Gaussian primitive functions in the gas phase and in three continuum models. See text for details.

N	$E^{gas}+128$ *Hartrees*	$E^{ons}+128$ *Hartrees*	ΔE^{ons} *mHartrees*	a_0 *Bohr*	$E^{pcm}+128$ *Hartrees*	ΔE^{pcm} *mHartrees*	$E^{ipcm}+128$ *Hartrees*	ΔE^{ipcm} *mHartrees*	V_c^{ipcm} $Bohr^3$
3	−0.432993	−0.433999	−1.006	4.61	−0.599086	−166.094	−0.582084	−149.091	172.04
4	−0.773519	−0.774158	−0.639	4.82	−0.940583	−167.064	−0.918516	−144.997	186.25
5	−0.834838	−0.835355	−0.517	4.91	−1.001730	−166.892	−0.982786	−147.947	179.04
6	−0.850104	−0.850602	−0.498	4.93	−1.016600	−166.496	−1.000012	−149.908	174.50
7	−0.858319	−0.858940	−0.622	4.61	−1.024601	−166.282	−1.007696	−149.377	175.85
8	−0.860794	−0.861343	−0.549	4.78	−1.027049	−166.255	−1.009474	−148.680	177.35
9	−0.860464	−0.860979	−0.515	4.88	−1.026786	−166.322	−1.009055	−148.591	177.45
10	−0.860212	−0.860808	−0.597	4.67	−1.026599	−166.387	−1.009148	−148.936	176.79
11	−0.860920	−0.861469	−0.550	4.78	−1.027324	−166.404	−1.010219	−149.299	176.26
12	−0.861890	−0.862510	−0.620	4.61	−1.028274	−166.384	−1.011324	−149.434	176.17
13	−0.862391	−0.862856	−0.465	5.03	−1.028751	−166.360	−1.011765	−149.374	176.35
14	−0.862306	−0.862856	−0.550	4.78	−1.028661	−166.355	−1.011563	−149.257	176.54
15	−0.862042	−0.862566	−0.523	4.86	−1.028411	−166.369	−1.011228	−149.186	176.60
16	−0.861963	−0.862500	−0.537	4.82	−1.028352	−166.389	−1.011149	−149.186	176.55
17	−0.862161	−0.862766	−0.605	4.65	−1.028564	−166.402	−1.011393	−149.231	176.47
18	−0.862497	−0.863039	−0.542	4.80	−1.028902	−166.405	−1.011777	−149.281	176.44

5 Discussion

It is important to re-iterate that the purpose of the present work is to investigate the convergence characteristics of calculations for solvated systems using continuum models when the solute is described by a matrix Hartree-Fock wave function for which systematically constructed even-tempered basis sets of Gaussian primitive functions are employed. Specifically, no attempt has been made to achieve high accuracy but the emphasis has been on the trends in molecular properties with increasing basis set size.

The results presented in the previous section will be analyzed in this section, first by examining the behaviour observed for different molecules, and then by comparing the results obtained with different continuum models.

5.1 Comparison of results obtained for different molecules

The gas phase energies recorded in Table 3 for the CO molecule decrease monotonically with increasing size of basis set for $N = 3, ..., 11$; for $N = 12$ there is a small increase in the energy and then it decreases further until $N = 17,\ 18$, where it is seen to increase again. Similar behaviour is seen in Table 4 for the BF molecule and in Table 5 for the NO^+ ion.

In Figure 1, the variation of the difference

$$L^x \equiv \log \mid E^x(N) - E^x(N-1) \mid,\ x = gas,\ ons,\ pcm,\ ipcm, \tag{12}$$

where $E^x(N)$ is the energy obtained with a basis set of size N, is shown for the gas phase and the three continuum models for each of the molecular species CO, BF and NO^+. For each system, the convergence pattern observed for the gas phase calculations is mirrored in the calculations for the three continuum models.

In previous studies of these isoelectronic systems[21] [81] in the gas phase, oscillation has been observed in the convergence pattern for the matrix Hartree-Fock energy for basis sets containing only atom centred basis functions of s- and p-type Gaussian functions. For values of N greater than $15 - 16$ this has been attributed to computational linear dependence in the basis set. For values of N in the range $10 - 15$ the oscillation is attributable to the absence of higher harmonics in the basis set since it has been found that addition of d- and f-type Gaussian functions attenuates their amplitude most significantly.

Figure 2 shows the observed convergence pattern for the difference in energy between the continuum model and gas phase calculations, ΔE^{x}, $x = ons, pcm, ipcm$, with increasing basis set size. The scales used in Figure 2 have been chosen to accommodate all three continuum models. In general, for basis sets with $N > 5$, the variation of ΔE^{x} with increasing basis set size is less significant than the energy differences with different continuum models.

5.2 Comparison of results obtained for different continuum models

The trends in the changes of ΔE^{ons} with increasing basis set size are displayed in Figure 3. The cavity radius, a_0, and the energy difference, ΔE^{ons}, oscillate in phase for each of the molecules studied as the basis sets are extended. This can be attributed to the fact that the molecular volume, and hence the cavity size, depends on the specification of the basis set. Increasing the molecular size creates a larger cavity, which results in the interaction energy, ΔE^{ons}, being less negative. In Figure 4, a similar same trend is seen for the variation of the dipole moment, μ^{ons}, with increasing size of basis set, as expected since the reaction field is related to the molecular dipole of the solute.

Figure 5 shows the difference in energy between the Polarized Continuum model and the gas phase, ΔE^{pcm}, together with the variation of the molecular dipole moment, μ^{pcm}. The results for CO follow a similar pattern to those in the Onsager Model. After $N = 6$, the oscillations in the energy for BF are much smaller than those for CO. NO^{+} shows little correlation between ΔE^{pcm} and μ^{pcm}.

For the Isodensity Polarised Continuum Model we have studied the variation of the cavity volume, V_c^{ipcm}, defined by the isodensity surface, together with ΔE^{ipcm}. The variations of V_c^{ipcm} and $\Delta E^{ipcm}$with increasing basis set size are in phase as is confirmed in Figure 6.

For the Isodensity Polarized Continuum Model, the variation of the dipole moment, μ^{ipcm}, shows little correlation with ΔE^{ipcm} as can be seen from Figure 7.

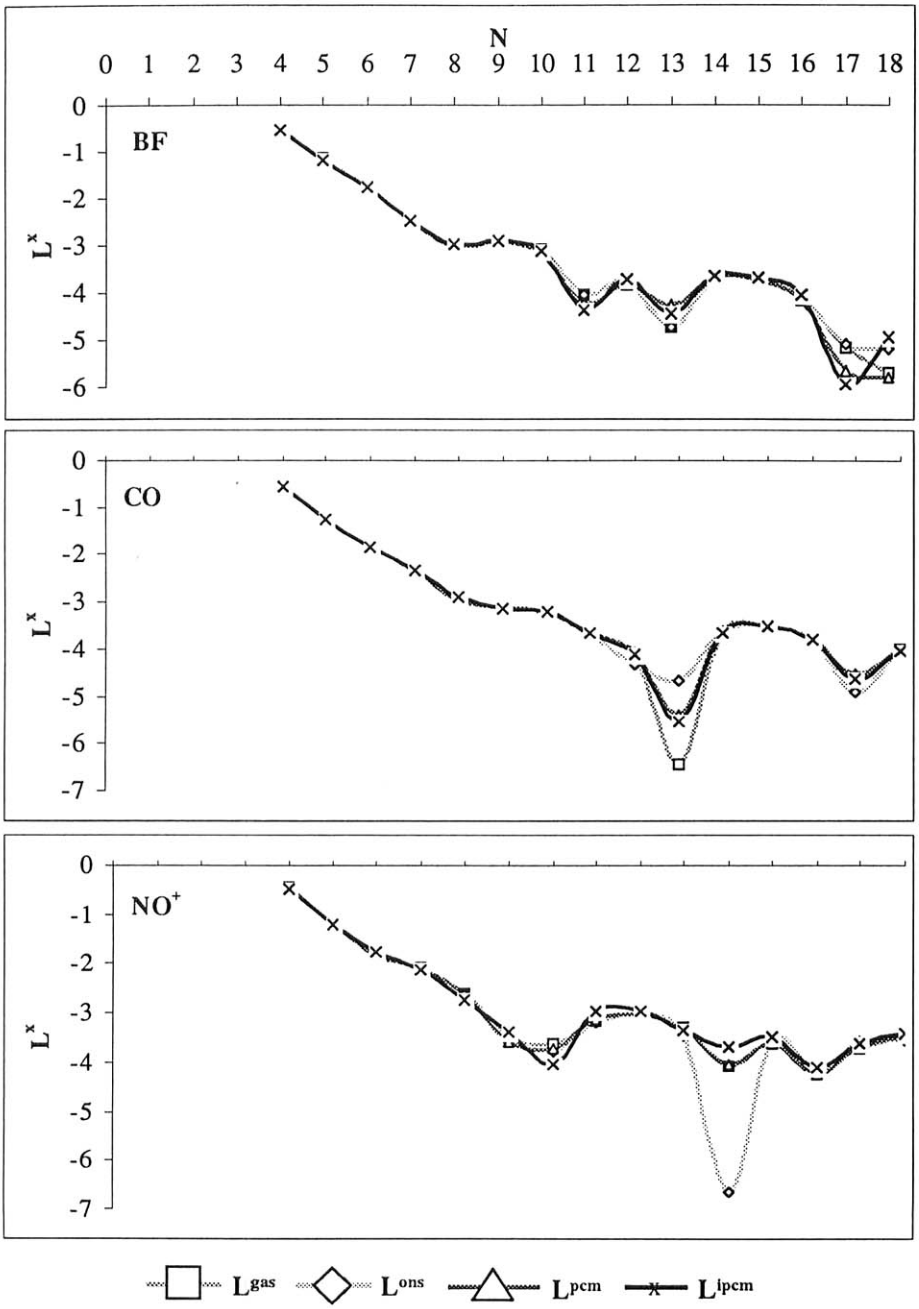

Figure 1: Variation of the difference L^x with increasing size of basis set, for the gas phase and three continuum models, for each of the molecular species *CO*, *BF* and *NO^+*.

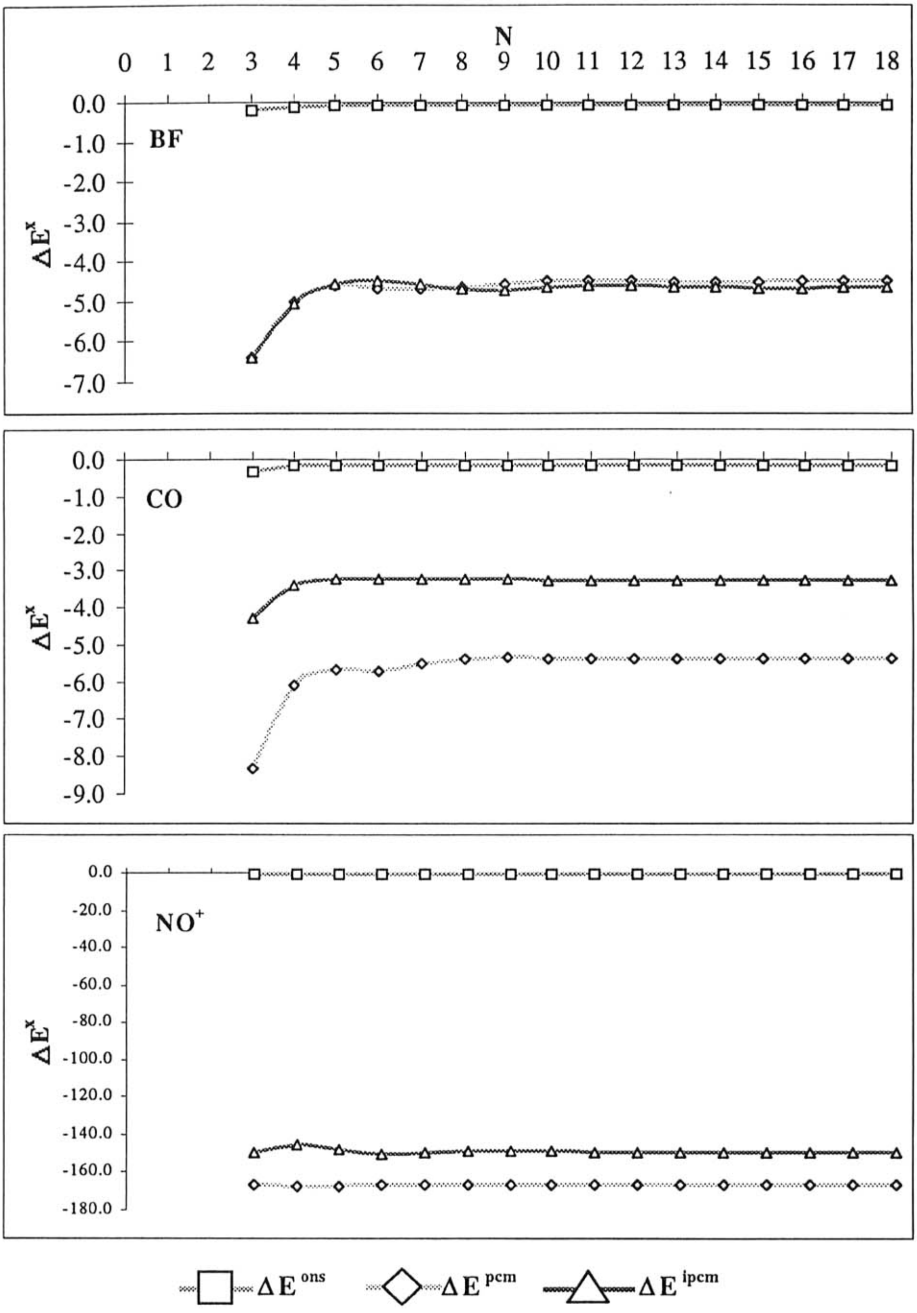

Figure 2: Convergence pattern for the difference in energy between the continuum model and gas phase calculations with increasing size of basis set.

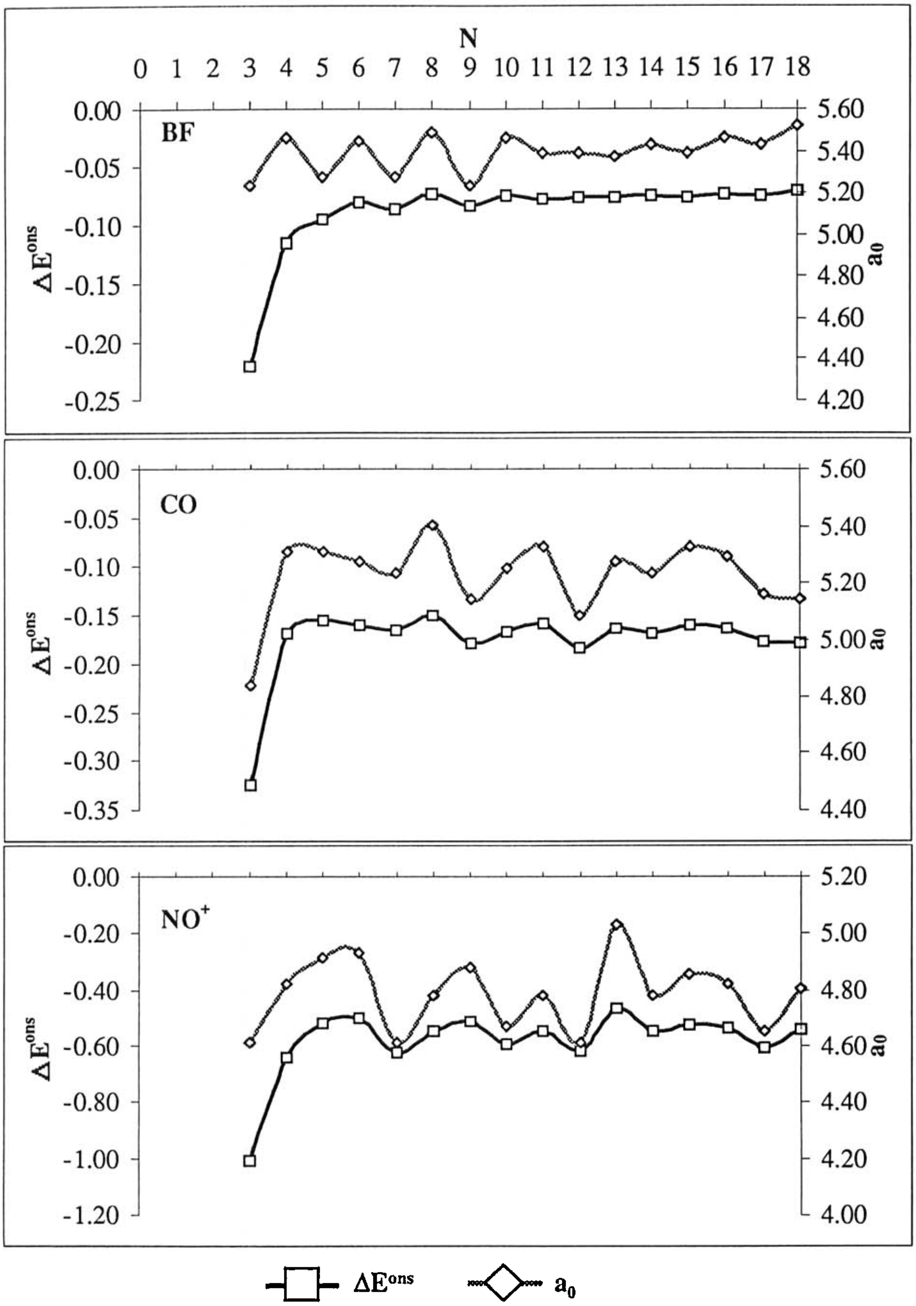

Figure 3: Energy difference for the quantum Onsager model with increasing size of basis set.

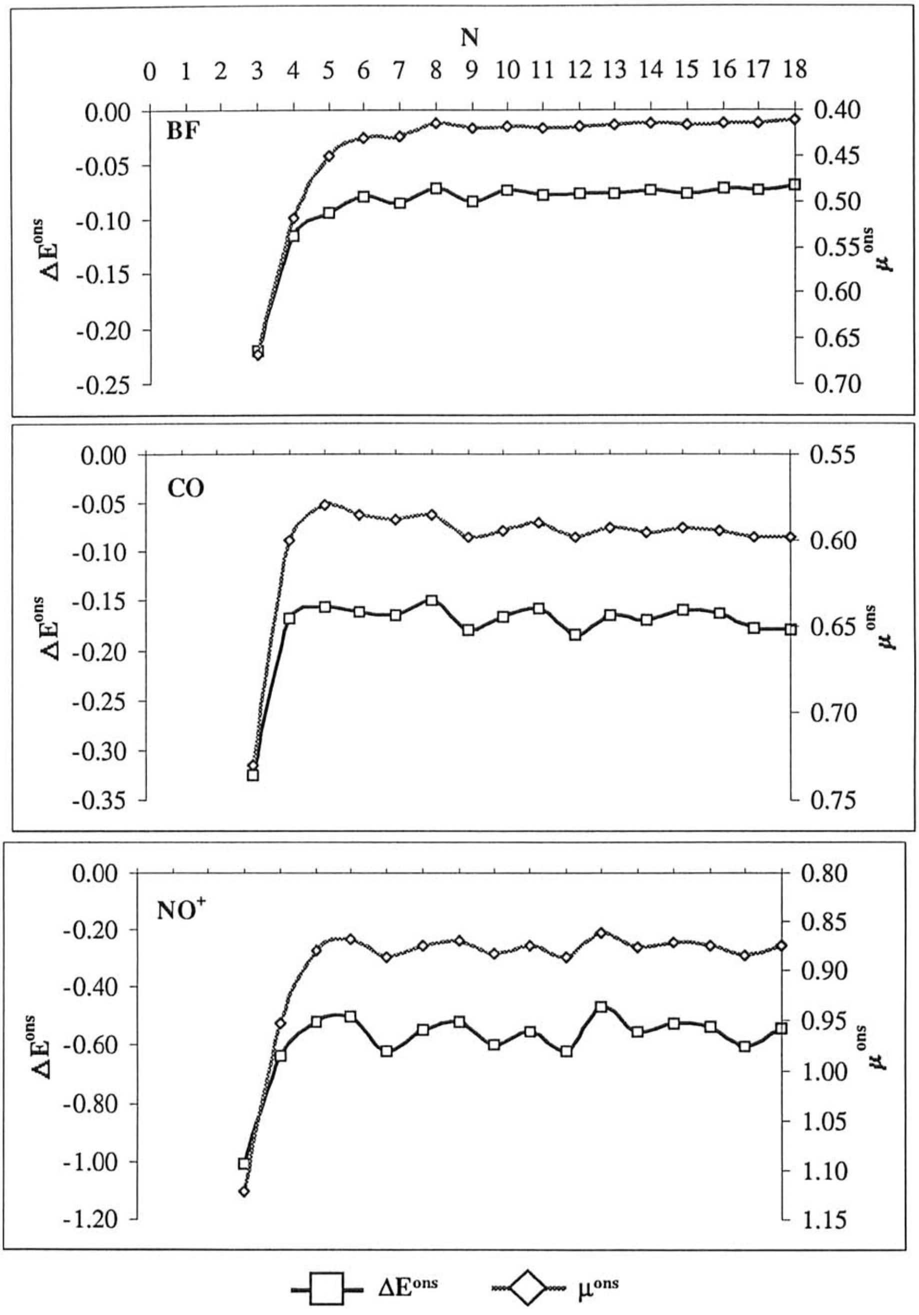

Figure 4: Dipole moment and energy difference for the quantum Onsager model with increasing size of basis set.

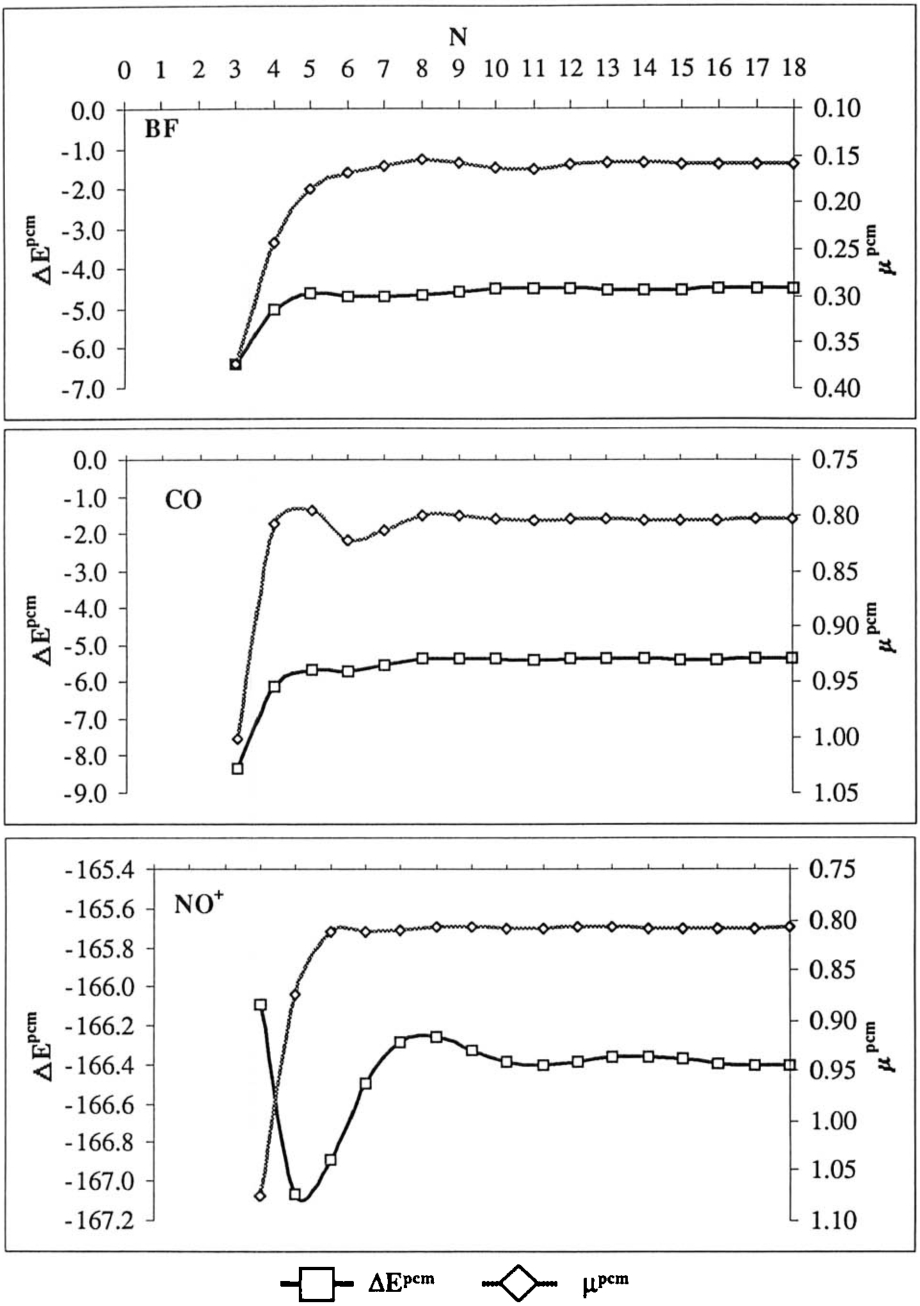

Figure 5: Energy difference and dipole moment for the Polarized Continuum model with increasing size of basis set.

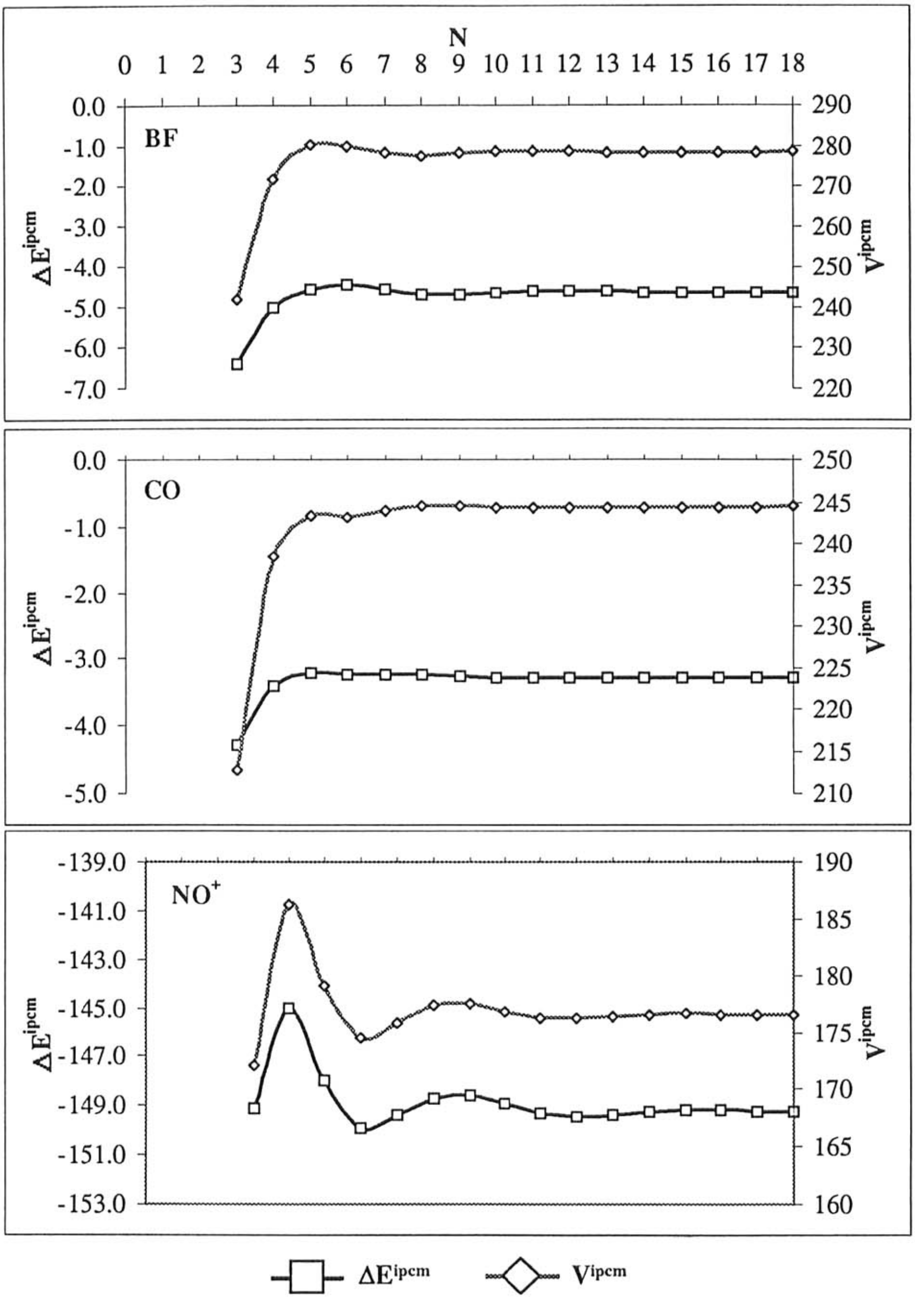

Figure 6: Energy difference and cavity volume for the Isodensity Polarized Continuum model with increasing size of basis set.

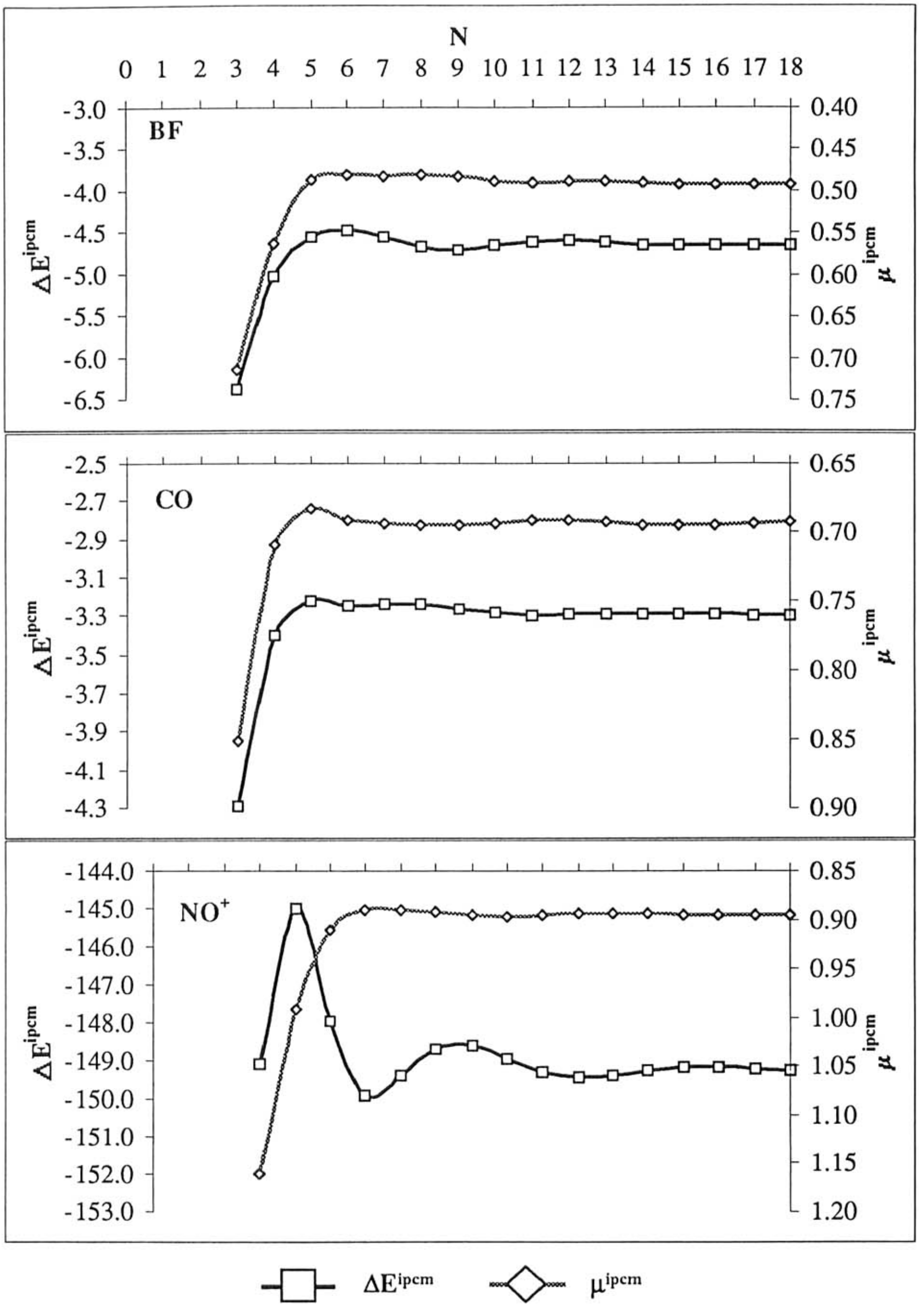

Figure 7: Energy difference and dipole moment for the Isodensity Polarized Continuum model with increasing size of basis set.

6 Conclusions

For the gas phase calculations reported in Tables 3, 4 and 5, the basis set truncation errors for the appropriate $30s15p$ even-tempered basis set are 72.8 mHartree for CO, 41.3 mHartree for BF and 115.7 mHartree for the NO^+ ion. It will be assumed that the basis set truncation errors in the calculations for the solvated species are of a comparable magnitude. For the neutral species, CO and BF, ΔE^{pcm} and ΔE^{ipcm} are, therefore, about an order of magnitude smaller than the corresponding basis set truncation error. For CO, ΔE^{pcm} and ΔE^{ipcm} have a magnitude of $\sim$ 7.4% and $\sim$ 4.5% of the basis set truncation error, whilst for BF, ΔE^{pcm} and ΔE^{ipcm} both have a magnitude of $\sim$ 11% of the basis set truncation error. The Quantum Onsager Model consistently predicts a much smaller solvation effect on the energies than both the Polarized Continuum Model and the Isodensity Polarized Continuum Model, largely due to the unrealistic description of the cavity. ΔE^{ons} has a magnitude of just 0.2% of the basis set truncation error for both CO and BF.

The convergence behaviour observed in the present study for continuum models of solvated species using systematic sequences of even-tempered basis sets of Gaussian primitive functions of s- and p- symmetry mirrors that observed for the gas phase molecular species. Gas phase matrix Hartree-Fock calculations for the isoelectronic molecules studied in the present work which approach a sub-$\mu Hartree$level of accuracy for the total energy have been reported elsewhere[18]-[25]. The present work demonstrates that this approach can be applied to molecules in solution by making use of continuum models. The basis set truncation error would then be $\sim$ 3 orders of magnitude smaller than the ΔE^x values.

Acknowledgment
One of us (S.W.) acknowledges the support of E.P.S.R.C. under Grant GR/L65567.

References

[1] K.P. Lawley (Ed.), *Ab initio Methods in Quantum Chemistry*, Adv. Chem. Phys. **67**, **68**, J. Wiley & Sons, Chichester (1987)

[2] R. McWeeny, *Methods of Molecular Quantum Mechanics*, 2^{nd} Edition, Academic Press, London (1989)

[3] S. Wilson and G.H.F. Diercksen (Ed.), *Methods in Computational Molecular Physics*, Plenum, New York (1992)

[4] E. Clementi and G. Corongui, *Methods and Techniques in Computational Chemistry*, METECC-95, STEF, Cagliari (1995)

[5] J. Tomasi and M. Persico, *Chem. Rev.* **94**, 2027 (1994)

[6] M. Karelson, *Adv. Quantum Chem.* **28**, 141 (1997)

[7] M. Karelson and G.H.F. Diercksen, in *Problem Solving in Computational Molecular Science: Molecules in Different Environments*, edited by S. Wilson and G.H.F. Diercksen, Kluwer, Dordrecht (1997)

[8] S. Wilson and G.H.F. Diercksen (Ed.), *Problem Solving in Computational Molecular Science: Molecules in Different Environments*, Kluwer, Dordrecht (1997)

[9] J. Tomasi, *Adv. Quantum Chem. (this volume)*

[10] S. Wilson, *Electron correlation in molecules*, Clarendon Press, Oxford (1984)

[11] T.H. Dunning, Jr., and P.J. Hay, *Methods in Electronic Structure Theory*, edited by H.F. Schaefer III, Plenum, New York (1977)

[12] R. Ahlrichs and P.R. Taylor, J. chim. Phys. **78**, 315 (1981)

[13] S. Wilson, in *Methods in Computational Molecular Physics*, edited by G.H.F. Diercksen and S. Wilson, NATO ASI Series C, Vol. 113, Reidel, Dordrecht, (1983)

[14] S. Huzinaga, Comput. Phys. Rept. **2**, 279 (1985)

[15] E.R. Davidson and D. Feller, Chem. Rev. **86**, 681 (1986)

[16] S. Wilson, Adv. Chem. Phys. **67**, 439 (1987)

[17] S. Wilson, in *Problem Solving in Computational Molecular Science: Molecules in Different Environments*, edited by S. Wilson and G.H.F. Diercksen, Kluwer, Dordrecht (1997)

[18] B.H. Wells and S. Wilson, J. Phys. B: At. Mol. Opt. Phys. **18**, 2731 (1985)

[19] B.H. Wells and S. Wilson, J. Phys. B: At. Mol. Opt. Phys. **22,** 1285 (1989)

[20] D. Moncrieff and S. Wilson, Chem. Phys. Lett. **209,** 423 (1993)

[21] D. Moncrieff and S. Wilson, J. Phys. B: At. Mol. Opt. Phys. **26,** 1605 (1993)

[22] J. Kobus, D. Moncrieff and S. Wilson, J. Phys. B: At. Mol. Opt. Phys. **27,** 5139 (1994)

[23] J. Kobus, D. Moncrieff and S. Wilson, J. Phys. B: At. Mol. Opt. Phys. **27,** 2867 (1994)

[24] D. Moncrieff, J. Kobus, and S. Wilson, J. Phys. B: At. Mol. Opt. Phys. **28**, 4555 (1995)

[25] J. Kobus, D. Moncrieff and S. Wilson, Molec. Phys. **86**, 1315 (1995)

[26] D. Moncrieff and S. Wilson, J. Phys. B: At. Mol. Opt. Phys. **28,** 4007 (1995)

[27] D. Moncrieff and S. Wilson, J. Phys. B: At. Mol. Opt. Phys. **29**, 2425 (1996)

[28] D. Moncrieff and S. Wilson, J. Phys. B: At. Mol. Opt. Phys. **29**, 6009 (1996)

[29] D. Moncrieff, J. Kobus and S. Wilson, J. Phys. B: At. Mol. Opt. Phys. **28**, 4555 (1995)

[30] W.J. Hehre, R.F. Stewart and J.A. Pople, J. Chem. Phys. **51**, 2657 (1969)

[31] J.B. Collins, P. v. R. Schleyer, J.S. Binkley and J.A. Pople, J. Chem. Phys. **64**, 5142 (1976)

[32] J.S. Binkley, J.A. Pople and W.J. Hehre, J. Amer. Chem. Soc. **102**, 939 (1980)

[33] M.S. Gordon, J.S. Binkley, J.A. Pople, W.J. Pietro and W.J. Hehre, J. Amer. Chem. Soc. **104**, 2797 (1982)

[34] W.J. Pietro, M.M. Francl, W.J. Hehre, D.J. Defrees, J.A. Pople and J.S. Binkley, J. Amer. Chem. Soc. **104**, 5039 (1982)

[35] R. Ditchfield, W. Hehre and J.A. Pople, J. Chem. Phys. **54**, 724 (1971)

[36] W. Hehre, R. Ditchfield and J.A. Pople, J. Chem. Phys. **56**, 2257 (1972)

[37] P.C. Hariharan and J.A. Pople, Molec. Phys. **27**, 209 (1974)

[38] M.S. Gordon Chem. Phys. Lett. **76**, 163 (1980)

[39] P.C. Hariharan and J.A. Pople, Theo. Chim. Acta. **28**, 213 (1973)

[40] M. J. Frisch, G. W. Trucks, H. B. Schlegel, P. M. W. Gill, B .G. Johnson, M. A. Robb, J. R. Cheeseman, T. Keith, G. A. Petersson, J. A. Montgomery, K. Raghavachari, M. A. Al-Laham, V. G. Zakrzewski, J. V. Ortiz, J. B. Foresman, J. Cioslowski, B. B. Stefanov, A. Nanayakkara, M. Challacombe, C. Y. Peng, P. Y. Ayala, W. Chen, M. W. Wong, J. L. Andres, E. S. Replogle, R. Gomperts, R. L. Martin, D. J. Fox, J. S. Binkley, D. J. Defrees, J. Baker, J. P. Stewart, M. Head-Gordon, C. Gonzalaz and J. A. Pople, GAUSIAN94 Rev. C.3, Gaussian Inc., Pittsburgh PA, (1995)

[41] O. Tapia and O. Goscinski, Molec. Phys. **29**, 1683 (1975)

[42] J.-L. Rivail and D. Rinaldi, Chem Phys. **18**, 233 (1976)

[43] M.M. Karelson, Org. React. **17**, 357 (1980)

[44] J.G. Kirkwood, J. Chem. Phys. **2**, 351 (1934)

[45] L. Onsager, J. Am. Chem. Soc. **58** 1486 (1936)

[46] C.J.F. Böttcher, *Theory of Electric Polarization*, Elsevier, Amsterdam (1952)

[47] C.J.F. Böttcher, *Theory of Electric Polarization*, Vol. I, Elsevier, Amsterdam (1973)

[48] C.J.F. Böttcher and P. Bordewijk, *Theory of Electric Polarization*, Vol. II, Elsevier, Amsterdam (1978)

[49] M. W. Wong, K. W. Wiberg, M. Frisch, J.Chem.Phys. **95**, 8991 (1991)

[50] S. Miertus, E. Scrocco, J. Tomasi, Chem. Phys. **55**, 117 (1981)

[51] J. Tomasi, R. Bonaccorsi, R. Cammi and F. J. O. d. Valle, J. Mol. Struct.: THEOCHEM **234** 401 (1991)

[52] J. Tomasi and R. Bonaccorsi, Croat. Chem. Acta. **65**, 29 (1992)

[53] I. Tunon, E. Silla, J. Tomasi, J. Phys. Chem. **96**, 9043 (1992)

[54] J. B. Foresman, Æ Frisch, *Exploring Chemistry with Electronic Structure Methods - A guide to using Gaussian*, Gaussian Inc. Ch.10 (1996)

[55] R. McWeeny, *Dissertation*, University of Oxford (1948)

[56] C. Reeves, J. Chem. Phys. **39**, 1 (1963)

[57] C. Reeves and M. Harrison, J. Chem. Phys. **39**, 11 (1963)

[58] K. Ruedenberg, R.C. Raffenetti and R. Bardo, in *Energy, Structure and Reactivity*, Proceedings of the 1972 Boulder Conference on Theoretical Chemistry, Wiley, New York (1973)

[59] R.C. Raffenetti and K. Ruedenberg, J. Chem. Phys. **59**, 5978 (1973)

[60] R.C. Raffenetti, J. Chem. Phys. **58**, 4452 (1973)

[61] R.C. Raffenetti, J. Chem. Phys. **59**, 5936 (1973)

[62] R.D. Bardo and K. Ruedenberg, J. Chem. Phys. **59**, 5956 (1973)

[63] R.D. Bardo and K. Ruedenberg, J. Chem. Phys. **59**, 5966 (1973)

[64] R.D. Bardo and K. Ruedenberg, J. Chem. Phys. **60**, 918 (1974)

[65] M. W. Schmidt, K. Ruedenberg, J. Chem. Phys. **71**, 3951 (1979)

[66] D.M. Silver, S. Wilson and W. Nieupoort, Intern. J. Quantum Chem.**14**, 635 (1978)

[67] D.M. Silver and W. Nieupoort, Chem. Phys. Lett. **57**, 421 (1978)

[68] D.M. Silver and S. Wilson, J. Chem. Phys. **69**, 3787 (1978)

[69] S. Wilson and D.M. Silver, Chem. Phys. Lett. **63**, 367 (1979)

[70] P. Mezey, Theoret. chim. Acta **53**, 187 (1979)

[71] S. Wilson and D.M. Silver, J. Chem. Phys. **72**, 2159 (1980)

[72] S. Wilson and D.M. Silver, J. Chem. Phys. **77**, 3674 (1982)

[73] S. Wilson, Theoret. chim. Acta **58**, 31 (1980)

[74] S. Wilson, Chem. Phys. Lett. **81**, 467 (1981)

[75] D. Sundholm, P. Pyykkö and L. Laaksonen, Intern. J. Quantum Chem. (1983)

[76] L. Laaksonen, P. Pyykkö and D. Sundholm, Comput. Phys. Reports **4**, 313 (1986)

[77] P. Pyykkö, in *Numerical Determination of the Electronic Structure of Atoms, Diatomic and Polyatomic Molecules*, edited by M. Defraneschi and J. Dehalle, NATO ASI Series C271, p. 161, Kluwer, Dordrecht (1989)

[78] J. Kobus, Chem. Phys. Lett. **202**, 7 (1993)

[79] J. Kobus, Comput. Phys. Comm. **78**, 247 (1994)

[80] J. Kobus, L. Laaksonen and D. Sundholm Comput. Phys. Comm. **98**, 346 (1996)

[81] D. Moncrieff and S. Wilson, J. Phys. B: At. Mol. Opt. Phys. **27**, 1 (1994)

Beyond the transition state treatment.

by
Jan Linderberg
(jan@kemi.aau.dk)
Department of Chemistry
Aarhus University
DK-8000 Aarhus C, Denmark

Abstract

Transmission coefficients are determined numerically for a simple two-state problem designed to simulate the passage of a chemical system through a transition state conformation where the electronic nature of the ground state changes substantially.

Contents

Motivation
R-matrix theory
Electronic model
Basis set expansion
Matrix algebra
Examples
Further comments
Acknowledgment
Appendix

ADVANCES IN QUANTUM CHEMISTRY, VOLUME 32
Copyright © 1999 by Academic Press. All rights of reproduction in any form reserved.
0065-3276/99 $30.00

Motivation

Emphasis is given in this note to the development of a model, which, with a modest numerical effort, can be used to incorporate the influence of an excited electronic state on the nuclear motion in the lowest electronic state. Such attempts have recently been undertaken by Shin and Light[1] and followed up by Qi and Bowman[2]. The rate of reactions, which are perceived to be well described by a ground state energy hypersurface, may be influenced to a considerable extent by excited electronic states. The simple model proposed in this note accommodates the interaction with one excited state and can be readily extended to several. Calculations are carried out and illustrate the effect of an excited state for varying degree of coupling.

R-matrix theory

The vehicle for the analysis of the scattering problem will be the Wigner-Eisenbud R-matrix formulation[3]. We consider a quantum system with two degrees of freedom represented by coordinates q for the nuclear motion and x for the electronic part. The domain for these variables will be such that the coupling between the two coordinates is considered only when q belongs to the interval $[r,p]$. The domain for the electronic coordinate is arbitrary, the space will instead be limited by a choice of two basis functions.

Most generally, the variational functional of R-matrix theory[4] takes the form

$$\begin{aligned} J(\Psi,\Phi) = {} & \iint_{\Omega} dq dx \left\{ \left[E - W(q,x) \right] \left| \Psi(q,x) \right|^2 - \left| \nabla \Psi(q,x) \right|^2 \right\} \\ & + \oint_{\Gamma} ds \left[\Psi^*(q,x) \Phi(q,x) + \Phi^*(q,x) \Psi(q,x) \right] \\ & - \oint_{\Gamma} ds \Phi^*(q,x) \oint_{\Gamma} ds' \mathfrak{R}(q,x;q',x') \Phi(q',x') \end{aligned} \tag{1}$$

where units and variables have been chosen so as to give as simple a form as possible. The gradient form in the first integral reads in expanded form

$$\left| \nabla \Psi(q,x) \right|^2 = \left| \frac{\partial \Psi(q,x)}{\partial x} \right|^2 + \left| \frac{\partial \Psi(q,x)}{\partial q} \right|^2 \tag{2}$$

The domain Ω is described above and Γ is its boundary with the measure ds. A stationary value of the functional J leads to the Schrödinger equation on Ω and two relations between Φ and Ψ on the boundary which combine[4] to give the amplitude Ψ on Γ as a functional of the outward gradient on Γ. We limit the electronic space by means of a set of two orthonormal basis functions, $u_r(x)$ and $u_p(x)$, and put

$$\Psi(q,x) = u_r(x) a_r(q) + u_p(x) a_p(q) \tag{3}$$

It should be observed here that the electronic basis is chosen to be independent of the nuclear coordinate. This an ideal situation but may have limited applicability. The form (3) results in substantial reductions in the functional (1) which becomes

$$
\begin{aligned}
J\left(a_r,a_p,\{b\}\right) = & \int_r^p dq\left\{\left[E-\alpha_r(q)\right]\left|a_r(q)\right|^2-\left|\frac{da_r(q)}{dq}\right|^2\right\} \\
& -\int_r^p dq\,\beta(q)\left[a_r^*(q)a_p(q)+a_p^*(q)a_r(q)\right] \\
& +\int_r^p dq\left\{\left[E-\alpha_p(q)\right]\left|a_p(q)\right|^2-\left|\frac{da_p(q)}{dq}\right|^2\right\} \\
& +a_r^*(r)b_{rr}+a_p^*(r)b_{pr}+a_r^*(p)b_{rp}+a_p^*(p)b_{pp} \\
& +b_{rr}^*a_r(r)+b_{pr}^*a_p(r)+b_{rp}^*a_r(p)+b_{pp}^*a_p(p) \\
& -\begin{bmatrix} b_{rr}^* & b_{pr}^* & b_{rp}^* & b_{pp}^* \end{bmatrix}
\begin{bmatrix}
\mathfrak{R}_{rr,rr} & \mathfrak{R}_{rr,pr} & \mathfrak{R}_{rr,rp} & \mathfrak{R}_{rr,pp} \\
\mathfrak{R}_{pr,rr} & \mathfrak{R}_{pr,pr} & \mathfrak{R}_{pr,rp} & \mathfrak{R}_{pr,pp} \\
\mathfrak{R}_{rp,rr} & \mathfrak{R}_{rp,pr} & \mathfrak{R}_{rp,rp} & \mathfrak{R}_{rp,pp} \\
\mathfrak{R}_{pp,rr} & \mathfrak{R}_{pp,pr} & \mathfrak{R}_{pp,rp} & \mathfrak{R}_{pp,pp}
\end{bmatrix}
\begin{bmatrix} b_{rr} \\ b_{pr} \\ b_{rp} \\ b_{pp} \end{bmatrix}
\end{aligned} \tag{4}
$$

Electronic features enter through the elements

$$
\begin{aligned}
\alpha_r(q) &= \int dx\left[W(q,x)\left|u_r(x)\right|^2+\left|\frac{du_r(x)}{dx}\right|^2\right] \\
\beta(q) &= \int dx\left[W(q,x)u_p^*(x)u_r(x)+\frac{du_p^*(x)}{dx}\frac{du_r(x)}{dx}\right] \\
\alpha_p(q) &= \int dx\left[W(q,x)\left|u_p(x)\right|^2+\left|\frac{du_p(x)}{dx}\right|^2\right]
\end{aligned} \tag{5}
$$

while the b-parameters are given by expressions like

$$
b_{rp} = \int dx\,u_r^*(x)\Phi(p,x) \tag{6}
$$

and the R-matrix is reduced to a four-by-four form. Variational stability of the functional (4) requires that the Euler equations,

$$
\begin{aligned}
\left[E-\alpha_r(q)\right]a_r(q)+\frac{d^2a_r}{dq^2} &= \beta(q)a_p(q) \\
\left[E-\alpha_p(q)\right]a_p(q)+\frac{d^2a_p}{dq^2} &= \beta(q)a_r(q)
\end{aligned} \tag{7}
$$

are satisfied together with the boundary conditions

$$\frac{da_r(r)}{dq}+b_{rr}=0;\frac{da_p(r)}{dq}+b_{pr}=0;-\frac{da_r(p)}{dq}+b_{rp}=0;-\frac{da_p(p)}{dq}+b_{pp}=0; \quad (8)$$

and

$$\begin{bmatrix} a_r(r) \\ a_p(r) \\ a_r(p) \\ a_p(p) \end{bmatrix} = \begin{bmatrix} \Re_{rr,rr} & \Re_{rr,pr} & \Re_{rr,rp} & \Re_{rr,pp} \\ \Re_{pr,rr} & \Re_{pr,pr} & \Re_{pr,rp} & \Re_{pr,pp} \\ \Re_{rp,rr} & \Re_{rp,pr} & \Re_{rp,rp} & \Re_{rp,pp} \\ \Re_{pp,rr} & \Re_{pp,pr} & \Re_{pp,rp} & \Re_{pp,pp} \end{bmatrix} \begin{bmatrix} b_{rr} \\ b_{pr} \\ b_{rp} \\ b_{pp} \end{bmatrix} \quad (9)$$

Four linearly independent solutions exist in general for the system (7) and when they can be found they specify the R-matrix uniquely.

We consider only the case that there is one open entrance channel and one open exit channel, characterized by the electronic states $u_r(x)$ and $u_p(x)$ respectively. This requires that

$$\begin{aligned} &E=\alpha_p(r)-\kappa_p^2;\kappa_p>0;E=\alpha_r(p)-\kappa_r^2;\kappa_r>0; \\ &E=\alpha_r(r)+k_r^2;k_r>0;E=\alpha_p(p)+k_p^2;k_p>0. \end{aligned} \quad (10)$$

It will be assumed that the boundary conditions are those for a constant potential outside the interval $[r,p]$ so that by standard notations

$$\begin{aligned} &a_r(r)=\frac{1-S_{rr}}{\sqrt{k_r}};\frac{da_r(r)}{dq}=i\sqrt{k_r}(1+S_{rr});\frac{da_p(r)}{dq}=\kappa_p a_p(r); \\ &a_p(p)=-\frac{S_{pr}}{\sqrt{k_p}};\frac{da_p(p)}{dq}=-i\sqrt{k_p}S_{pr};\frac{da_r(p)}{dq}=-\kappa_r a_r(p); \end{aligned} \quad (11)$$

we introduce elements of the S-matrix. Additional phase factors should be considered in order to relate asymptotic states. There are four unknowns in the set (11) and they can be solved for from the system (9) in the form

$$\begin{gathered} \begin{bmatrix} \Re_{pr,pr}+\frac{1}{\kappa_p} & \Re_{pr,rp} \\ \Re_{rp,pr} & \Re_{rp,rp}+\frac{1}{\kappa_r} \end{bmatrix} \begin{bmatrix} b_{pr} \\ b_{rp} \end{bmatrix} + \begin{bmatrix} \Re_{pr,rr} & \Re_{pr,pp} \\ \Re_{rp,rr} & \Re_{rp,pp} \end{bmatrix} \begin{bmatrix} -i\sqrt{k_r}(1+S_{rr}) \\ -i\sqrt{k_p}S_{pr} \end{bmatrix} = 0; \\ \begin{bmatrix} \Re_{rr,rr}+\frac{i}{k_r} & \Re_{rr,pp} \\ \Re_{pp,rr} & \Re_{pp,pp}+\frac{i}{k_p} \end{bmatrix} \begin{bmatrix} -i\sqrt{k_r}(1+S_{rr}) \\ -i\sqrt{k_p}S_{pr} \end{bmatrix} + \begin{bmatrix} \Re_{rr,pr} & \Re_{rr,rp} \\ \Re_{pp,pr} & \Re_{pp,rp} \end{bmatrix} \begin{bmatrix} b_{pr} \\ b_{rp} \end{bmatrix} = \begin{bmatrix} \frac{2}{\sqrt{k_r}} \\ 0 \end{bmatrix} \end{gathered} \quad (12)$$

which is seen to reduce to the problem

$$\begin{bmatrix} \Re^o_{rr} + \dfrac{i}{k_r} & \Re^o_{rp} \\ \Re^o_{pr} & \Re^o_{pp} + \dfrac{i}{k_p} \end{bmatrix} \begin{bmatrix} \sqrt{k_r}(1+S_{rr}) \\ \sqrt{k_p}S_{pr} \end{bmatrix} = \begin{bmatrix} \dfrac{2i}{\sqrt{k_r}} \\ 0 \end{bmatrix} \tag{13}$$

The reduced R-matrix connects only open channels and is symmetric which guarantees a symmetric and unitary S-matrix. The transmission probability, which will be the quantity to calculate, equals the square modulus of the off diagonal S-matrix element:

$$P_{p\leftarrow r}(E) = \left|S_{pr}(E)\right|^2 \tag{14}$$

and depends on the energy through the R-matrix elements and the wave numbers k_r and k_p.

Electronic model.

Particular assumptions are introduced with regard to the functional form of the matrix elements (5) for the electronic states. There should be no coupling between the two at the entrance and exit of the domain, thus

$$\beta(r) = \beta(p) = 0, \tag{15}$$

and the open channels should have a smooth connection to a constant potential outside the domain so that

$$\frac{d\alpha_r(r)}{dq} = \frac{d\alpha_p(p)}{dq} = 0. \tag{16}$$

The simplest forms to satisfy these conditions are

$$\begin{aligned} \alpha_r(q) &= \alpha_r(r) + \tfrac{1}{2}\alpha_r''(r)(q-r)^2, \\ \beta(q) &= \beta_0(q-r)(p-q), \\ \alpha_p(q) &= \alpha_p(p) + \tfrac{1}{2}\alpha_p''(p)(q-p)^2. \end{aligned} \tag{17}$$

which is the one-dimensional version of a two-dimensional potential model used earlier[5]. The closed channels cannot be connected to a constant asymptotic potential with this form and maintain a continuous derivative. Five parameters characterize the electronic model, the two energies $\alpha_r(r)$ and $\alpha_p(p)$ determine the endo- or exothermicity of the process. The other three give the properties of the adiabatic barrier, its height, position, and curvature. They are connected by the conditions that the adiabatic energy should have a maximum at the transition point. Energies are conveniently referred to the top of the barrier as the zero of energy. The coordinate at the top is called t and an auxiliary parameter γ is introduced in order to simplify the analysis.

Both diabatic states will have positive energies at the transition geometry and since the adiabatic ground state is at zero energy it holds that

$$\alpha_r(t)\alpha_p(t) = \beta^2(t). \tag{18}$$

The maximum property requires that

$$\alpha_r'(t)\alpha_p(t)+\alpha_r(t)\alpha_p'(t)=2\beta(t)\beta'(t). \tag{19}$$

We find from the forms (17) and Eqs. (18) and (19) that

$$\frac{\alpha_r'(t)}{\alpha_r(t)}-\frac{2}{t-r}=\frac{2}{t-p}-\frac{\alpha_p'(t)}{\alpha_p(t)}=\frac{2}{\gamma}. \tag{20}$$

which leads to the expressions

$$\alpha_r''(r)=2\alpha_r(r)\frac{\gamma+t-r}{(r-t)^3};\quad \alpha_p''(p)=2\alpha_p(p)\frac{\gamma+p-t}{(t-p)^3};\quad \beta_0^2=\frac{\alpha_r(r)\alpha_p(p)\gamma^2}{(r-t)^3(t-p)^3}. \tag{21}$$

A negative value is chosen for β_0. The energy gap between the top of the barrier and the upper state in the adiabatic picture is

$$\Delta E=\alpha_r(t)+\alpha_p(t)=\left[\frac{\alpha_r(r)}{r-t}+\frac{\alpha_p(p)}{t-p}\right]\gamma \tag{22}$$

and the radius of curvature ρ on top of the barrier derives from the relation

$$\rho\left(\frac{8}{\gamma}+\frac{6}{t-r}+\frac{6}{p-t}\right)=\frac{t-r}{\alpha_r(r)}+\frac{p-t}{\alpha_p(p)}. \tag{23}$$

It is negative since the function is convex in the vicinity of the top. Either Eq. (22) or Eq.(23) can be used to set a desirable value of the parameter γ.

Figure 1. These are the diabatic, $\alpha_r(q)$ and $\alpha_p(q)$, and adiabatic energies for the model with ε_r = -0.03319E_h, r = -0.1419Å, t = 0, ε_p = -0.03255E_h, p = 0.1409Å, and γ = 0.043Å.

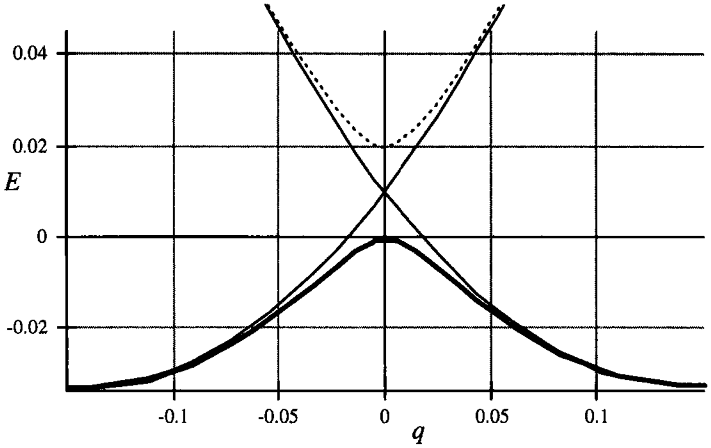

Basis set expansion.

No readily useful analytical solutions are available for the system (7) and we resort to an expansion of the amplitude functions in a basis set. The discrete variable representation[6] is a convenient means and we chose to employ a localized basis associated with the Lobatto quadrature rule[7]. It is convenient then to choose units and displacement such that the interval $[r,p]$ equals the standard one, $[-1,1]$. A basis of $n+1$ Lagrange interpolation functions is defined from the Legendre polynomial $P_n(q)$ as follows

$$u_j(q) = \frac{\left(1-q^2\right)P'_n(q)}{n(n+1)\left(q_j - q\right)P_n\left(q_j\right)}, \qquad q_j \in \left\{q \middle| \left(1-q^2\right)P'_n(q) = 0\right\} \tag{24}$$

so that the amplitude functions are given as

$$a_s(q) = \sum_0^n a_s\left(q_j\right)u_j(q), \qquad s = r,p. \tag{25}$$

Integrals over the interval are given by the rule

$$\int_{-1}^{1} dq f(q) = \sum_0^n w_j f\left(q_j\right); \qquad w_j = \frac{2}{n(n+1)P_n^2\left(q_j\right)}, \tag{26}$$

with an error term proportional to the $(2n)$-th derivative of $f(q)$. All integrals in the functional (4) with the elements (17) will be accurate if the amplitude functions are constrained to polynomials of degree n-2. This gives the conditions

$$0 = \sum_0^n \frac{a_s\left(q_j\right)}{P_n\left(q_j\right)} = \sum_0^n \frac{q_j a_s\left(q_j\right)}{P_n\left(q_j\right)}, \qquad s = r,p. \tag{27}$$

A set of two amplitudes should be eliminated. Those at the end points are readily expressed in terms of the others by means of Eq. (27). Thus,

$$\begin{aligned} \frac{a_s(-1)}{P_n(-1)} + \frac{a_s(1)}{P_n(1)} &= -\sum_1^{n-1} \frac{a_s\left(q_j\right)}{P_n\left(q_j\right)}, & s &= r,p, \\ -\frac{a_s(-1)}{P_n(-1)} + \frac{a_s(1)}{P_n(1)} &= -\sum_1^{n-1} \frac{q_j a_s\left(q_j\right)}{P_n\left(q_j\right)}, & s &= r,p. \end{aligned} \tag{28}$$

or resolved

$$\begin{aligned} a_s(-1) &= -P_n(-1)\sum_1^{n-1} \frac{\left(1-q_j\right)a_s\left(q_j\right)}{2P_n\left(q_j\right)}, & s &= r,p, \\ a_s(1) &= -P_n(1)\sum_1^{n-1} \frac{\left(1+q_j\right)a_s\left(q_j\right)}{2P_n\left(q_j\right)}, & s &= r,p. \end{aligned} \tag{29}$$

where it should be observed that the sums on the right hand side do not involve the points given on the left hand side. This is explicit for the first and third but implicit in the second of Eqs. (29).

The derivatives of the amplitude functions have the values

$$\frac{da_s(q_k)}{dq}=\sum_{j\neq k}^{0,n}\frac{a_s(q_j)P_n(q_k)}{(q_k-q_j)P_n(q_j)}+\frac{a_s(q_k)P_n'(q_k)}{2P_n(q_k)},s=r,p, \tag{30}$$

where the last term occurs only at the end points. There is no reason to make an explicit substitution of the forms (29) in the expression (30).

The basis set expansion reduces the functional (4) to a sesquilinear form in the amplitudes at the grid points and we have

$$\begin{aligned}
J(\{a_s(q_j)\},\{b\}) = {} & \sum_0^n w_j\left\{\left[E-\alpha_r(q_j)\right]\left|a_r(q_j)\right|^2-\left|\frac{da_r(q_j)}{dq}\right|^2\right\} \\
& -\sum_0^n w_j\beta(q_j)\left[a_r^*(q_j)a_p(q_j)+a_p^*(q_j)a_r(q_j)\right] \\
& +\sum_0^n w_j\left\{\left[E-\alpha_p(q_j)\right]\left|a_p(q_j)\right|^2-\left|\frac{da_p(q_j)}{dq}\right|^2\right\} \\
& +a_r^*(r)b_{rr}+a_p^*(r)b_{pr}+a_r^*(p)b_{rp}+a_p^*(p)b_{pp} \\
& +b_{rr}^*a_r(r)+b_{pr}^*a_p(r)+b_{rp}^*a_r(p)+b_{pp}^*a_p(p) \\
& -\begin{bmatrix} b_{rr}^* & b_{pr}^* & b_{rp}^* & b_{pp}^* \end{bmatrix}\begin{bmatrix} \mathfrak{R}_{rr,rr} & \mathfrak{R}_{rr,pr} & \mathfrak{R}_{rr,rp} & \mathfrak{R}_{rr,pp} \\ \mathfrak{R}_{pr,rr} & \mathfrak{R}_{pr,pr} & \mathfrak{R}_{pr,rp} & \mathfrak{R}_{pr,pp} \\ \mathfrak{R}_{rp,rr} & \mathfrak{R}_{rp,pr} & \mathfrak{R}_{rp,rp} & \mathfrak{R}_{rp,pp} \\ \mathfrak{R}_{pp,rr} & \mathfrak{R}_{pp,pr} & \mathfrak{R}_{pp,rp} & \mathfrak{R}_{pp,pp} \end{bmatrix}\begin{bmatrix} b_{rr} \\ b_{pr} \\ b_{rp} \\ b_{pp} \end{bmatrix}
\end{aligned} \tag{31}$$

It should be kept in mind that this form depends on the amplitudes given in Eqs. (29) and that in order to construct the Euler equations, one utilizes those forms.

Matrix algebra.

The sesquilinear form (31) is stationary when a set of linear equations in the amplitudes $\{a_s(q_j)\}$ and $\{b_{ss'}\}$ is satisfied. These equations can be written as a matrix equation with the partitioned structure

$$\begin{bmatrix} \mathbf{A} & \mathbf{d} \\ \mathbf{d}^\dagger & -\mathbf{R} \end{bmatrix}\begin{bmatrix} \mathbf{a} \\ \mathbf{b} \end{bmatrix}=0 \tag{32}$$

where the **R**-block is the desired entity. It follows that

$$\mathbf{R}=-\mathbf{d}^\dagger\mathbf{A}^{-1}\mathbf{d} \tag{33}$$

and the solution exists as long as the block **A** is not singular.

The matrix elements of the block **A** are obtained from the form (29) as

$$\mathbf{A}_{sj,s'k} = \frac{\partial^2 J}{\partial a_{sj}^* \partial a_{s'k}} \tag{34}$$

by taking into account that the end point amplitudes are given in Eqs. (29). Elements of the block **d** derive from the end point amplitudes,

$$\mathbf{d}_{sj,s's''} = \frac{\partial^2 J}{\partial a_{sj}^* \partial b_{s's''}} \tag{35}$$

and are

$$\left.\begin{aligned} d_{sj,s'r} &= -\delta_{ss'} P_n(-1) \frac{1-q_j}{2P_n(q_j)}, \\ d_{sj,s'p} &= -\delta_{ss'} P_n(1) \frac{1+q_j}{2P_n(q_j)}, \end{aligned}\right\} j = 1,2,\ldots n-1, s, s' = r, p. \tag{36}$$

The matrix equation (32) can be modified to give the S-matrix elements directly. To this end we retain the first rows of the partitioned problem and add the boundary conditions from Eqs. (8) and (11) as

$$\begin{aligned} a_r(r) + \frac{i}{k_r} b_{rr} &= \frac{2}{\sqrt{k_r}}; \quad a_r(p) + \frac{1}{\kappa_r} b_{rp} = 0; \\ a_p(r) + \frac{1}{\kappa_p} b_{pr} &= 0; \quad a_p(p) + \frac{i}{k_p} b_{pp} = 0. \end{aligned} \tag{37}$$

The result is the system of equations comprehensively written as

$$\begin{bmatrix} \mathbf{A} & \mathbf{d} \\ \mathbf{d}^\dagger & i\mathbf{k}^{-1} \end{bmatrix} \begin{bmatrix} \mathbf{a} \\ \mathbf{b} \end{bmatrix} = \begin{bmatrix} \mathbf{0} \\ \mathbf{c} \end{bmatrix} \tag{38}$$

with the diagonal matrix **k** and the right hand side **c** are defined by

$$(\mathbf{k})_{ss',ss'} = k_r \delta_{sr} \delta_{rs'} + k_p \delta_{sp} \delta_{ps'} + i\kappa_r \delta_{sr} \delta_{ps'} + i\kappa_p \delta_{sp} \delta_{rs'}. \tag{39}$$

and

$$(\mathbf{c})_{ss'} = \frac{2}{\sqrt{k_r}} \delta_{sr} \delta_{rs'} \tag{40}$$

It is only necessary to find the element b_{pp} in order to determine the transition probability from Eq. (14):

$$P_{p \leftarrow r}(E) = |S_{pr}(E)|^2 = \frac{1}{k_p} |b_{pp}|^2. \tag{41}$$

The presence of the imaginary elements on the left hand side of the matrix equation (38) ensures that there is a solution for every energy E.

An actual solution of the system (38) in complex arithmetic is not warranted since there are only two elements which are complex. They are purely imaginary and it is then advantageous to separate the problem by considering the real and imaginary parts of the diagonal matrix **k**, that is into parts corresponding to open and closed channels respectively:

$$\mathbf{k} = \mathbf{k}_o + i\mathbf{k}_c, \tag{42}$$

and to rewrite (38) in the form

$$\begin{bmatrix} \mathbf{A} & \mathbf{d} \\ \mathbf{d}^\dagger & \mathbf{k}_c^{-1} \end{bmatrix} \begin{bmatrix} \mathbf{a} \\ \mathbf{b} \end{bmatrix} = \begin{bmatrix} \mathbf{0} \\ \mathbf{c} - i\mathbf{k}_o^{-1}\mathbf{b} \end{bmatrix}. \tag{43}$$

Inversion of the real symmetric matrix on the left hand side allow us to consider only two equations, those relating b_{rr} and b_{pp} . A suitable notation for the elements of the inverse is

$$\left\{ \begin{bmatrix} \mathbf{A} & \mathbf{d} \\ \mathbf{d}^\dagger & \mathbf{k}_c^{-1} \end{bmatrix}^{-1} \right\}_{ss,s's'} \equiv \Omega_{s,s'}, s, s' = r, p. \tag{44}$$

and leads to the form

$$\begin{bmatrix} \Omega_{r,r} - ik_r & \Omega_{r,p} \\ \Omega_{p,r} & \Omega_{p,p} - ik_p \end{bmatrix} \begin{bmatrix} ik_r^{-1} b_{rr} \\ ik_p^{-1} b_{pp} \end{bmatrix} = \begin{bmatrix} \Omega_{r,r} \\ \Omega_{p,r} \end{bmatrix} \frac{2}{\sqrt{k_r}} \tag{45}$$

and the result

$$P_{p\leftarrow r}(E) = \frac{1}{k_p} \left| b_{pp} \right|^2 = 4k_p k_r \left| \Omega_{p,r} \right|^2 \begin{Vmatrix} \Omega_{r,r} - ik_r & \Omega_{r,p} \\ \Omega_{p,r} & \Omega_{p,p} - ik_p \end{Vmatrix}^{-2}, \tag{46}$$

where the magnitude of the determinant enters. There may be energy values for which the inverse matrix in the expression (44) does not exist. A numerical problem occurs then, but the transmission probability is analytic on account of cancellation of singularities in denominator and numerator.

The real symmetric matrix on the left hand side of the system (43) depends on the energy variable linearly through the elements of the block **A** and otherwise in the block $\mathbf{k}_C$. Its inverse will be singular at real values E_n when there is a state with zero amplitude in the open channels at the boundary. We may conclude that the elements (44) have the appearance

$$\Omega_{s,s'} = \tfrac{1}{\varepsilon} v_s v_{s'} \pm u_s u_{s'} \tag{47}$$

for $\varepsilon = E - E_n$ and derive the result

$$\lim_{\varepsilon \to 0} P_{p\leftarrow r}(E_n + \varepsilon) = \frac{4k_p v_p^2 k_r v_r^2}{\left(k_p v_r^2 + k_2 v_p^2\right)^2 + \left(u_r v_p - u_p v_r\right)^4}, \tag{48}$$

which remains finite as stated above.

Examples.

Illustrations of the preceding model are offered by calculations on potentials derived for the nitrogen inversion of 2-methylaziridine (Fig. 2).

Figure 2. Diagram of 2-methylaziridine:

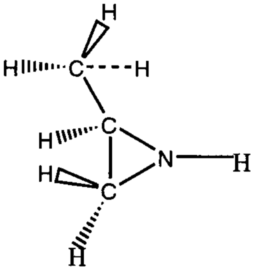

This is a preliminary exploration of the possibilities for describing processes with potential significance for stereospecificity in chemical reactions. Accurate electronic structure calculations by Ida M. B. Nielsen[9] at the second order Møller-Plesset perturbation theory level with a (6-31g*) Gaussian basis set puts the trans-form 33.19 milliHartree (mE_h) below the transition state while the cis-form is 32.55 mE_h below. The optimal distances[10,5] are 0.2678 Bohr radii (a_o) and 0.2663 a_o respectively. This gives a nearly symmetric potential barrier in the present model. The total mass of the system is 57.058 *u*.

The model is determined from one additional parameter, the energy gap at the transition state between the two adiabatic levels, as defined in Eq. (22). Calculations have been performed for three values of the energy gap, $5mE_h$, $10mE_h$, $20mE_h$. The transmission probability has been evaluated in the two-state formulation and in the single adiabatic state approximation. A relatively large gap, $20mE_h$, leads to very similar results for the two cases, Fig. 3 , as long as the system energy is less than the bottom of the upper adiabatic state energy curve. Resonances occur at higher energies when a nearly bound state can be formed in the upper level. A gap of the size $10mE_h$ give results displayed in Fig. 4 , and show essentially the same thing. The smallest gap, $5mE_h$, exhibits (Fig. 5) a substantial decrease in the transmission probability above the top of the adiabatic barrier and illustrates the significance of the coupling between adiabatic channels.

Figure 3. Transmission probability derived from a single adiabatic state model (heavy line) and the two-state treatment (normal line) with an energy gap at the top of the barrier of $20mE_h$.

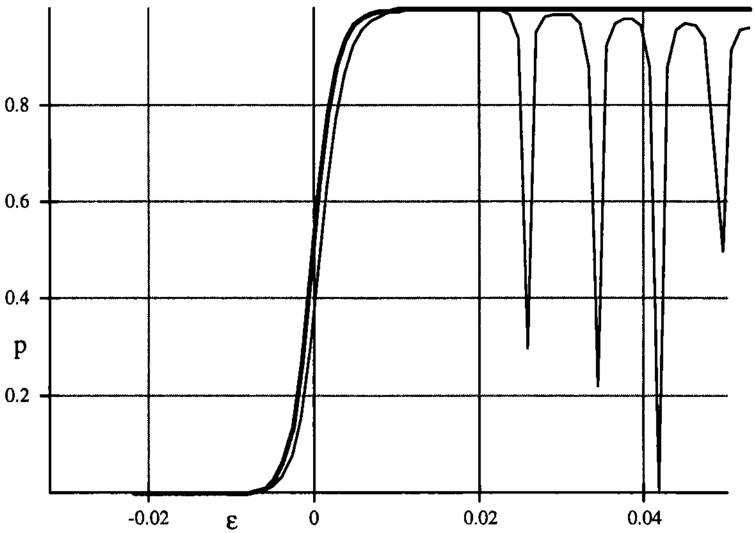

Figure 4. Transmission probability derived from a single adiabatic state model (heavy line) and the two-state treatment (normal line) with an energy gap at the top of the barrier of $10 mE_h$.

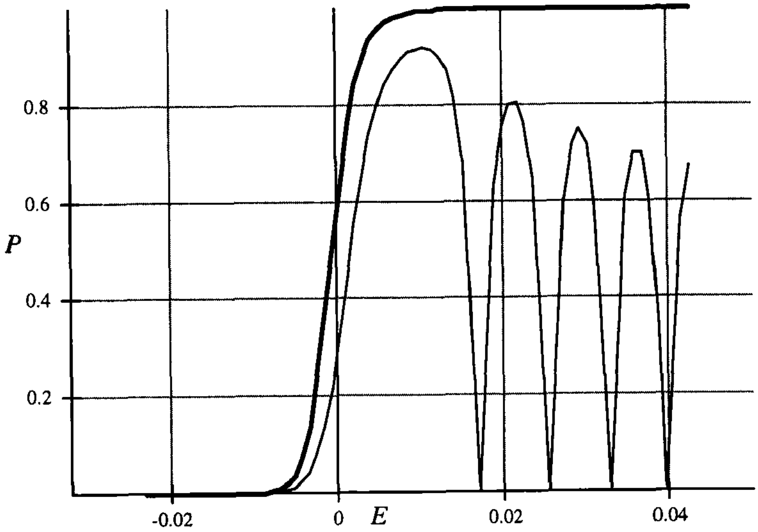

Figure 5. Transmission probability derived from a single adiabatic state model (heavy line) and the two-state treatment (normal line) with an energy gap at the top of the barrier of $5 mE_h$.

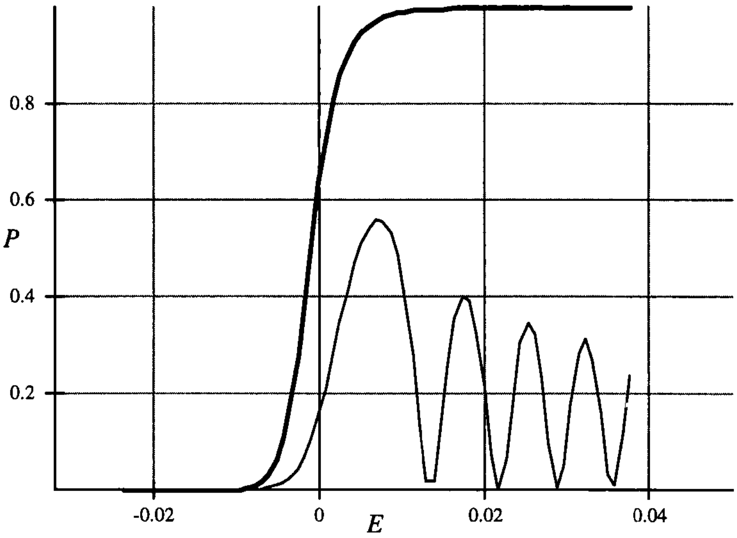

Further comments.

A simple model is proposed in this note. It is shown to incorporate the possibility of including several potential energy curves in a treatment of scattering processes in a linear geometry based on very limited information from electronic structure calculations. The present demonstration of the feasibility will be followed by more detailed examinations and possible comparisons with more elaborate theoretical work and even experimental findings. Extensions to two and higher dimensions appear to be within reach[5] and in conjunction with a geometrical characterization of the molecular conformation space based on a distance concept derived from a quantification of the Rice-Teller least motion principle[5,10] there opens an avenue towards detailed descriptions of chemical processes from basic principles.

Acknowledgment.

Support for part of the present work has been forthcoming from the Carlsbergfoundation, in particular for the computational equipment. The present calculations, graphics, and word processing have all been performed on a Macintosh Powerbook with a PowerPC processor.
The interest in enantioselectivity and the aziridines has been aroused in the author by Professor Göran Bergson.

Bibliography

1 S. Shin and J. C. Light, *J. Chem. Phys.* **101**, 2836 (1994).

2 J. Qi and J. M. Bowman, *J. Chem. Phys.* **104**, 7545 (1996).

3 E. P. Wigner and L. Eisenbud, *Phys. Rev.* **72** (1947) 29.

4 J. Linderberg, *Comp. Phys. Rep.* **6** (1987) 209.

5 J. Linderberg, *J. Chem. Soc., Faraday Trans.,* **93** (1997) 893.

6 J. C. Light, I. P. Hamilton, and J. V. Lill, *J. Chem. Phys.* **82** (1985) 1400, see also R. M. Whitnell and J. C. Light, *ibid.* **90** (1989) 1774; S. E. Choi and J. C. Light, *ibid.* **90** (1989) 2593.

7 M. Abramowitz and I. A. Stegun, *Handbook of Mathematical Functions,* (Dover, New York 1968) p. 888

8 G. H. Golub and J. H. Welsch, *Math. Comp.* **23** (1969) 221.

9 I. M. B. Nielsen, to be published

10 P. E. Larsson and J. Linderberg, *Theor. Chim. Acta* **93** (1996) 79.

Appendix: Lobatto integration rule.

The nodes, $\{q_j\}$, and weights, $\{w_j\}$, for the Lobatto integration rule are found from an eigenvalue problem[8] derived from the recurrence relation for the associated Legendre polynomials, in the normalized form,

$$\tilde{P}^1_{k-1}(q)\sqrt{\frac{(k-1)(k+1)}{(2k-1)(2k+1)}}+\tilde{P}^1_{k+1}(q)\sqrt{\frac{k(k+2)}{(2k+1)(2k+3)}}=\tilde{P}^1_k(q)q;$$
$$\tilde{P}^1_k(q)=-\sqrt{1-q^2}\sqrt{\frac{2k+1}{2k(k+1)}}\frac{dP_k(q)}{dq}. \tag{A1}$$

The eigenvalue problem arises when the condition

$$\tilde{P}^1_n(q)=0 \tag{A2}$$

is invoked. A set of eigenvalues and orthonormal vectors are calculated, $\{q_j, c_{kj} | j,k = 1,2,\ldots n-1\}$ and it is concluded that there is a proportionality so that

$$\tilde{P}^1_k(q_j)=-\sqrt{1-q_j^2}\,\frac{c_{kj}}{c_{1j}} \tag{A3}$$

and consequently

$$P_n(q_j)=\sqrt{\frac{2n-2}{n(2n-1)}}\,\frac{c_{n-1,j}}{c_{1j}} \tag{A4}$$

which gives the weights from Eq. (26)

$$w_j=\frac{2}{n(n+1)P_n^2(q_j)}=\frac{(2n-1)}{(n-1)(n+1)}\left|\frac{c_{1,j}}{c_{n-1j}}\right|^2;\, j=1,2,\ldots n-1. \tag{A5}$$

and

$$w_j=\frac{2}{n(n+1)},\quad j=0,n;\quad q_0=-1;\quad q_n=1. \tag{A6}$$

It is observed that the integral rule, applied to $P_n{}^2(x)$, gives an error,

$$\int_{-1}^{1} dq P_n^2(q)-\sum_0^n w_j P_n^2(q_j)=\frac{2}{2n+1}-\frac{2}{n}=-\frac{2(n+1)}{n(2n+1)} \tag{A7}$$

in agreement with the standard formula[7]

$$R_{n+1}=-\frac{2^{2n+1}}{(2n+1)!}\binom{2n}{n}^{-1}\binom{2n}{n-1}^{-1}\frac{d^{2n}}{dq^{2n}}P_n^2(q) \tag{A8}$$

since

$$\frac{d^{2n}}{dq^{2n}}P_n^2(q)=\binom{2n}{n}\left[\frac{d^n}{dq^n}P_n(q)\right]^2=\binom{2n}{n}\left[\binom{2n}{n}\left(\tfrac{1}{2}\right)^n n!\right]^2 \tag{A9}$$

The integration rule overestimates this integral by more than 100% and thus it is necessary to be aware of the range of validity and to impose constraints in the variational expression where the discrete variable representation is employed.

Index

A

ABCS theory, *see* Aquilar–Balslev–Combes–Simon theory
Ab initio calculations
  BSSE free, intermolecular interaction potential, 267–271
  2-hydroxy-acetamide, 95–96
  water–water interaction energy, 271–273
Above-threshold ionization process
  for atom, 198–200
  in photoelectron spectrum, 202–204
Adiabatic effects, basis to diabatic representation, 132–133
Algebra, matrix, equations, 322–324
Algorithms
  CASVB algorithm, 52–65
  McMurchie–Davidson algorithm, 28
  Peaceman–Rachford algorithm, 201–202
Amine group, in methylamine
  H wagging, 148–152
  H wagging and bending, 152–155
Ammonium ion, oscillatory strength and Einstein emission coefficients, 187–193
Apparent surface charge, and PCM, for basic electrostatic problem, 229–230
Aquilar–Balslev–Combes–Simon theory, relationship to CCR method, 209–210
ASC, *see* Apparent surface charge
ATI process, *see* Above-threshold ionization process
Atomic states, Sc and Sc^+, 71–72
Atoms
  electric properties, 213
  four-electron, resonance spectrum, 220
  in static electric and magnetic field, 211–212
  theoretical model, 198–200
  three-electron atoms, 218–220
  two-electron atoms, 216–218

B

Barium, resonance spectrum, 220–221
Basis sets
  even-tempered, Gaussian primitive functions, 294–295
  expansion, with Lobatto quadrature rule, 321–322
  finite, in restricted HF calculations, 97
  in gas phase matrix studies, 291–293
  Legendre, triatomic molecules, 131–132
  for resonance, 214–216
  Slater, minimal, in variational treatments, 9
Basis set superposition errors, interaction potential, 267–271
Bending
  amine H in methylamine, 152–155
  double torsion and bending, 160–161
Benzene, application of CASVB algorithm, 54–57
BERTHA program
  determination of Dirac–Hartree–Fock equation, 31–32
  large molecule electronic structures, 39–43
Beryllium, resonance spectrum, 220
Bethe–Salpeter equation, in relativistic many-electron theory, 13–14
BO approximation, *see* Born–Oppenheimer approximation
Born–Oppenheimer approximation
  in Dirac equation, 6–7
  potential energy surface, 146–148
Boron fluoride
  analysis with standard basis sets, 291–293
  gas phase energies, 299–300
Breit operator, matrix operator, 29
BSSE, *see* Basis set superposition errors

C

Carbon monoxide
  analysis with standard basis sets, 291–293
  gas phase energies, 299–300
  ground state, HF energy, 294–295
CASSCF wave function, *see* Complete active space self-consistent field wave function
CASVB algorithm, *see* Complete active space valence bond algorithm
Cavity surface
  error correction, 244–246
  PCM with UATM extension, 253–254
  tessellation
    non-atomic sphere-based tessellation, 255–256
    variable, PCM, 253–254
CCR method, *see* Complex coordinate rotation method
Charge density, charged particles, 173–177
Charged particles
  charge–current density, 173–177
  electrodynamic properties, 170–173
Charge operator, matrix elements, 26–27, 27–28
Complete active space self-consistent field wave function
  benzene, 54–57
  FeH, 57–60
  invariance, 52
  method, 70–71
  model polyene systems, 60–65
  normalized wave function, 52–54
Complete active space valence bond algorithm
  application
    to benzene, 54–57
    to FeH, 57–60
    to model polyene systems, 60–65
  normalized CASSCF wave function, 52–54
  strategy, 52
Complex coordinate rotation method
  atoms in external fields, 211–212
  Ba, 220–221
  Be, 220
  exotic systems, 221
  H^-, 216–217
  H^{2-}, 219–220
  He, 217
  He^-, 218–219
  He-like ions, 218
  Li, 219
  Li^-, 220
  Li-like ions, 220
  nonvariational methods, 210–211
  photons, 212–213
  relationship to ABCS theory, 209–210
  Sr, 220–221
Computer programs
  BERTHA, 31–32, 39–43
  GAUSSIAN94, 97, 114
  MOTECC, 273–274
Conformational analysis
  energy
    TA, 120
    (*R*,*R*)-tartamide, 120–121
    (*R*,*R*)-tetramethyltartramide, 120–121
  gas, with GAUSSIAN94, 114
  2-hydroxy-acetamide, 94–95
Conical intersections
  nonadiabatic effects, 129–131
  triatomic molecules, 131–132
Continuum models
  description, 288
  Gaussian primitive function even-tempered basis sets, 294–295
  isodensity polarized continuum model, 290, 300
  polarizable
    analytical geometry derivatives, 246–249
    basic electrostatic problem, 229–230
    basic specifications, 230–233
    COSMO-PCM, 238–239
    different formulations of electrostatic problem, 236–238
    extensions for cavity definition
      UATM, 253–254
      variable tessellation, 254–255
    formulation, 233
    HF formalism, dispersion and repulsion, 233–236
    IEF-PCM, 239–242
    molecular response functions, 249–253
    PCM-QINTn, 242–244
    in solvation studies, 289–290
  quantum Onsager model, 288–289
Correlation energy
  electron

    finite basis set HF calculations, 97
    2-hydroxy-acetamide, 96
  2-hydroxy-acetamide, 101
  second-order, 2-hydroxy-acetamide, 103
COSMO-PCM, definition, 238–239
Coulomb operator, matrix elements, 28
Current density, charged particles, 173–177
Current operator, matrix elements, 26–27, 27–28

D

DA, *see* (*R*,*R*)-Tartaric acid diamide
DEFPOL method, in cavity surface tessellation, 255–256
DHF calculations, *see* Dirac–Hartree–Fock calculations
Diabatic electronic representation, adiabatic basis, 132–133
Dimethylamine, double torsion, 155–159
Dipole moment, variation, isodensity polarized continuum model, 300
Dirac–Coulomb–Breit operator, in continuum dissolution, 14–15
Dirac–Coulomb Hamiltonian, in relativistic treatments, 11–12
Dirac equation
  forms, 5–7
  in N-electron problem, 15–18
  in Undheim–Hylleraas–Macdonald theorem, 8–9
Dirac–Hartree–Fock calculations
  determination with BERTHA, 31–32
  large molecules, 39–43
  in relativistic many-body theory, 18–20
Dispersion, in HF formalism of PCM, 233–236
Dissolution, continuum, in relativistic many-electron theory, 14–15
Double torsion, in dimethylamine
  torsion, 155–159
  torsion and bending, 160–161

E

Einstein emission coefficients, Rydberg electron, 187–193
Electric field
  atoms, 213
  static, atoms, 211–212
Electric polarization field, charged particles, 170–173
Electrodynamics, charged particles, 170–173
Electron correlation effects
  finite basis set HF calculations, 97
  2-hydroxy-acetamide, 96
Electron–electron interaction, in relativistic many-electron theory, 12–13
Electronic model, matrix elements, 319–320
Electronic state, excited, numerical model, 316
Electron–positron virtual pair, 24–26
Electrostatics, different formulations of problem, 236–238
Energy
  correlation
    electron
      finite basis set HF calculations, 97
      2-hydroxy-acetamide, 96
    2-hydroxy-acetamide, 101
    second-order, 2-hydroxy-acetamide, 103
  ground state
    2 $^4\Sigma^-$, ScB^+, 76–78
    1 $^2\Pi$, ScB^+, 79–81
    2 $^2\Pi$, ScB^+, 81–82
    hydrogenic, variational treatment, 9–11
    Ne, Dirac–Hartree–Fock ground state, 31–32
    X $^4\Sigma^-$ (1 $^4\Sigma^-$), ScB^+, 72–75
  interaction, water–water dimer, 271–273
  potential
    BO approximation of surface, 146–148
    water–water dimer, 274–279
  total, through second-order, 2-hydroxy-acetamide, 98–100, 102–103
Energy conformational analysis
  TA, 120
  (*R*,*R*)-tartamide, 120–121
  (*R*,*R*)-tetramethyltartramide, 120–121
Excited state
  1 $^2\Delta$ and 2 $^2\Delta$, ScB^+, 83–85
  1 $^2\Sigma^-$, ScB^+, 87–88
  1 $^2\Sigma^+$ and 2 $^2\Sigma^+$, ScB^+, 85–87

F

Finite basis sets, in restricted HF calculations, 97

Four-electron atoms
  resonance spectrum
    Be, 220
    Li^-, 220
  two-electron, resonance spectrum, 216–218

G

Gas conformational analysis, with GAUSSIAN94, 114
Gas phase
  energies, 299–300
  matrix studies with standard basis sets, 291–293
GAUSSIAN94 program
  finite basis set HF calculations, 97
  in gas conformational analysis, 114
Gaussian primitive functions, even-tempered
  basis sets, 294–295
  systematic sequences, 290–291
Geometry, derivatives, calculations with PCM, 246–249
GEPOL method, in cavity surface tessellation, 255–256
Germanocene, DHF calculations, 39–43
Ground state energy
  2 $^4\Sigma^-$, ScB^+, 76–78
  1 $^2\Pi$, ScB^+, 79–81
  2 $^2\Pi$, ScB^+, 81–82
  hydrogenic, variational treatment, 9–11
  Ne, Dirac–Hartree–Fock ground state, 31–32
  X $^4\Sigma^-$ (1 $^4\Sigma^-$), ScB^+, 72–75

H

HA, *see* 2-Hydroxyacetic acid
Hamiltonian, continuous effective, basic classification, 229–230
Hartree–Fock calculations
  CO ground state, 294–295
  finite basis set, for electron correlation effects, 97
  gas phase matrix, 291–293
  matrix restricted, 2-hydroxy-acetamide, 98, 102
  PCM, dispersion and repulsion, 233–236
  restricted, TA, DA, and TMDA, 114–116
  Sc and Sc^+, 71–72
HD, *see* 2-Hydroxyacetamide
Helium, resonance spectrum, 217
  He, 217
  He^-, 218–219
  He-like ions, 218
HF calculations, *see* Hartree–Fock calculations
HMD, *see* 2-Hydroxy-*N,N*-dimethylacetamide
Hydrogen
  on methylamine amine group
    wagging, 148–152
    wagging and bending, 152–155
  resonance spectrum, H^{2-}, 219–220
Hydrogenic ground state energy, variational treatment, 9–11
2-Hydroxyacetamide
  ab initio calculations, 95–96
  conformational analysis, 94–95
  correlation energy, 101
  electron correlation effects, 96
  finite basis set HF calculations, 97
  matrix restricted HF calculations, 102
  as model system, 113–114, 116–119, 121–123
  restricted matrix HF calculations, 98
  second-order correlation energy, 103
  total energy through second-order, 98–100, 102–103
2-Hydroxyacetic acid, as model system, 113–114, 116–119, 121–123
2-Hydroxy-*N,N*-dimethylacetamide, as model system, 113–114, 116–119, 121–123

I

IEF-PCM, definition, 239–242
Infrared spectrum, water–water dimer, 279
Interaction energy, water–water dimer, 271–273
Interaction potential
  charged particles, 170–173
  intermolecular, BSSE free *ab initio*, 267–271
  water–water, 265–267
Intersections, conical
  nonadiabatic effects, 129–131
  triatomic molecules, 131–132

Ionization, ATI process
  for atom, 198–200
  in photoelectron spectrum, 202–204
Iron hydride, application of CASVB algorithm, 57–60
Isodensity polarized continuum model
  dipole moment variation, 300
  in solvation studies, 290

L

Legendre basis functions, triatomic molecules, 131–132
Lithium, resonance spectrum
  Li, 219
  Li^-, 220
  Li-like ions, 220
Lobatto integration rule, description, 330
Lobatto quadrature rule, in basis set expansion, 321–322

M

Magnetic field, static, atoms, 211–212
Magnetic polarization field, charged particles, 170–173
Many-body perturbation theory, relativistic, methods, 23–24
Many-body theory, relativistic
  Dirac–Hartree–Fock equation, 18–20
  N-electron problem, general formulation, 15–18
Many-electron theory, relativistic
  continuum dissolution, 14–15
  electron–electron interaction, 12–13
  treatments, 11–12
Matrix algebra, equations, 322–324
Matrix elements
  Breit operator, 29
  charge and current operator, 26–27
  charge–current operator, 27–28
  coulomb operator, 28
  moment integrals, 28
McMurchie–Davidson algorithm, generalization, 28
Methylamine
  amine H wagging, 148–152
  amine H wagging and bending, 152–155
  methyl torsion, 148–152
2-Methylaziridine, nitrogen inversion, potentials, 325
Methyl group, torsion in methylamine, 148–152
Minimal Slater basis set, in variational treatments, 9
Model systems
  atoms, 198–200
  electronic model, 319–320
  HA, 113–114, 116–119, 121–123
  HD, 113–114, 116–119, 121–123
  HMD, 113–114, 116–119, 121–123
  isodensity polarized continuum model, 290, 300
  for 2-methylaziridine nitrogen inversion, 325
  nuclear motion, 316
  polarizable
    analytical geometry derivatives, 246–249
    basic electrostatic problem, 229–230
    basic specifications, 230–233
    COSMO-PCM, 238–239
    different formulations of electrostatic problem, 236–238
    extensions for cavity definition
      UATM, 253–254
      variable tessellation, 254–255
    formulation, 233
    HF formalism, dispersion and repulsion, 233–236
    IEF-PCM, 239–242
    molecular response functions, 249–253
    PCM-QINTn, 242–244
    in solvation studies, 289–290
  polyene systems, application of CASVB algorithm, 60–65
  quantum Onsager model, 288–289
  united atom topological model, 253–254
Molecular dynamics, water–water dimer, 273–274
Molecules
  analysis with standard basis sets, 291–293
  chiral, parity violation, 36–39
  gas phase energies, 299–300
  large, DHF calculations, 39–43
  small, NMR shielding tensors, 32–36
  triatomic, conical intersections, 131–132
Møller–Plesset calculations, TA, DA, and TMDA, 114–116, 121

Moment integrals, matrix elements, 28
MOTECC program, application to water–water dimer, 273–274
MQDT, *see* Multichannel quantum defect theory
Multichannel quantum defect theory, Rydberg radicals, 182–184

N

N-electron problem, general formulation, 15–18
Neon, Dirac–Hartree–Fock ground state of atom, 31–32
Nitrogen
  analysis with standard basis sets, 291–293
  inversion, 2-methylaziridine, potentials, 325
Nitrogen dioxide, nonadiabatic spectrum
  beginning, 134–137
  development, 137–142
  methods, 133–134
Nitrogen oxide cation
  analysis with standard basis sets, 291–293
  gas phase energies, 299–300
NMR, *see* Nuclear magnetic resonance
Nonadiabatic effects
  from conical intersection, 129–131
  NO_2 spectrum
    beginning, 134–137
    development, 137–142
    methods, 133–134
Non-relativistic quantum mechanics
  relativistic corrections, 21–23
  in variation theory, 7
Nonvariation, in CCR method, 210–211
Nuclear magnetic resonance, shielding tensors in small molecules, 32–36
Nuclear motion, model systems, 316
Numerical computations
  excited electronic state, 316
  TDSE, 198, 201–202

O

Oscillator strength, Rydberg electron, 187–193

P

Parity, violation in chiral molecules, 36–39
Particles, charged
  charge–current density, 173–177
  electrodynamic properties, 170–173
PCM, *see* Polarizable continuum model
PCM-QINTn, definition, 242–244
Peaceman–Rachford algorithm, in TDSE, 201–202
Perturbation theory, many-body, relativistic, methods, 23–24
Photoelectron spectrum
  from atomic wave function, 201–202
  laser and harmonic, 202–204
Photons, interaction, application of CCR method, 212–213
Polarizable continuum model
  analytical geometry derivatives, 246–249
  basic electrostatic problem, 229–230
  basic specifications, 230–233
  COSMO-PCM, 238–239
  different formulations of electrostatic problem, 236–238
  extensions for cavity definition
    UATM, 253–254
    variable tessellation, 254–255
  formulation, 233
  HF formalism, dispersion and repulsion, 233–236
  IEF-PCM, 239–242
  molecular response functions, 249–253
  PCM-QINTn, 242–244
  in solvation studies, 289–290
Polarization fields
  and charge–current density, 173–177
  in charged particles, 170–173
Polyene systems, application of CASVB algorithm, 60–65
Position, resonance, 208
Positron–electron virtual pair, 24–26
Positronium ion, resonance spectrum, 221
Potential energy
  BO approximation of surface, 146–148
  water–water dimer, 274–279
Potentials, 2-methylaziridine nitrogen inversion, 325

Q

QDO method, *see* Quantum defect orbital method
Quantum defect orbital method
  NH_4, 187–193
  Rydberg electron, 184–186
Quantum mechanics
  non-relativistic
    relativistic corrections, 21–23
    in variation theory, 7
  relativistic, in variation theory, 7–9
Quantum Onsager model, in solvation studies, 288–289

R

Raman spectrum, water–water dimer, 279
Rayleigh quotient, in variational treatments, 9
Relativistic corrections, to non-relativistic quantum chemistry, 21–23
Relativistic many-body perturbation theory, methods, 23–24
Relativistic many-body theory
  Dirac–Hartree–Fock equation, 18–20
  N-electron problem, general formulation, 15–18
Relativistic many-electron theory
  Bethe–Salpeter equation, 13–14
  continuum dissolution, 14–15
  electron–electron interaction, 12–13
  treatments, 11–12
Relativistic quantum mechanics, in variation theory, 7–9
Repulsion, in HF formalism of PCM, 233–236
Resonance
  Ba, 220–221
  basis sets for, 214–216
  Be, 220
  exotic systems, 221
  H^-, 216–217
  H^-, 219–220
  He, 217
  He^-, 218–219
  He-like ions, 218
  Li, 219
  Li^-, 220
  Li-like ions, 220
  partial widths, 211
  position and width, 208
  Sr, 220–221
Response functions, molecular, PCM, 249–253
Restricted Hartree–Fock calculations, TA, DA, and TMDA, 114–116
R-matrix theory, scattering problem, 316–319
Rydberg electron
  application of QDO method, 184–186
  Einstein emission coefficients, 187–193
  oscillator strength, 187–193
Rydberg states, definition, 182–184

S

Scattering, application of R-matrix theory, 316–319
ScB^+
  $1\,^2\Delta$ and $2\,^2\Delta$ states, 83–85
  $1\,^2\Sigma^+$ and $2\,^2\Sigma^+$ states, 85–87
  $1\,^2\Sigma^-$ state, 87–88
  $2\,^4\Sigma^-$ state, 76–78
  $1\,^2\Pi$ state, 79–81
  $2\,^2\Pi$ state, 81–82
  Hartree–Fock energies, 71–72
  $X\,^4\Sigma^-$ $(1\,^4\Sigma^-)$ state, 72–75
Schrödinger equation
  one-electron, for Rydberg electron, 184–186
  time-dependent, numerical treatment, 198, 201–202
Self-consistent field, SCF-MI, water–water dimer, 271–273
Self-consistent reaction field, in solvation studies, 288–289
Semiempirical calculations, TA, DA, and TMDA, 112–113
Slater basis set, minimal, in variational treatments, 9
Solvation studies
  isodensity polarized continuum model, 290
  polarized continuum model, 289–290
  Quantum Onsager model, 288–289
Spectra, nonadiabatic, NO_2
  beginning, 134–137
  development, 137–142
  methods, 133–134
Spheres, atomic, and cavity surface tessellation, 255–256

Strontium, resonance spectrum, 220–221
Surface charge, apparent, and PCM, for basic electrostatics, 229–230

T

TA, *see* (*R*,*R*)-Tartaric acid
(*R*,*R*)-Tartamide, energy conformational analysis, 120–121
(*R*,*R*)-Tartaric acid
  energy conformationl analysis, 120
  RHF and MP2 energy, 114–116
  role in organic and pharmaceutical chemistry, 109–110
  semiempirical calculations, 112–113
(*R*,*R*)-Tartaric acid diamide
  RHF and MP2 energy, 114–116
  semiempirical calculations, 112–113
(*R*,*R*)-Tartaric acid *N*,*N*,*N*,*N*-tetramethyl diamide
  RHF and MP2 energy, 114–116
  semiempirical calculations, 112–113
TDSE, *see* Time-dependent Schrödinger equation
Tensors, shielding, in small molecules, NMR, 32–36
Tessellation, cavity surface
  non-atomic sphere-based tessellation, 255–256
  variable tessellation, 254–255
(*R*,*R*)-Tetramethyltartramide, energy conformational analysis, 120–121
Three-electron atoms, resonance spectrum
  H^{2-}, 219–220
  He^-, 218–219
  Li, 219
  Li-like ions, 220
Time-dependent Schrödinger equation, numerical treatment, 198, 201–202
TMDA, *see* (*R*,*R*)-Tartaric acid *N*,*N*,*N*,*N*-tetramethyl diamide
Torsion
  double, in dimethylamine
    torsion, 155–159
    torsion and bending, 160–161
  methyl group in methylamine, 148–152
Two-electron atoms, resonance spectrum
  H^-, 216–217
  He, 217
  He-like ions, 218

U

UATM, *see* United atom topological model
Undheim–Hylleraas–Macdonald theorem, in Dirac equation, 8–9
United atom topological model, for cavity definition, 253–254

V

Valence bond, wavefunction for water–water dimer, 271–273
Variation theory
  application to hydrogenic ground state energies, 9–11
  non-relativistic quantum mechanics, 7

W

Wagging, amine H in methylamine, 148–155
Water–water dimer
  interaction energy, 271–273
  interaction potential, 265–267
  IR spectrum, 279
  molecular dynamics, 273–274
  Raman spectrum, 279
  simulation results, 274–279
Wave functions
  atomic, photoelectron spectrum, 201–202
  CASSCF
    benzene, 54–57
    FeH, 57–60
    invariance, 52
    method, 70–71
    model polyene systems, 60–65
    normalized wave function, 52–54
  VB, for water–water dimer, 271–273
Width
  partial, in resonance, 211
  resonance, 208

Z

Zeeman effect, in quantum mechanics, 30–32